Analysis of Accelerated Corrosion Experiment on Reinforced Concrete Slabs Using Half-Cell Potential Measurements

BY

CARLOS JAQUEZ
Bachelor of Science, University of Massachusetts Lowell

SUBMITTED IN PARTIAL FULFILLMENT OF THE REQUIREMENTS
FOR THE DEGREE OF MASTER OF SCIENCE
DEPARTMENT OF CIVIL AND ENVIRONMENTAL ENGINEERING
UNIVERSITY OF MASSACHUSETTS LOWELL

Signature of the Author .....
Department of Civil and Environmental Engineering
March, 2013

Signature of Thesis Supervisor .....
Tzu-Yang Yu
Assistant Professor

Committee Member Signature .....
Professor Donald Leitch
Department of Civil and Environmental Engineering

Committee Member Signature .....
Professor Susan Faraji
Department of Civil and Environmental Engineering

Analysis of Accelerated Corrosion Experiment on Reinforced Concrete Slabs Using Half-Cell Potential Measurements

BY

CARLOS JAQUEZ
Bachelor of Science, University of Massachusetts Lowell

ABSTRACT OF A THESIS SUBMITTED TO THE FACULTY OF THE
DEPARTMENT OF CIVIL AND ENVIRONMENTAL ENGINEERING
IN PARTIAL FULFILLMENT OF THE REQUIREMENTS
FOR THE DEGREE OF
MASTER OF SCIENCE
UNIVERSITY OF MASSACHUSETTS LOWELL
2013

Thesis Supervisor: Tzu-Yang Yu
Title: Assistant Professor

Corrosion of steel reinforcement is know to be the primary cause of deterioration for reinforced concrete structures. It is one of the foremost factors that affect the durability of concrete structures. The corrosion of steel reinforcement is most commonly caused by the action of chloride ions on the steel reinforcement. These chloride ions cause the breakdown of the passive film formed around the reinforcement due to the highly alkaline environment of the concrete. Damage to the concrete eventually manifests itself in the form of cracking and eventually spalling of the concrete. End of service life for the corrosion affected structures is characterized by the loss of concrete cover of the reinforcement. At this stage, the reinforcement is no longer protected against further degradation from corrosion. In this research, corrosion in reinforced concrete structures is induced by means of accelerated corrosion experiment. Reinforced concrete slabs were cast with various different cover thickness for the steel reinforcement (1.5-in, 2.0-in and 2.5-in) and the effects of chloride induced corrosion studied and analyzed by means of half-cell potential measurements. A separate accelerated corrosion experiment was performed on an individual steel rebar to measure the anticipated mass loss from corrosion. These results were compared against the analysis of the half-cell potential data and correlated. Furthermore, a cover meter survey was performed on the reinforced concrete slabs to determine the reliability of the cover meter sensor when corrosion is known to be present in the reinforcement. The sampling rate for the half-cell potential measurements was 8 inches while the sampling rate for the cover meter survey was 5 inches.

Acknowledgements

I would like to express my deepest and sincere gratitude to my research advisor, Professor Tzu-Yang Yu, for his encouragement and support through this thesis. Prof. Yu continually and convincingly provided me with the guidance needed to make this thesis a reality. Without your assistance, this thesis would not have been possible.

I would also like to extend gratitude to my committee members, Prof. Susan Faraji and Prof. Donald Leitch for their valuable inputs and comments through this journey.

This research was supported by the U.S. Department of Commerce, National Institute of Science and Techology (NIST) Technology Innovation Program (TIP) Grant #5049557805 and I am thankful to the VOTERS (Versatile Onboard Traffic Embedded Roaming Sensors) project and Prof. Ming Wang, from Northeastern University, for providing me with the opportunity to perform the experimental work.

In addition, I would like to thank of all my friends and colleagues at the SERG group, for their friendship and support over the years. In particular, Hao Liu, Shafique Ahmed, CheFu Su and Ross Gladstone.

Finally, it is with immense gratitude that I give my deepest appreciation to my wife, Yomayra, for her support and care throughout my time at UMass Lowell. I dedicate this thesis to you.

Contents

List of Figures

List of Tables

Chapter 1

Introduction

1.1 Background

Reinforcement corrosion, primarily resulting in the deterioration of concrete structures, is a problem well known to the civil engineering community. A 2002 study by the Federal Highway Administration (FHWA), estimated that total annual direct costs of corrosion in the U.S. is approximately $276 billion, with approximately $8.3 billion directly affecting the infrastructure of highways and bridges [26]. To reduce the economic impact of corrosion, corrosion engineers and scientists aim to reduce the losses, material and economic, that result in the corrosion of pipes, tanks, machines, ships, bridges and the like. Rebuilding of corroded equipment and infrastructure requires further investment of human, mechanical and ecological resources [40].

Due to the high cost for replacement and rehabilitation of infrastructure, it is essential that proper scientific studies are performed, in order to quantify the

corrosion damage potential. For reinforced concrete structures, the final corrosion products, as a result of the natural volumetric expansion of the byproducts, is the primary cause of cracking and spalling in the concrete [21]. Additional damage resulting from corrosion of steel reinforcement includes delamination reduction of steel areas and debonding between rebars and concrete [22].

Ample research can be found in the literature in regards to the assessment of aging concrete structures due to corrosion [22], deterioration [8], chloride-contaminated concrete [19], reduced load carrying capacity [41], detrimental effect on the reinforcing bars [1], among others. Experimental investigations similar in nature to the one presented in this thesis, have indicated that several factors affect the bond strength of reinforcing steel bars. Among them are (a) permeability of the concrete matrix; (b) cover thickness; (c) the electric current applied; (d) density of the solution used and; (e) the environmental temperature.

Studies have been made also on the effect of water to cement (w/c) ratio, concrete cover depth and area of anode to cathode ratio during corrosion propagation under macro cell corrosion condition. It was found that the rate of corrosion on the anode mainly depends on the chloride content and oxygen supply in concrete [43]. In practice, chloride ingress into reinforced concrete takes many years, providing time for the concrete to mature and the steel to equilibrate in the alkaline environment, before the steel encounters the chlorides and corrosion is initiated [36].

For laboratory experiments it is impractical to wait many years in order to obtain results. Therefore, several studies have been undertaken using accelerated

corrosion experiments to assess the condition of reinforced structures. These studies use a variety of mechanisms to develop corrosion in the rebars from imbedding the concrete with NaCl [21], partially immersing the concrete in NaCl solution [8] and utilizing impressed anodic current [1].

Depending on the corrosion state of the structure, different remediation strategies can be undertaken for repair, rehabilitation or outright replacement. Durable and cost effective repairs can only be obtained based on reliable information on the level and rate of corrosion. Half-cell potential (HCP) mapping has been shown to be a powerful, rapid and non-destructive technique both in condition assessment and in repair work [12] [28] [38].

1.2 Research Objectives

While the effects of corrosion on concrete infrastructure have been studied extensively, less research has been devoted to the actual methods used to develop the understanding needed to assess the degree of corrosion within the reinforcement. The most common method to ascertain the degree of reinforcement corrosion with 100% accuracy is a destructive test [8] [1] [27] [14] [10]. Other researchers have experimented with non-destructive methods to assess the degree of corrosion within the steel reinforcement [12] [29] [23] [31] [28] [42] [44] [34] [38]. The most widely cited and relied on standard for assessing non-destructively corrosion in concrete has been ASTM C876-09 "Standard Test Method for Corrosion Potentials of Uncoated Reinforcing Steel in Concrete" (ASTM C876)[4].

Based on this information the research objectives can be summarized in the following:

- To develop an accelerated corrosion model based on experimental data to assess the degree of corrosion within concrete.
- To investigate the effect of differing concrete cover thickness on the HCP measurements from reinforced concrete slabs subjected to an accelerated corrosion experiment.
- To determine the reliability of other non-destructive sensors on corroded steel reinforcement.

1.3 Research Approach

To achieve the research objectives, a comprehensive approach to study the effects of corrosion on the non-destructive sensors is adopted. Three different experiments are conducted to collect information in regards to all three research objectives.

First experiment. A section of steel reinforcement is placed into 15% NaCl solution for the period of time necessary to achieve 15% corrosion mass loss. The specimen is placed within a small plastic container and wired to a piece of copper that serves as the cathode of the electrochemical cell. Mass loss measurements are taken at different intervals by removing the rust accumulated throughout the experiment and measuring the cumulative mass loss of the steel reinforcement.

Second experiment. Four reinforced concrete slabs are cast with different

concrete cover thicknesses and with two rows of reinforcement. The dimensions of the slabs are 4-ft by 6-ft by 7-in. The reinforcement for slabs 1 and 2 is placed in the y-direction. The concrete cove thickness for slab 1 is 1.5-in while the thickness for slab 2 is 2.0-in. The reinforcement for slabs 3 and 4 is placed in the x-direction. The concrete cover thickness for slab 3 and 4 are 1.5-in, 2.0-in and 2.5-in. Slabs 1, 2 and 3 are subjected to accelerated corrosion [11] [6], while slab 4 is held as the control slab. HCP measurements, are taken every week. The results are analyzed using MATLAB® and per ASTM G16-95 "Standard Guide for Applying Statistics to Analysis of Corrosion Data" (ASTM G16)[7].

Third experiment. Covermeter measurements are taken at the beginning of the accelerated corrosion experiment on all four slabs. Measurements are then collected at the end of the accelerated corrosion experiment, again on all four slabs. The data is analyzed against known concrete cover thickness and correlated with corresponding half-cell measurements.

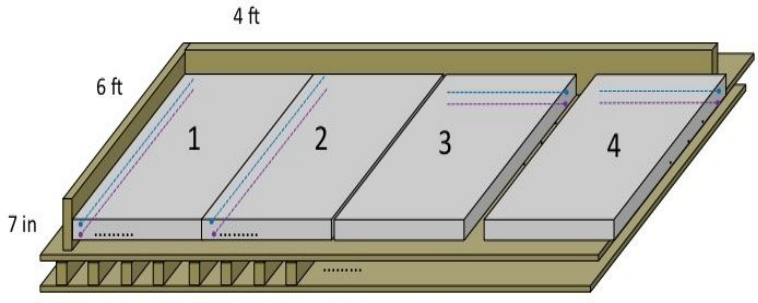

Figure 1-1: Layout of Reinforced Concrete Slabs

1.4 Organization of the Thesis

This thesis is organized as outlined below.

Chapter 2 reviews the comprehensive body of literature regarding the corrosion process and experimental studies using accelerated corrosion. The half-cell reaction as the basis behind the HCP method is discussed and explained. The theoretical framework for eddy currents is outlined and studies past experiments on civil infrastructure.

Chapter 3 presents the accelerated corrosion experimental program.

Chapter 4 provides data analysis, summarizes and discusses the results obtained.

Chapter 5 concludes the findings obtained from the research program.

Chapter 2

Literature Review

In this chapter we will explain the theoretical background to the various processes that have been performed during this research program. Corrosion mechanisms are explained and summarized, along with the monitoring standards utilized during the experiment. Additional information is provided for the covermeter sensor and the theory behind the operation of the device.

2.1 The Corrosion Process

2.1.1 Reaction Mechanisms

The corrosion of steel in concrete is essentially an electrochemical process. Iron and plain carbon steels are thermodynamically unstable materials [30]. Under neutral conditions, such as steel imbedded in concrete, the process of rust formation within the steel requires the presence of both water and oxygen to initiate the corrosion process. This process ordinarily proceeds by forming electrochem-

ical cells with anodic and cathodic areas on the steel surface. Different types of iron oxides may be formed depending on the exposure conditions [30]:

$$Fe + H_2O + O_2 \rightarrow Fe(OH)_2/Fe_3O_4/Fe_2O_3 \tag{2.1}$$

This overall reaction may be divided into two half-cell reactions, which are running simultaneously at two adjacent locations, either very close (microscopic) or very far away (macroscopic). One of these reactions, called the anodic reaction, is the dissolution of iron, i.e. an oxidation of iron to form ferrous ions and leaving behind electrons in the metal. This is the electrode at which the chemical oxidation occurs (or positive "+" electricity leaves the electrode and enters the electrolyte). This is called the anode. Examples of anodic reactions are:

$$Zn \rightarrow Zn^{2+} + 2e^- \tag{2.2}$$

$$Al \rightarrow Al^{3+} + 3e^- \tag{2.3}$$

$$Fe^{2+} \rightarrow Fe^{3+} + e^- \tag{2.4}$$

For corrosion of steel reinforcement, the anodic process is related to the dissolution of iron, passing into the concrete pore solution as positively charged divalent ferrous ions and leaving free electrons in the metal, according to the oxidation reaction in Eq. (2.4).

The excess free electrons flow through the body of the steel reinforcement to the cathodic sites where they are consumed in a reduction reaction. In the highly

alkaline environment normally present in the concrete, it is commonly accepted that the cathodic reaction is the reduction of oxygen. The liberated electrons are consumed by oxygen in the presence of water to form hydroxyl (OH^-). In this reaction, oxygen is electrochemically reduced from O_2 (oxidation state 0) to OH^- (oxidation state -2).

The electrode at which the chemical reduction occurs (or positive "+" current enters the electrode from the electrolyte) is called the cathode. Examples of cathodic reactions are:

$$H^+ \rightarrow \frac{1}{2}H_2 - e^- \tag{2.5}$$

$$Cu^{2+} \rightarrow Cu - 2e^- \tag{2.6}$$

$$Fe^{3+} \rightarrow Fe^{2+} - e^- \tag{2.7}$$

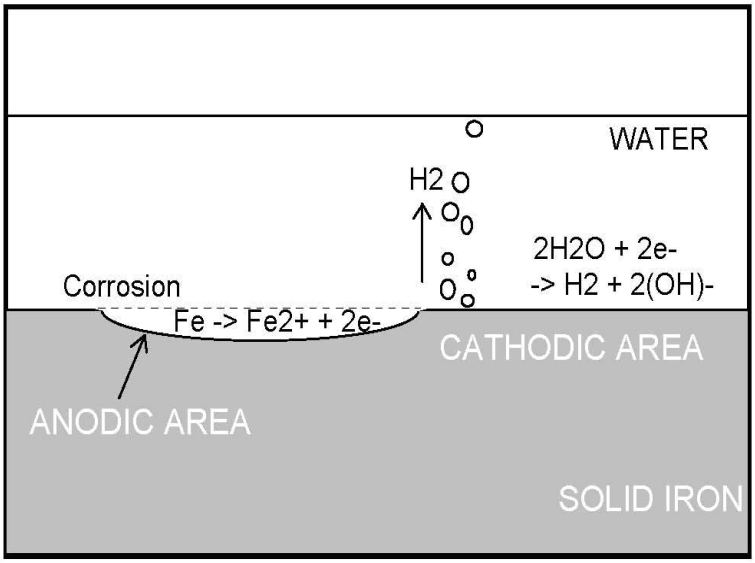

Figure 2-1: Schematic Illustration of Steel Corrosion [Source: Corr Science, Inc.]

Concrete structures freely exposed to the atmosphere usually have an adequate supply of oxygen diffusing through the concrete to support the cathodic reactions [19]. In galvanic cells, the cathode is the positive pole, whereas the anode is the negative pole. Unlike galvanic cells, when the current is impressed by a generator or an external battery, reduction occurs at the electrode connected to the negative pole of the external current source, and this electrode consequently is called the cathode. Similarly, the electrode connected to the positive pole of the generator is the anode.

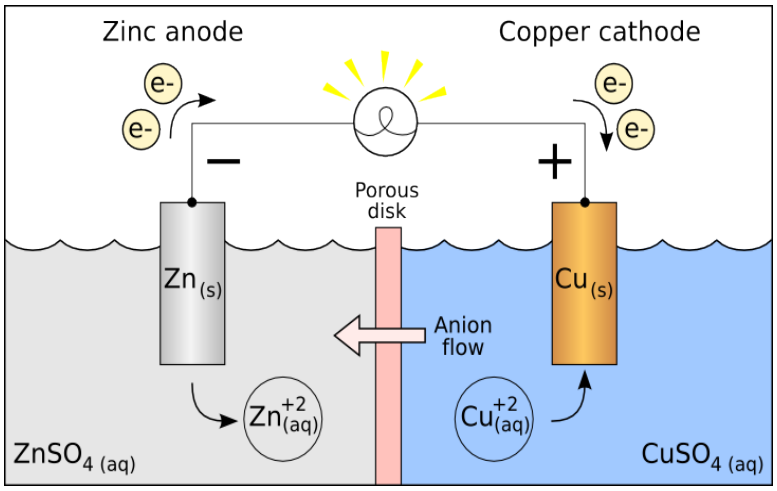

Figure 2-2: Galvanic Cell [Source: Wikipedia]

2.1.2 Thermodynamics of Corrosion

Electrochemical reactions imply the transport of electric charges and the rates of such reactions are normally given as electric current densities. The corrosion current densities of steel in concrete may vary a lot in the range of 10^{-2} to 10^{2} μA/cm^2. Very low current densities indicate passivity, and higher current densities

indicate active corrosion [30].

Using Faraday's law of electrochemical equivalence, the corrosion rate in terms of the amount of mass loss of steel may be calculated by:

$$m = \frac{ita}{nF} \tag{2.8}$$

where:

m = mass of iron per area dissolved at the anode (g/m^2)

i = electric current density (A/m^2)

t = time (s)

a = atomic mass of iron (55.8 g/mol)

n = number of electrons liberated in the anodic reaction

(2 for $Fe \rightarrow Fe^{2+} + 2e^{-}$)

F = Faraday's constant (96,487 C/mol)

Assuming the mass density of iron to be 7.87 g/cm^3, Faraday's law can be expressed as:

$$V_{corr} = 11.6 i_{corr} \tag{2.9}$$

where:

V_{corr} = corrosion rate (μm/year)

i_{core} = corrosion current density (μA/cm^2)

A corrosion current density of $1\mu A/cm^2$ corresponds to 11.6 μm steel section loss per year.

2.1.3 Factors Affecting the Corrosion Rate

According to Markeset and Myrdal [30], several factors can affect the corrosion rate of steel reinforcement in concrete. Of these factors we can itemize the following:

- **Temperature**. Temperature affects the corrosion rate directly, as in all chemical reactions. The rate of corrosion increases significantly with increasing temperature at normal ambient temperature range, but at high temperatures (40 °C), the corrosion rate decreases due to the lack of oxygen.

- **Oxygen Supply**. The rate of the oxygen supply to the reaction is directly dependent on the porosity of the concrete, the degree of moisture in these pores, the concrete cover thickness and the temperature. For atmospherically exposed concrete structures the porous system is partly open, which allows transport of oxygen (in the gaseous state) into concrete. The higher the oxygen supply, the higher is the corrosion rate of the steel rebar.

- **Relative Humidity**. The moisture content of the pore system affects the corrosion rate by requiring a minimum amount of moisture in the pores in contact with the steel, by the moisture content of concrete and by associating the electrical resistivity of the concrete with the moisture content. The

corrosion reaction can only proceed in liquid water, and water is a reactant that is consumed in the reaction. This requires a minimum of moisture in the pores in contact with the steel. If the pores dry out, the electrochemical reaction stops.

- **Chloride Concentration**. The active corrosion rate is increased by increasing the amount of chloride present and almost uniform corrosion may be the result, leading to an overall increase in the corrosion rate. However, several researchers have noted that chemically bound chloride does not contribute to corrosion. It is necessary to have a certain degree of dissolved chloride ions in the pore water to affect the corrosion rate [30].

- **Alkalinity**. The pH value of the concrete cover may affect the corrosion rate in three ways: (a) with decreasing pH, the corrosion cell potential increases, (b) with decreasing pH, the dissolution of chemically bound chlorides increases and, (c) an increase in the concentration ratio [Cl]/[OH] may increase the corrosion rate.

- **Resistivity**. Research indicates that the single most important factor affecting the corrosion rate of depassivated reinforcement is the resistivity of the concrete. The resistivity of concrete affects the rate of electric current driven by the potential differences between the cathodic and anodic areas [18] [2]. This current is equal to the rate of corrosion. Low resistivity favors the migration of ions, therefore increasing the corrosion rate.

- **Galvanic Interactions**. A galvanic macrocell is a corrosion cell where an active rebar, acting as the anode, is separated from a passive rebar, serving as the cathode. This macrocell interaction increases as the difference in the electrochemical potentials between the anodic and cathodic areas increases.

- **Rust layer formation**. Some researchers have noted that after the depassivation of steel, the continuous formation of rust on the surface of steel reinforcement influences the rate of corrosion of the steel rebar. For metals in general, the rate is highest at the beginning and later becoming reduced due to the accumulation of less protective corrosion products on the metal surface [30].

2.1.4 Experimental Investigations on Accelerated Corrosion

Some researchers have performed extensive studies on different types of accelerated corrosion mechanisms. Since the corrosion process itself may take years to fully affect the performance of reinforced concrete structures, it is necessary to perform accelerated experiments to study these effects. The following paragraphs summarize different approaches taken by researchers to study the corrosion process.

Arya and Vassie (1995) [2] conducted experiments measuring the electrical resistivity of concrete by dosing the concrete mix with 3% Cl to initiate corrosion. By measuring the current density between the cathode and the anode, they con-

cluded that corrosion current increases with increasing cathode/anode area ratio up to 190. Beyond this ratio the rate of increase decreases as the ratio increases.

Huang and Yang (1997) [22] impressed electrical current on reinforced concrete beams in order to accelerate corrosion. An impressed current of 5 A/mm^2 was applied to the beam specimens using a DC power supply.

Gulikers (1996) [19] induced macrocell corrosion by ponding a two-rebar layer reinforced concrete with sodium chloride solution on the top of the concrete.

Glass and Buenfeld (1997) [17] reported that total chloride content relative to the alkaline reserves of the concrete, may be able to present the threshold level of chloride in concrete.

Rodriguez *et al.* (1997) [41] stated that the reduction of corroded steel section can be estimated from the measurement of the corrosion intensity in concrete structures.

Almusallam (2001) [1] indicated that there is a close relationship between the failure characteristics of steel rebars and slabs with corroded reinforcement. A sudden failure of slabs in flexure was noted when the degree of reinforcement corrosion was more than 13%.

Lee *et al.* (2002) [27] reported that, as the corrosion percentage increases, the maximum bond strength decreases. Also, as the corrosion percentage increases, the bond rigidity decreases rapidly.

Elsener (2002) [13] indicated that most of the DC currents applied by an external counter electrode on concrete surface placed over an active/passive macrocell flows to the local anode, despite the large cathode area (anode/cathode area ratio

of 1:60).

Chung *et al.* (2004) [9] stated that 2% is the critical corrosion level affecting the bond strength between the steel reinforcement and concrete.

Huang *et al.* (2005) [20] reported that, after HCl corrosion, the flexural strength of high-strength concrete is larger than the one of normal-strength concrete, indicating that the sensitivity of HCl corrosion increases in the increased grade strength of the concrete.

2.2 Half-Cell Potential Method

2.2.1 The Half-Cell Potential and Electrode Potentials

The tendency for any chemical reaction to go, is measured by the Gibbs free-energy change ΔG. The more negative the ΔG, the greater the tendency for the reaction to go. A positive ΔG, indicates that the reaction has no tendency to go at all. The tendency to corrode is not a measurement of the reaction rate. A large negative ΔG may or may not be accompanied by a high corrosion rate, but when ΔG is positive, it can be stated with certainty that the reaction will not go at all under the particular conditions described [40]. The Gibbs free energy of a particular reaction can be described by:

$$E = \frac{-\Delta G}{nF} \tag{2.10}$$

where:

E = electrochemical potential (V)

ΔG = free energy of reaction (J/mol)

n = number of electrons transferred during the reaction

F = Faraday's constant (96,487 C/mol)

The higher the numerical (positive) voltage, the higher the driving force for that particular reaction [30].

The tendency of a metal to corrode can also be expressed in terms of the electromotive force (emf) of the corrosion cells that are an integral part of the corrosion process. Since electrical energy is expressed as the products of volts by coulombs, the relationship between ΔG and emf in volts, E, is defined by Eq. (2.10).

Since the emf of a cell is always the algebraic sum of two electrode potentials or of two HCPs, it is convenient to calculate each electrode potential separately. The emf series is an orderly arrangement of the standard potentials for all metals. The more negative values correspond to the more reactive metals. Position of the metal in the emf series is determined by the equilibrium potential of a metal in contact with its ions at a concentration level equal to 1[40]. Of two metals forming a cell, the more active metal in the series is the anode. Measured or calculated values of standard potentials at 25 °C are listed in most electrochemistry books. Some values are listed on Table 2.1.

Because of the limitations of the emf series in predicting galvanic reactions,

Electrode Reaction	**Standard Potential in volts at** $25\,^{\circ}\mathrm{C}$
$Au^{3+} + 3e^- = Au$	1.50
$Pt^{2+} + 2e^- = Pt$	1.2
$Pd^{2+} + 2e^- = Pd$	0.987
$Hg^{2+} + 2e^- = Hg$	0.854
$Ag^{+} + e^- = Ag$	0.800
$Hg_2^{2+} + 2e^- = 2Hg$	0.789
$Cu^{+} + e^- = Cu$	0.521
$Cu^{2+} + 2e^- = Cu$	0.342
$AgCl^{+} + e^- = Ag + Cl$	0.222
$2H^{+} + 2e^- = H_2$	0.000
$Pb^{2+} + 2e^- = Pb$	-0.126
$Sn^{2+} + 2e^- = Sn$	-0.136
$Mo^{3+} + 3e^- = Mo$	-0.2
$Ni^{2+} + 2e^- = Ni$	-0.250
$Co^{2+} + 2e^- = Co$	-0.277
$Tl^{+} + e^- = Tl$	-0.336
$In^{3+} + 3e^- = In$	-0.342
$Cd^{2+} + 2e^- = Cd$	-0.403
$Fe^{2+} + 2e^- = Fe$	-0.440
$Ga^{3+} + 3e^- = Ga$	-0.53
$Cr^{3+} + 3e^- = Cr$	-0.74
$Zn^{2+} + 2e^- = Zn$	-0.763
$Cr^{2+} + 2e^- = Cr$	-0.91
$Nb^{3+} + 3e^- = Hg$	-1.1
$Mn^{2+} + 2e^- = Mn$	-1.18
$Zr^{4+} + 4e^- = Zr$	-1.53
$Ti^{2+} + 2e^- = Ti$	-1.63
$Al^{3+} + 3e^- = Al$	-1.66
$Hf^{4+} + 4e^- = Hf$	-1.70
$U^{3+} + 3e^- = U$	-1.80
$Be^{2+} + 2e^- = Be$	-1.85
$Mg^{2+} + 2e^- = Mg$	-2.37
$Na^{+} + e^- = Na$	-2.71
$Ca^{2+} + 2e^- = Ca$	-2.87
$K^{+} + e^- = K$	-2.93
$Li^{+} + e^- = Li$	-3.05

Table 2.1: Electromotive Force (Emf) Series [Source: Revie and Uhlig (2008)[40]]

and also because alloys are not included in Table 2.1, the galvanic series has been developed. The galvanic series is an arrangement of metals and alloys in accordance with their actual measured potentials in a given environment [40]. The potentials that determine the position of a metal in the galvanic series may include steady-state and reversible values; this is why alloys and passive metals are included. The galvanic series for metals is included in Fig. 2-3.

The damage incurred by coupling two metals depends not only on how far apart they are in the galvanic series, but also on their relative areas and the extent to which they are polarized. The potential difference between the electrodes and the conductivity of a corrosive environment determines how much current can flow between them [40].

2.2.2 Methodology

The method of HCP measurements normally involves measuring the potential of an embedded reinforcing rebar relative to the know potential of another electrode (usually referred to as the reference electrode) placed on the surface of the concrete. The half-cell is usually copper/copper-sulfate or silver/silver-chloride. The concrete functions as an electrolyte and the risk of corrosion in the reinforcement in the region of the test location may be related empirically to the measured potential differential [25]. ASTM C876[4] is the most widely followed standard for the measurements of HCP in concrete structures.

A HCP measurement system mainly consists of the following:

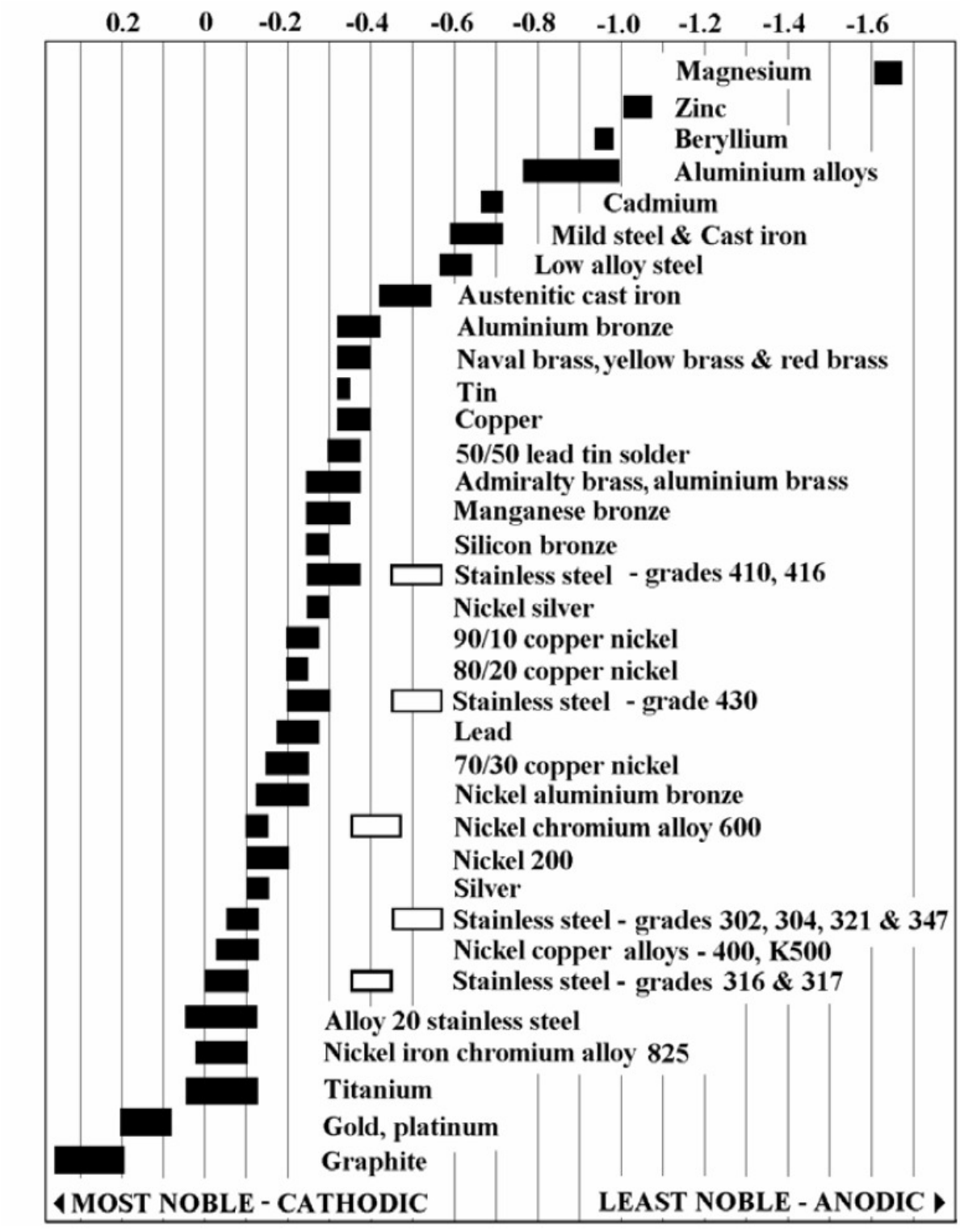

Figure 2-3: Galvanic Series [Source: Corr Science, Inc.]

- **Half-cell**. The cell consists of i) a rigid tube or container composed of dielectric material that is non-reactive with copper or copper sulphate, ii) a plastic plug that remains wet by capillary action, and iii) a copper rod that is immersed within the tube in a saturated solution of copper sulphate. The solution is prepared using reagent grade copper sulphate dissolved to saturation in a distilled or deionized water [25].

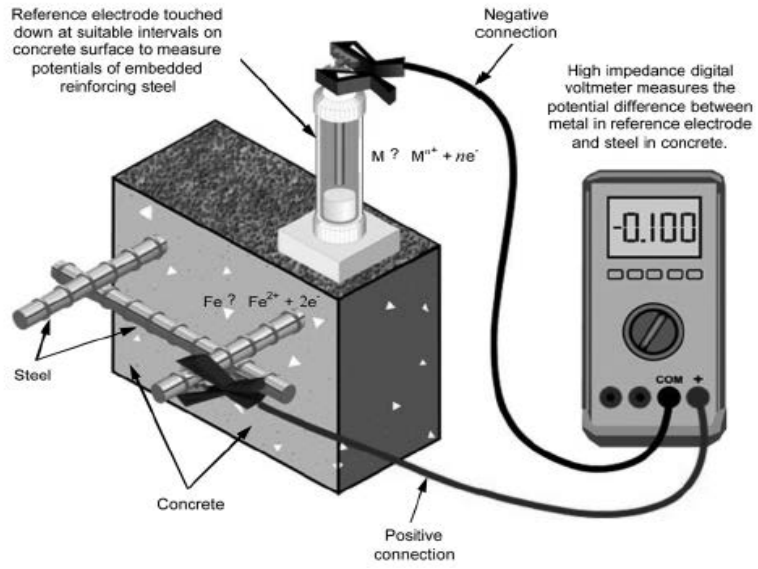

Figure 2-4: Half-cell [Source: ASTM International]

- **Electrical junction device**. An electrical junction device is used to provide a low electrical resistance liquid bridge between the surface of the concrete and the half-cell. It consists of a sponge or several sponges pre-wetted with a low electrical resistance contact solution.

- **Electrical contact solution**. In order to standardize the potential drop through the concrete portion of the circuit, an electrical contact solution is used to wet the electrical junction device. ASTM [4] recommends a mixture

of 95 mL of wetting agent (commercially available wetting agent) or a liquid household detergent thoroughly mixed with 5 gal (19 L) of potable water.

- **Voltmeter**. The voltmeter should be battery operated and have an accuracy of ± 3% end of scale accuracy at the voltage ranges in use. The input impedance should not be less than 10 MΩ when operating at a full scale of 100 mV. The divisions in the scale should be such that a potential of 0.02 V or less can be read without interpretation.

- **Electrical lead wires**. The electrical lead wire should be such that its electrical resistance for the length used does not disturb the electrical circuit by more than 0.0001 V. This can be accomplished by using no more than a total of 150 m of at least AWG No. 24 wire. The wire should be properly coated with direct burial type of insulation.

HCP measurements are made in either a grid or random pattern. The spacing between two HCP measurements is generally chosen such that adjacent readings are less than 150 mV with the minimum spacing so that there is at least 100 mV between the readings. A direct electrical connection is made to the reinforcing steel with a compression clamp or by brazing or welding a protruding rod. To get low electrical resistance connection, the rod should be scraped or brushed before connecting it to the reinforcing rebar. Sometimes it may be necessary to drill into the concrete to expose a reinforcing rebar. The rebar is connected to the positive terminal of the voltmeter. One end of the lead wire is connected to the half-cell and the other end is connected to the negative terminal of the voltmeter. Under

some circumstances the concrete surface has to be pre-wetted with a wetting agent (e.g., water). This is necessary and recommended if the readings fluctuates with time when it is placed in contact with the concrete. The electrical HCPs are recorded to the nearest 0.01 V.

HCPs reflect the chemistry of the electrode environment. Interpretation is complicated when concrete is saturated with water, where the concrete is carbonated at the depth of the reinforcing steel, where the steel is coated and under many other conditions. Increasing concentrations of chloride ions can reduce the ferrous ion concentration at a steel anode and consequently, lowering (making more negative) the HCP.

The HCP method has the advantage of being simple. This allows an almost non-destructive survey to be made to produce isopotential contour maps of the surface of the concrete member. Zones of varying degrees of corrosion risk may be identified from these maps [25]. The limitations of the HCP method is that it cannot indicate the actual corrosion rate. It may require to drill a small hole in the concrete to enable electrical contact with the reinforcement inside the member under examination. Meanwhile, surface preparation may also be required. It is important to recognize that the use and interpretation of HCP results obtained from the test require an experienced operator who will be aware of other limitations such as the effect of protective or decorative coatings applied to the concrete [25].

2.2.3 Experiments Using Half-Cell Potential Measurements

The HCP method is the most widely used method to assess the probability of corrosion in steel reinforcement embedded within concrete. Researchers have used this technique to assess the level of corrosion of reinforced concrete structures. The following paragraphs describe the use of this method reported in the literature.

Ohtsu and Yamamoto (1997) [33] provided a compensation procedure for HCP measurements based on boundary element method analysis.

Leelakerkiet *et al.* (2004)[28] utilized the HCP method to correlate it against a three-dimensional and inverse boundary element method analysis of potential distributions, current flows of rebar and identify the different corrosion states.

Assouli *et al.* (2008)[3] recommended that, in addition to taking into account environmental factors while assessing the results of the survey, direct visual and chemical inspections by removing a small section of concrete cover, as well as the corrosion rate measurements of reinforced concrete are necessary to confirm or to cancel the probabilities of corrosion predicted by ASTM C876.

Pradhan and Bhattacharjee (2009) [38] analyzed the suitability of HCP as a determining parameter for corrosion initiation in chloride contaminated concrete. The HCP method was found to be suitable and stable determining the parameters indicating rebar corrosion.

Poursaee and Hansson (2009) [36] suggested that, for interpreting the data, environmental factors should be taken into account and, whenever possible, repeated condition analyses should be conducted at the same time of the year. It

is also recommended that a large area of the structure be wet and measurements begin no sooner than 15 min after the area of the first measurement is wet.

Pour-Ghaz *et al.* (2009) [35] provided a quantitative assessment of the HCP method surveys based on numerical simulation and with recommendations for practicing engineers and field technicians. It was found that potential readings should be interpreted in accordance with the resistivity of the system; otherwise, the results can be misleading.

Pradhan and Bhattacharjee (2011) [39] used the HCP values obtained from earlier experiments to correlate against the chloride concentration within specific area of a structure. They observed that, HCP values obtained from internal chloride exposure lie mostly either in passive zone or in active zone whereas in some cases the potential values lie in pitting zone at higher dosage of internal chloride.

Hussain (2011) [24] determined that the HCP values for reinforced concrete specimens submerged underwater are not the true representative of corrosion rate and need to be re-calibrated. For this purpose, detailed bench mark testing was conducted in this paper involving a variety of material and environmental variables.

2.3 Electromagnetic Testing

2.3.1 Electromagnetic Theory of Covermeter Sensor

Electromagnetic testing as a form of nondestructive testing, consists in the process of inducing electro current or magnetic fields or both inside a test object and observing the electromagnetic response [15]. The term electromagnetic testing covers an expanding number of electromagnetic and magnetic test methods. For the purposes of our discussion we will concentrate specifically on eddy currents as the main working principle of the covermeter sensor used in this research program.

Eddy current sensors are based on electromagnetic induction and can be applied to electrically conductive materials for detection of cracks, porosity, and inclusions, and to measure the thickness of nonconductive coatings on a conductive metal [32]. In a standard eddy current sensor a circular coil carrying current is placed in proximity to the test specimen. The current flow creates a magnetic field that opposes the primary field created by the alternating current flow in the coil.

The presence of a surface or near surface discontinuity in the conductor will alter the magnetic field and can be sensed as a change in the flow of the current in a secondary coil in the probe or change of inductance in the probe. The output signal from the detection circuit is fed to an output device, typically a meter, oscilloscope or chart recorder [32]. Flaw size is indicated in extent of the response change as the probe is scanned along the test object. Eddy current techniques do not require direct contact with the test piece, and paint or coatings do not have to be removed

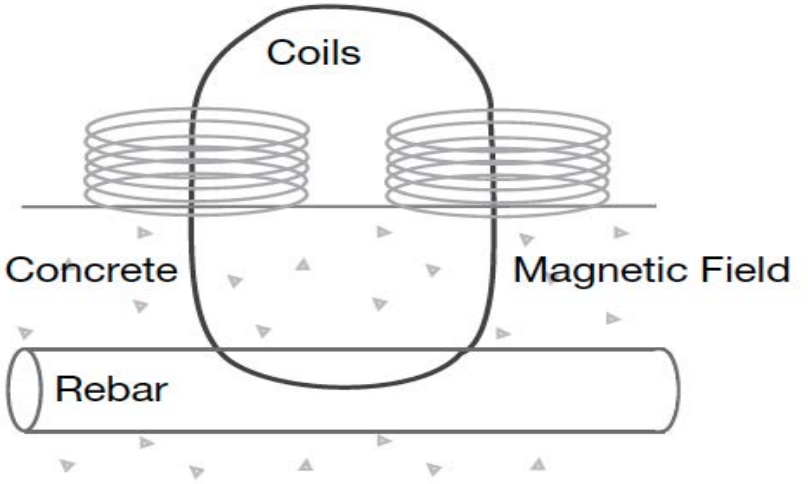

Figure 2-5: Eddy Current Principle [Source: Proceq®]

prior to its application [32]. Eddy current sensors can detect very small cracks in or near the surface of the material, the surfaces need minimal preparation, and physically complex geometries can be investigated. Only conductive materials can be tested, the surface of the material must be accessible, the finish of the materials may cause bad readings, depending on its composition and the depth of penetration into the material is limited [15].

2.3.2 Experimental Investigations of Magnetic Testing of Steel under Concrete

Many researchers have invested tremendous efforts into the non-destructive inspection of concrete. These techniques use a variety of different sensing methods including ultrasound, acoustic emission, X-ray, microwave and radar, light and eddy current induction [16]. The most reliable method of assessing the condition

of the steel is removal of the concrete cover for direct visual inspection but this practice is destructive in nature and ultimately undesirable. An ideal inspection procedure is a system that images the steel through the concrete. The following paragraphs describe in more detail the approach taken by different researchers as it relates to the inspection steel under concrete, particularly related to magnetic inspection methods.

Gaydecki *et al.* (2000) [16] developed a portable inductive scanning system for imaging steel-reinforcing rebars embedded within concrete. The sensing element detects the magnetic field generated by the steel due to eddy currents induced on their surfaces by an excitation coil. The sensor is mounted within within a computer that controls an x-y scanner used to collect the data.

Makar and Desnoyers (2001) [29] presented the results of a non-destructive evaluation of concrete using magnetic flux leakage measurements as a method to detect broken pre-stressing steel. The measurements produced detectable signals only when the cable was completely severed.

Miller *et al.* (2003) [31] described a new inductive sensor that exploits the principle of frequency shift and phase sensitive detection to identify and image corrosion on the surface of steel reinforcing rebars intended for embedment within concrete. A search coil radiating a time-varying magnetic field experiences impedance changes when conductive and/or permeable targets are brought within its vicinity. The change in its inductance is the condition that is the primary effect with corrosion product.

Prabakar *et al.* (2007) [37] performed a cover thickness survey and concrete

surface profile on a earth retaining reinforced concrete structure. A commercially available rebar locator was utilized for the survey. The sensor was designed in combination with the pulse induction method. The interaction between the sensor and the steel is primarily due to physical properties of steel, i.e. its magnetic permeability and electrical conductivity.

Yashiro *et al.* (2008) [44] developed a new magnetic corrosion probe for the non-destructive evaluation of concrete against corrosion of reinforcing rebar. Two types of magnetic corrosion probes were examined. One was a thin iron wire and the other was iron-plated copper bar. The probes were expected to change their residual magnetization as their iron faces are lost with progress of corrosion.

2.4 Summary

Many researchers have utilized accelerated corrosion experiments to assess the performance and condition of reinforced concrete structures. The ability to extrapolate these results and to compare them against field conditions indicates the reliability of accelerated corrosion as a methodology to simulate the corrosion process under laboratory environment. However, this methodology is hindered by the lack of quantitative analysis on the degree of corrosion in the reinforcement. Each method has its advantages and limitations in assessing the degree of corrosion in the reinforcement. Some researchers presented similar or dissimilar results with different types of accelerated corrosion approaches. This indicates that further research is needed in order to develop a better approach in assessing the degree

of corrosion in the reinforcement.

As outlined in the literature review on previous research, HCP has proved to be a reliable method for assessing the probability of corrosion within the steel reinforcement imbedded in concrete. Care must be taken while obtaining the experimental data, as factors like relative humidity, temperature, concrete surface condition, degree of moisture in concrete and others may affect the final HCP values as provided by the voltmeter. Should all these parameters be taken into consideration, the ease of the HCP method allows anyone with little to no experience in gathering data to obtain reliable information.

According to the literature review, the non-destructive evaluation of civil infrastructure can be performed using magnetic and eddy current based inspected methods. The main role of these methods is to provide an assessment of the health of the structure, without having to require to cumbersome, expensive and destructive methodologies. Commercial sensors based on eddy current methods have been developed pursuant to this goal and have already seen useful applications in the field.

Figure 2-6: Field Inspection Using Covermeter [Source: Proceq®]

Figure 2-7: Commercial Covermeter [Source: Proceq®]

Chapter 3

Accelerated Corrosion Experimental Program

The experimental program utilized in this research project is described below. This chapter presents all three different experiments as part of the research to study the corrosion process. This program is presented in detail in Fig. 3-1 and in subsequent sections of this chapter.

3.1 Corrosion Reactor Design

As part of the first set of experimental data, we attempted to determine the amount of time and corrosion current level that would be needed to achieve a certain level of corrosion. Based on the findings of Fang *et al.* (2004) [14] and Chung *et al.* (2004) [9], we determined that 2% mass loss would be an optimal corrosion level for our experiment. These studies showed, after a 2% corrosion

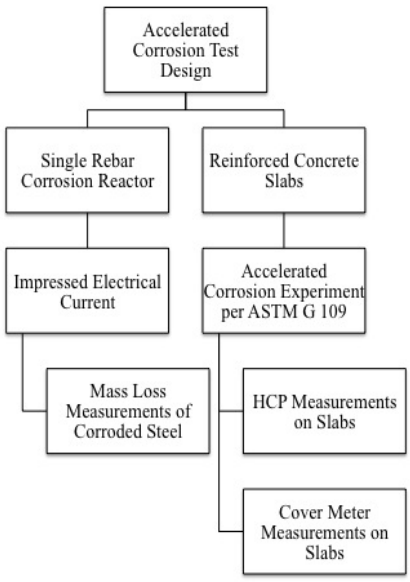

Figure 3-1: Experimental Program Flowchart

level, the rib of the reinforced rebar no longer exists. When the corrosion level is increased even more, the resisting force rapidly decreased.

In order to reflect the actual level of NaCl concentration that would be encountered on the second experimental set, we utilized the same NaCl concentration level of 15%. The steel reinforcement was of a No. 4 rebar diameter. Since we wanted to achieve mass loss on the steel reinforcement to reflect the same behavior observed by long term corrosion of reinforcement, we utilized an electrochemical corrosion cell in an aqueous environment. This environment along with the concentration of NaCl would facilitate the electron transfer mechanism that would help to achieve the desired mass loss on the steel reinforcement, based on electrochemical corrosion theory. To achieve this, we selected our steel reinforcement as our anode and selected a section of copper pipe as our cathode (see Fig. 3-3).

For our current inducing device we selected a Digi-Ivy® DY 2300 Series Poten-

tiostat with a maximum current range of ±100 mA. This potentiostat would allow us to regulate the amount of current that is impressed on the corrosion cell at any give point in time and will also record the amount of current being impressed on the reactor. To complete the corrosion cell we utilized an Ag/AgCl reference electrode with a known potential. An image of the potentiostat is included in Fig. 3-2.

Figure 3-2: Digi-Ivy DY 2300 Series Potentiostat [Source: Digi-Ivy®]

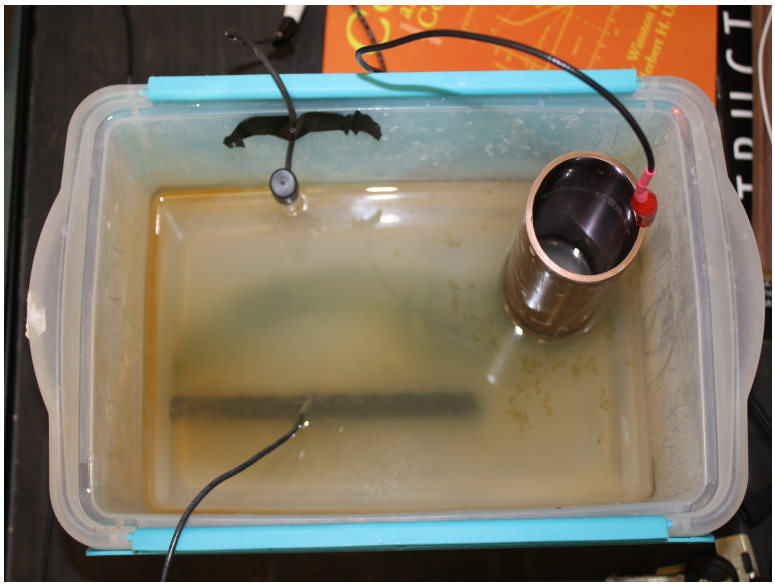

Figure 3-3: Corrosion Reactor

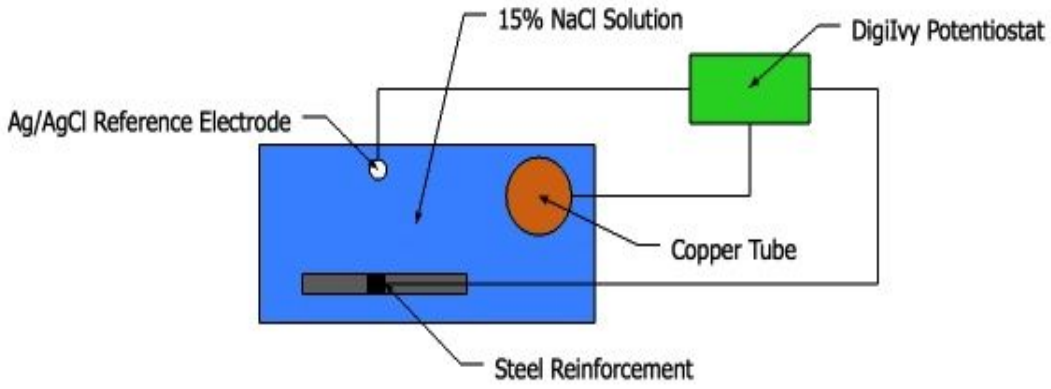

Figure 3-4: Corrosion Reactor Diagram

Once the corrosion reactor was assembled the external current was impressed on the steel reinforcement, the test was run for predetermined amounts of time in order to to be able to quantify the amount of mass loss for each experimental run. These results will be presented and discussed in Chapter 4.

3.2 Reinforced Concrete Slab Design

3.2.1 Concrete Mix Design

For this experimental setup, the Portland Cement Association (PCA) volume method was used to calculate the concrete mix design specifications. The amount of cement, sand, gravel and water reducer additive was 564 lb, 1600 lb, 1600 lb and 16.9 oz, respectively. This mix design proportion was used for all four slabs. The amount of mixing water was adjusted in order to compensate loss of water

absorbed by surface-dry sand and surface-dry gravel. The w/c ratio utilized for the mix design was 0.52. We utilized a relatively high w/c ratio to allow a more permeable concrete, allowing an easy path for the chloride to migrate through the concrete into the steel. A summary of the mix design used for the slabs is present in Table 3.1.

Component (lb)	**0.52 (w/c)**
Cement	564
Sand	1600
Gravel	1600
Water	292.03
Water Reducer	1.06
Total	**4057.09**

Table 3.1: Mix Design for Slabs

3.2.2 Reinforced Concrete Slab Preparation

Four reinforced concrete slabs were cast. All four slabs were cast with two rows of No. 4 rebar reinforcement. The bottom row of rebars were cast at a depth of 1-in from the bottom face of the slab, while the top row of rebars were cast at varying different concrete thickness. All distances are measured to the center of the rebar.

All four slabs were cast with the dimensions of 4-ft by 6-ft by 7-in. The reinforcements for slabs 1 and 2 were laid in the y-direction and the reinforcements for slabs 3 and 4 were laid in the x-direction. The steel reinforcement was prepared pursuant to the recommendations of ASTM G109 - 07 “Standard Test Method for Determining Effects of Chemical Admixtures on Corrosion of Embedded Steel

Reinforcement in Concrete Exposed to Chloride Environments" (ASTM G109) [6]. Detailed information related to the design and arrangement of the slabs and the preparation of the reinforcement is presented in the next subsection and in Figs. 3-5 to 3-10

3.2.3 Steel Reinforcement Preparation

All steel reinforcement used in the experimental setup were No. 4 rebars. All of the rebars were cleaned and any evidence of rust accumulation on the surface was removed by a bench-top wire brush. After the rust was removed, a stainless steel screw with two nuts were drilled and tapped to the end of each rebar. Each rebar end was covered with electroplaters tape so that the exposed portion of the rebar was covered. A 3.5-in section of neoprene tubing over the electroplaters tape was placed at the end of each rebar. The length of tubing protruding from the rebar ends was covered with a two-part epoxy. A small section of electrical wire was attached to the end of each rebar for measurement of the voltage in each rebar.

3.3 Experimental Setup for Concrete Covermeter

Change of steel reinforcement cross-section as a result of the mass loss due to the corrosion process is crucial in the study of concrete cover measurements. Therefore, a covermeter sensor was used for concrete cover measurements. In the fol-

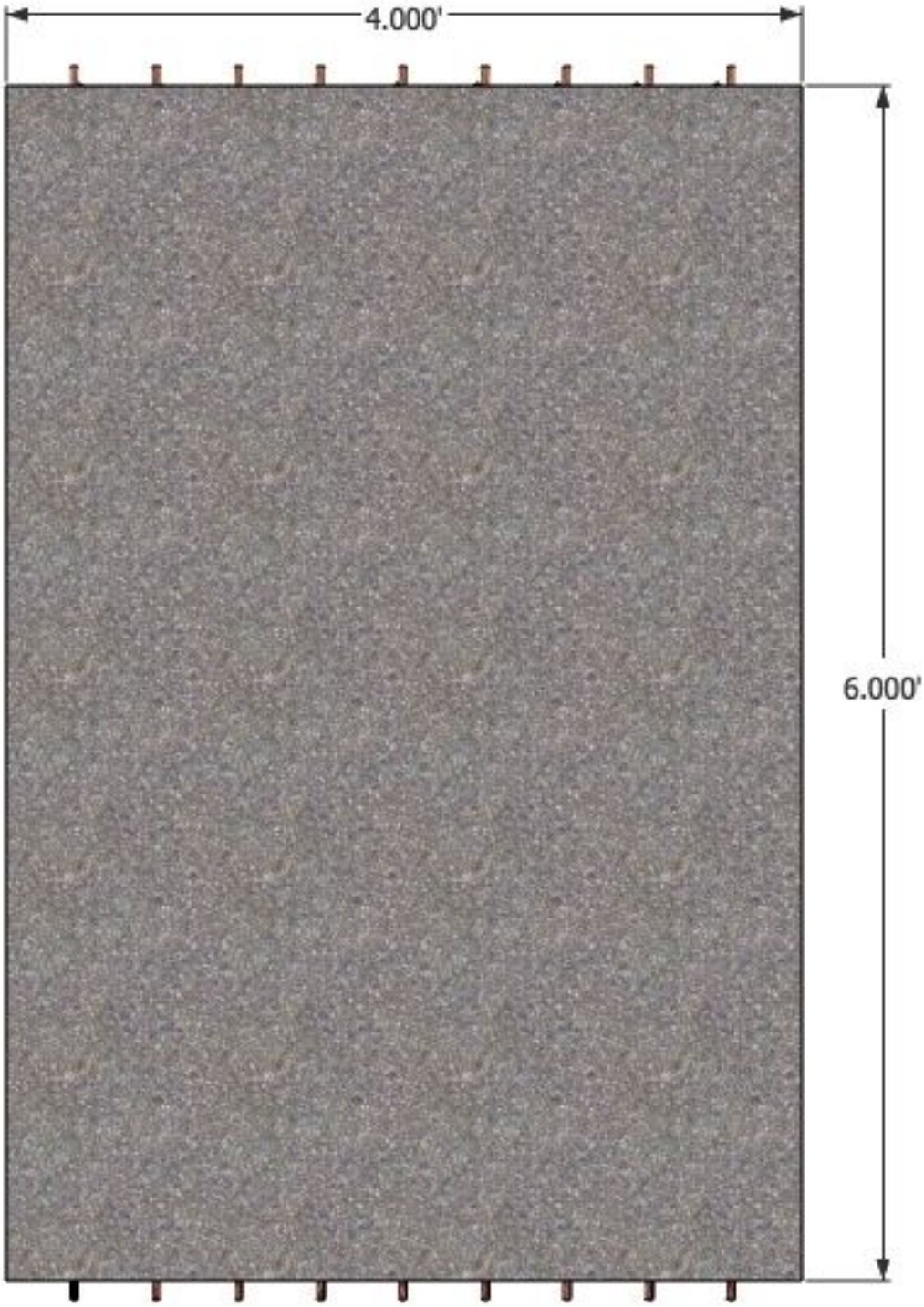

Figure 3-5: Slabs 1 and 2 - Plan View

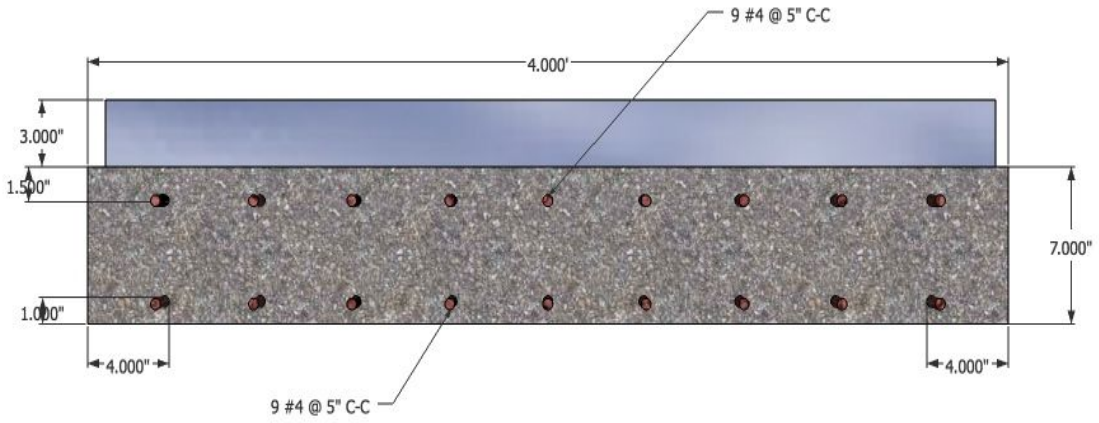

Figure 3-6: Slab 1 - Section View

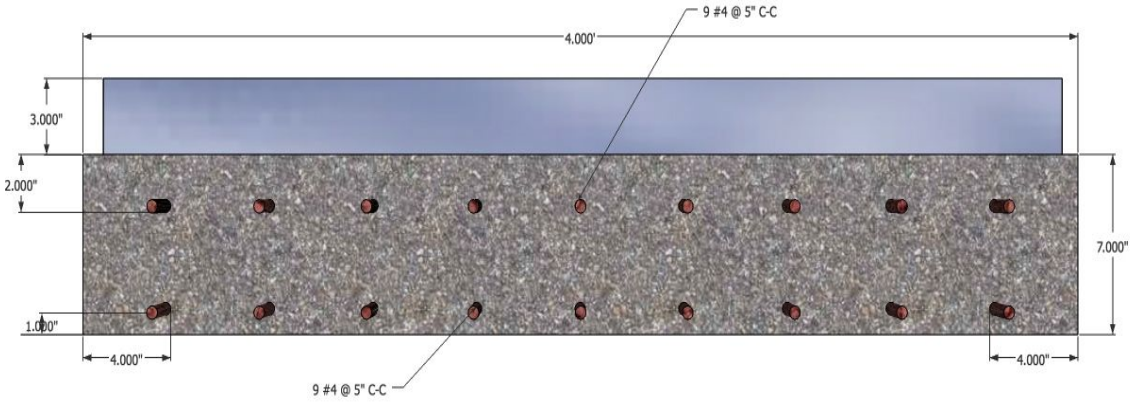

Figure 3-7: Slab 2 - Section View

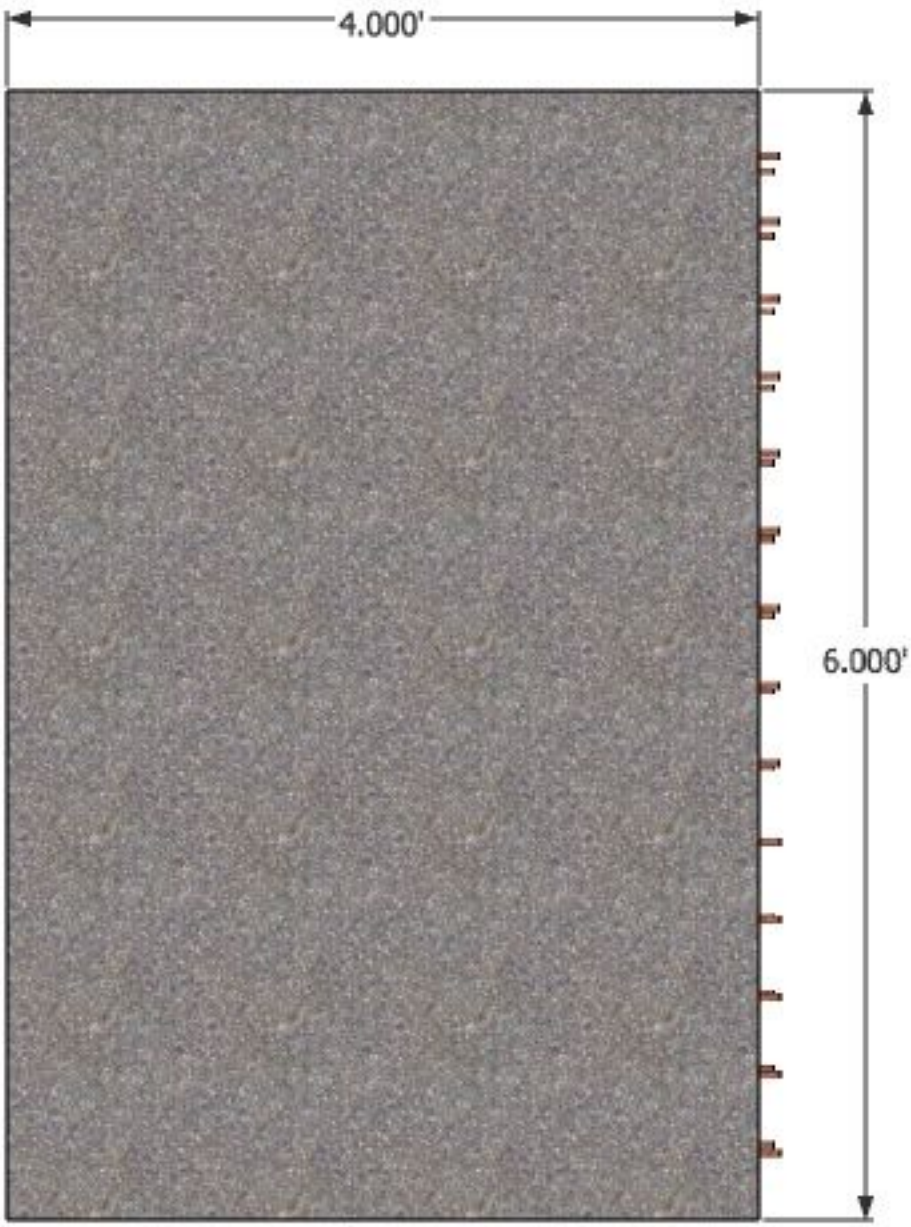

Figure 3-8: Slabs 3 and 4 - Plan View

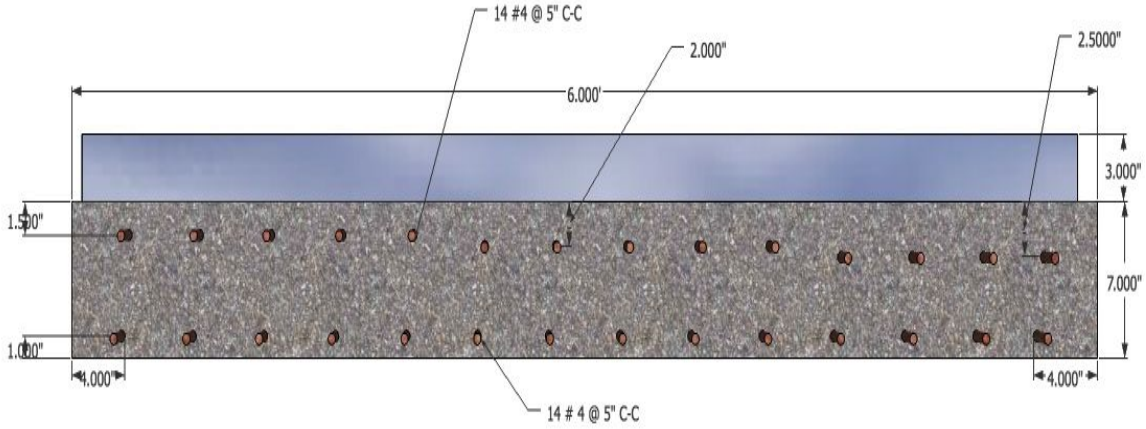

Figure 3-9: Slab 3 - Section View

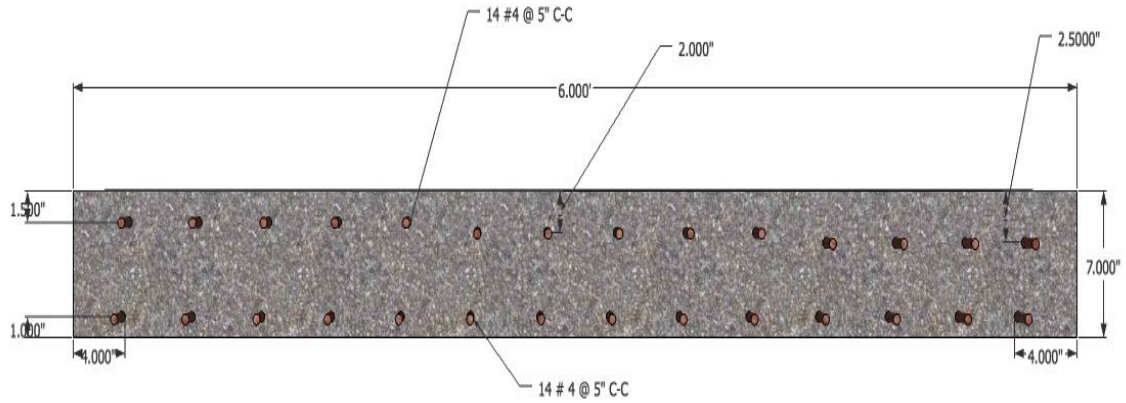

Figure 3-10: Slab 4 - Section View

lowing subsection, the calibration and validation of the coveremeter sensor are presented.

3.3.1 Covermeter Sensor Calibration Method and Result

1. Install the ProfoLink® software onto the computer used for the sensor.

2. Plug the Profoscope® sensor into a USB port of the computer.

3. Start the ProfoLink® software.

4. Download all the values from the Profoscope® sensor.

5. Remove the sensor from the USB port of the computer.

6. Use the ProfoLink® software to review, export and save the recorded data.

Two calibration tests were performed to determine the accuracy of the Profoscope® sensor. The calibration test was performed with a calibration that accompanied the covermeter sensor; the kit is composed of two pieces of stainless steel No. 5 rebar imbedded in a nonconductive material to allow passage of the electromagnetic waves. Two different concrete cover thicknesses were measured with the sensor and were compared against the know value of the cover thickness. The measurements from the sensor had an accuracy of $\pm$ 0.10-in.

3.4 Summary

The experimental program has been set up with the goal of establishing a clear line between the research problem and the conclusions that are drawn based on the results of the experiments. For this, we designed the corrosion reactor with the goal of being able to assume under which conditions we would obtain a reasonable level of corrosion in order to operate the covermeter sensor. The probability of corrosion is evaluated using the HCP method. Chapter 4 provides the results and evaluation part of the research program in order to determine the reliability of the covermeter sensor under a corrosion environment. This is the research problem that we are attempting to solve.

Chapter 4

Data Analysis and Discussion

In this chapter, experimental work on the corrosion reactor, the HCP method and covermeter measurements is reported. The research program was divided into three experimental sets. First, the data acquired from the corrosion reactor was analyzed and the results are presented for future use in other research programs with similar corrosion environments. Second, the HCP data was studied for determining the probability of corrosion on all four slabs. Lastly, the HCP data was correlated with the covermeter data and analyzed, using statistical analysis to determine the reliability of the covermeter sensor under a corrosion environment.

Experiment No.	**Description**
1	Corrosion Reactor
2	HCP Measurements
3	Covermeter Survey

Table 4.1: Summary of Experimental Program

4.1 First Experimental Set - Corrosion Reactor

The preliminary phase of the accelerated corrosion experiment was primarily characterized by the attempt to increase the external current being applied to the experiment to a rate closer to the maximum output of the potentiostat (i=±100 mA). During the preliminary phase, the experiment utilized a platinum counter electrode. However, while utilizing this counter electrode the electrical current output ranged between 0.296 to 0.949 mA, well below the maximum output of the equipment. After further studying the corrosion cell arranged for this experiment, the platinum counter electrode was replaced with a copper counter electrode. The electrical current output with the new copper electrode increased to an average of i=94.9 mA, well near the maximum output of the potentiostat and an increase of 10,000% of the initial current output utilizing the copper counter electrode.

During phase 1 of the accelerated corrosion experiment we attempted to extrapolate the time necessary to corrode a steel rebar in the corrosion reactor. The time required to achieve 15% corrosion will be calculated based on the data points from the experiment. While the preliminary corrosion experiment consisted of submerging only a section of the rebar, during phase 1 of the experiment we submerged the steel rebar completely in the NaCl solution. This yielded more precise results by neglecting the effect of water evaporation that needed to be taken into account during the preliminary phase of the experiment.

4.1.1 Results

The steel rebar was subjected to an average electrical current of i = 94.9 mA for a period of 8 hours (28,800 s), immersed in a 15% NaCl solution. The mass loss was measured at intervals of 4 hours. A qualitative assessment of the corrosion rate of the steel rebar at t = 0 s and t = 14,400 s is presented in Figs. 4-1 and 4-2. It is clear from the images how the steel rebar in Fig. 4-2 has been subjected to a significant level of accelerated corrosion, under a period of 4 hours. This level is better appreciated once we observe the state of the steel rebar before the experiment, in Fig. 4-1.

Figure 4-1: Rebar at t = 0 s

Approximately 14.9699% of mass loss was achieved. This percent of mass loss is enough to achieve a reasonable trendline estimate as outlined below. The average electrical current applied throughout the experiment was i=94.7 mA.The amount of data obtained will yield a reasonable trendline estimate to be used in further

Figure 4-2: Rebar at t = 14,400 s

experiments. The trendline estimates from this experiment are presented in Fig. 4-3. It is clear that a directly proportional relationship is established between mass loss and time. This relationship is possible due to the stable corrosion rate of the experiment, more particularly described in Table 4.3.

Using a linear fitting for the graph in Fig. 4-3 we have:

$$\Delta m(\%) = 0.31t - 0.31 \tag{4.1}$$

$$\text{for } \Delta m(\%) = 15$$

$$t = 5.72 \text{ days}$$

Using a quadratic fitting for the graph in Fig. 4-3 we have:

$$\Delta m(\%) = 0.0005t^2 + 0.29t - 0.11 \tag{4.2}$$

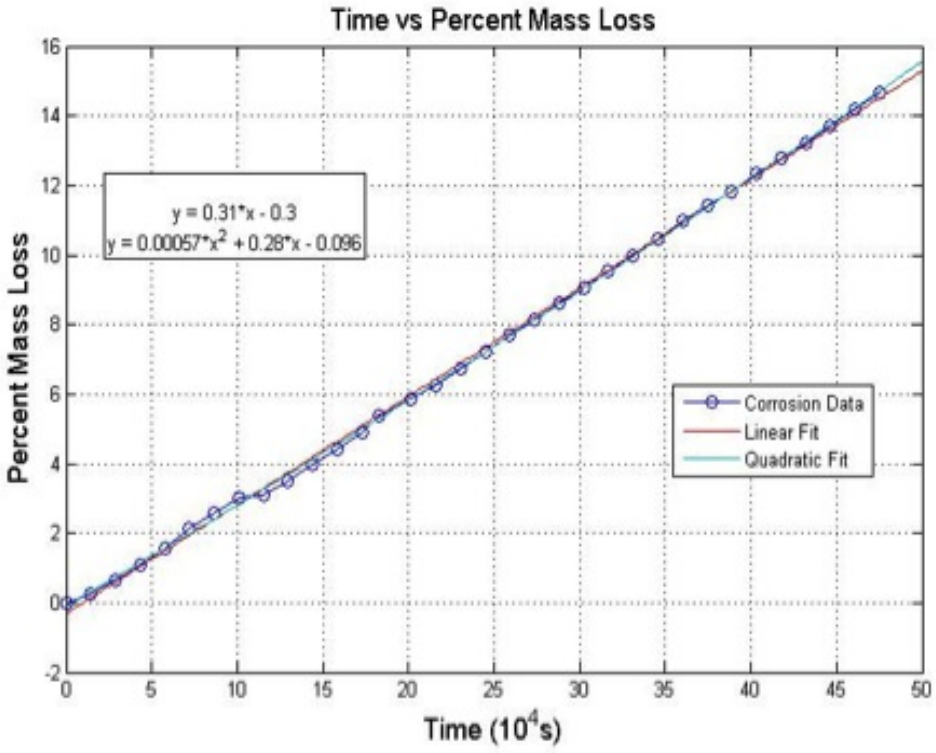

Figure 4-3: Percent Mass Loss of a Steel Rebar

for $\Delta m(\%) = 15$

$$t = 5.57 \text{ days}$$

From the trendline estimates and the results presented on Table 4.1 below, we will be using Eq. (4.1), since the results obtained from this equation yield the least percent difference from the actual corrosion results.

	Corrosion Time for 14.9699% Mass Loss (s)	**% Difference from Actual**
Actual	489600	-
Linear Fit	492900	0.674019608
Quadratic Fit	480234	1.912990196

Table 4.2: Comparison of Corrosion Time Estimates

The covermeter sensor that will be utilized under experiment No. 3 measures the concrete cover depth of the steel reinforcement. Once the corrosion process initiates on the steel reinforcement, the diameter of the rebar begins to decrease due to the mass transfer effect. These changes in diameter will be reflected by an increase in the concrete cover depth of the steel reinforcement. Table 4.2 illustrates the measurement of the corrosion rate throughout the experiment. The average corrosion rate for the entire experiment was 45.31 μg/s, including the outliers at t = 14,400 s and t = 115,200 s.

4.1.2 Discussion

In Fig. 4-3, the corrosion rate from the steel rebar specimen remains constant throughout the entire experiment. The corrosion rate throughout the experiment

Time (s)	**Corrosion Rate (μg/s)**
0	0
14400	27.77777778
28800	41.66666667
43200	45.13888889
57600	48.61111111
72000	59.02777778
86400	48.61111111
100800	45.13888889
115200	6.944444444
129600	41.66666667
144000	48.61111111
158400	45.13888889
172800	45.13888889
187200	48.61111111
201600	48.61111111
216000	41.66666667
230400	45.13888889
244800	48.61111111
259200	45.13888889
273600	45.13888889
288000	45.13888889
302400	41.66666667
316800	48.61111111
331200	41.66666667
345600	45.13888889
360000	48.61111111
374400	45.13888889
388800	34.72222222
403200	48.61111111
417600	41.66666667
432000	41.66666667
446400	45.13888889
460800	41.66666667
475200	45.13888889
489600	43.66582492

Table 4.3: Corrosion Rate Data from a Rebar - Experiment No. 1

was measured by taking the mass at the beginning and the end of the test runs and by dividing the mass the amount of time of the experiment. The corrosion rate is primarily affected by the mass loss between predetermined time intervals during the experiment. This mass loss is due to the electron transfer mechanism between the cathode and the anode. The electron transfer is directly proportional to the electrical current generated by the potentiostat.

Corrosion rate variations are not discernible in the experiment because the electrical current applied to the experiment was kept at a constant rate (i.e. i = 94.9 mA). This electrical current was also close to the maximum current output the potentiostat was able to produce (i.e. i=$\pm$100 mA).

The procedure for measuring the actual mass loss was based on the recommendations of ASTM G1 - 03 "Standard Practice for Preparing, Cleaning, and Evaluating Corrosion Test Specimens" (ASTM G1-03)[5]. The reason for using the corrosion mass loss as a corrosion rate index is explained as follows. During the corrosion process, the corrosion product itself will become a passive film such that the corrosion rate will slow down and the corrosion open circuit will become nobler. Therefore, the instantaneous corrosion rate will not increase with respect to time. However, rebar thickness loss (mass loss) does increase with respect to time. This long-term trend of mass loss measurements allows us to make a better judgment in regards to the corrosion rate.

The maximum amount of mass loss of the steel rebar specimen was 21.15 g, corresponding to an experiment time of 489,600 s. All of the mass loss followed the same proportional pattern which leads to the stable corrosion rate measurements,

as presented in Table 4.2. These measurements obtained from the experiments are as expected since no parameters were changed or modified during the entire duration of the experiment (e.g. NaCl concentration, current output, cathode to anode ratio).

Based on the analysis of the mass loss measurements from Fig. 4-3 and Table 4.2, the following findings are obtained:

1. This electrochemical test can be used for rapid determination of steel corrosion in concrete. There are limitations to this assumption. One has to consider that concrete cover may delay the onset of corrosion compared to the exposed environment within the experiment. Accurately assessing the field conditions of the concrete may allow this method to estimate the corrosion rate and cross-sectional area loss of the embedded steel rebar.

2. In Fig. 4-3, a near perfect fit with the actual corrosion rate data was obtained from data fitting. This produces a mathematical model useful for predicting the degree of corrosion on an environment subject to accelerated corrosion based on the mass loss of steel from the corrosion process.

3. For experimental programs, one can easily replicate the results obtained by carefully adjusting the electrical current output to obtain the same numerical values. This electrical current is in turn directly proportional to the corrosion rate.

4.2 Second Experimental Set - Half-Cell Potential Mapping

Four reinforced concrete slabs with dimensions 4-ft by 6-ft by 7-in were cast on December 9, 2011. Two of these slabs were cast with the rebar in the x-direction and the other two were cast on the y-direction. Detailed description of the experimental setup was already presented in Chapter 3. In order to study the macro-cell mechanism, three of the slabs were submitted to a corrosion process in a NaCl water environment in a simulated cyclic ponding-and-drying condition. An artificial climate environmental tent was constructed around the four slabs. Two small portable heaters and one humidifier were installed inside the tent to help maintaining the desired temperature and relative humidity (RH) levels inside the tent (i.e., 90 °F and 50 ± 5% RH) per ASTM G109. The tent was made of a general purpose tarp commercially available at any general hardware store. The alternating ponding-and-drying cycles include 4 days of ponding and 3 days of drying. These alternating cycles were performed on slabs 1, 2 and 3. Slab 4 was not subjected to the ponding-and-drying cycles, as it was the control slab.

Six 4-in diameter concrete cylinders taken from the cast date of 12/9/11 were tested for the compressive strength on 1/6/12 at the 28-day mark. The results of the compressive tests are outlined in Fig. 4-5.

Further information about Fig. 4-5 can be found in Table 4.3. The noticeable increase in the slump of the mix is due to the addition of water during the casting process to improve the workability issues with the mix. The average strain value

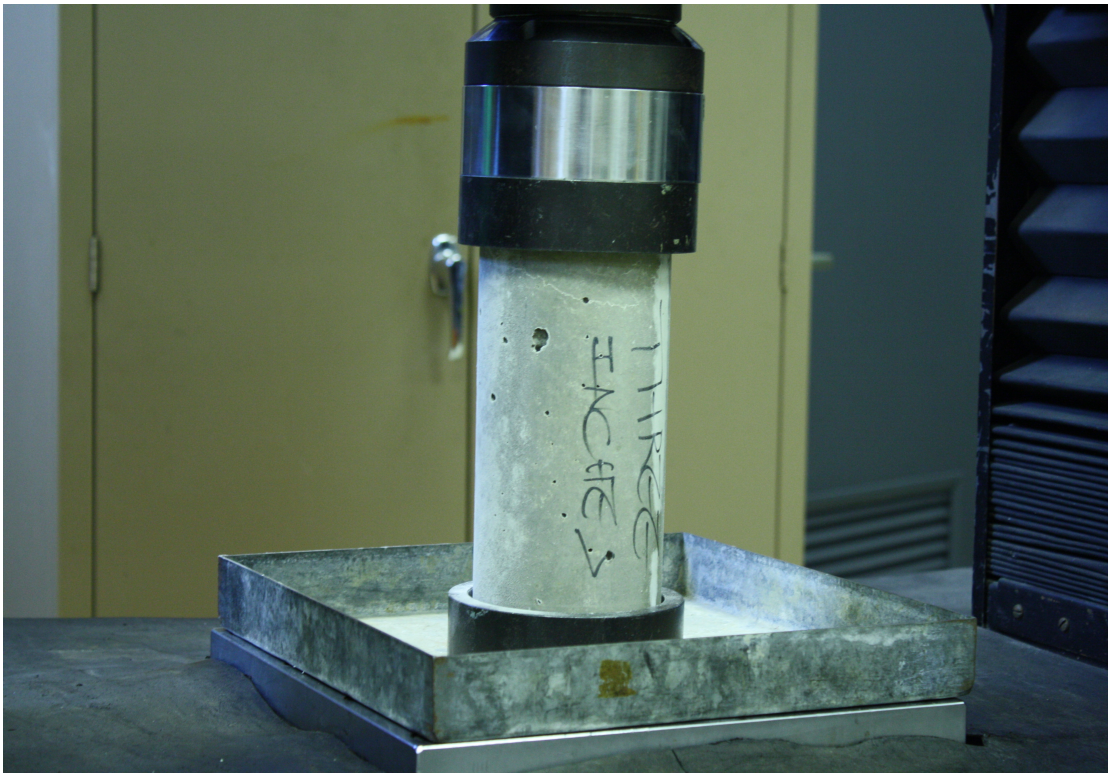

Figure 4-4: Test Cylinder

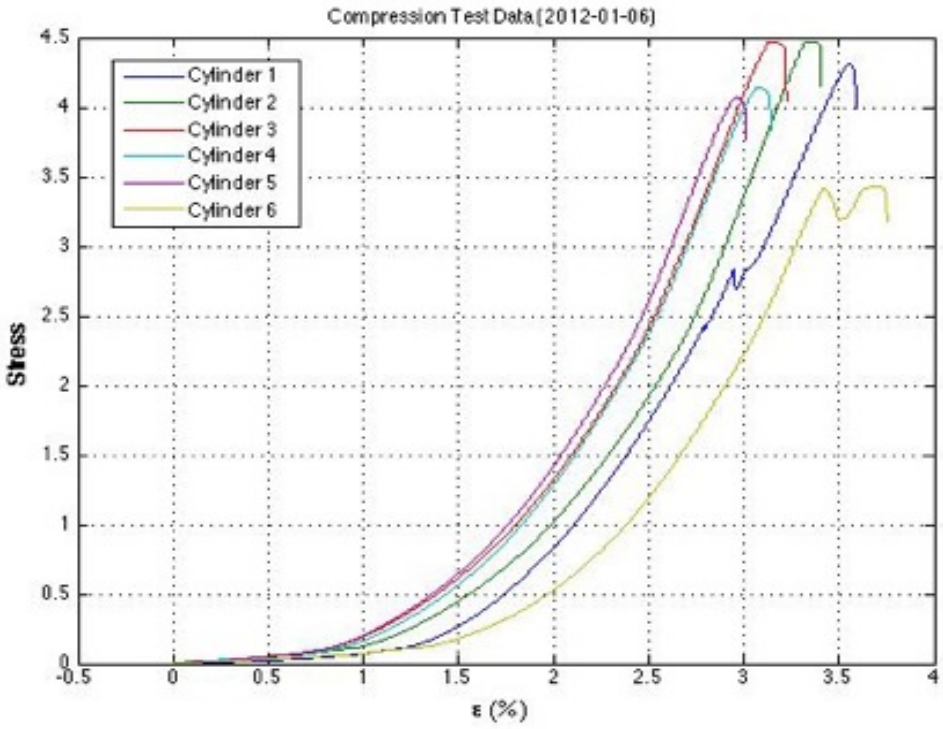

Figure 4-5: Stress vs. Strain Graph for 28-day Compressive Strength of Concrete Cylinders

of the concrete mix was 3.03%, while the average maximum compressive strength value was 4.15 ksi.

Sample	Slump (in)	Max. Compressive Load (lbf)	Compressive Strain at Max. Compressive Load (%)	Compressive Stress at Max. Compressive Load (ksi)
Cylinder 1	1	54101.83	3.56	4.31
Cylinder 2	2	56205.25	3.36	4.47
Cylinder 3	2	56203.90	3.14	4.47
Cylinder 4	2.25	52026.15	3.08	4.14
Cylinder 5	2.25	51119.88	2.97	4.06799
Cylinder 6	3	43134.23	3.71	3.43251

Table 4.4: Results from Compressive Strength Tests

HCP was measured by a portable covermeter, as presented in Fig. 2-3, with a silver/silver chloride reference electrode (Ag/AgCl). The surface of the concrete was divided into 72 meshes as illustrated in Fig. 4-6. The measurement was conducted at the points indicated in Fig. 4-6 from No.1 to No. 72. The probability of corrosion was estimated by following ASTM C876 standard. Because this reference electrode was an Ag/AgCl electrode and the ASTM standard is based on a copper/copper sulfate ($Cu/CuSO_4$), the conversion from Ag/AgCl to $Cu/CuSO_4$ is conducted by the following equation:

$$HCP_{Cu} = HCP_{Ag} - 119 \tag{4.3}$$

where HCP_{Cu} and HCP_{Ag} are the HCPs of the $Cu/CuSO_4$ and Ag/AgCl reference electrodes respectively.

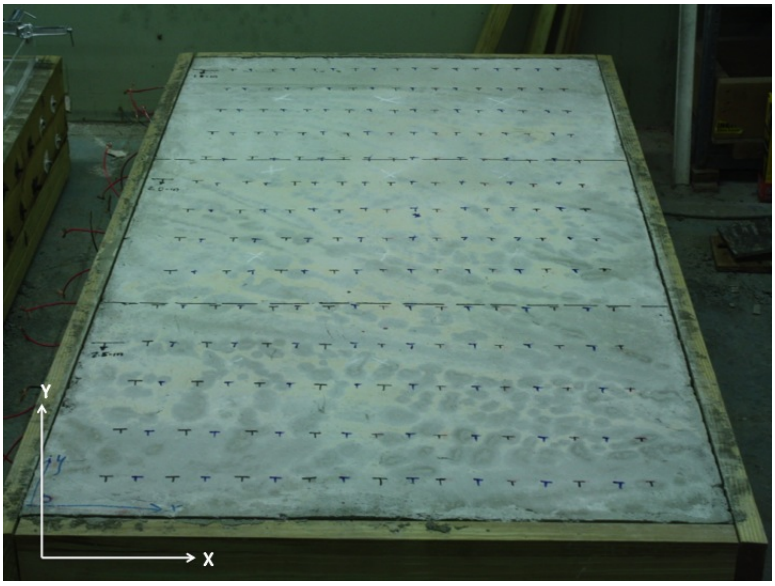

Figure 4-6: Testing Mesh

4.2.1 Results

After 28 days of curing in fresh water, the RC slabs were firstly measured by the HCP sensor. The HCP of the top steel rebar was measured with reference to the Ag/AgCl electrode by placing it on top of the concrete surface just above the steel rebar. After that, the potential difference between the top steel rebar and the surface of the concrete was measured. The measurements were carried weekly at the end of the drying period just before the next ponding cycle. A graphical representation of the HCP data collected during this period is presented in Fig. 4-7 and in Appendix A. The red areas signify areas where HCP reached values lower than -350 mV ($Cu/CuSO_4$). A statistical analysis model pursuant to the recommendations of ASTM G16-95[7] has been included for reference in Appendix B.

4.2.2 Discussion

After 13 weeks of the ponding-and-drying cycle, HCP of the specimens during the dry conditions reached -350 mV in slabs 1 and 3, concentrated around rebars No. 1 and No. 8 (slab 1) and rebar No. 7 (slab 3), respectively. The cover of these rebars were 1.5-in (rebar No. 1 and 8) and 2.0-in (rebar No. 7). It is clearly visible that the potentials are more negative in areas where the concrete cover is less and higher in areas where the concrete cover is more. The HCPs of all slabs are presented in the form of equipotential contour maps. It was found that all areas where the concrete cover was between 1.5-in and 2.0-in the potentials tend to be more negative than the other areas. According to the results of the half-cell measurements, it may be summarized that some parts of rebars No. 1 and No. 8 in slab 1 and rebars No. 4 thru No. 7 in slab 3 in the anodic region were corroded, while a little rust might have been initiated in some other areas. Some portions of slab 1, particularly in the bottom left and right corners of the diagrams indicated some corrosion level within the reinforcement, as shown in Fig. 4-7.

Although all slabs were designed with specific concrete cover depths that are consistent throughout each slab, the HCP results indicated that the areas for corrosion are highly localized. Some areas within slab 1 exhibited HCP values as high as -123 mV and as low as -516 mV, even though the entire slab has a concrete cover depth of 1.5-in. Likewise for slab 3, reinforcements with a cover depth of 2.0-in exhibit a range of values between -136 mV and -528 mV. In comparison, slab 2 was cast with all of the reinforcement at a concrete cover depth of 2.0-in

and the values at this slab range from -121 mV to -226 mV. According to ASTM C876, the confidence level of probability of corrosion of these values is very low.

In terms of the probability of corrosion for the slabs, a normal distribution analysis was performed on a weekly basis on all slabs to determine the probability of any slab reaching a less than -350 mV value during the course of the experiment. The results showed that slab 2 did not exhibit a significant change in probability during the timeframe of the measurements. On 3/23/12 the probability of slab 2 having a HCP value less than -350 mV was 2.33 x 10^{-25}%. On 8/24/12 this probability was 1.57 x 10^{-29}%. Likewise for slab 4, this probability was 8.37 x 10^{-84}% on 3/23/12 and 2.92 x 10^{-108}% on 8/24/12. The most marked change occurred on slab 1 where the probability increased from 1.71% to 15.6%. Slab 3 decreased from 28.5% to 16.1%. It is important to note that these probabilities represent the chance that any value from the slabs is less than -350 mV and therefore representing a chance of greater than 90% of corrosion per ASTM C876. This does not represent the actual level of corrosion but the probability for a chance of corrosion.

Comparing these results to the visual inspection of the slabs, it is observed that results of the HCP measurements are in good agreement with physical evidence of corrosion in the reinforcement, particularly in slabs 1 and 3. The visual inspection for slab 1 shows that the rebar of the upper layer exhibits evidence of corrosion near the bottom left area of the graphs for slab 1. This area, in particular, was subject to continuously exposed to direct NaCl solution, due to a leakage from the plexiglass dam. The visual inspection for slab 3 also indicates that the rebar of the

upper layer, particularly rebar No. 7, exhibits considerable evidence of corrosion in the reinforcement, to the degree that a large rust stain is seen at this location in the reinforcement. Coincidentally, this observation also agrees with the most negative measurements taken from slab 3. No visible evidence of corrosion was observed on slabs 2 and 4. According to these HCP results, it is concluded that HCP measurements can be used as an indicator for the probability of corrosion for steel reinforcement embedded within concrete.

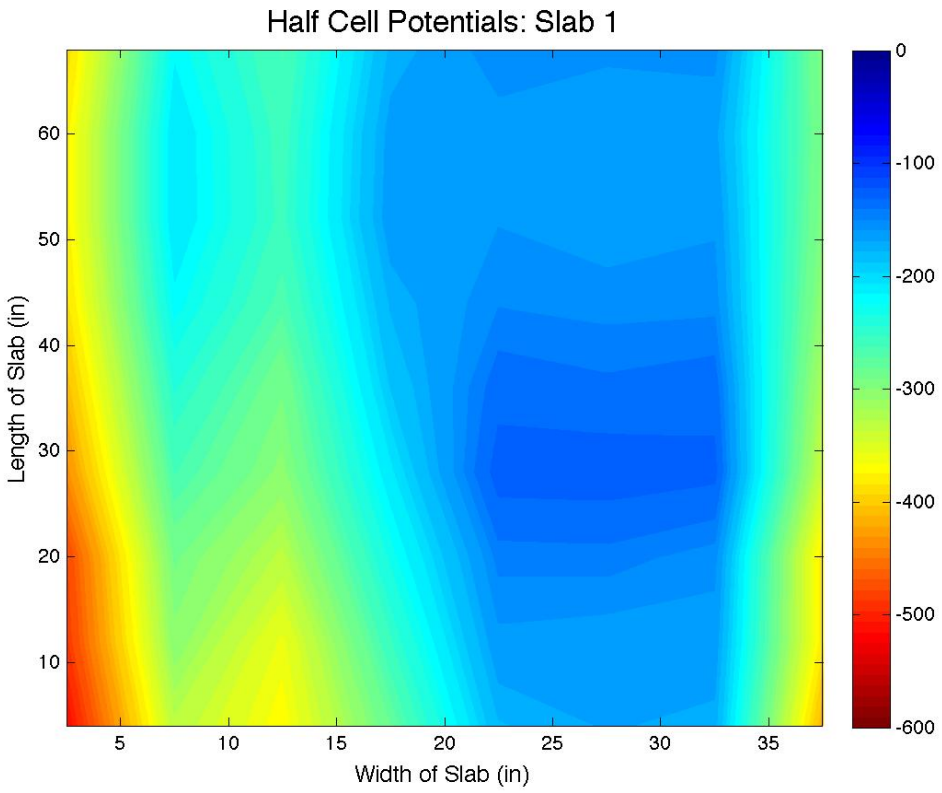
Half Cell Potentials: Slab 1
Length of Slab (in)
Width of Slab (in)
10
20
30
40
50
60
5
10
15
20
25
30
35
0
-100
-200
-300
-400
-500
-600

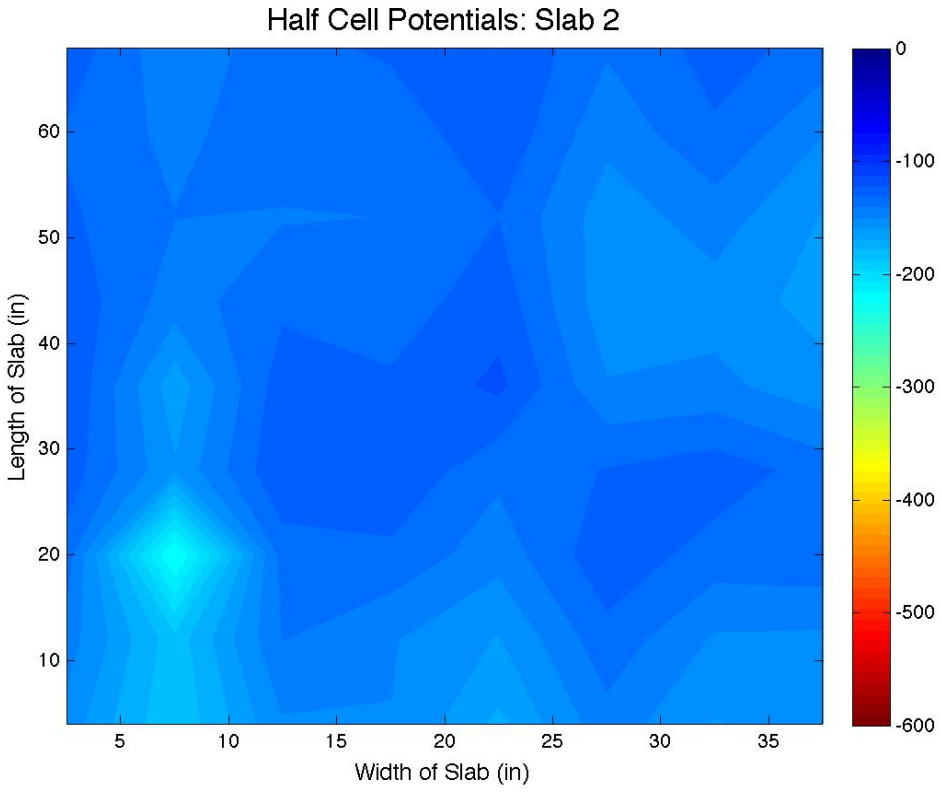
Half Cell Potentials: Slab 2
Length of Slab (in)
Width of Slab (in)
10
20
30
40
50
60
5
10
15
20
25
30
35
0
-100
-200
-300
-400
-500
-600

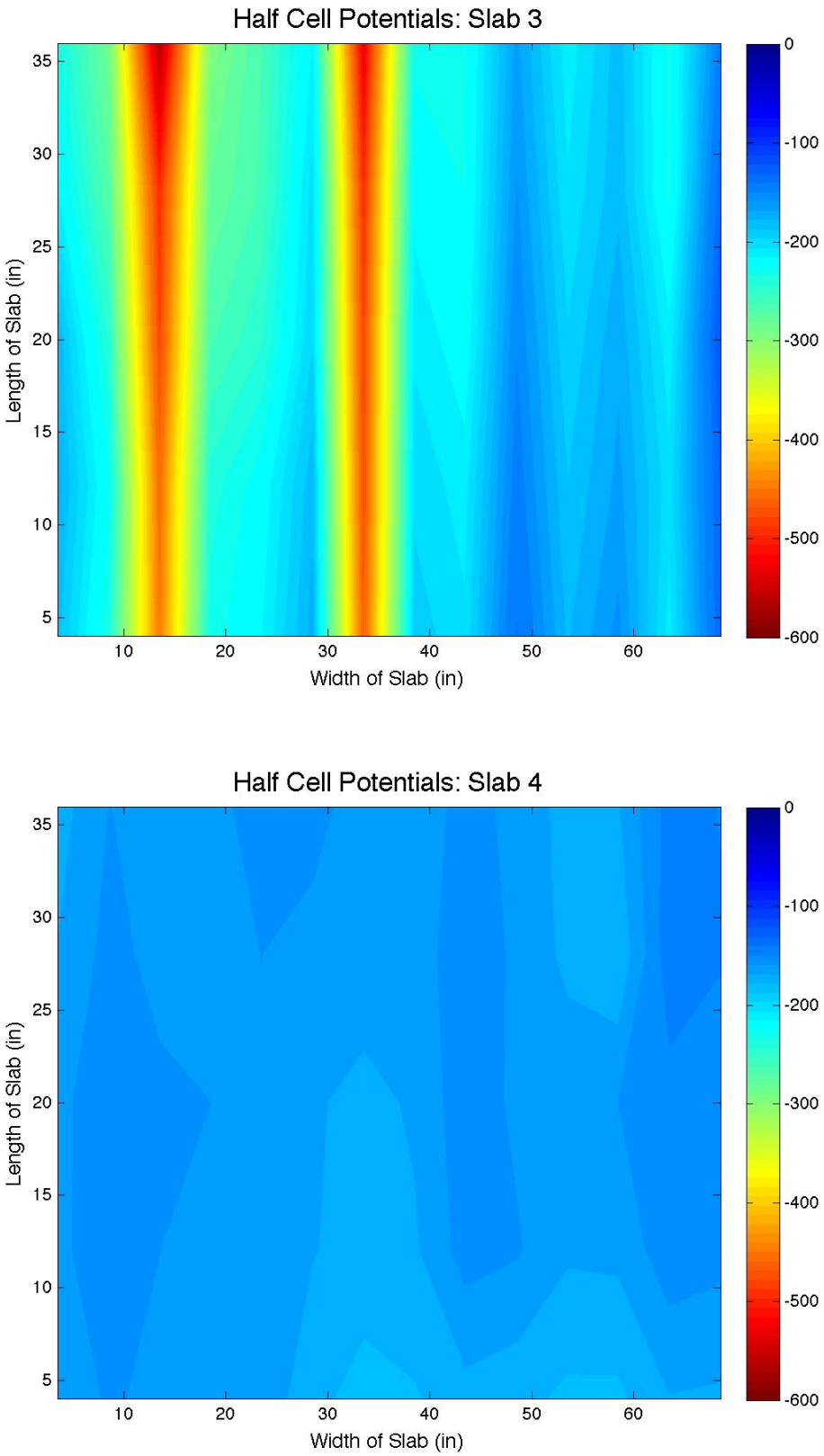

Figure 4-7: Week of August 24, 2012

4.3 Third Experimental Set - Covermeter Survey

For the third experimental set a Profometer® rebar locator was used to measure the concrete cover depth of all four slabs at the beginning and at the end of the experiment period. This instrument is designed in combination with the pulse induction method, as explained previously in Chapter 3. The covermeter is electromagnetic in principle. Electric currents in a coil winding in the search head generate a magnetic field which propagates through the concrete and interacts with the buried metal present in the concrete, such as steel rebars. This interaction happens mainly due to the magnetic properties of steel rebars. The signal will increase with increasing rebar diameter and will decrease with increasing concrete cover. This instrument was calibrated by means of a calibration kit that was provided by the manufacturer. For comparison purposes the measurements for the concrete cover depth of the rebar was taken at the same locations as the measurement for the HCP.

4.3.1 Results

In order to analyze the concrete cover depth, an extensive graphical analysis was performed on slabs 3 and 4. These two slabs were selected since they were the only two slabs cast with identical concrete cover depths and also due to one of them being the control slab (slab 4) and the other being the experimental slab (slab 3). The results of these tests consist the following:

- Figs. 4-8 and 4-9 show the data comparison between the expected value of the concrete cover depth, the measured value and the error in the measurements. The data comparison chart compares these measurements side by side for slabs 3 and 4.

- Figs. 4-10 thru 4-12 illustrate error analyses for both slabs. In particular, the mean squared error, the error percentage and the standard deviation of the measurement values.

- Fig. 4-13 presents the measurement error data contained in the covermeter survey of slabs 3 and 4 (Fig. 4-8). This measurement error data analysis covers the entire range of measurements for both slabs, not the average values that are presented on Fig. 4-8.

4.3.2 Discussion

The data from the cover thickness survey was analyzed. The data obtained using the covermeter survey was used to plot the curves presented in Figs. 4-8 thru 4-13. The main purpose of the covermeter survey was to gauge the accuracy and reliability of the covermeter sensor when the existing rebar has been subject to corrosion. In order to achieve this, the covermeter survey data was fed into MATLAB® and the concrete cover depth profiles were generated and illustrated.

The rebar profiles drawn by MATLAB® appear to reasonably agree with the general location of the rebar and actual cover depth values. In Fig. 4-9 we can

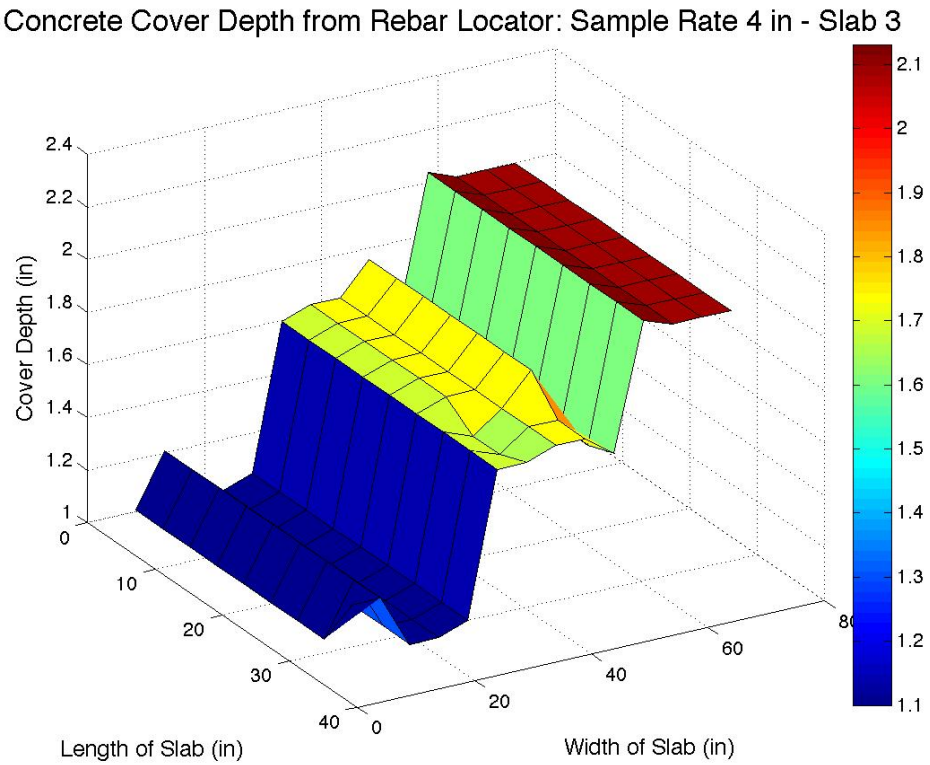

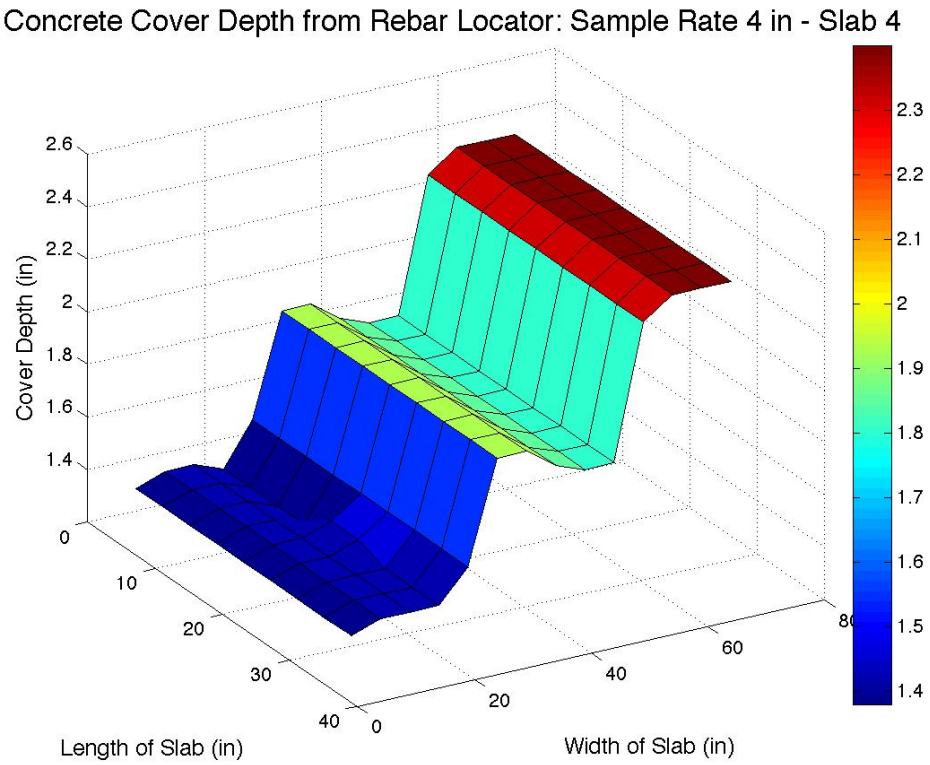

Figure 4-8: Concrete Cover Depth

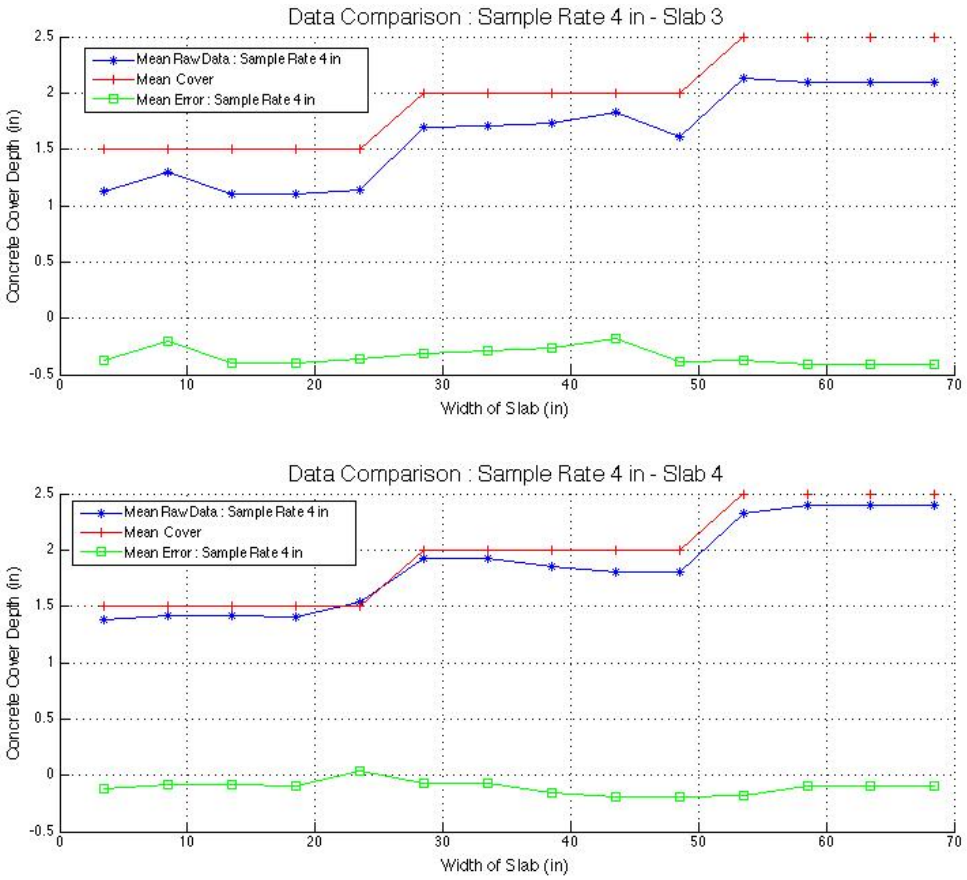

Figure 4-9: Data Comparison

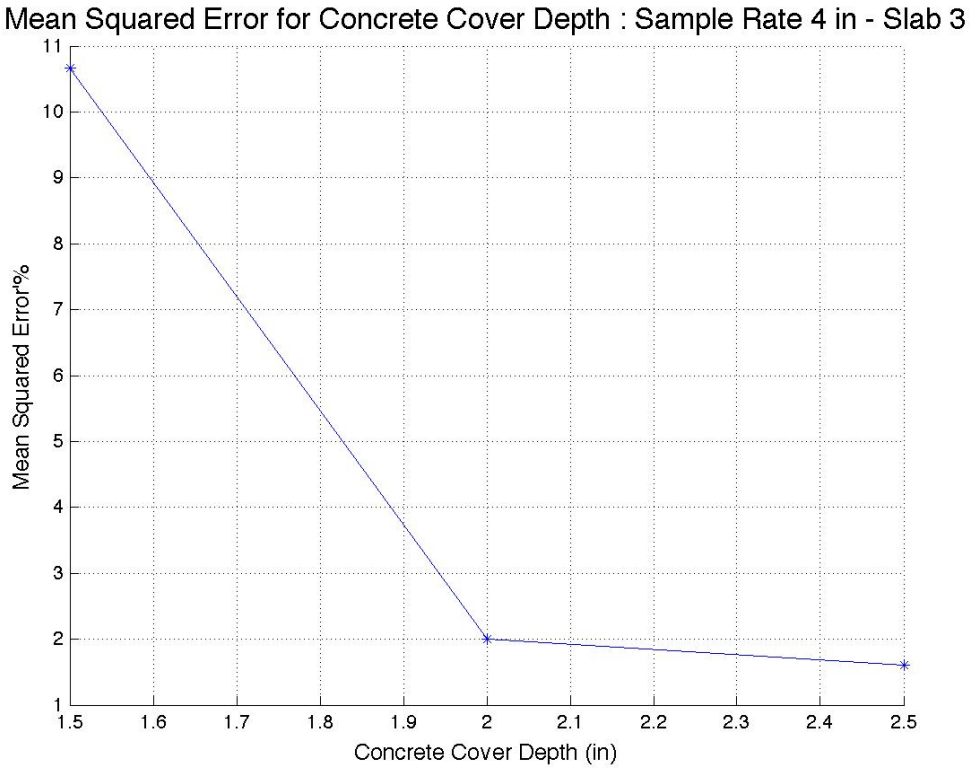

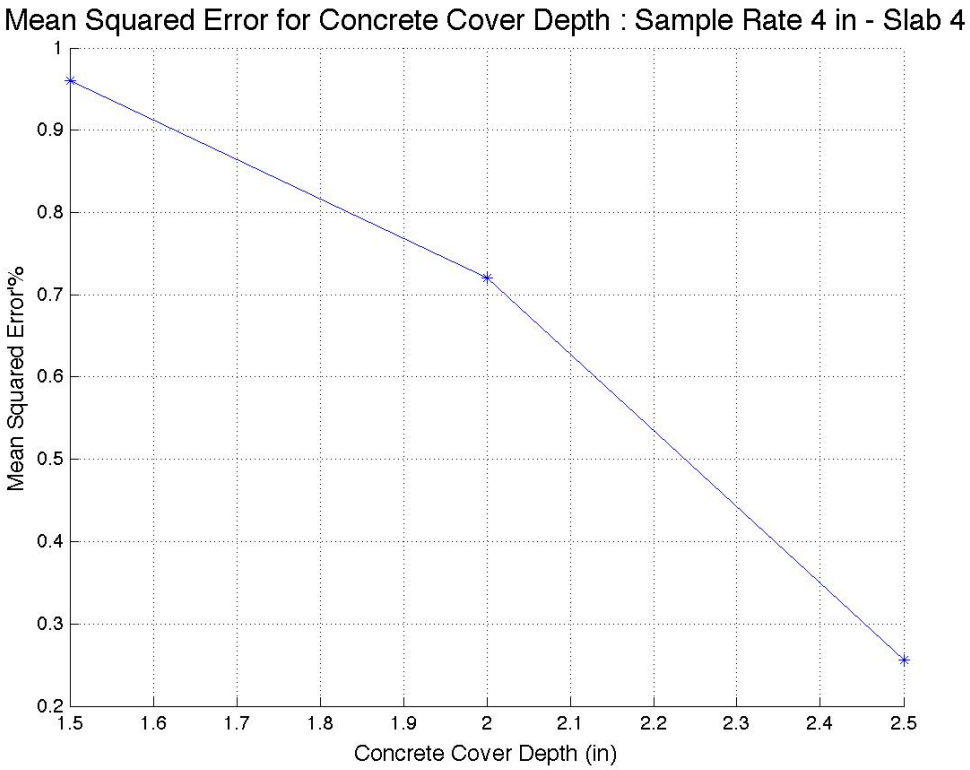

Figure 4-10: Mean Squared Error

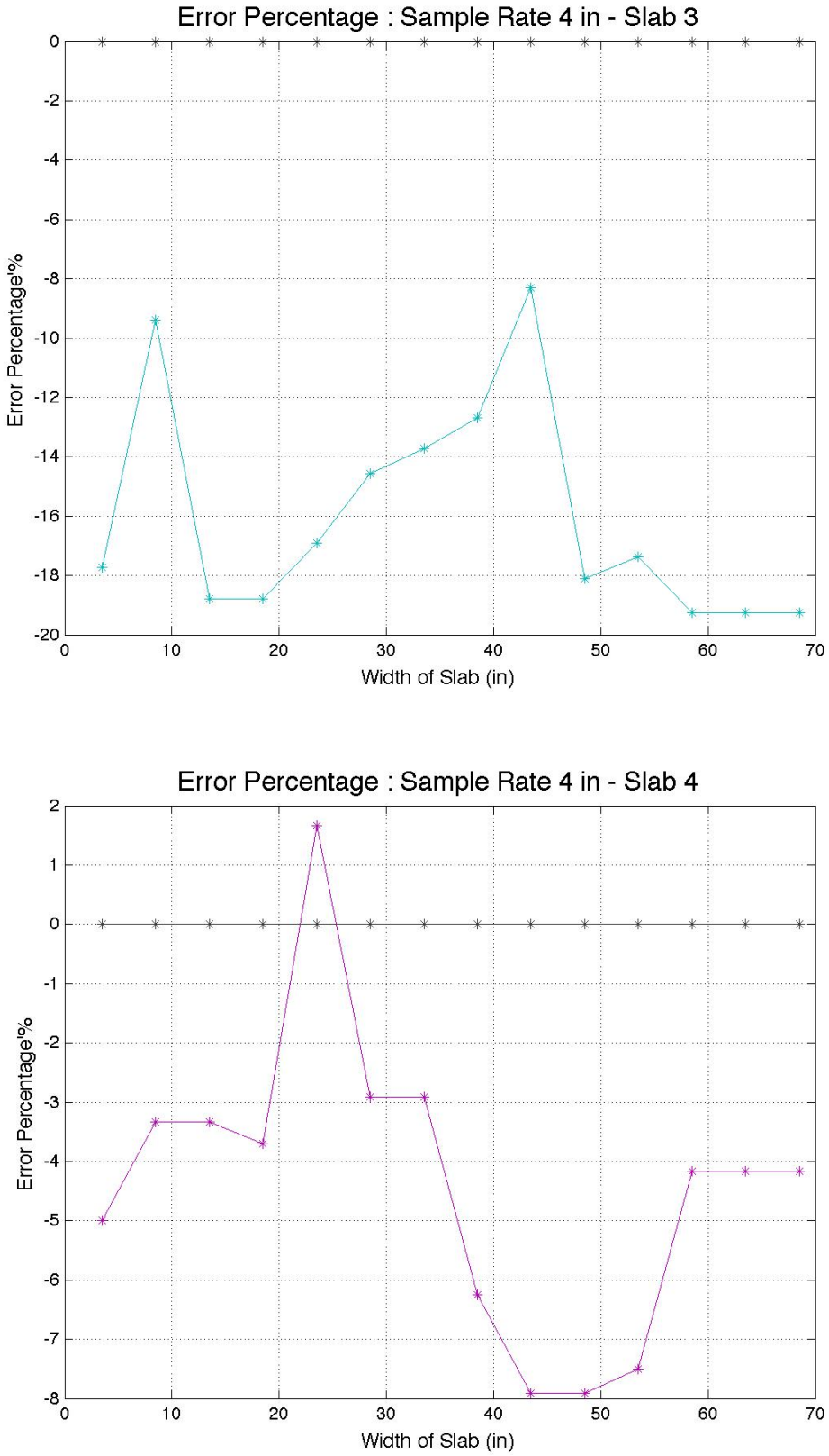

Figure 4-11: Error Percentage

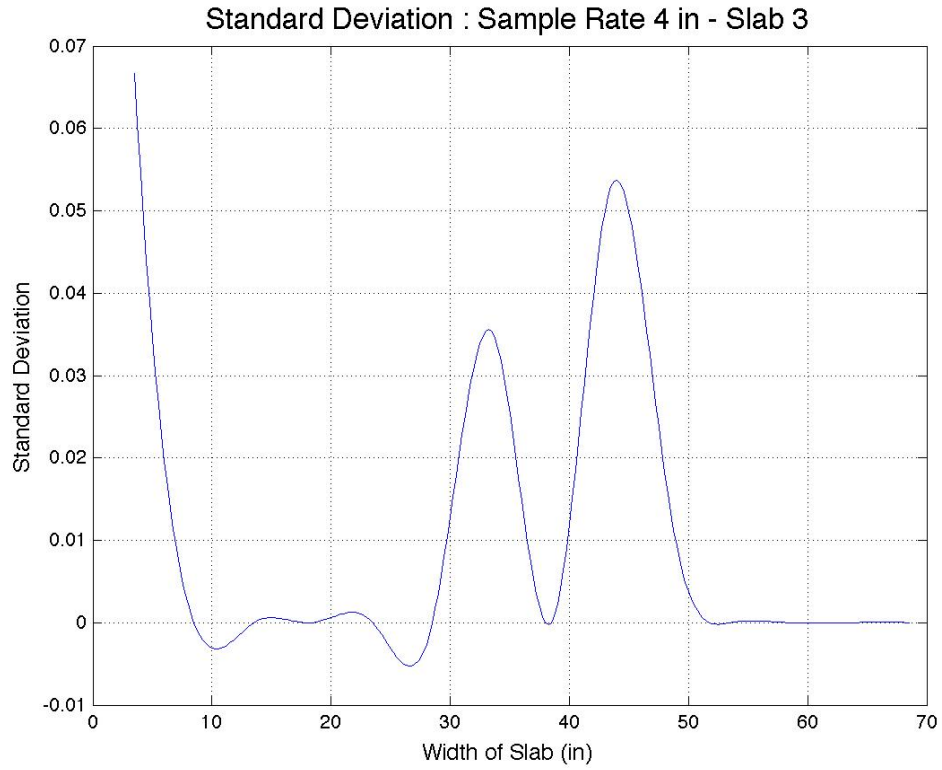

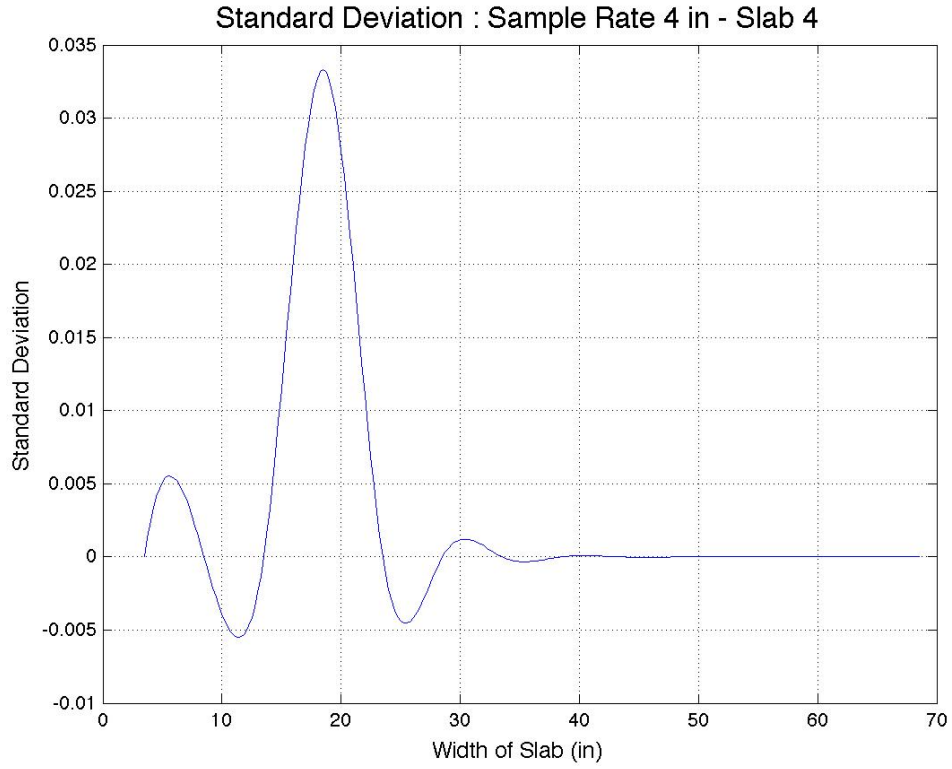

Figure 4-12: Standard Deviation

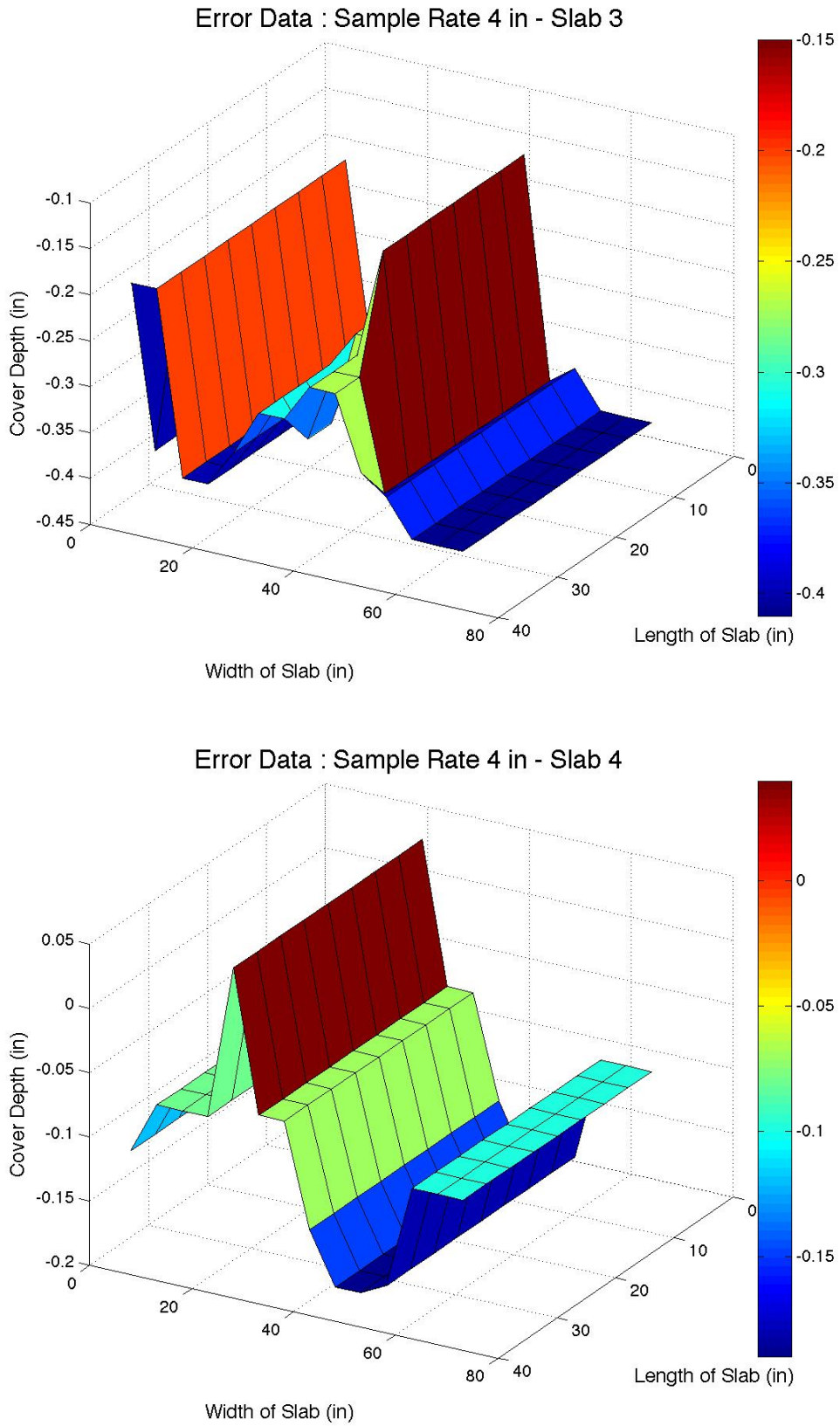

Figure 4-13: Measurement Error in the Covermeter Survey of Slabs 3 and 4

clearly appreciate the average concrete cover depth for each rebar located along both slabs. The red line represents the actual known values of the concrete cover depth, the blue line represents the concrete cover depth as measured by the covermeter and the green line represents the difference in error of the known cover depth vs. the measured cover depth. It is clear from these graphs that measured cover values on the control slab (i.e., slab 4) are more close to the actual cover values than the values measured on slab 3. Comparing this data against the HCP values on slab 3, as indicated in Fig. 4-7, less HCP values occur at rebar No. 3 and rebar No. 7, which indicates areas where a larger probability of corrosion occurs. The location of rebar No. 3 also shows a large discrepancy between the known concrete cover values vs. the measured concrete cover values. However, this discrepancy is not present at rebar No. 7.

The error values become more pronounced once we consider the mean squared error of the covermeter data. Fig. 4-10 illustrates how the mean squared error values on slab 3 ranges between 1.9% and 10.5%. This 10.5% value represents the discrepancy for the cover depth value of 1.5-in. This area along the slab also accounts for some of the lowest HCP values of this slab. This error value decreases to approximately 2% for the cover depth value of 2.0-in. When we compare these values against the data obtained from the covermeter survey on slab 4, we notice a significant decrease in the mean squared error values. For the concrete cover depth value of 1.5-in the error value is approximately 0.95%, while for the cover depth values of 2.0-in and 2.5-in the errors are 0.71% and 0.25%.

Error percentage values and standard deviation values for the localized sections

of data among both slabs also correlate, as presented in Figs. 4-11 and 4-12. These two figures represent the error analysis in terms of percentage and the standard deviation, respectively. Fig. 4-13 represents a 3-D analysis of the green line presented in Fig. 4-8 but with an exaggerated scale such that the high and low values of the error data are easier to distinguish from one another.

The analysis of these figures and trendlines of data can lead us to a conclusion. Although there is a discernible correlation between the probability of corrosion and the covermeter values, it is possible that these trendlines have more to do with factors other than the degree of corrosion in the rebar. Although in Fig. 4-9 one can vividly appreciate the difference between the measured values of the covermeter survey and the known values of the concrete cover, there are no swift changes in the cover values where the HCP measurements indicate a higher probability of corrosion. When one compares the surveys of slab 3 and slab 4, what is more discernible from this data is not so much significant changes in covermeter values from one point to another. Rather, the same trendline of data is presented on both slabs, albeit slab 4 displays less discrepancy and slab 3 displays more. This difference between concrete cover values for both of these slabs could be attributed to i) the level of NaCl already presenting in the concrete or ii) the level of moisture in the concrete. It is known that the covermeter utilized for the survey is electromagnetic in nature. It is conceivable that NaCl contaminated water may cause a misreading from the equipment due to some interference between the electromagnetic waves and the moisture within the concrete. This conclusion is preliminary in its nature as more research in the future should be performed to

discern any possible change on the readings with various levels of moisture within the concrete.

4.4 Summary

In the first experiment, when all other factors were kept constant in the corrosion reactor experiment, it was found that corrosion degree, or more accurately mass loss level, is directly proportional to the level of external current applied on the steel rebar. This was found during the preliminary and subsequent phases of the corrosion reactor experiment. This result allowed us to develop a mathematical model for the degree of mass loss for a steel rebar. The result also permits us to have a physical benchmark for measuring the corrosion level. This method is, unfortunately, more appropriate for laboratory settings than actual field conditions.

For the second experiment, three reinforced concrete slabs were subjected to ponding-and-drying cycles of 15% NaCl solution. The development of corrosion was measured by ASTM C876, which relies on a probability scale of HCP measurements. These measurements indicated that corrosion activity was localized within the three slabs, with some areas of the slabs at the same concrete cover exhibiting no probability (i.e. no significantly negative HCP values) of corrosion. Some areas of these slabs did, however, exhibited a high probability of corrosion.

In third experiment, we selected slabs 3 and 4 for being the only two identical slabs in the experiment; one being an experimental slab and the other the control slab, for further experimentation with a concrete covermeter. These slabs were

surveyed with the covermeter. The data was analyzed against the known values of concrete cover and the areas that exhibited a higher probability of corrosion, based on the HCP analysis. The results indicated that a correlation between the areas of corrosion and a discrepancy between the measured and actual values of concrete cover are found. However, this discrepancy was consistent throughout both slabs and may be due to other factors, such as degree of moisture within the concrete and level of NaCl already present in the concrete.

Chapter 5

Conclusion

Corrosion of steel reinforcement embedded within concrete and subjected to artificial accelerated corrosion by means of NaCl solution was studied in this thesis research. Three different and interrelated experimental setups were implemented and developed. First, a small section of steel reinforcement was subjected to external electrical current while immersed in 15% NaCl solution. The external current was applied by means of a potentiostat device in an electrochemical cell. The mass loss of the steel reinforcement, as one of the primary effects of corrosion, was taken as a measurement for the specimen. The mass loss was compared against the time elapsed during the experiment and a mathematical relationship was developed between these two factors. During the second experimental setup, reinforced concrete slabs were cast and placed in a controlled environmental and subject to ponding-and-drying cycles of 15% NaCl solution. While the slabs were subject to accelerated corrosion, HCP measurements per the specifications of ASTM C876, were taken on all four slabs to measure the potential drops of the steel reinforce-

ment due to the ingress or migration of the NaCl solution inside concrete. For the third experimental setup, the concrete cover of the slabs was measured by means of a covermeter sensor. The objective of this experiment was to evaluate the difference in concrete cover measurements between the control slab (slab 4) and the experimental slab (slab 3).

Each analysis of the data was performed for the last experiment cycle (the last week of August 2012). For all four slabs the amounts of cement, gravel, sand and w/c ratio were kept constant. Slabs 3 and 4 had the same exact layer of reinforcement while slabs 1 and 2 had different concrete cover thicknesses.

5.1 Corrosion Rate and Evaluation

For the first experimental setup, a very stable and linear relationship was observed among the increased mass loss of a steel rebar with increased time and electrical current. The average corrosion rate was kept constant throughout the duration of the experiment.

For the second experimental setup, the HCP measurements generated a very good corrosion profile for all four slabs. The most marked potential drops occurred in areas where either i) there was visible evidence of corrosion or ii) where minimal concrete cover above the steel reinforcement was present. Where no physical evidence of corrosion was present, the potential measurements tended to be more positive with increasing concrete cover.

For the third experimental setup, the concrete cover measurements marked

variably in comparing the results between slabs 3 and 4. The profile measurements for slab 4 were closer in numerical value to the known concrete cover data. In contrast, slab 3 data generated values with significant error differences for particular sections of the concrete surface.

5.2 Recommendations for Future Research

Although the purpose of this research was to be as comprehensive as possible, future work is necessary to further understand the behavior of steel reinforcement subject to artificial accelerated corrosion and its assessment by other non-destructive sensors.

Furthermore, the following explicit recommendations are provided:

- Evaluate further options for additional impressed external currents on corrosion electrochemical cells and determine it's effects on the corrosion rate of the specimen. Compare this corrosion rate against the mass loss of the specimen and correlate them.

- Perform additional statistical analysis of the half-cell measurements in order to establish develop a better understanding of the actual corrosion potentials, taking into account the localized effects of the ponding-and-drying cycles. Validate these results against actual corrosion measurements using destructive methods.

- Expand the concrete covermeter surveys for various different known levels of

corrosion instead of probabilities of corrosion. Compare these measurements against the section loss of the rebar and measure the corrosion rate of the rebars.

Appendix A

Half-Cell Potential Data

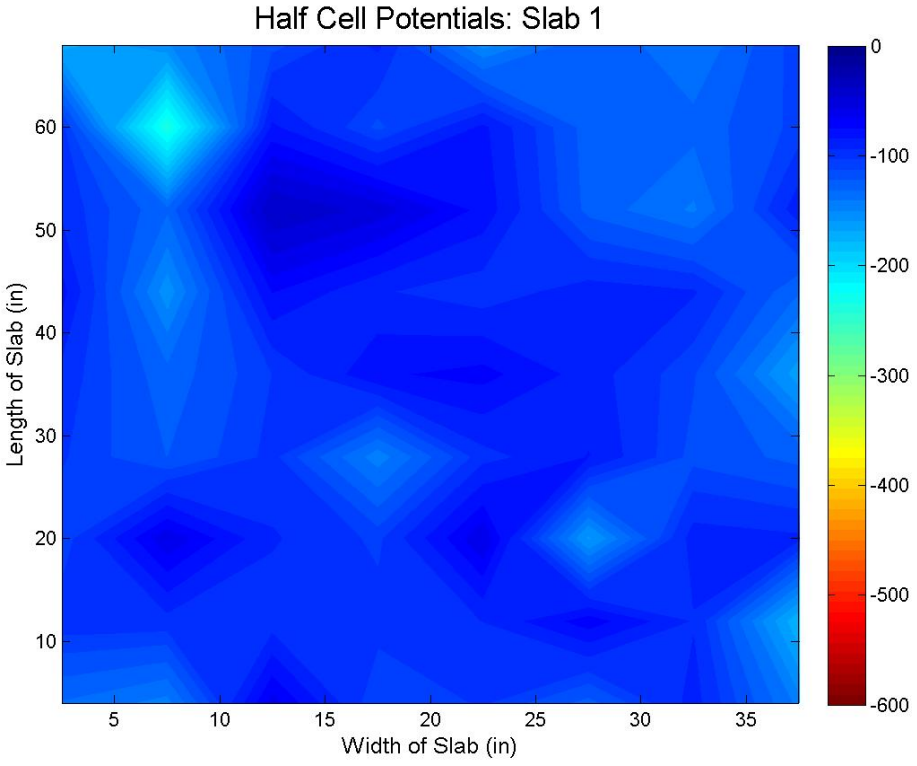
Half Cell Potentials: Slab 1
Length of Slab (in)
Width of Slab (in)
10
20
30
40
50
60
5
10
15
20
25
30
35
0
-100
-200
-300
-400
-500
-600

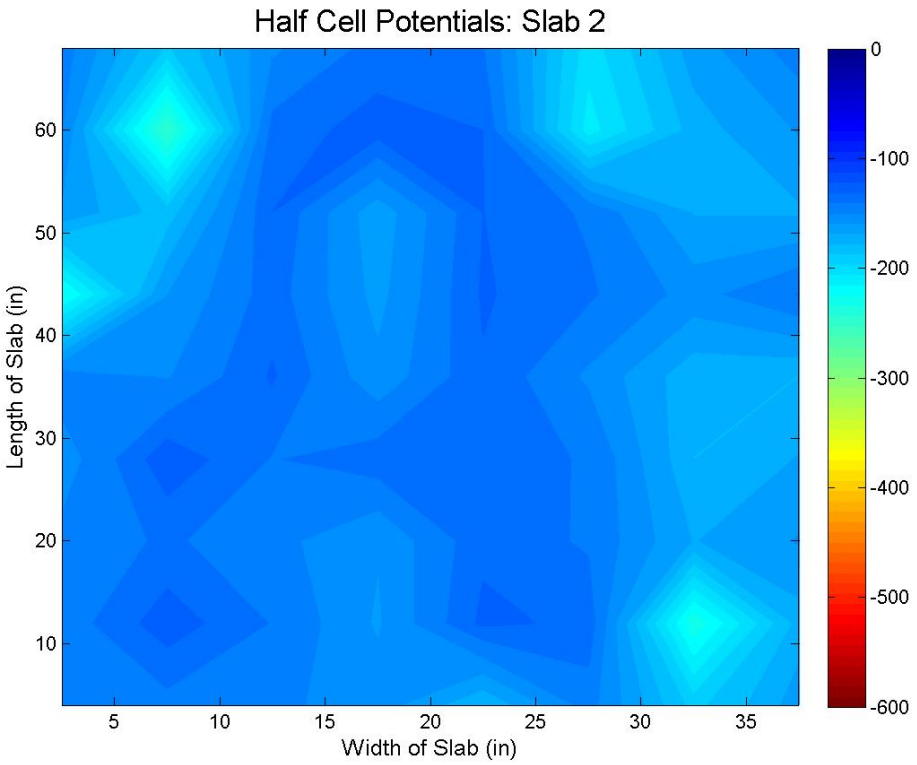
Half Cell Potentials: Slab 2
Length of Slab (in)
Width of Slab (in)
10
20
30
40
50
60
5
10
15
20
25
30
35
0
-100
-200
-300
-400
-500
-600

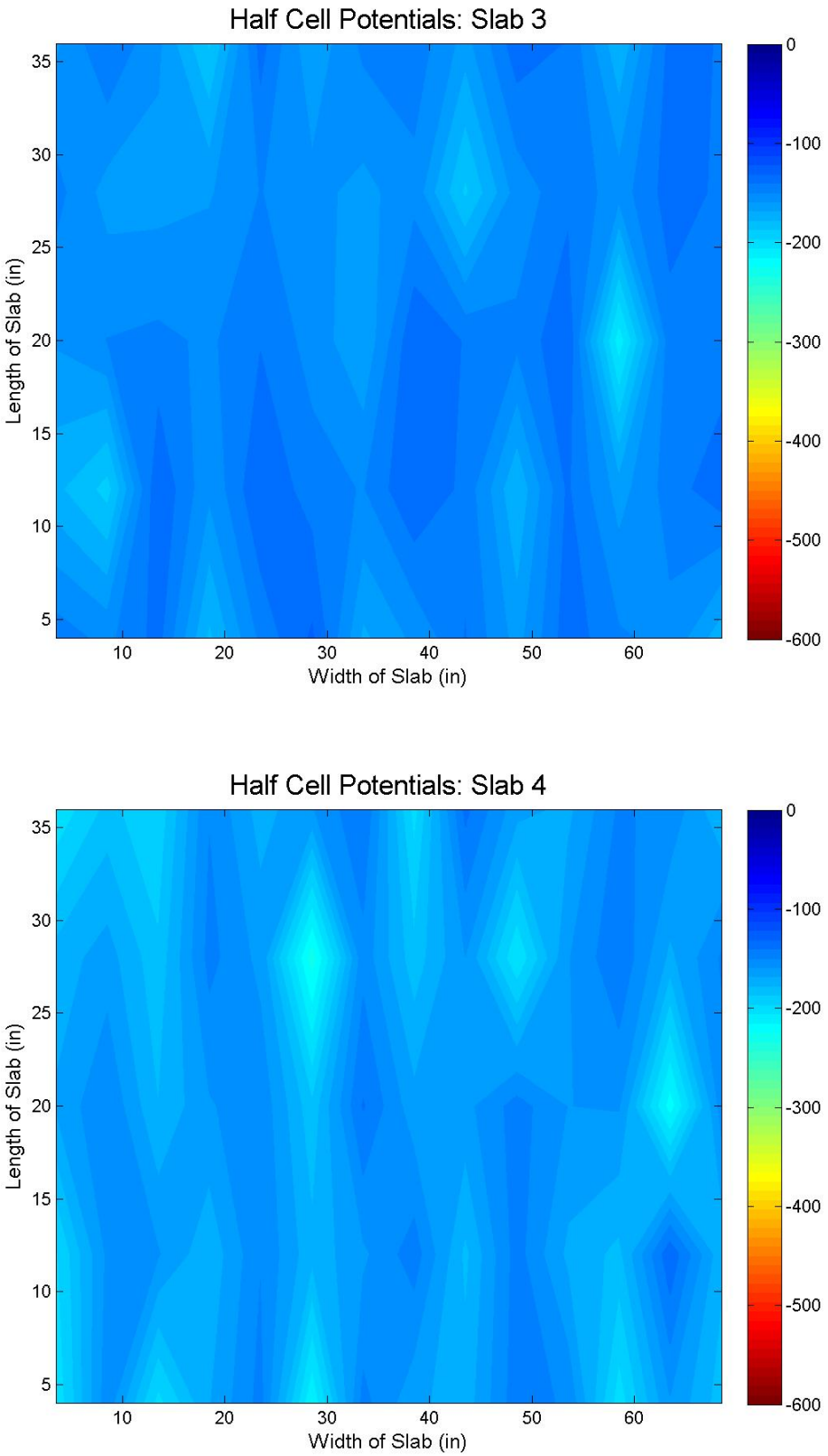

Figure A-1: Week of December 22, 2011

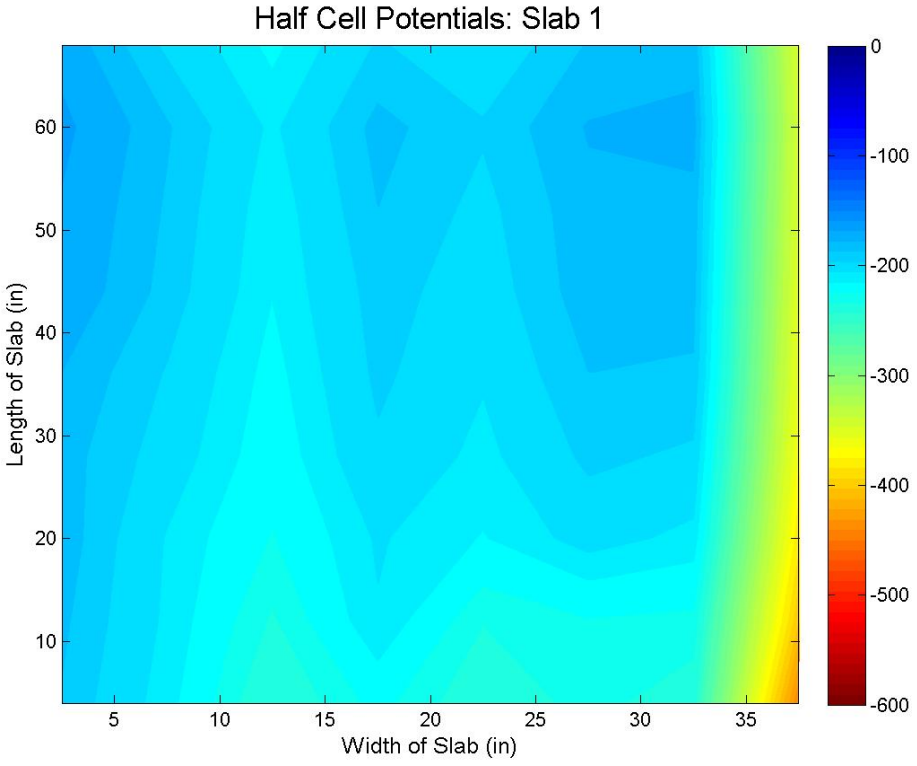
Half Cell Potentials: Slab 1
Length of Slab (in)
Width of Slab (in)
10
20
30
40
50
60
5
10
15
20
25
30
35
0
-100
-200
-300
-400
-500
-600

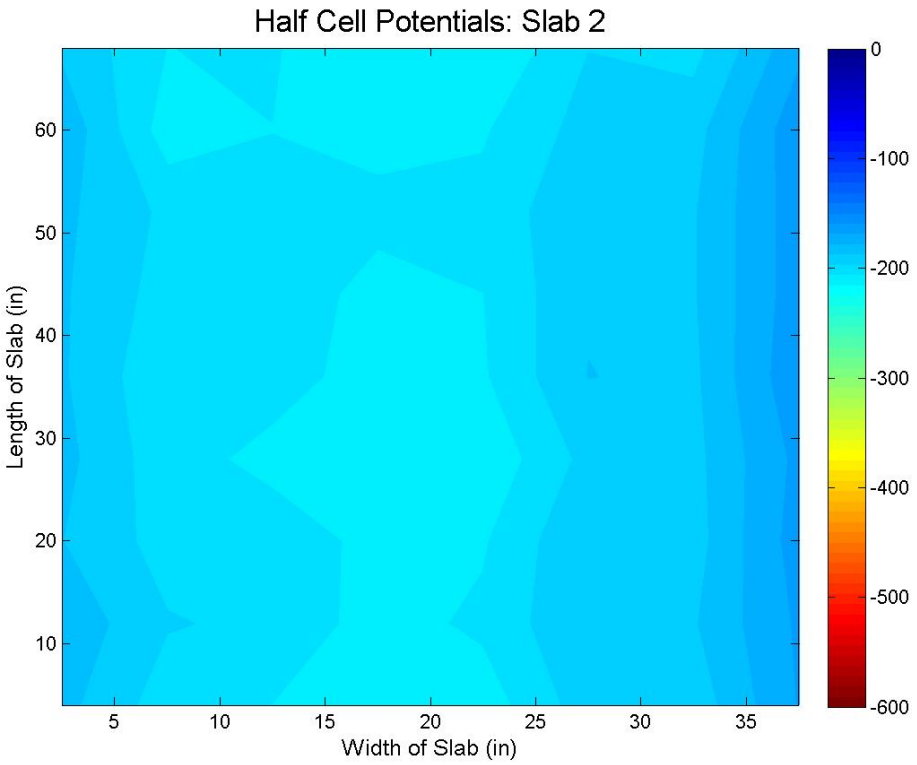
Half Cell Potentials: Slab 2
Length of Slab (in)
Width of Slab (in)
10
20
30
40
50
60
5
10
15
20
25
30
35
0
-100
-200
-300
-400
-500
-600

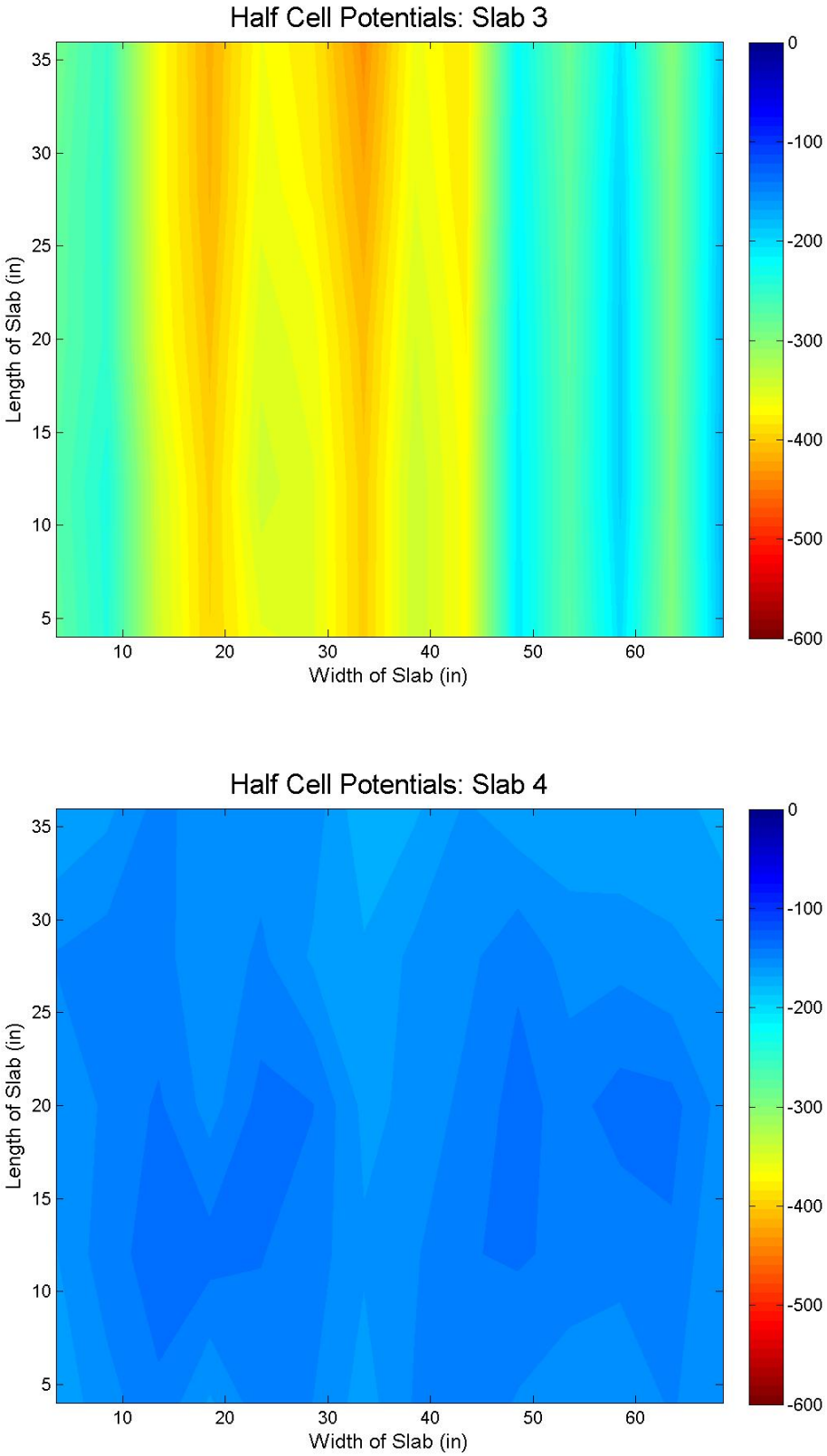

Figure A-2: Week of March 23, 2012

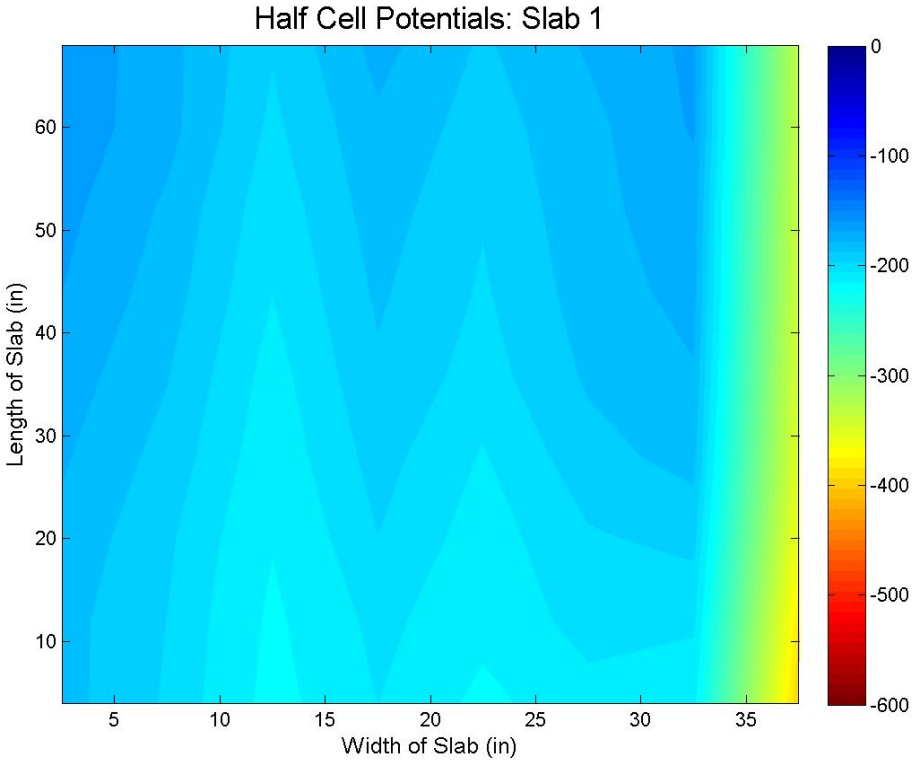
Half Cell Potentials: Slab 1
Length of Slab (in)
Width of Slab (in)
10
20
30
40
50
60
5
10
15
20
25
30
35
0
-100
-200
-300
-400
-500
-600

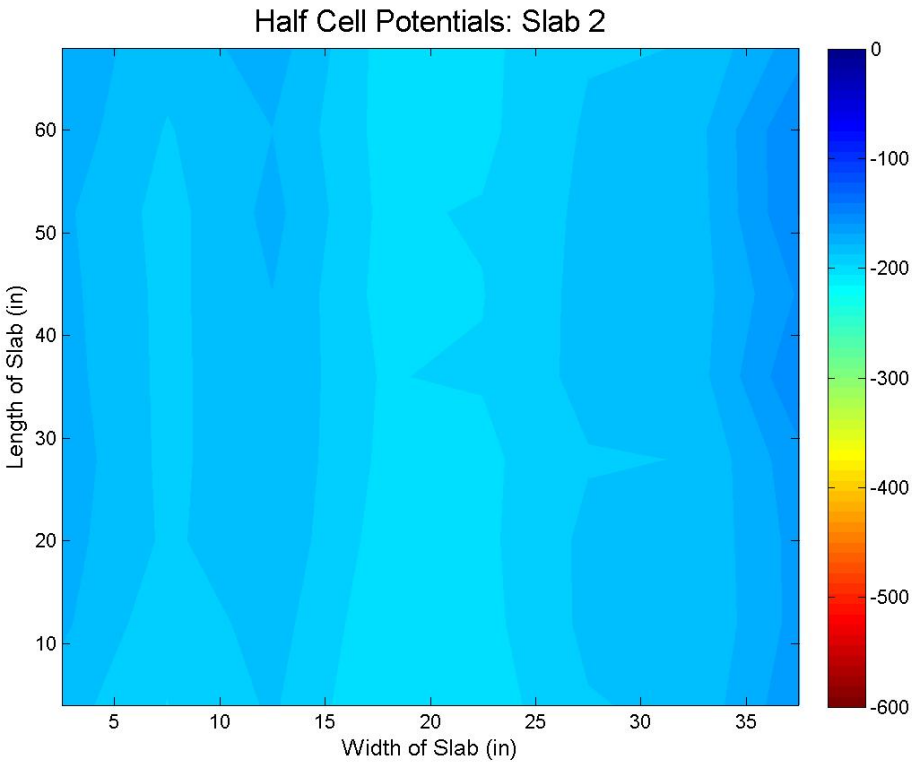
Half Cell Potentials: Slab 2
Length of Slab (in)
Width of Slab (in)
10
20
30
40
50
60
5
10
15
20
25
30
35
0
-100
-200
-300
-400
-500
-600

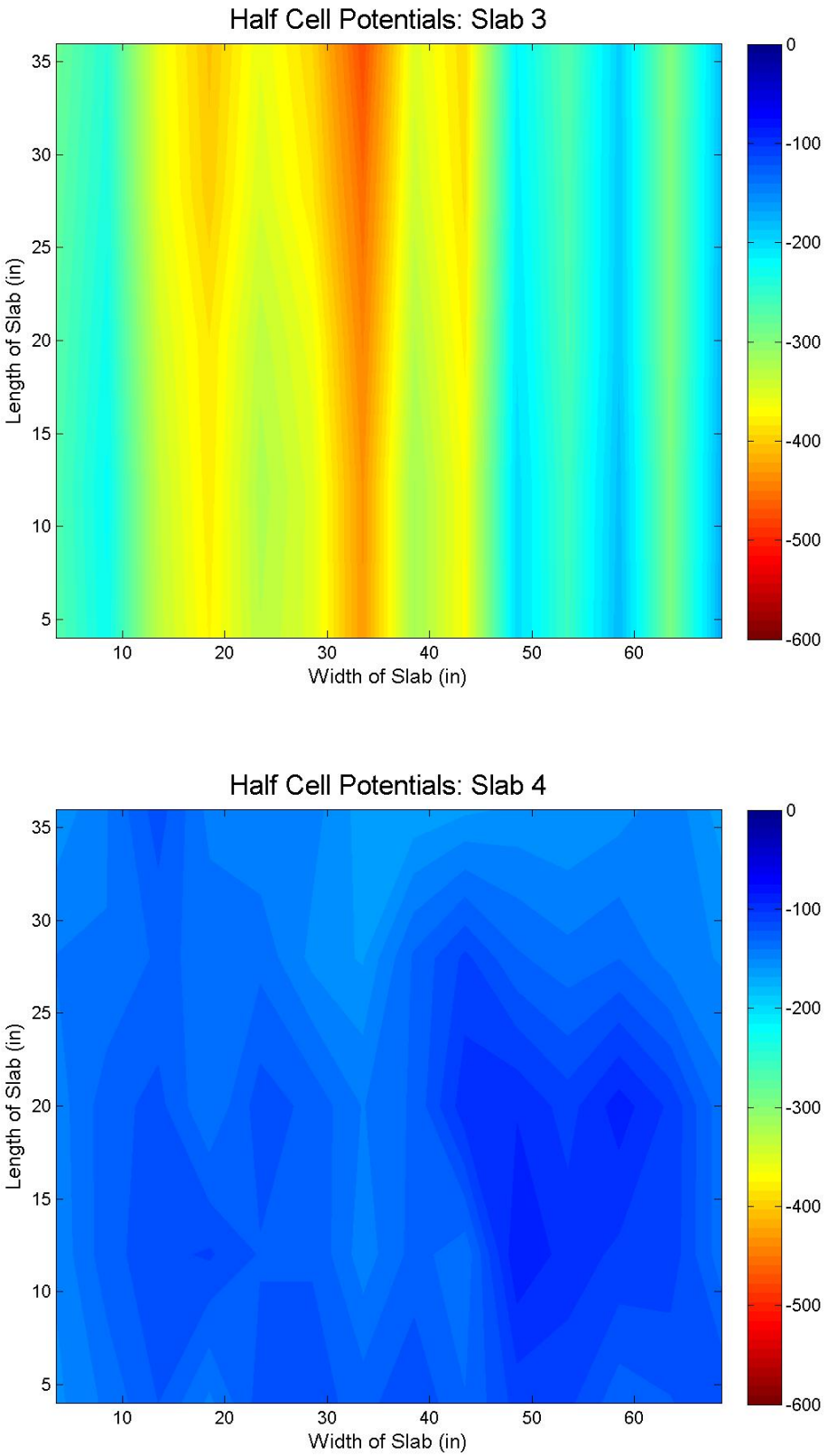

Figure A-3: Week of March 30, 2012

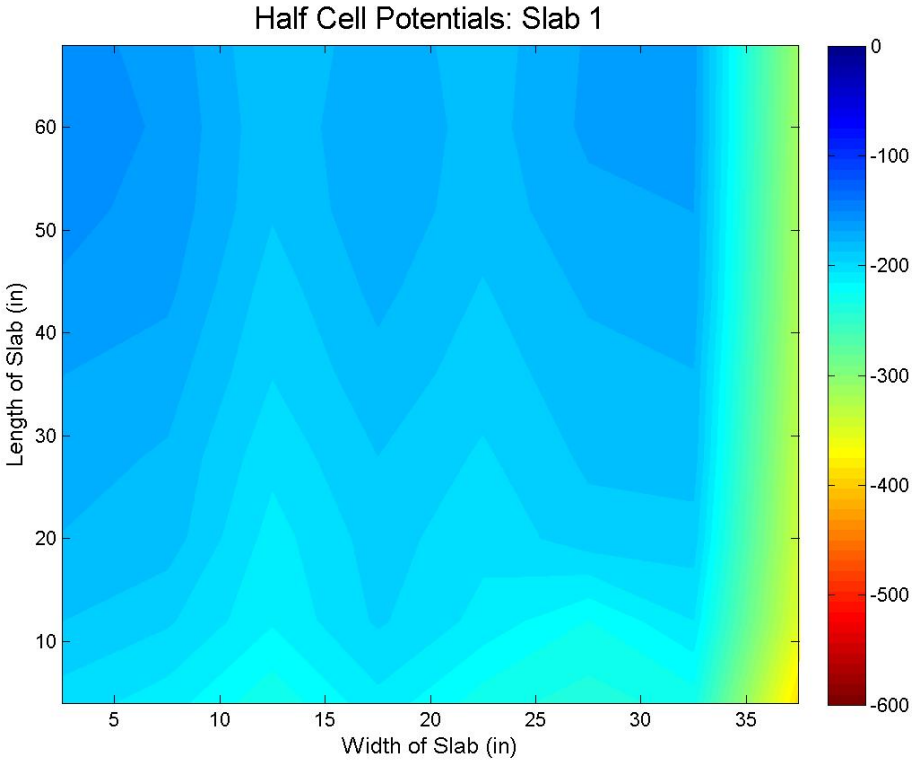
Half Cell Potentials: Slab 1
Length of Slab (in)
Width of Slab (in)
10
20
30
40
50
60
5
10
15
20
25
30
35
0
-100
-200
-300
-400
-500
-600

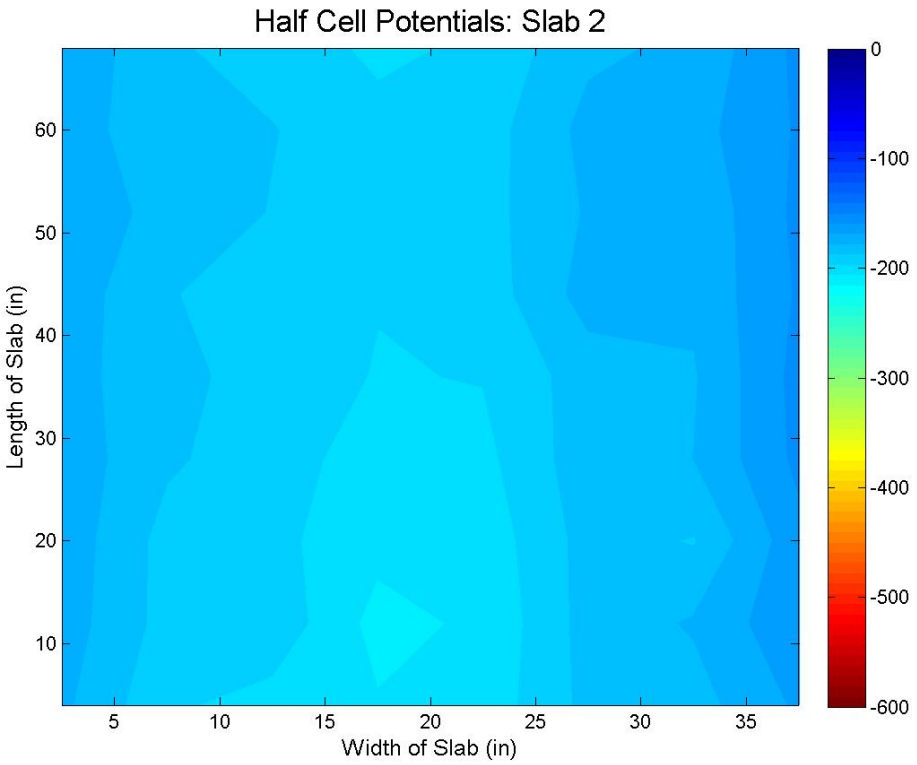
Half Cell Potentials: Slab 2
Length of Slab (in)
Width of Slab (in)
10
20
30
40
50
60
5
10
15
20
25
30
35
0
-100
-200
-300
-400
-500
-600

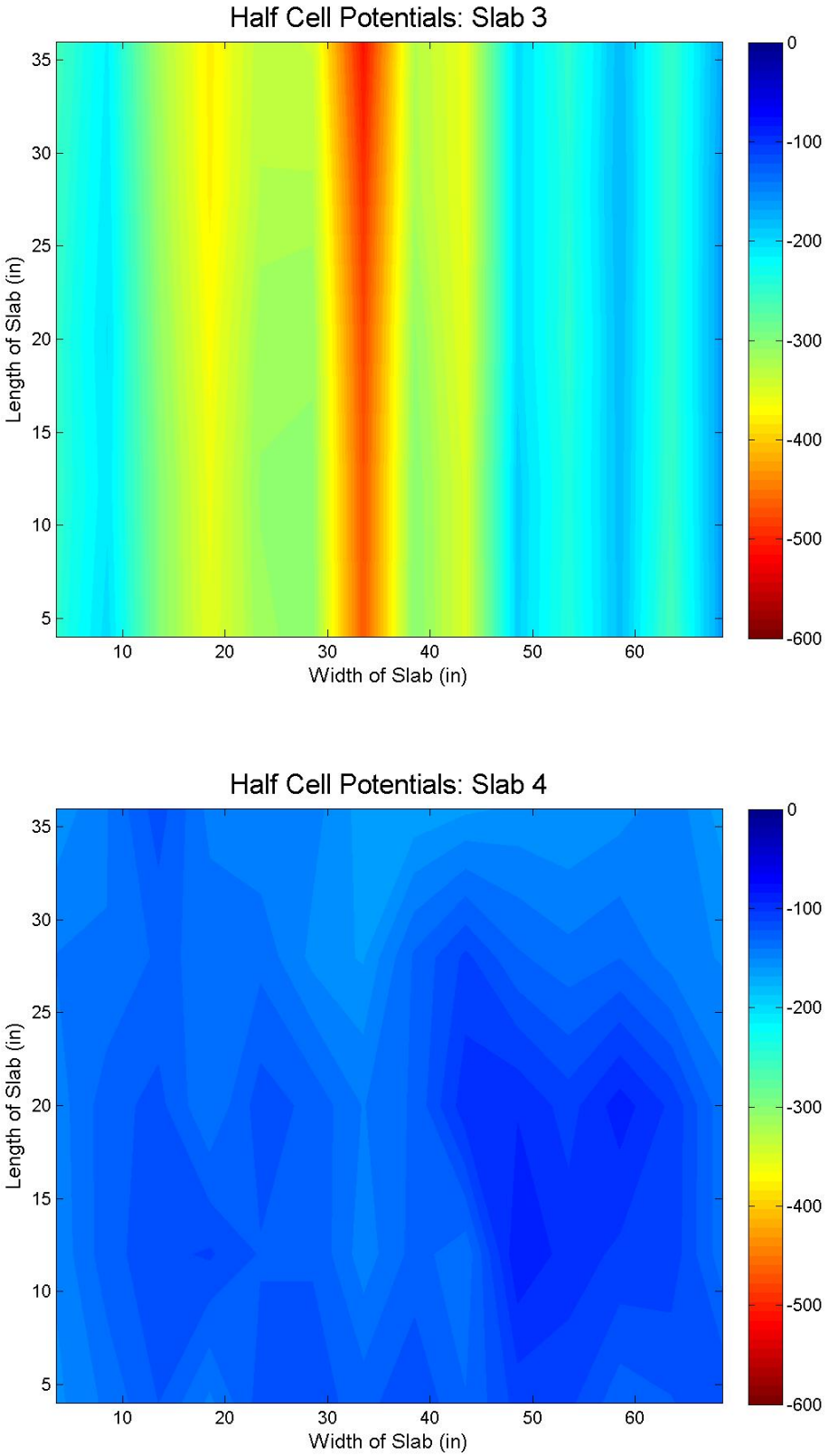

Figure A-4: Week of April 6, 2012

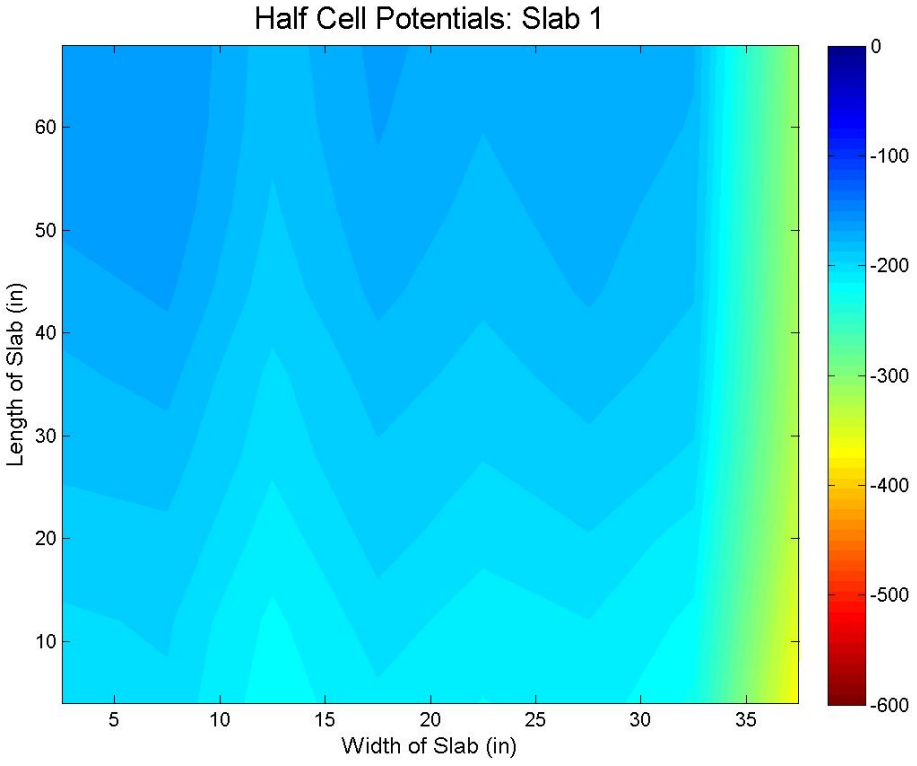
Half Cell Potentials: Slab 1
Length of Slab (in)
Width of Slab (in)
10
20
30
40
50
60
5
10
15
20
25
30
35
0
-100
-200
-300
-400
-500
-600

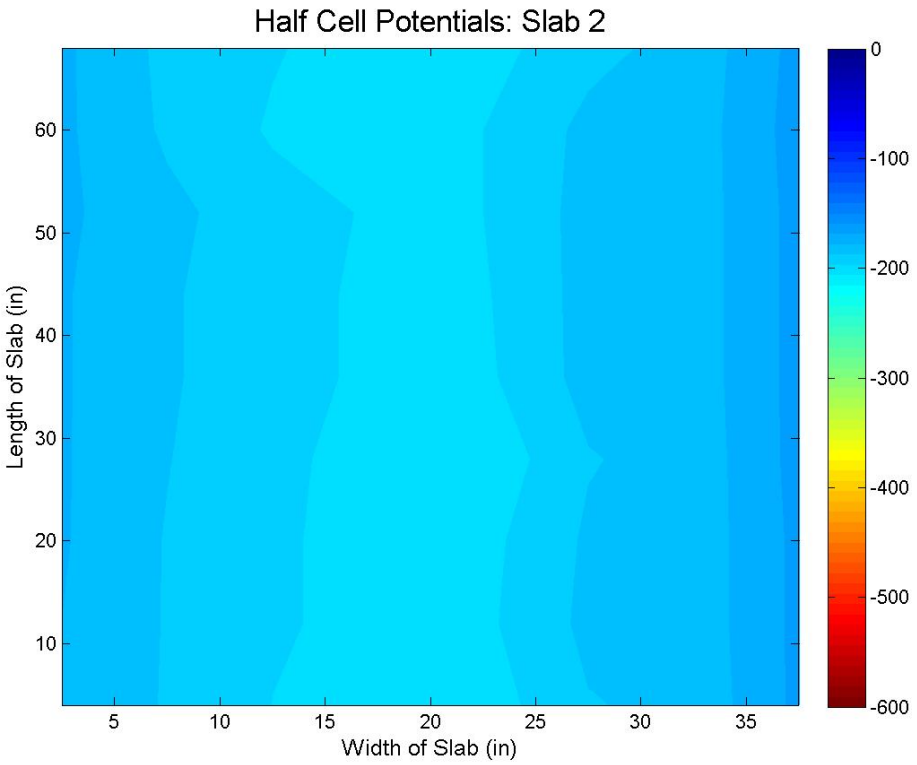
Half Cell Potentials: Slab 2
Length of Slab (in)
Width of Slab (in)
10
20
30
40
50
60
5
10
15
20
25
30
35
0
-100
-200
-300
-400
-500
-600

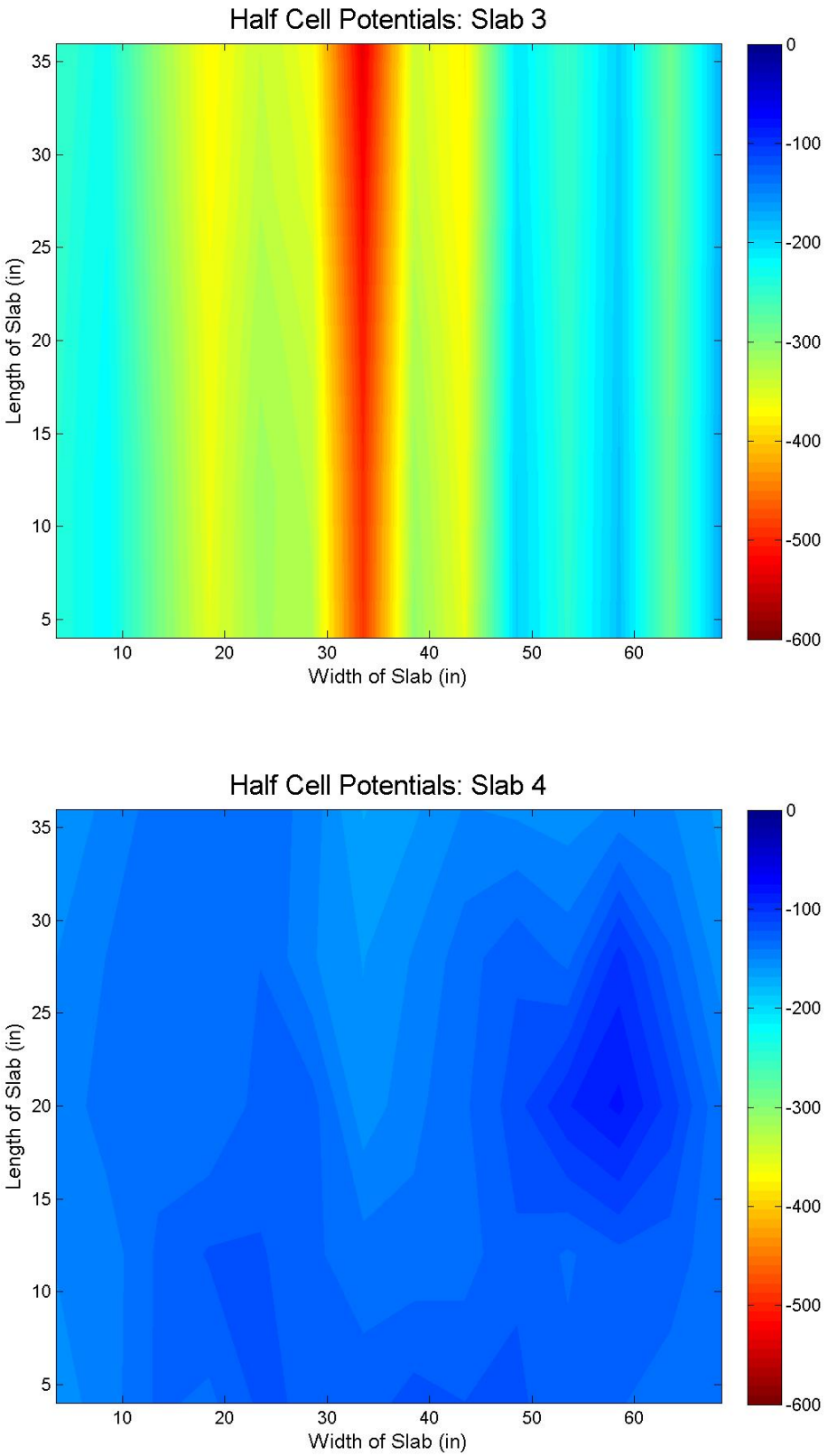

Figure A-5: Week of April 13, 2012

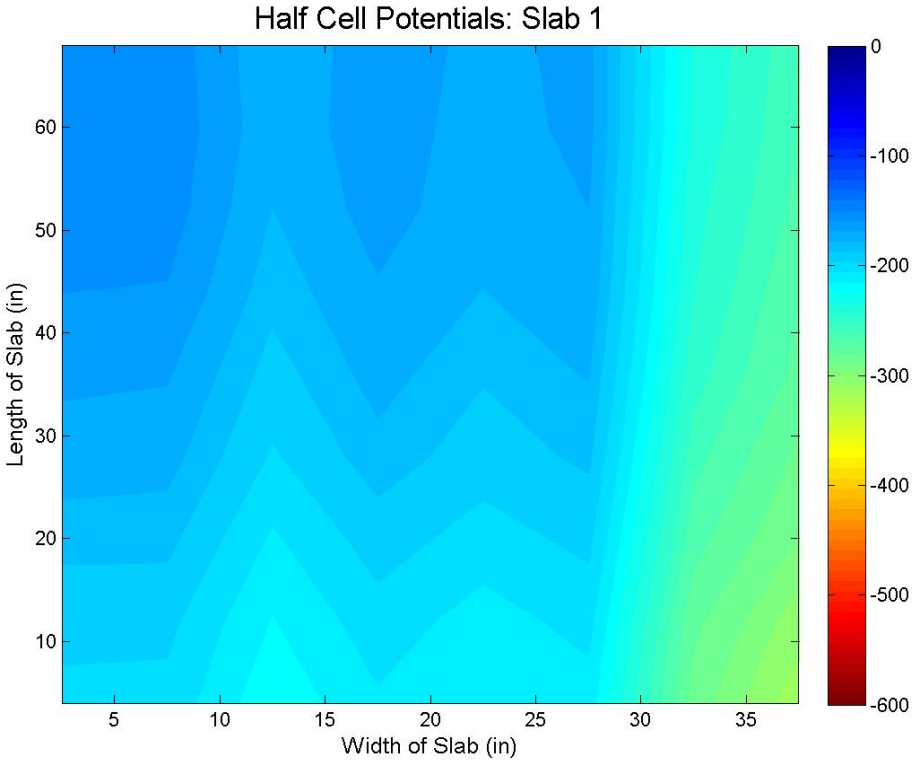
Half Cell Potentials: Slab 1
Length of Slab (in)
Width of Slab (in)
10
20
30
40
50
60
5
10
15
20
25
30
35
0
-100
-200
-300
-400
-500
-600

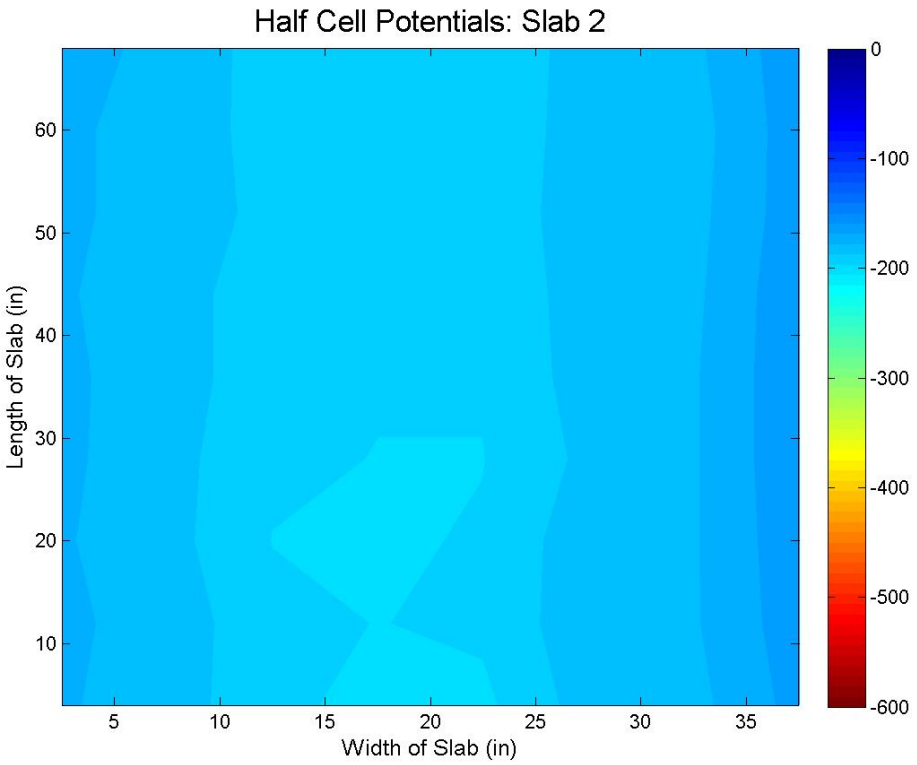
Half Cell Potentials: Slab 2
Length of Slab (in)
Width of Slab (in)
10
20
30
40
50
60
5
10
15
20
25
30
35
0
-100
-200
-300
-400
-500
-600

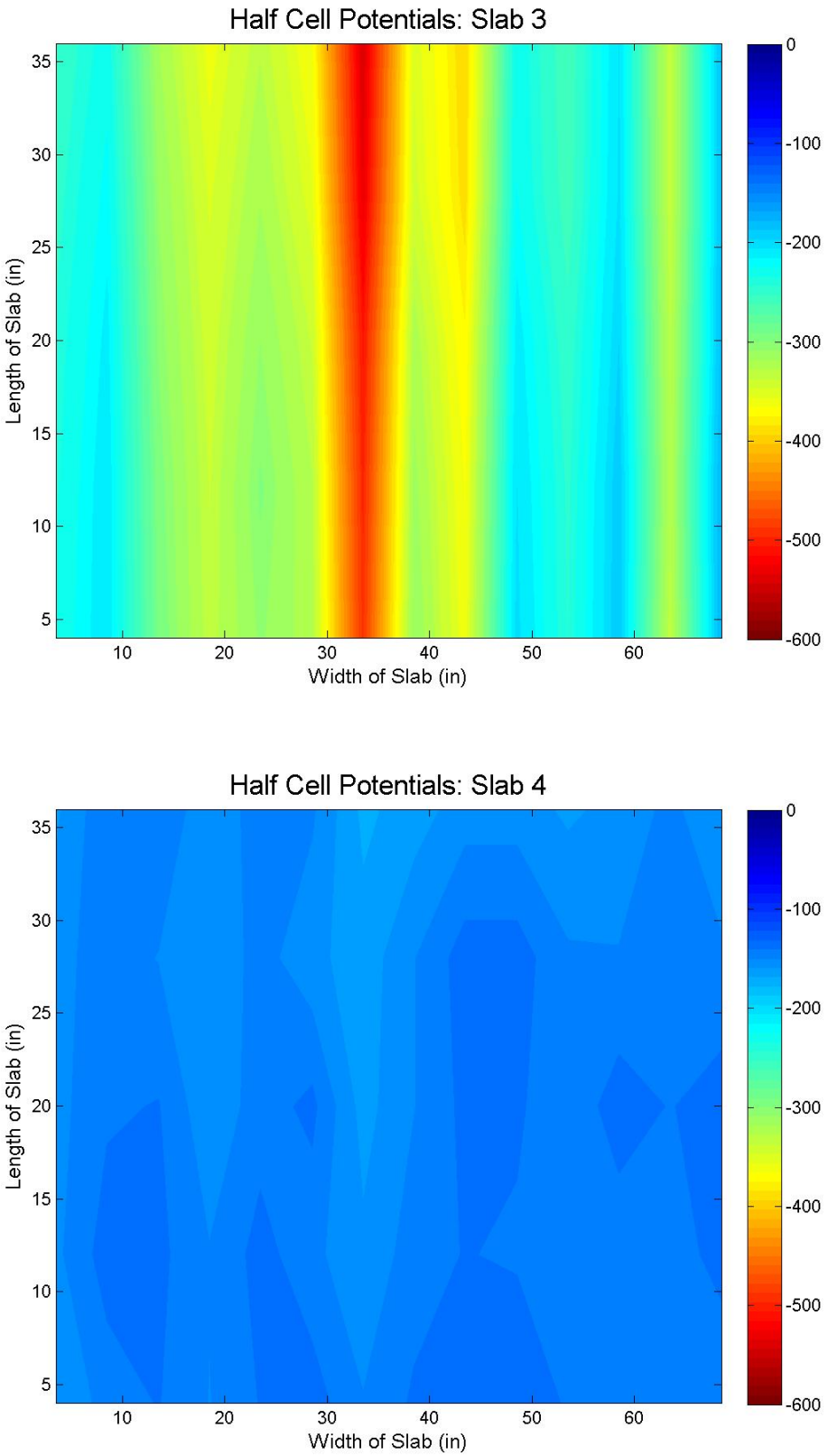

Figure A-6: Week of April 20, 2012

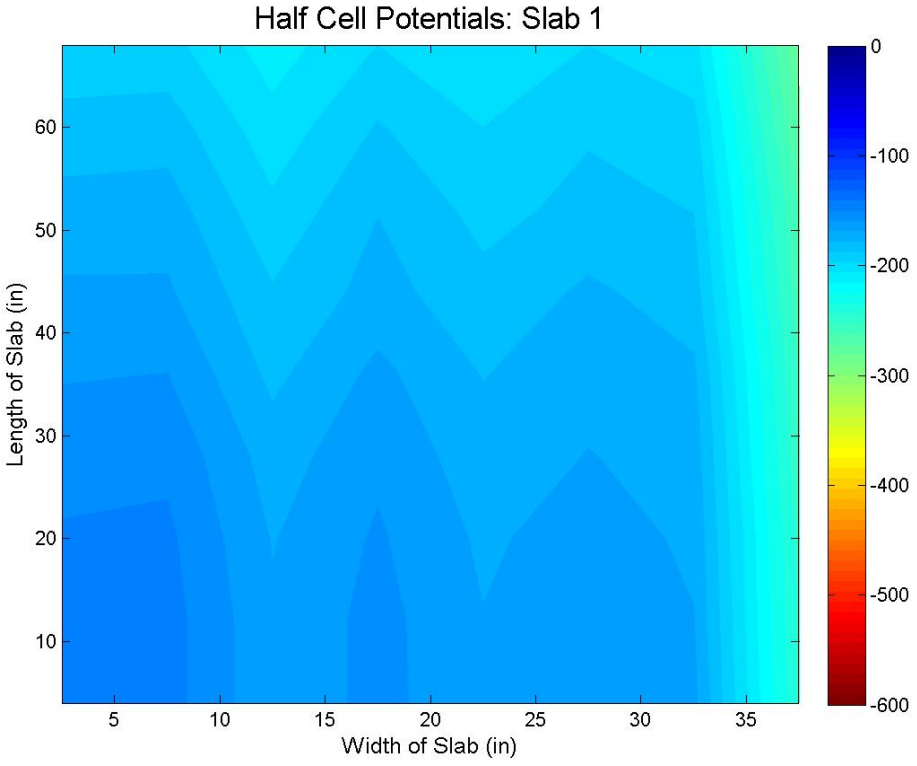
Half Cell Potentials: Slab 1
Length of Slab (in)
Width of Slab (in)
10
20
30
40
50
60
5
10
15
20
25
30
35
0
-100
-200
-300
-400
-500
-600

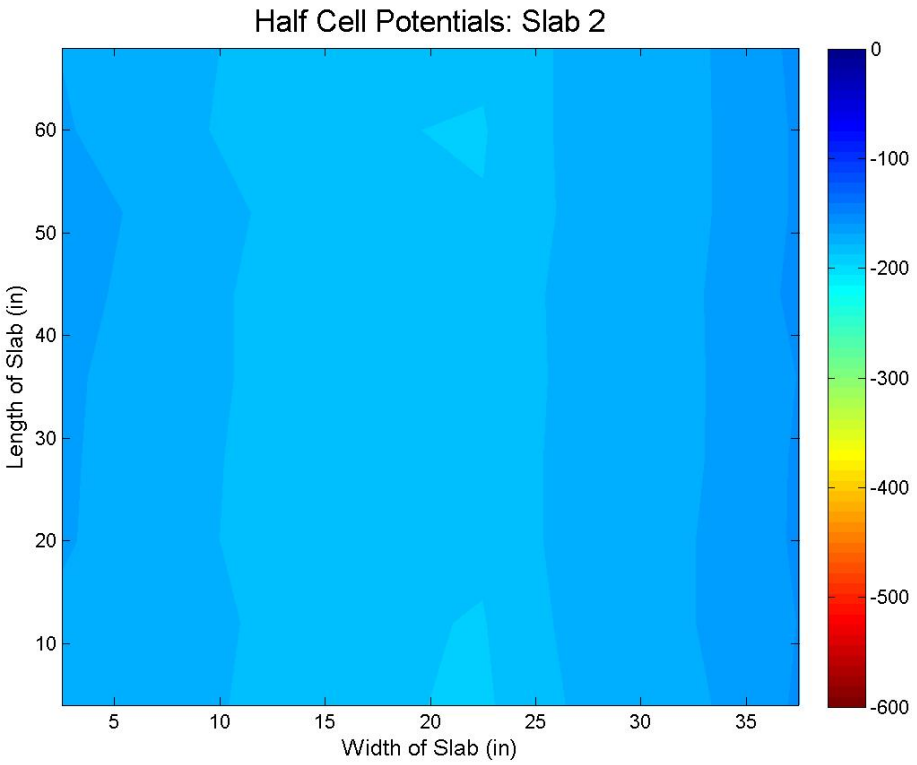
Half Cell Potentials: Slab 2
Length of Slab (in)
Width of Slab (in)
10
20
30
40
50
60
5
10
15
20
25
30
35
0
-100
-200
-300
-400
-500
-600

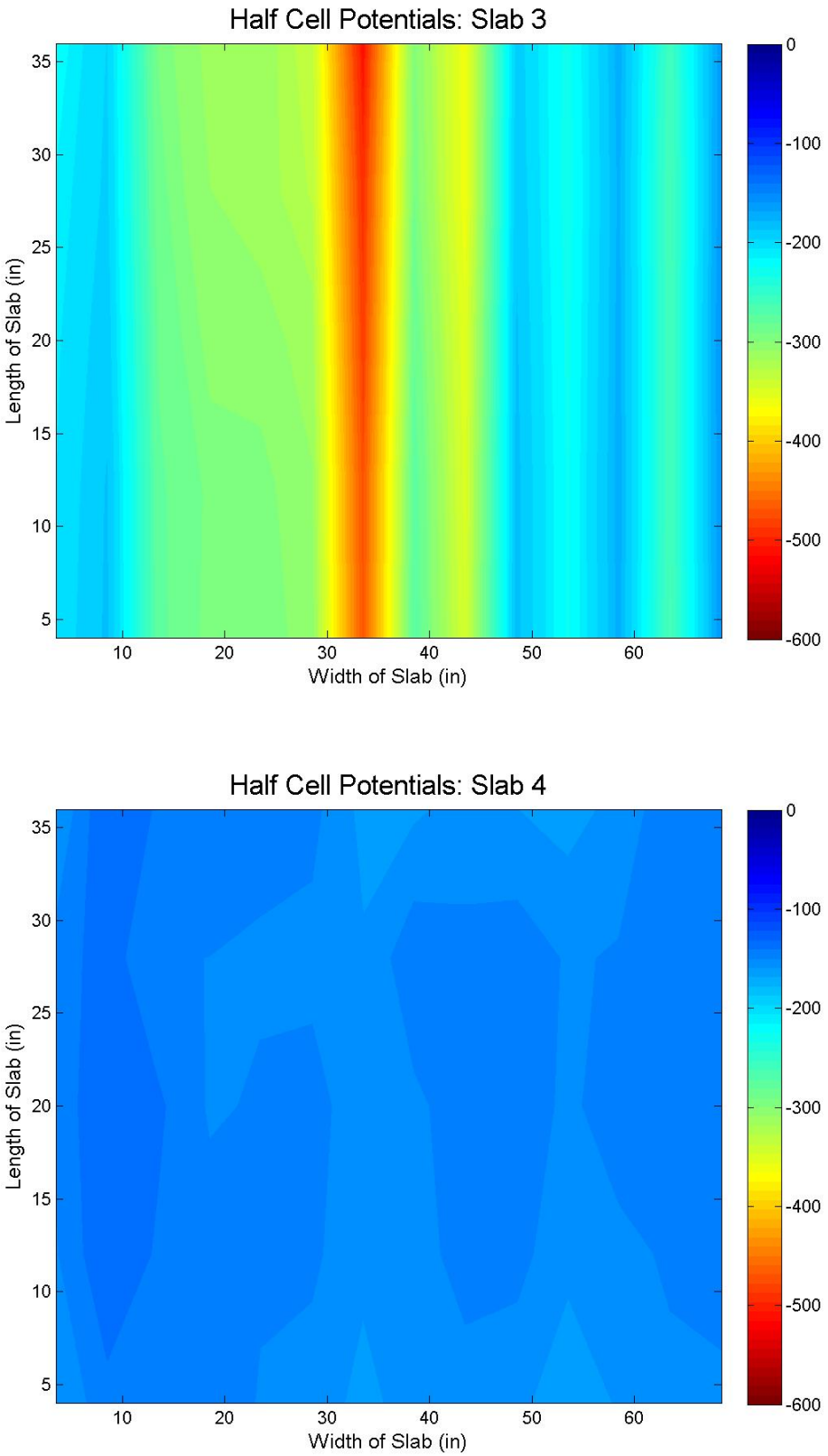

Figure A-7: Week of April 27, 2012

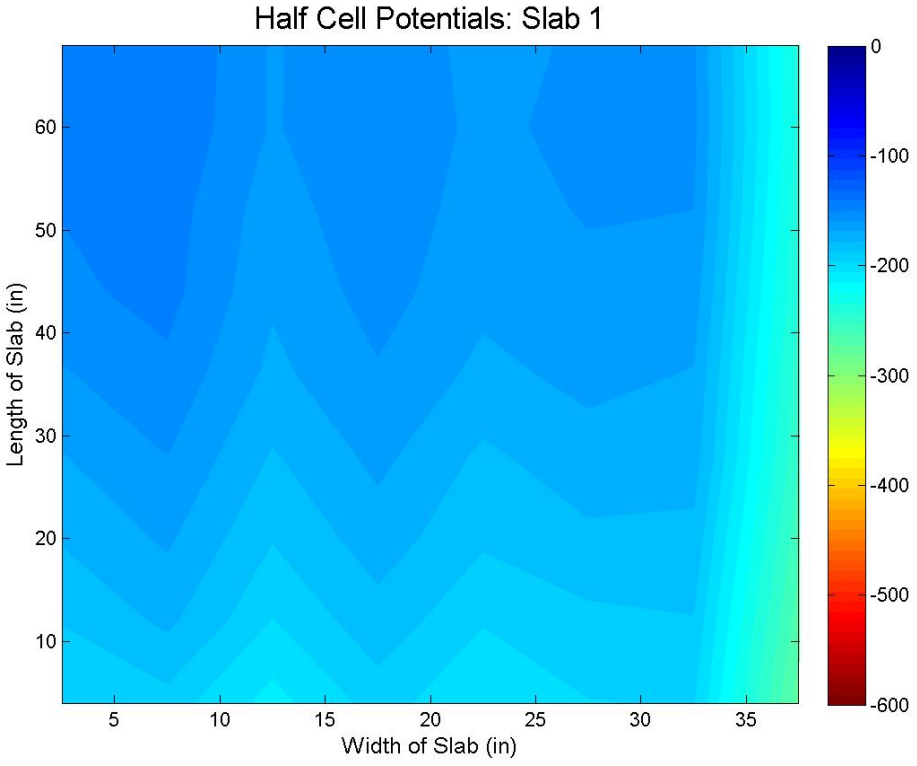
Half Cell Potentials: Slab 1
Length of Slab (in)
Width of Slab (in)
10
20
30
40
50
60
5
10
15
20
25
30
35
0
-100
-200
-300
-400
-500
-600

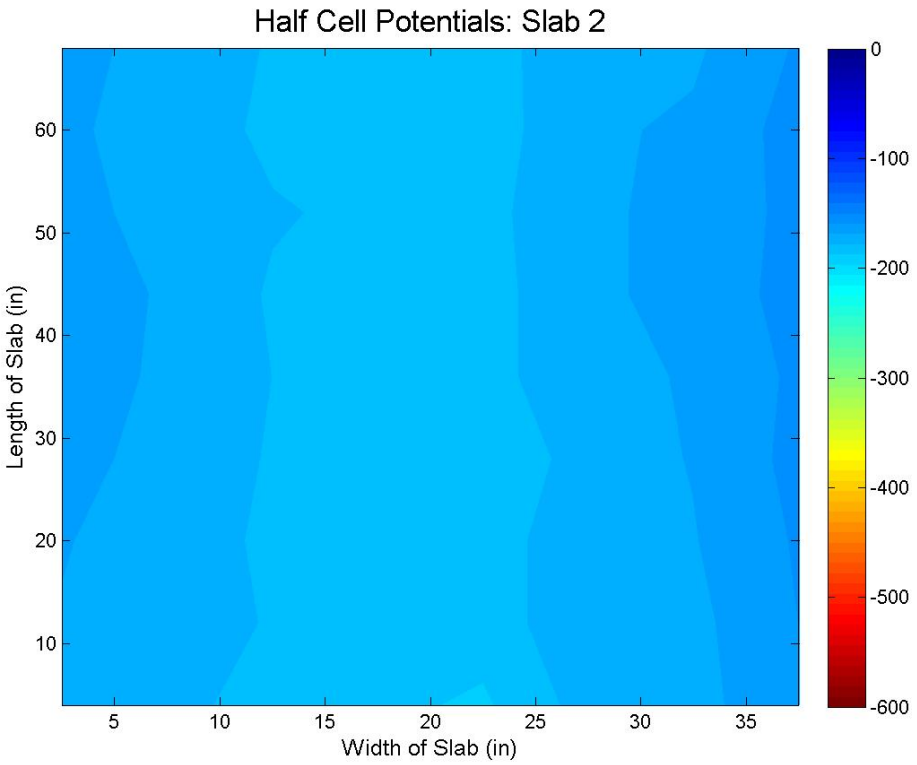
Half Cell Potentials: Slab 2
Length of Slab (in)
Width of Slab (in)
10
20
30
40
50
60
5
10
15
20
25
30
35
0
-100
-200
-300
-400
-500
-600

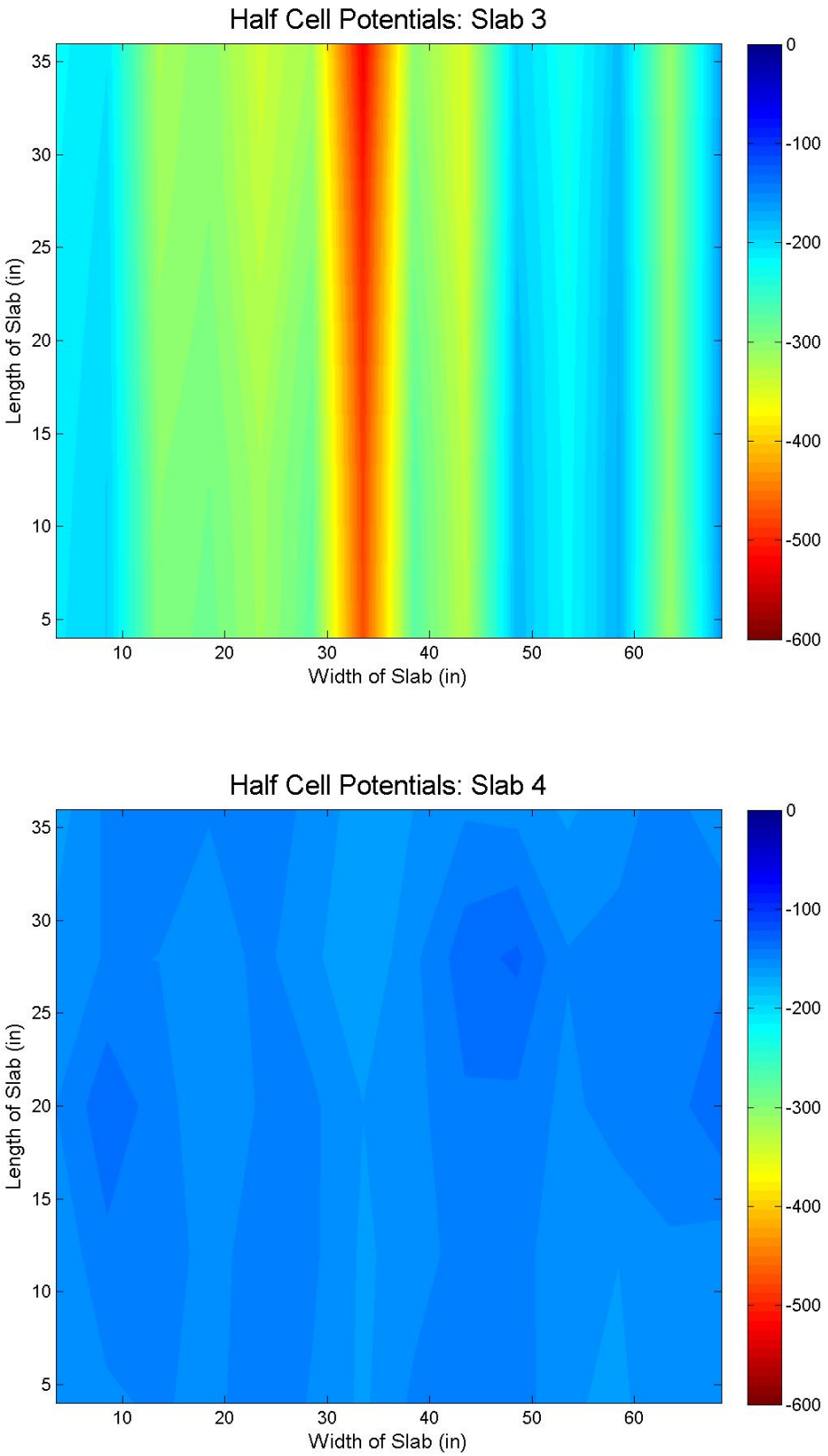

Figure A-8: Week of May 4, 2012

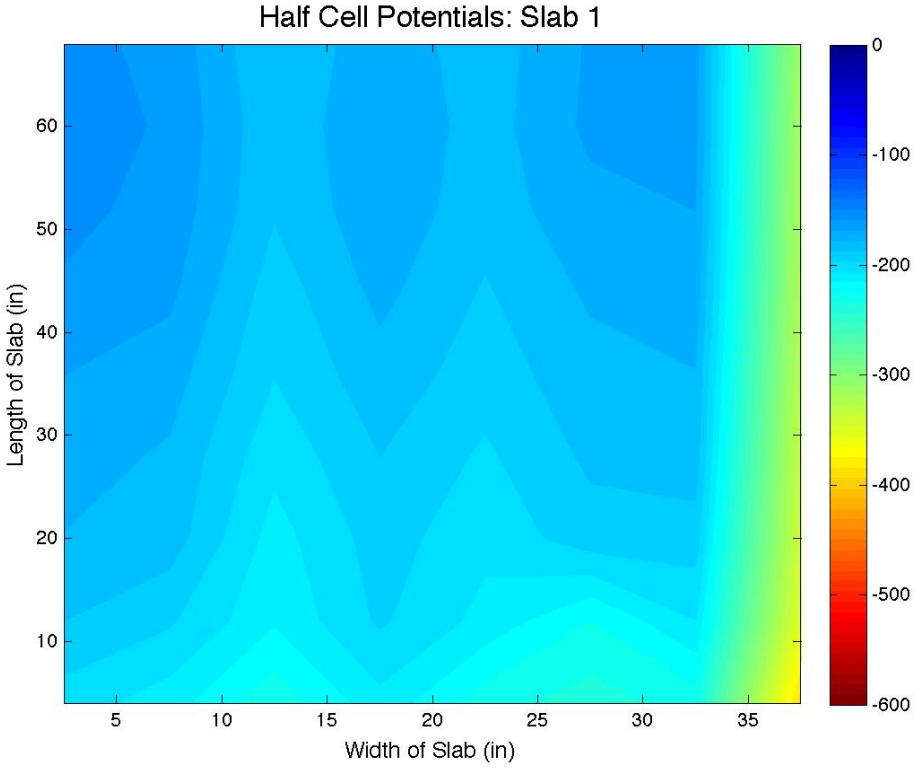
Half Cell Potentials: Slab 1
Length of Slab (in)
Width of Slab (in)
10
20
30
40
50
60
5
10
15
20
25
30
35
0
-100
-200
-300
-400
-500
-600

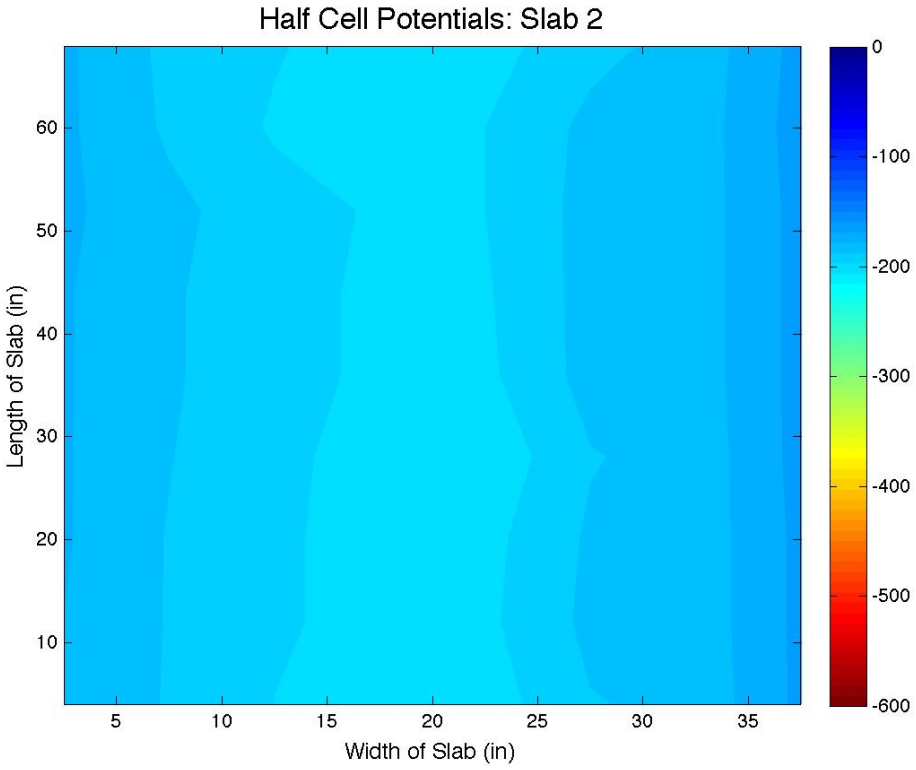
Half Cell Potentials: Slab 2
Length of Slab (in)
Width of Slab (in)
10
20
30
40
50
60
5
10
15
20
25
30
35
0
-100
-200
-300
-400
-500
-600

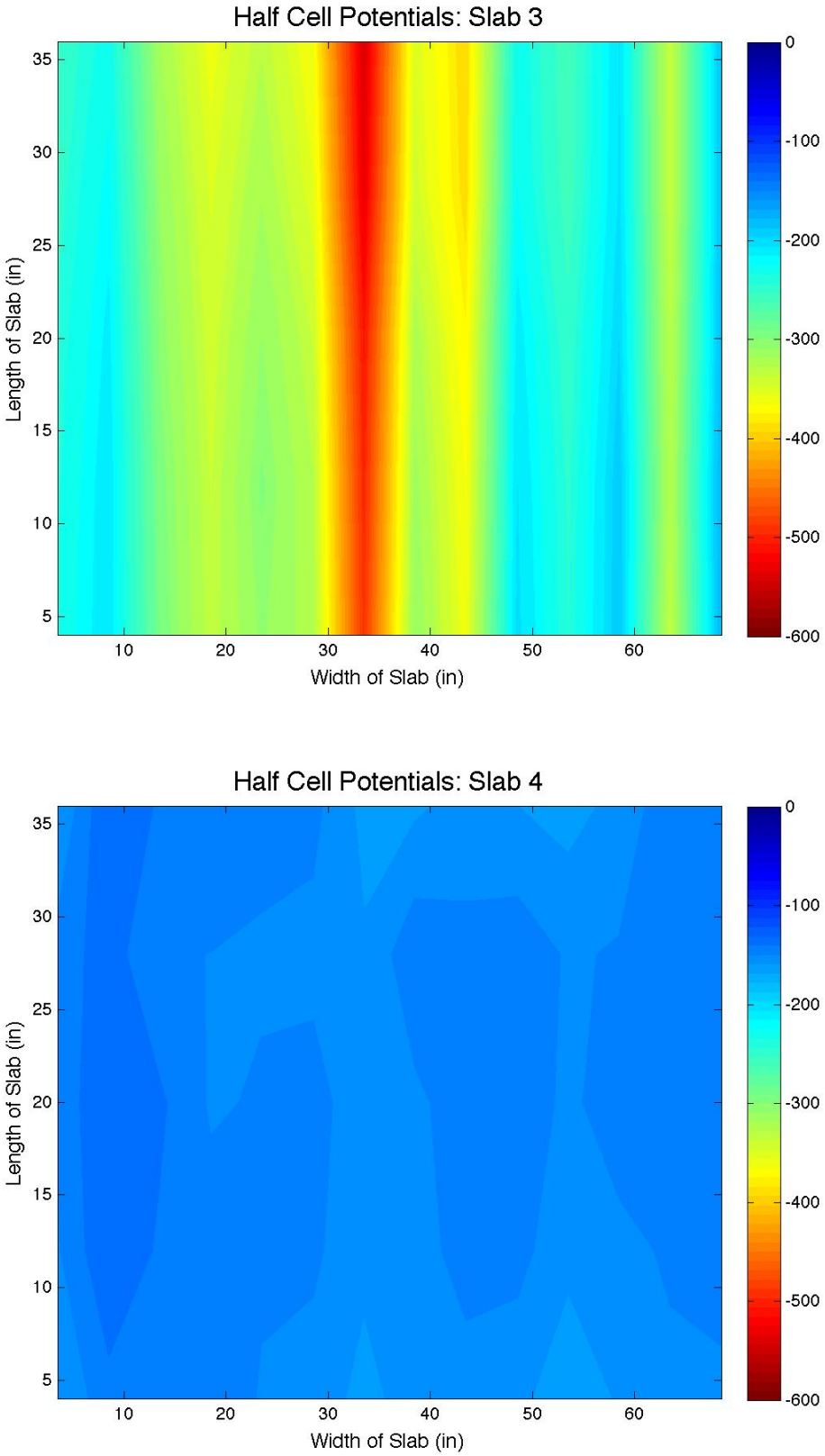

Figure A-9: Week of May 11, 2012

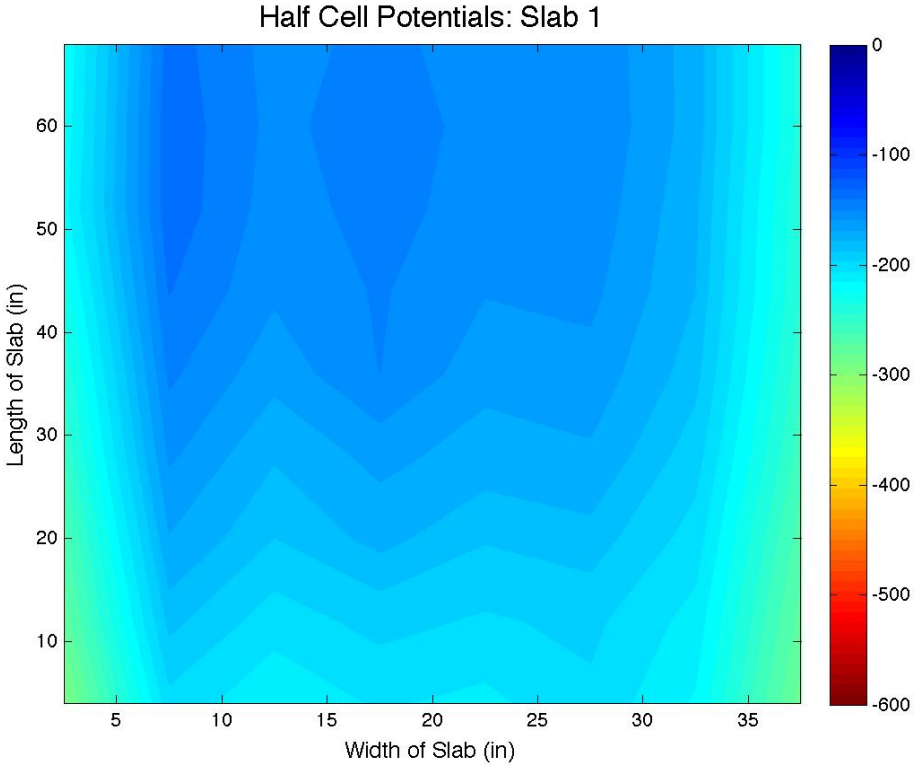
Half Cell Potentials: Slab 1
Length of Slab (in)
Width of Slab (in)
10
20
30
40
50
60
5
10
15
20
25
30
35
0
-100
-200
-300
-400
-500
-600

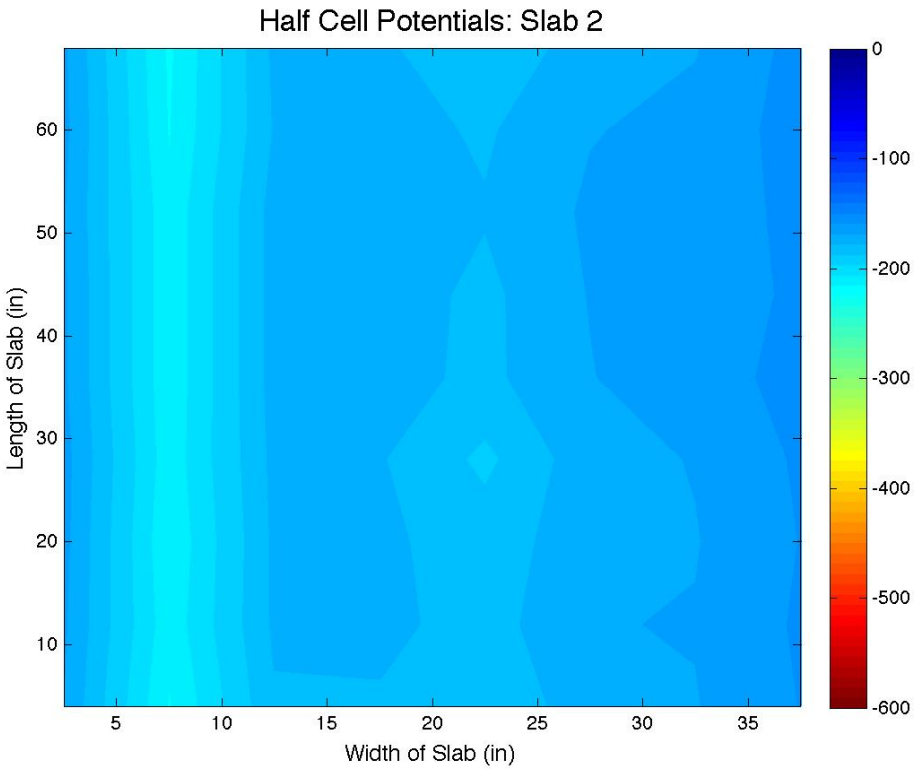
Half Cell Potentials: Slab 2
Length of Slab (in)
Width of Slab (in)
10
20
30
40
50
60
5
10
15
20
25
30
35
0
-100
-200
-300
-400
-500
-600

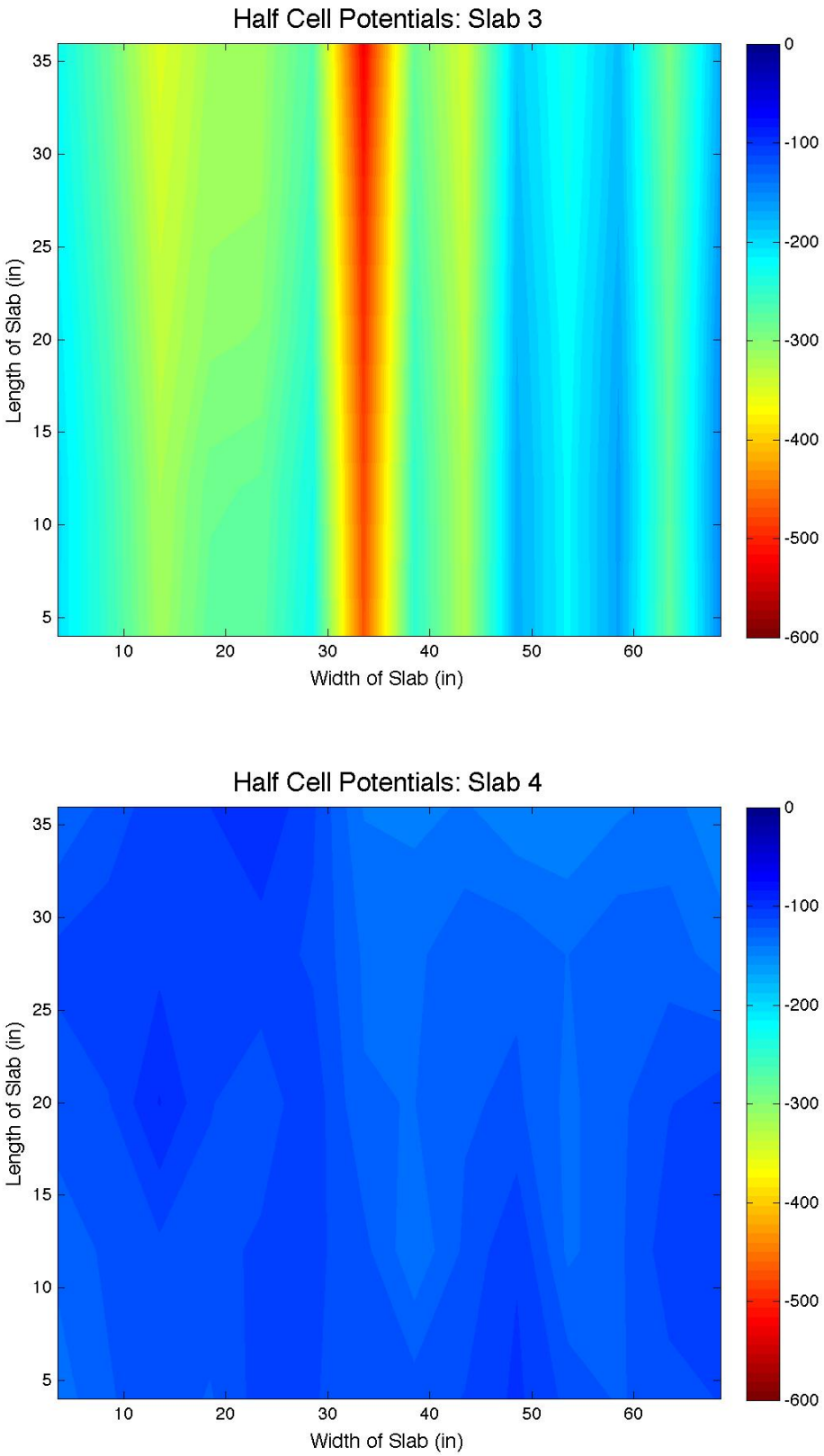

Figure A-10: Week of May 25, 2012

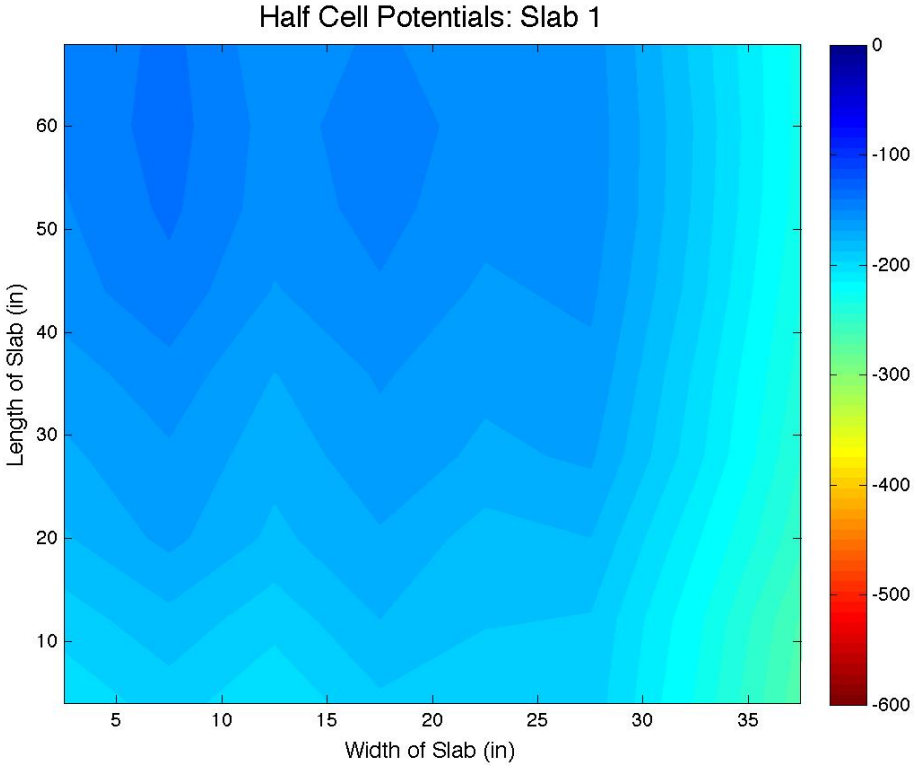
Half Cell Potentials: Slab 1
Length of Slab (in)
Width of Slab (in)
10
20
30
40
50
60
5
10
15
20
25
30
35
0
-100
-200
-300
-400
-500
-600

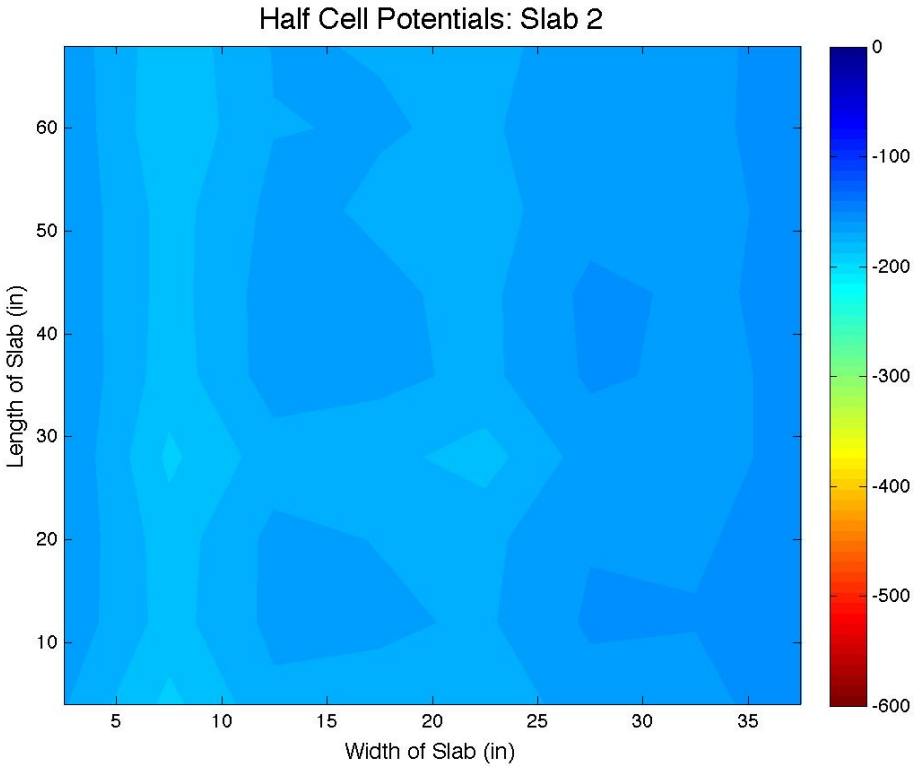
Half Cell Potentials: Slab 2
Length of Slab (in)
Width of Slab (in)
10
20
30
40
50
60
5
10
15
20
25
30
35
0
-100
-200
-300
-400
-500
-600

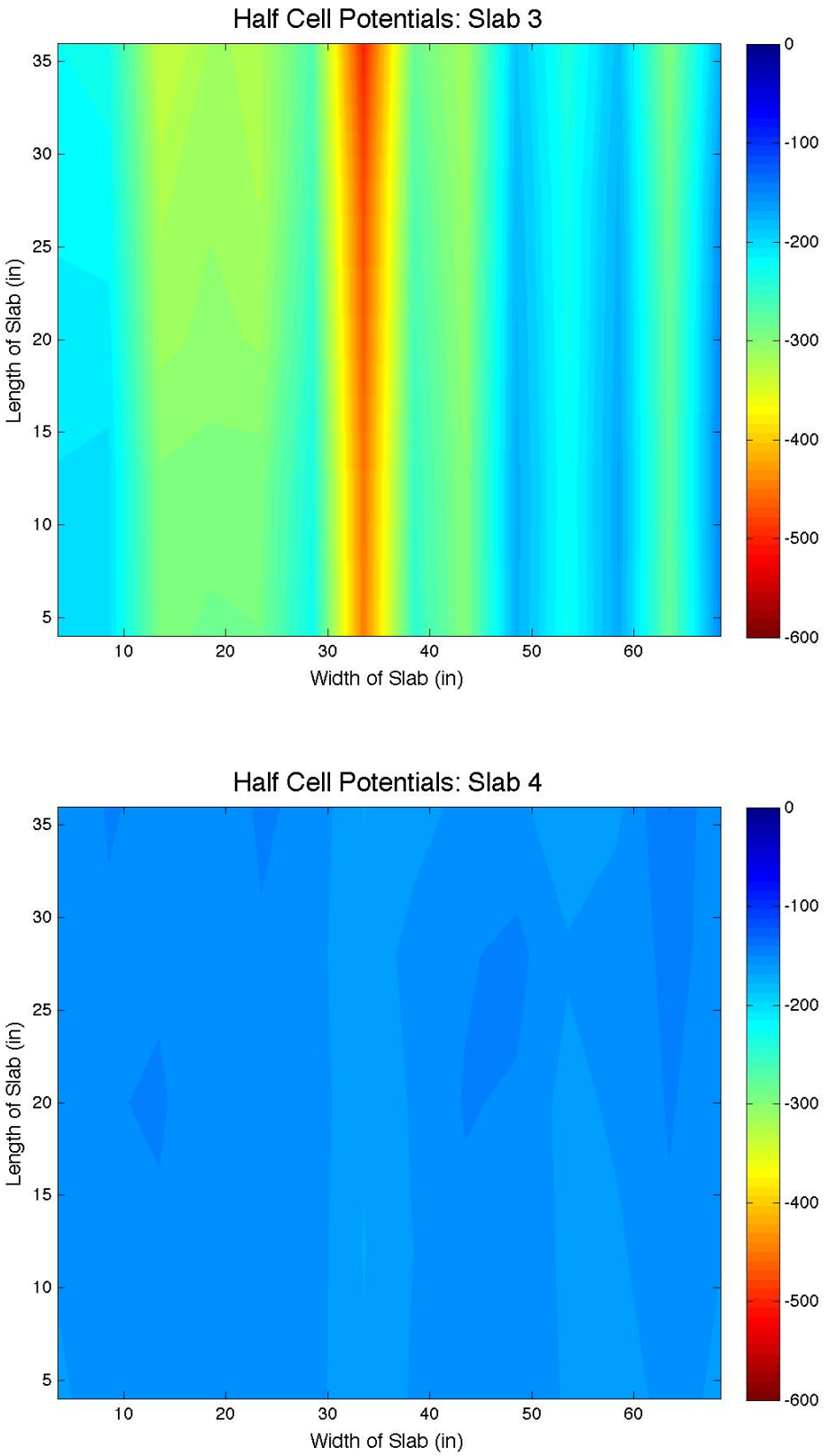

Figure A-11: Week of June 1, 2012

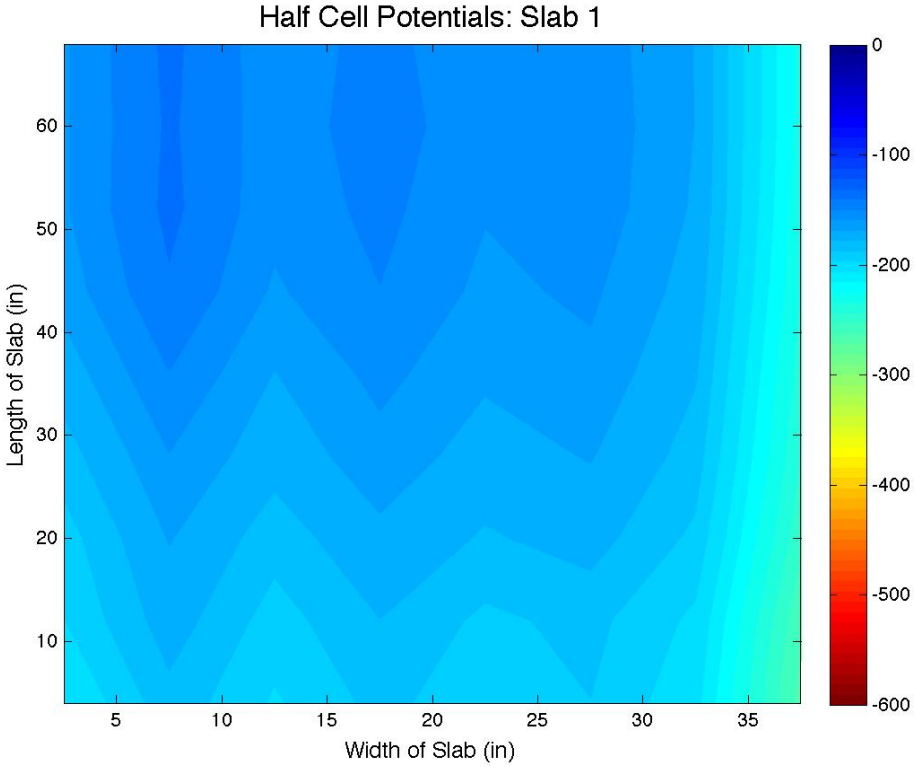
Half Cell Potentials: Slab 1
Length of Slab (in)
Width of Slab (in)
10
20
30
40
50
60
5
10
15
20
25
30
35
0
-100
-200
-300
-400
-500
-600

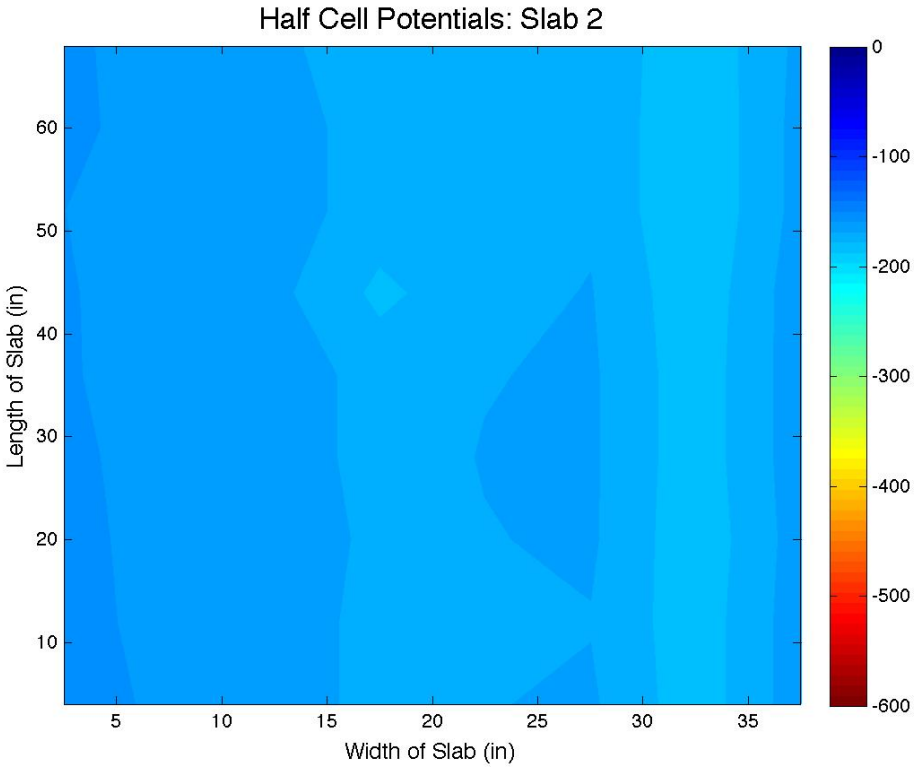
Half Cell Potentials: Slab 2
Length of Slab (in)
Width of Slab (in)
10
20
30
40
50
60
5
10
15
20
25
30
35
0
-100
-200
-300
-400
-500
-600

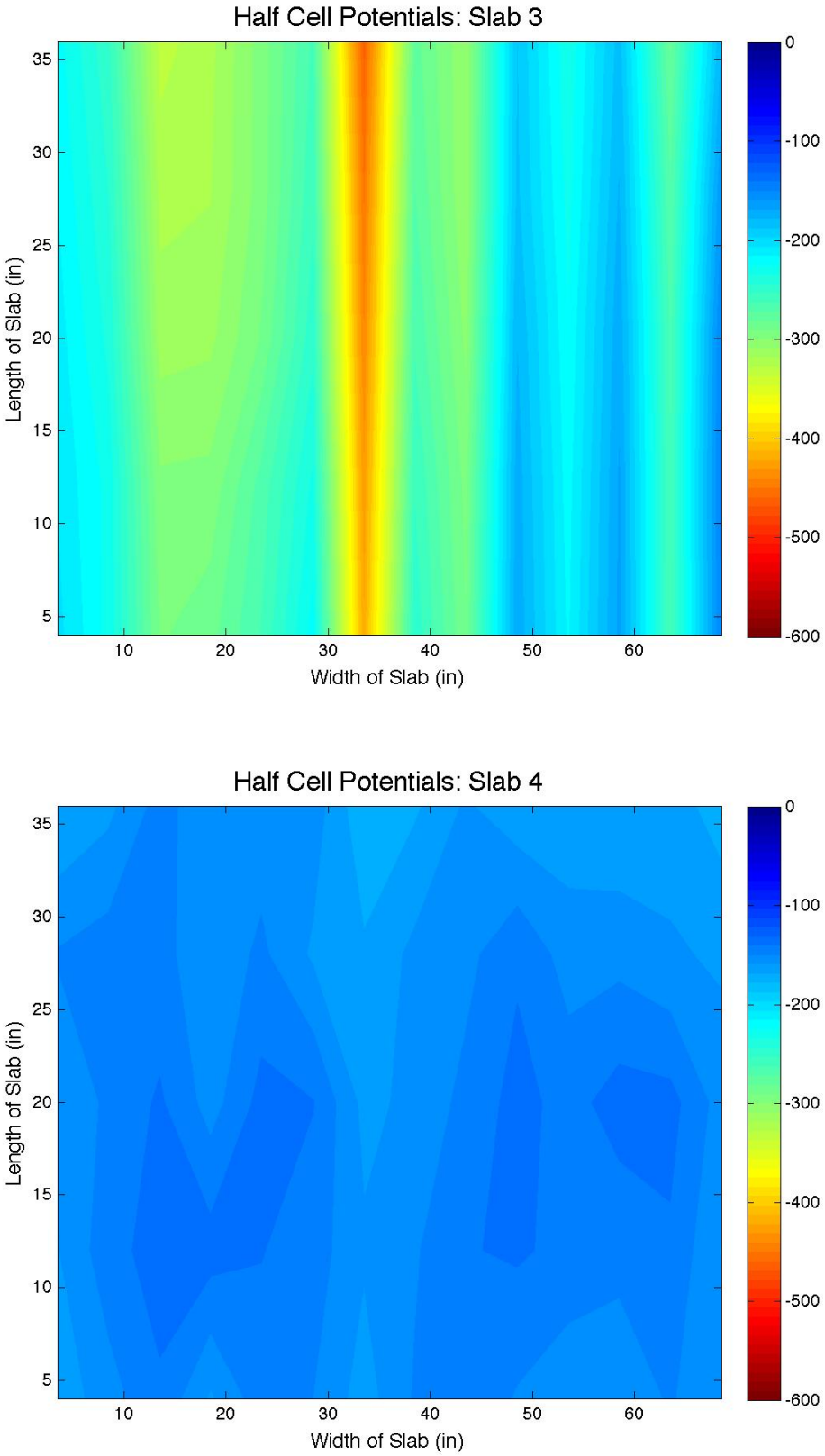

Figure A-12: Week of June 8, 2012

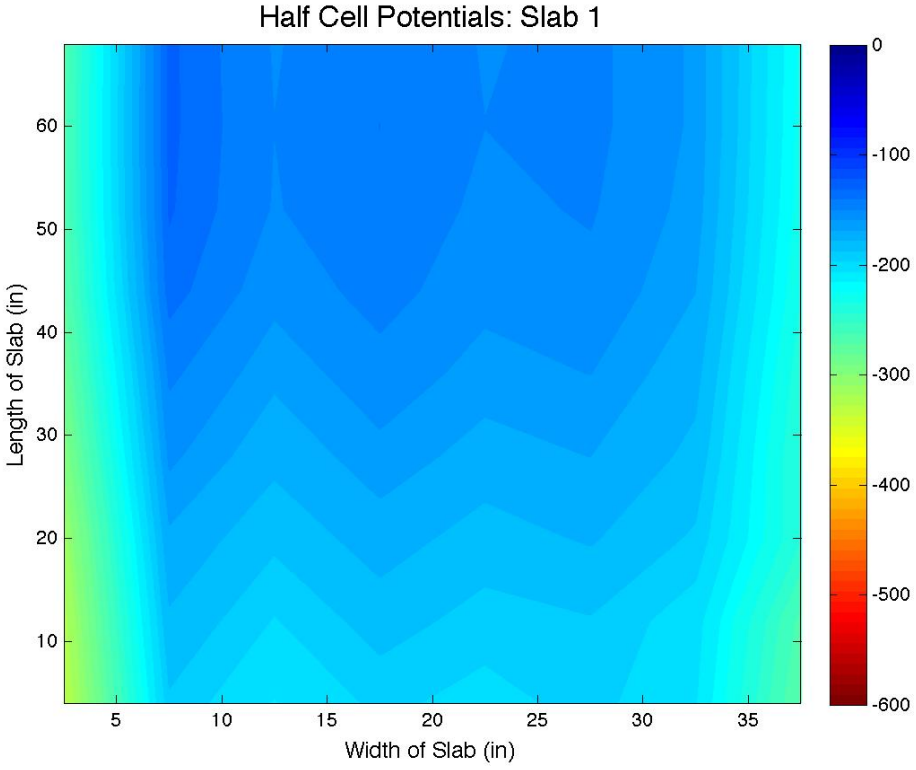
Half Cell Potentials: Slab 1
Length of Slab (in)
Width of Slab (in)
10
20
30
40
50
60
5
10
15
20
25
30
35
0
-100
-200
-300
-400
-500
-600

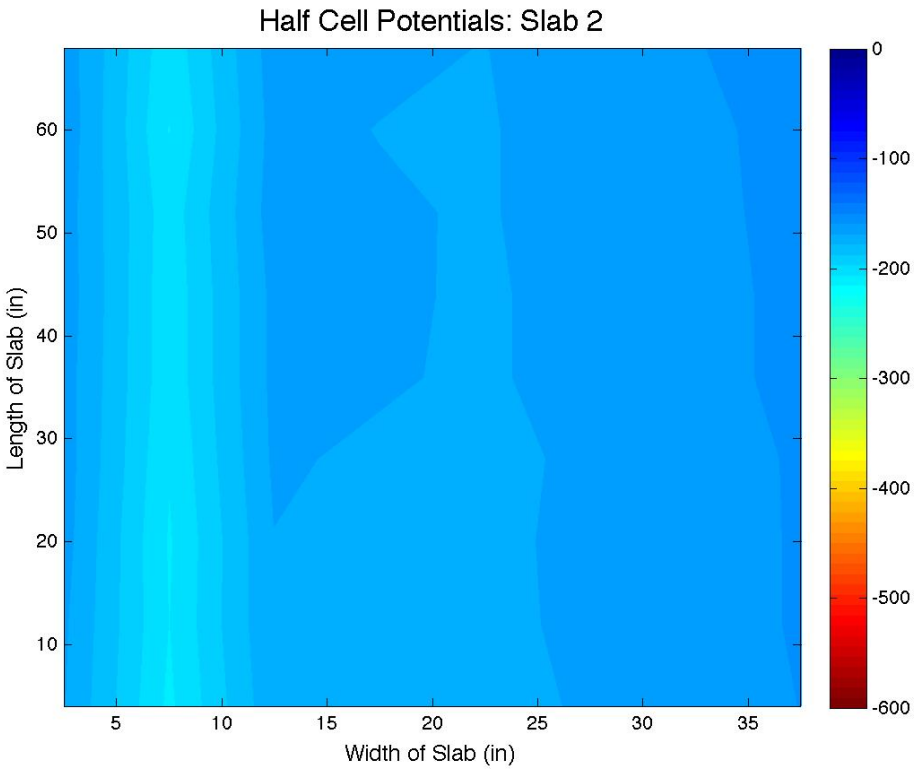
Half Cell Potentials: Slab 2
Length of Slab (in)
Width of Slab (in)
10
20
30
40
50
60
5
10
15
20
25
30
35
0
-100
-200
-300
-400
-500
-600

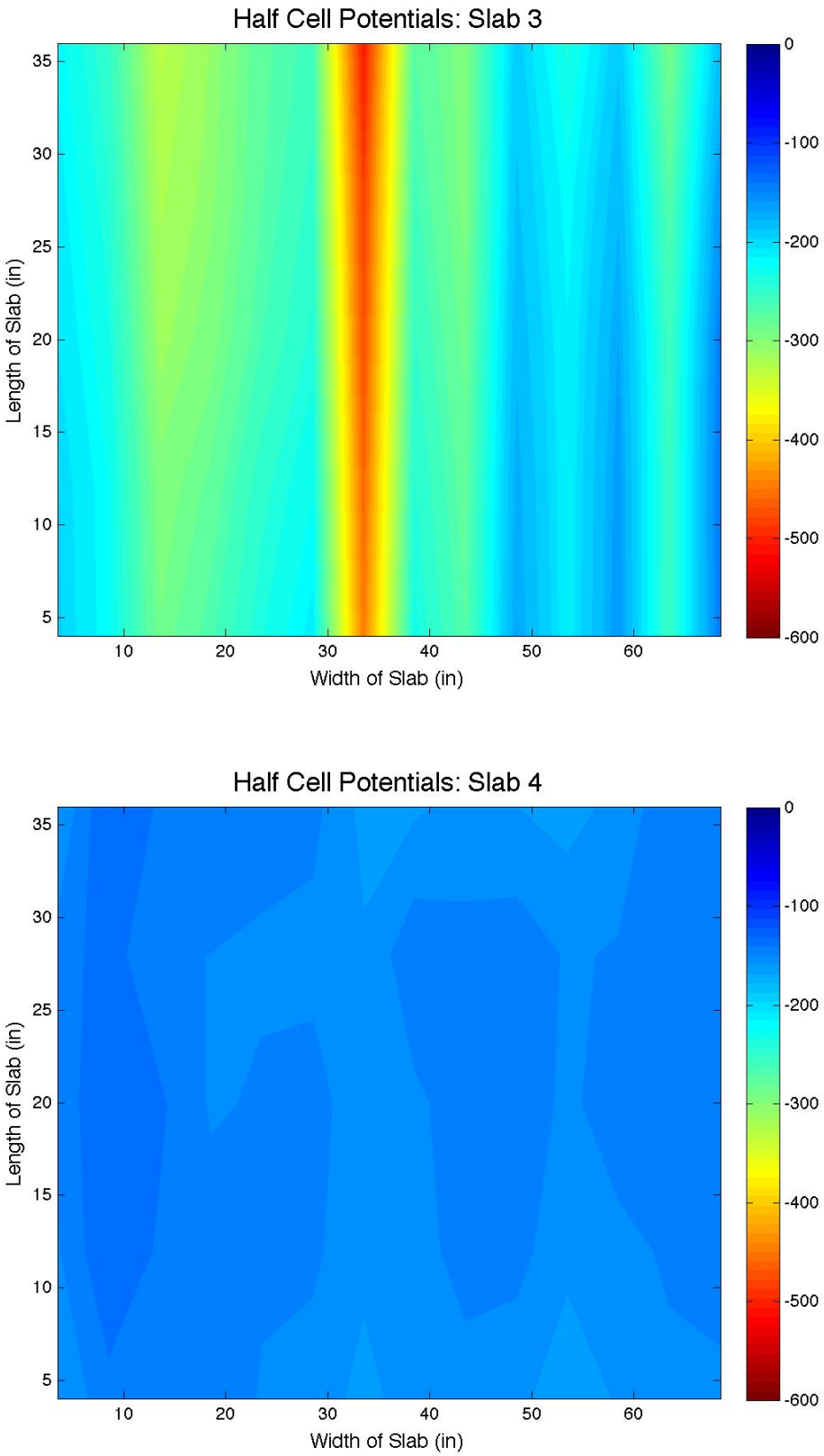

Figure A-13: Week of June 15, 2012

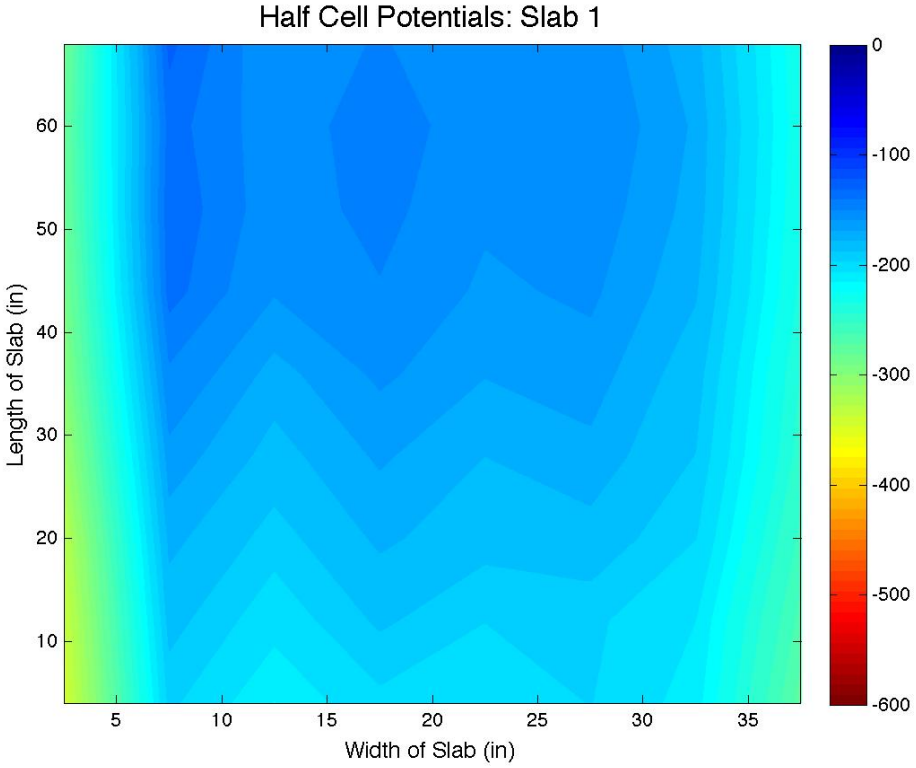
Half Cell Potentials: Slab 1
Length of Slab (in)
Width of Slab (in)
10
20
30
40
50
60
5
10
15
20
25
30
35
0
-100
-200
-300
-400
-500
-600

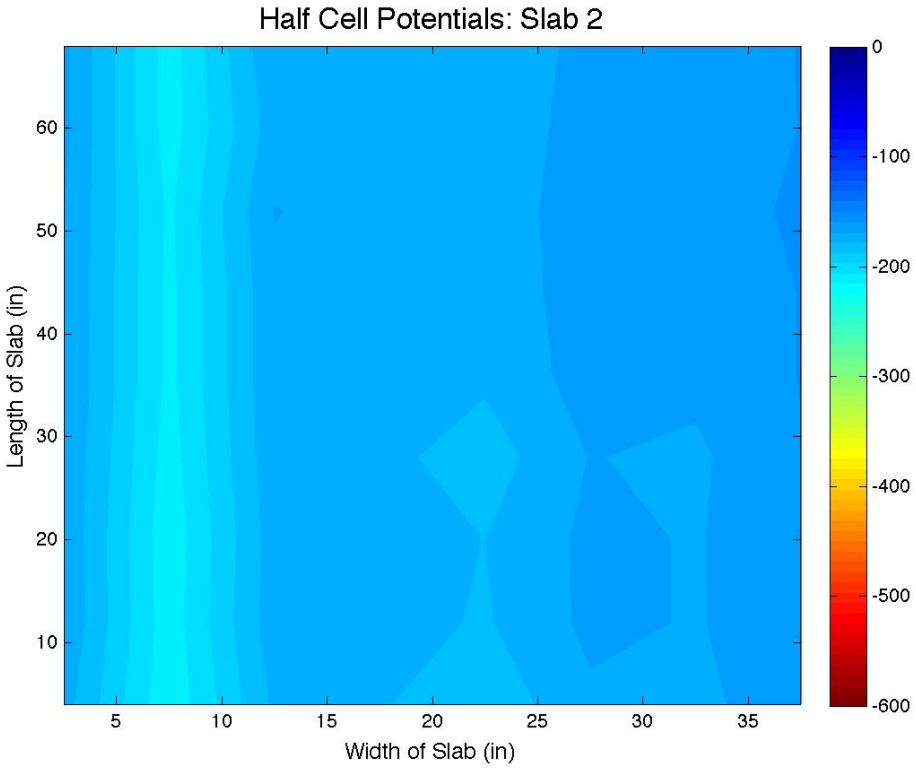
Half Cell Potentials: Slab 2
Length of Slab (in)
Width of Slab (in)
10
20
30
40
50
60
5
10
15
20
25
30
35
0
-100
-200
-300
-400
-500
-600

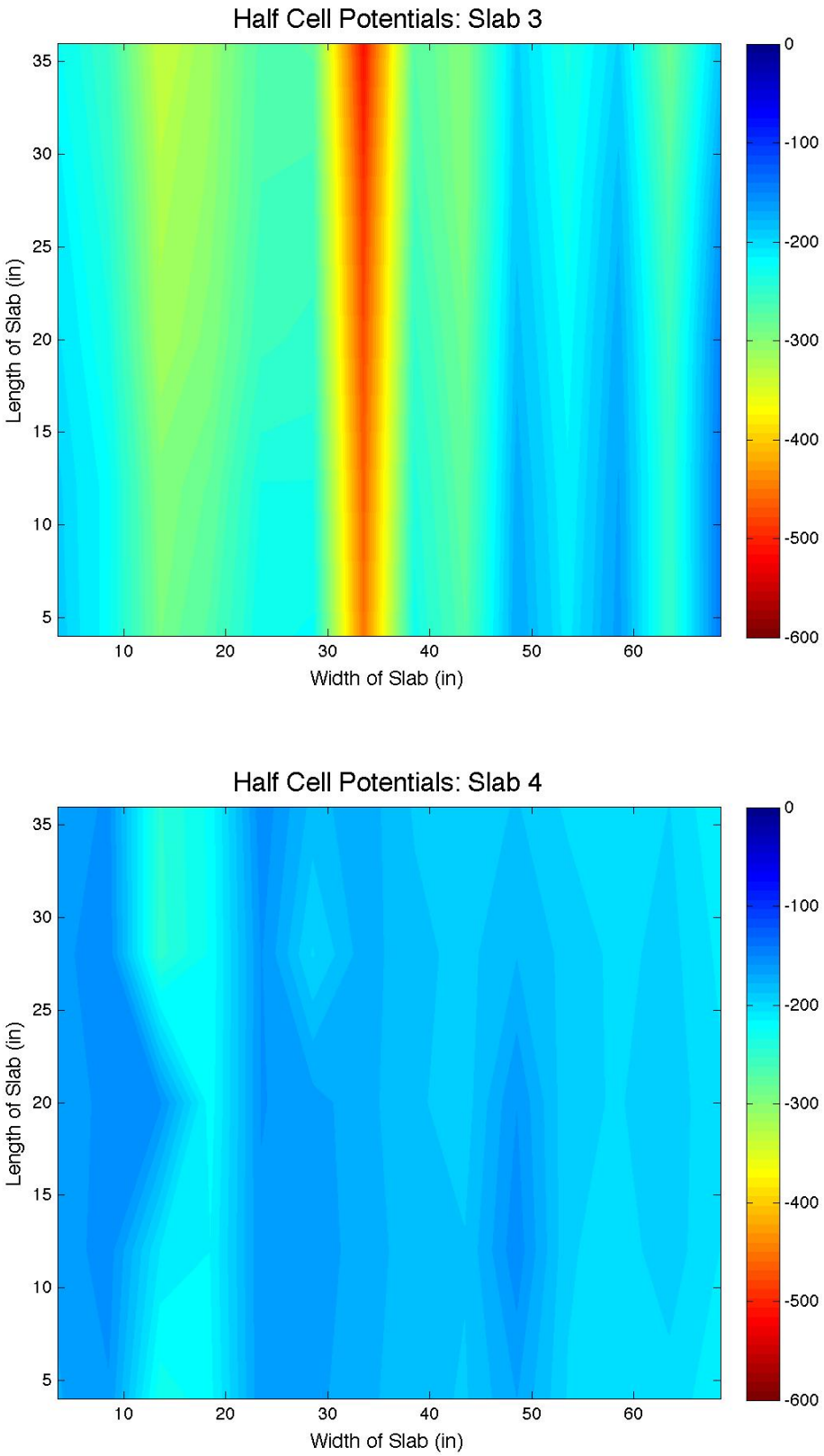

Figure A-14: Week of June 22, 2012

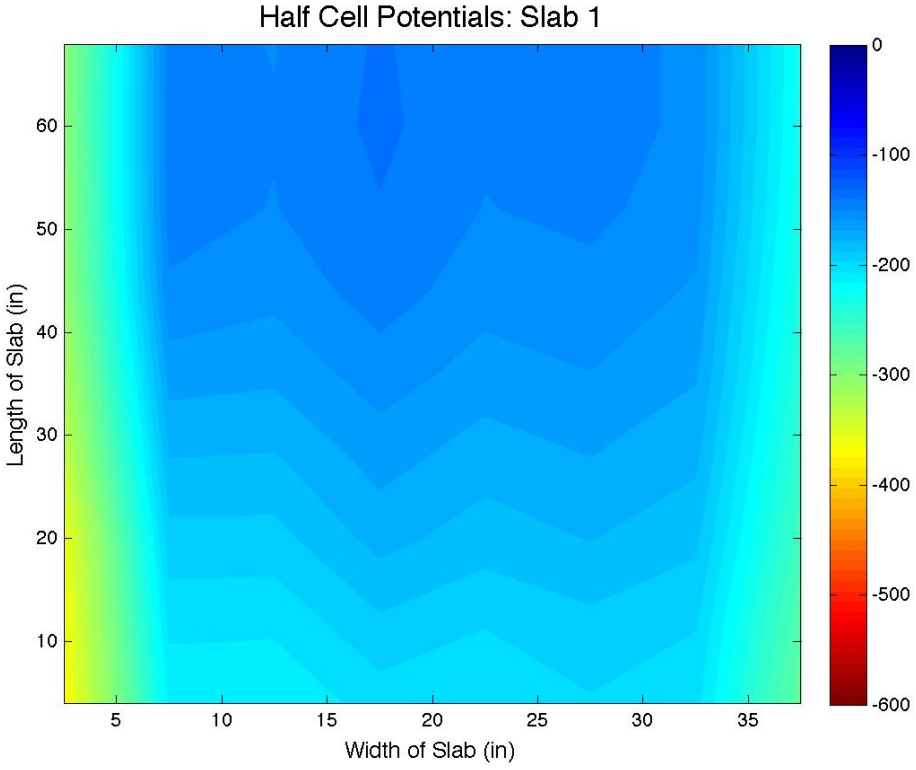
Half Cell Potentials: Slab 1
Length of Slab (in)
Width of Slab (in)
10
20
30
40
50
60
5
10
15
20
25
30
35
0
-100
-200
-300
-400
-500
-600

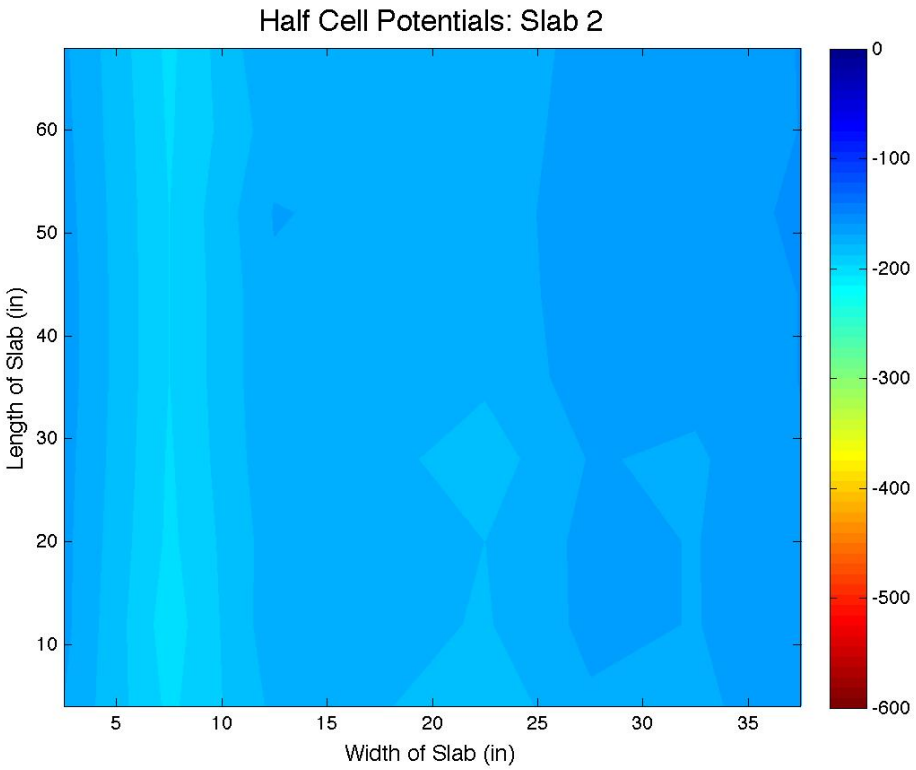
Half Cell Potentials: Slab 2
Length of Slab (in)
Width of Slab (in)
10
20
30
40
50
60
5
10
15
20
25
30
35
0
-100
-200
-300
-400
-500
-600

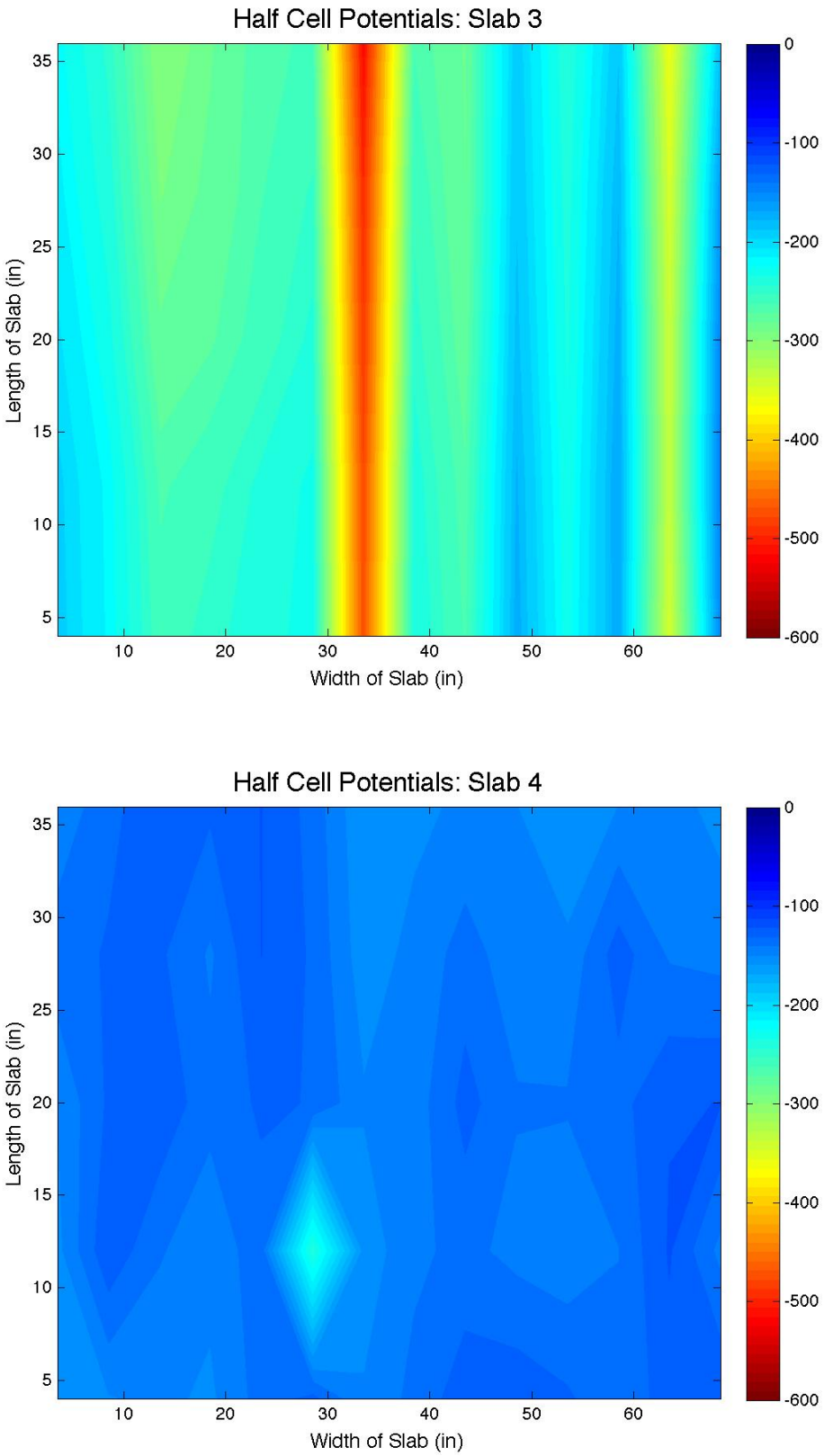

Figure A-15: Week of June 29, 2012

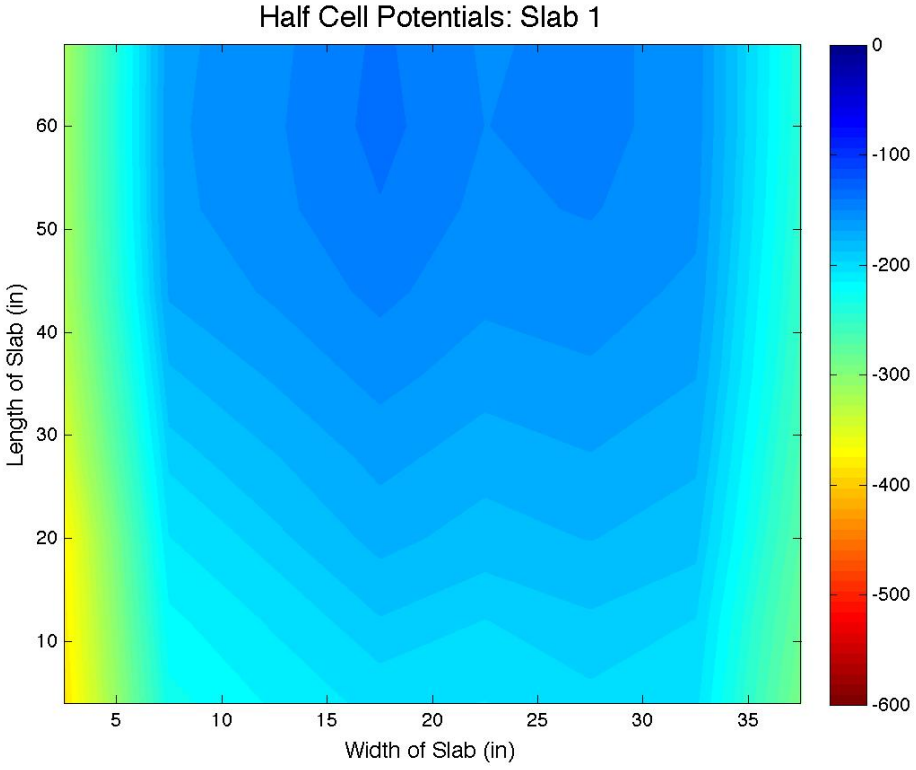
Half Cell Potentials: Slab 1
Length of Slab (in)
Width of Slab (in)
10
20
30
40
50
60
5
10
15
20
25
30
35
0
-100
-200
-300
-400
-500
-600

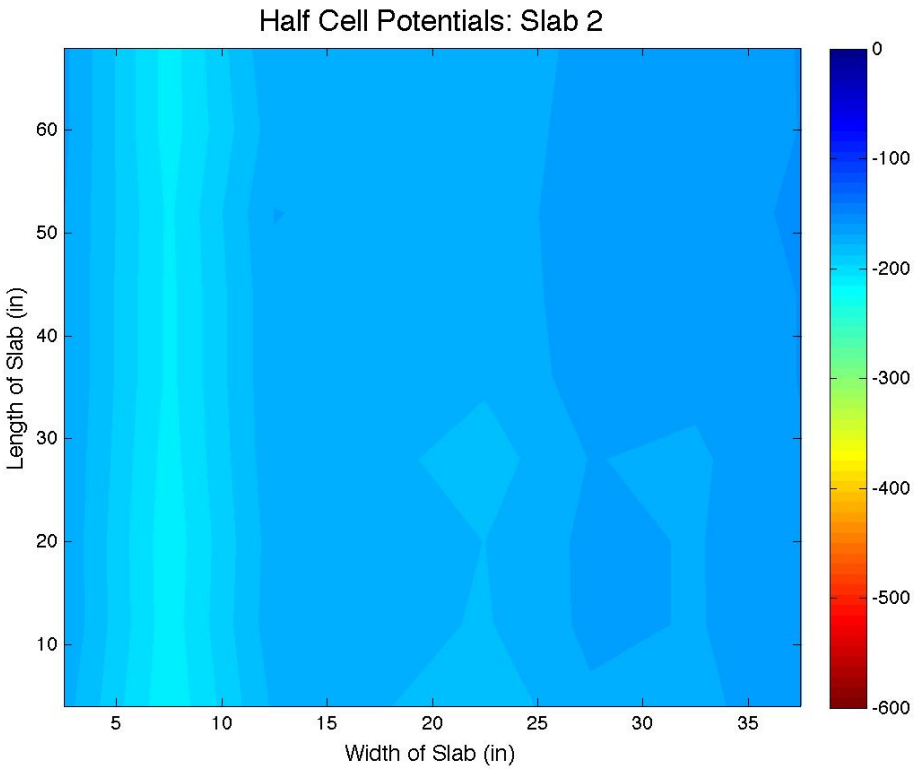
Half Cell Potentials: Slab 2
Length of Slab (in)
Width of Slab (in)
10
20
30
40
50
60
5
10
15
20
25
30
35
0
-100
-200
-300
-400
-500
-600

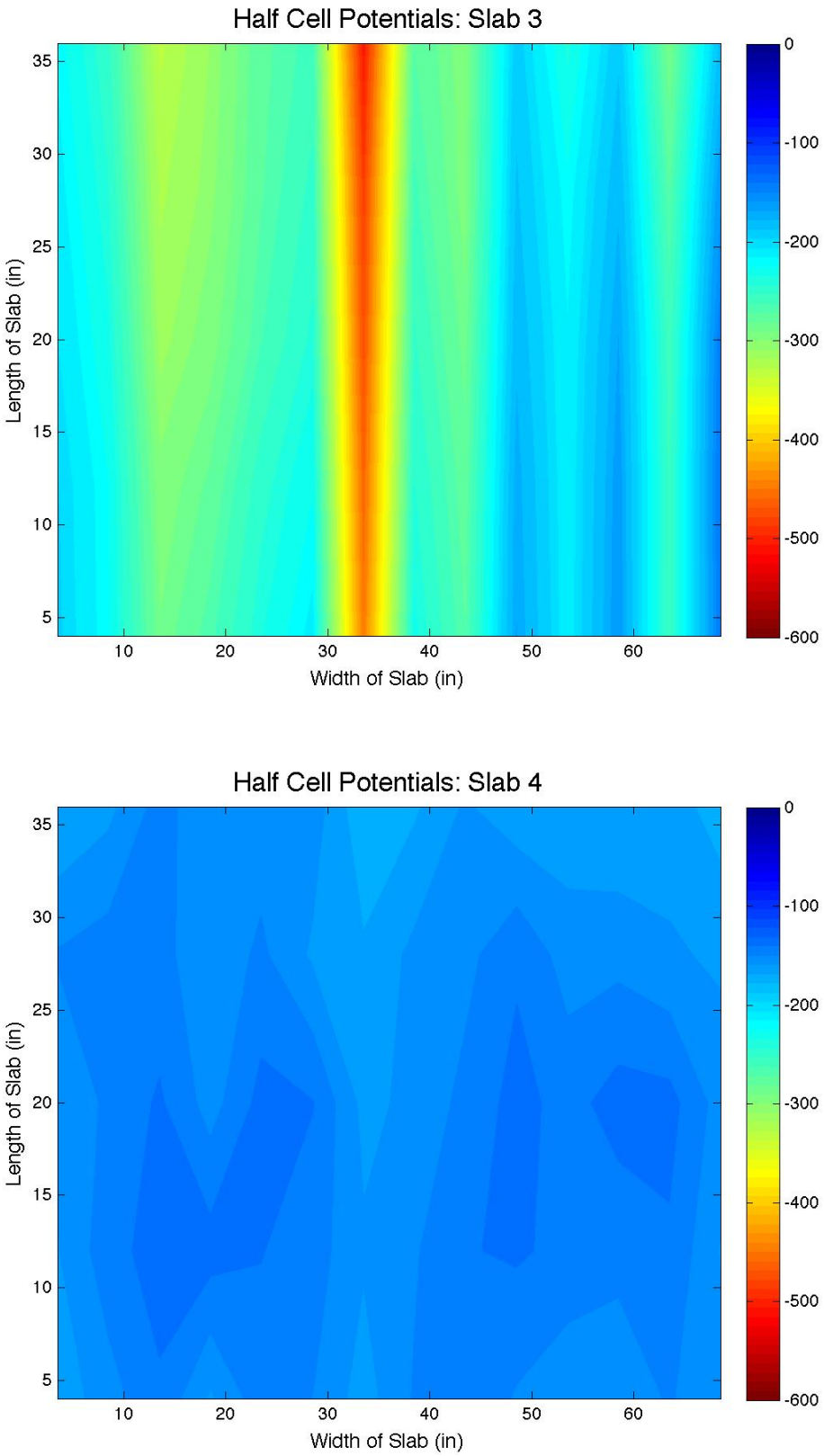

Figure A-16: Week of July 6, 2012

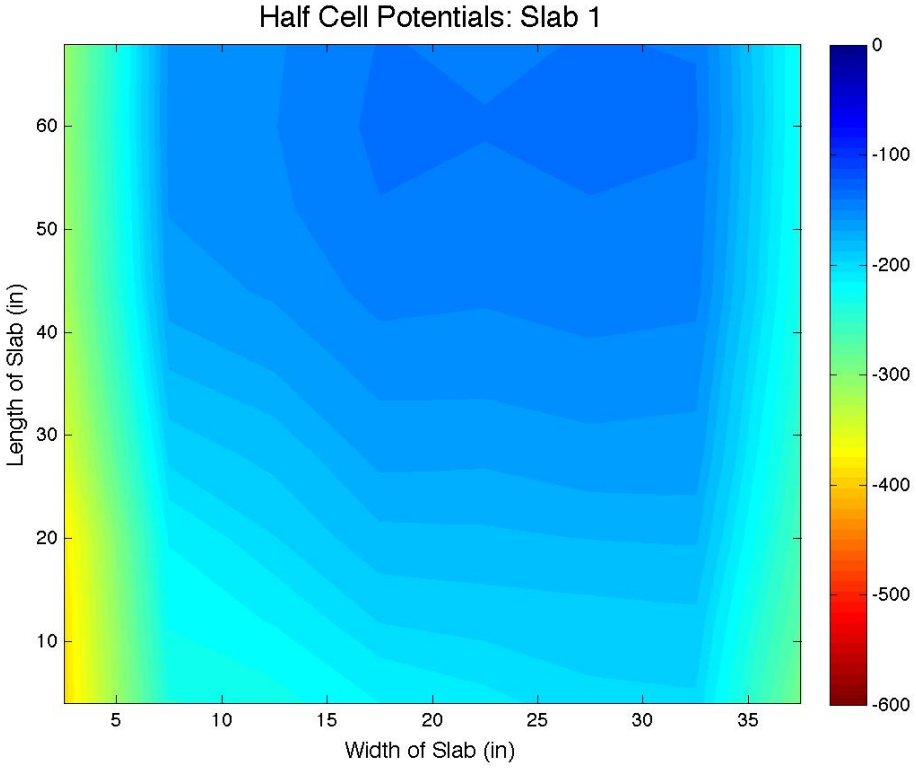
Half Cell Potentials: Slab 1
Length of Slab (in)
Width of Slab (in)
10
20
30
40
50
60
5
10
15
20
25
30
35
0
-100
-200
-300
-400
-500
-600

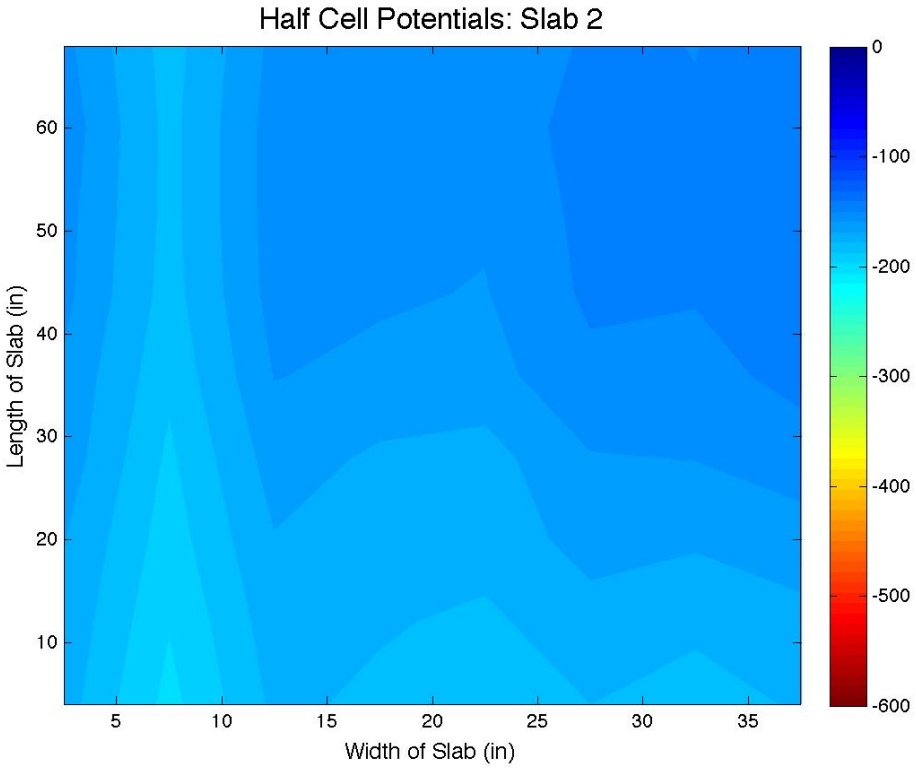
Half Cell Potentials: Slab 2
Length of Slab (in)
Width of Slab (in)
10
20
30
40
50
60
5
10
15
20
25
30
35
0
-100
-200
-300
-400
-500
-600

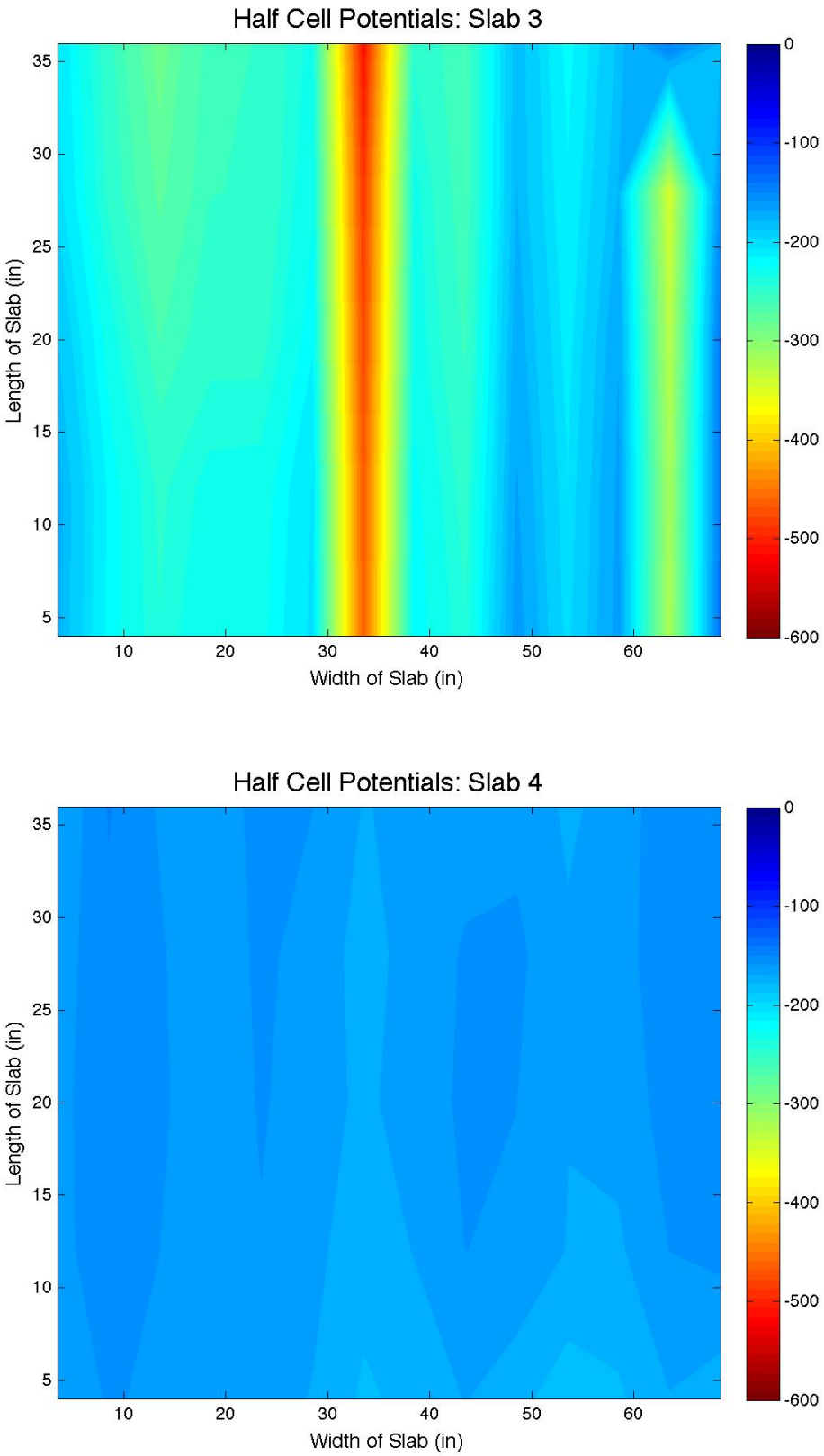

Figure A-17: Week of July 13, 2012

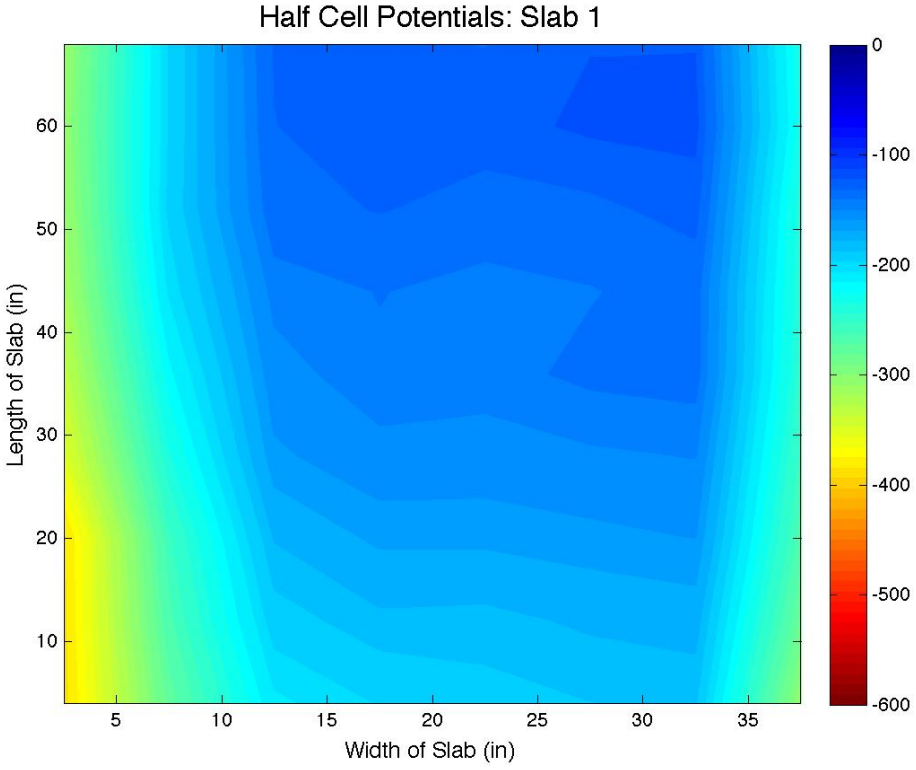
Half Cell Potentials: Slab 1
Length of Slab (in)
Width of Slab (in)
10
20
30
40
50
60
5
10
15
20
25
30
35
0
-100
-200
-300
-400
-500
-600

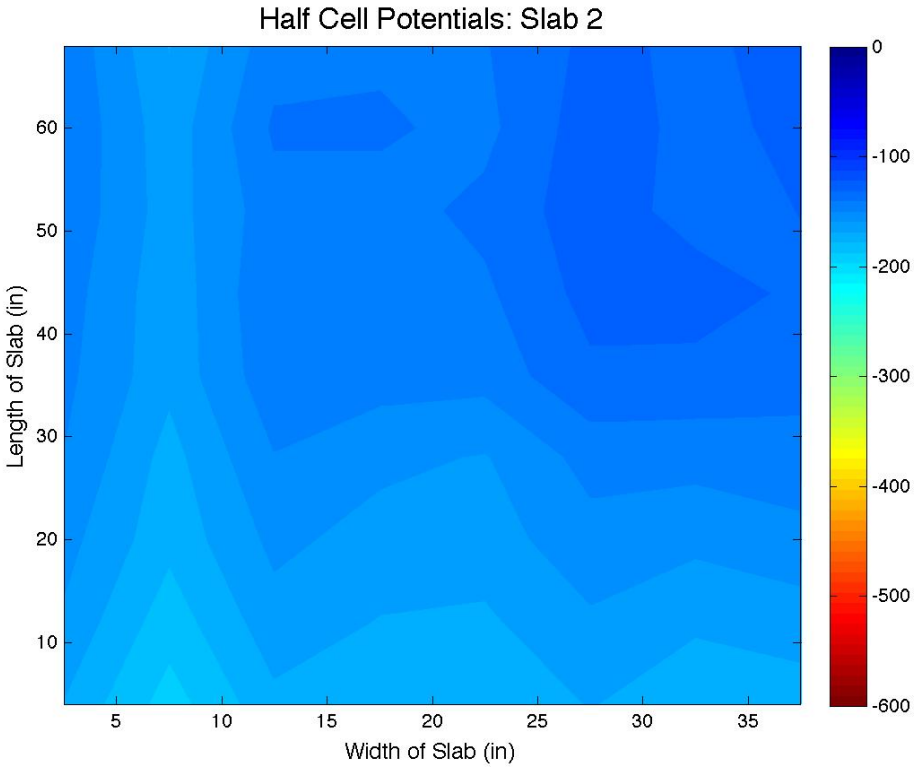
Half Cell Potentials: Slab 2
Length of Slab (in)
Width of Slab (in)
10
20
30
40
50
60
5
10
15
20
25
30
35
0
-100
-200
-300
-400
-500
-600

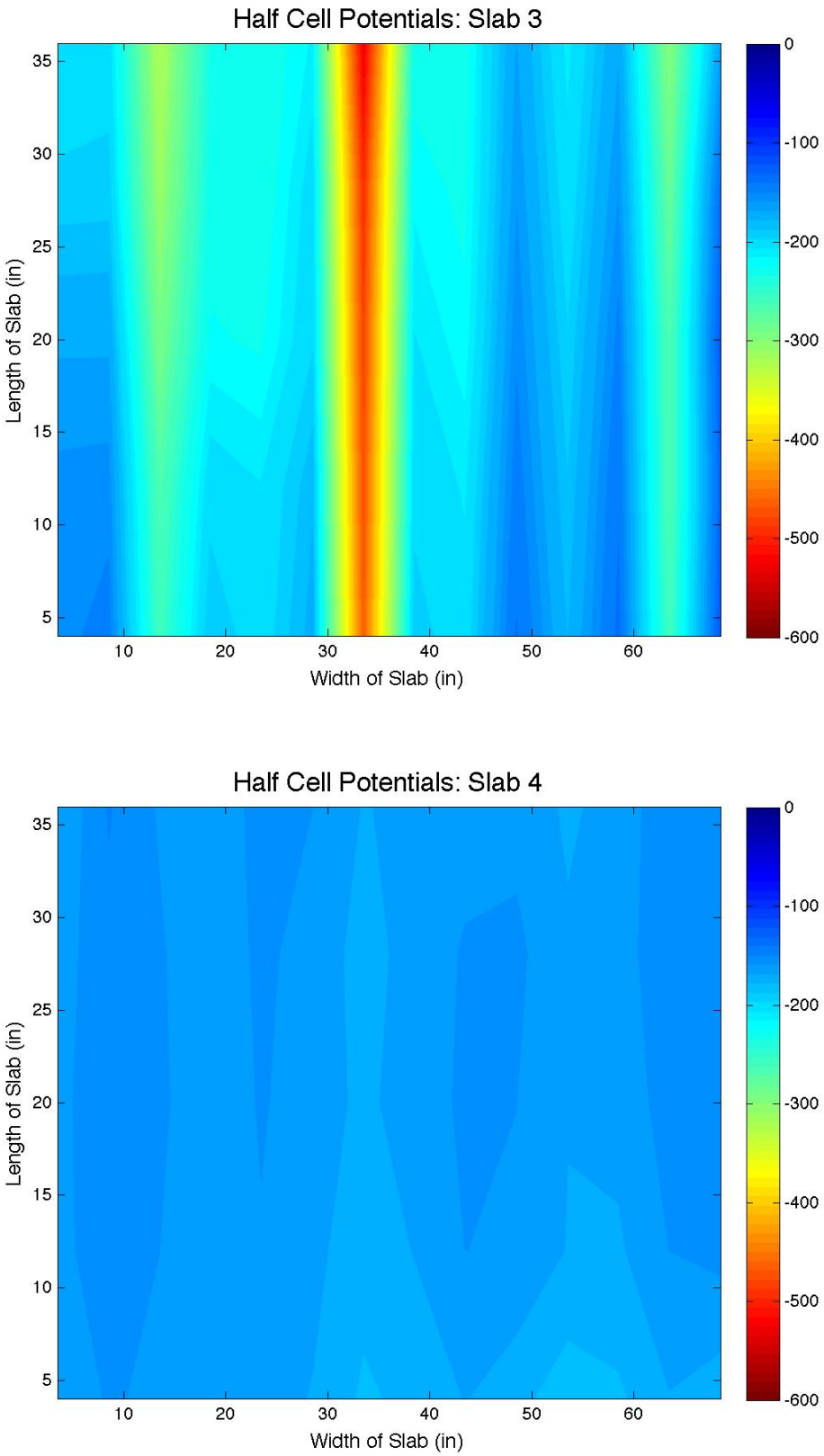

Figure A-18: Week of July 20, 2012

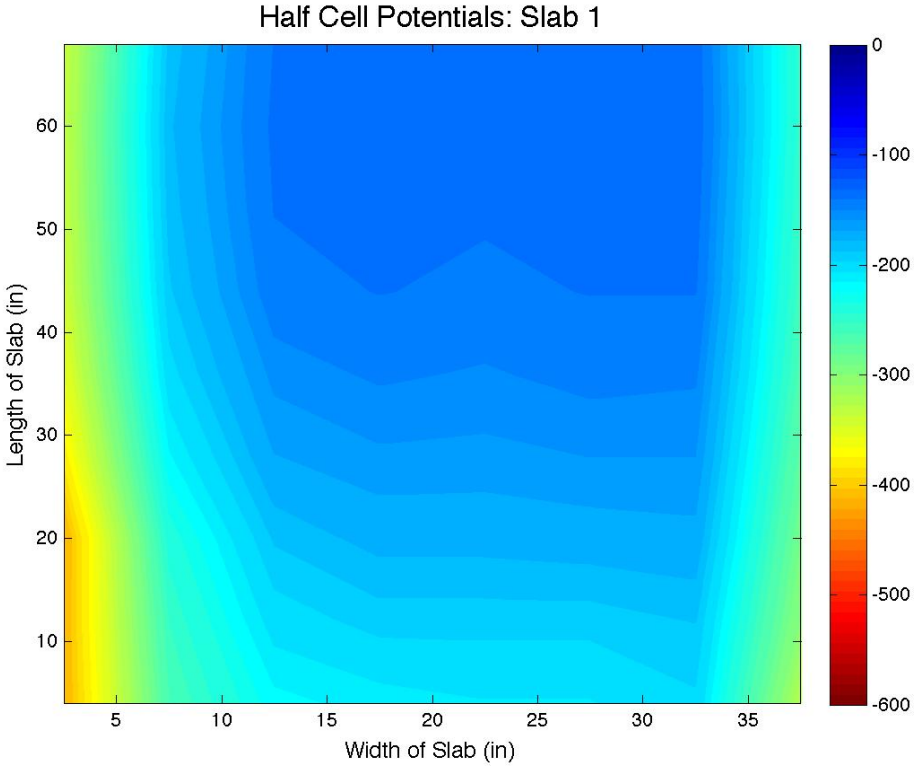
Half Cell Potentials: Slab 1
Length of Slab (in)
Width of Slab (in)
10
20
30
40
50
60
5
10
15
20
25
30
35
0
-100
-200
-300
-400
-500
-600

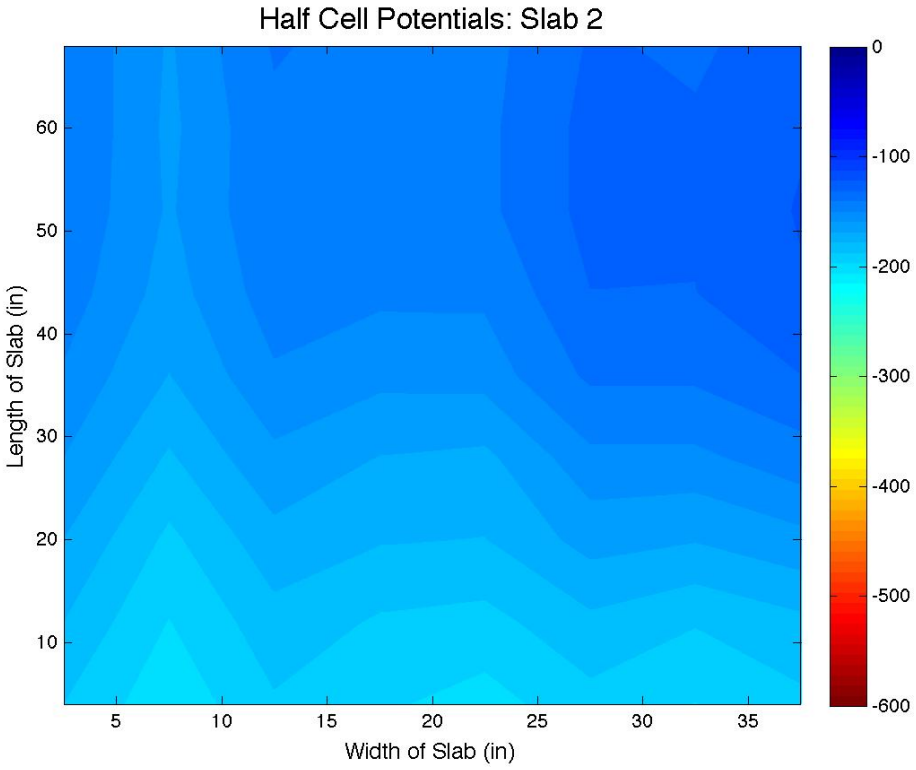
Half Cell Potentials: Slab 2
Length of Slab (in)
Width of Slab (in)
10
20
30
40
50
60
5
10
15
20
25
30
35
0
-100
-200
-300
-400
-500
-600

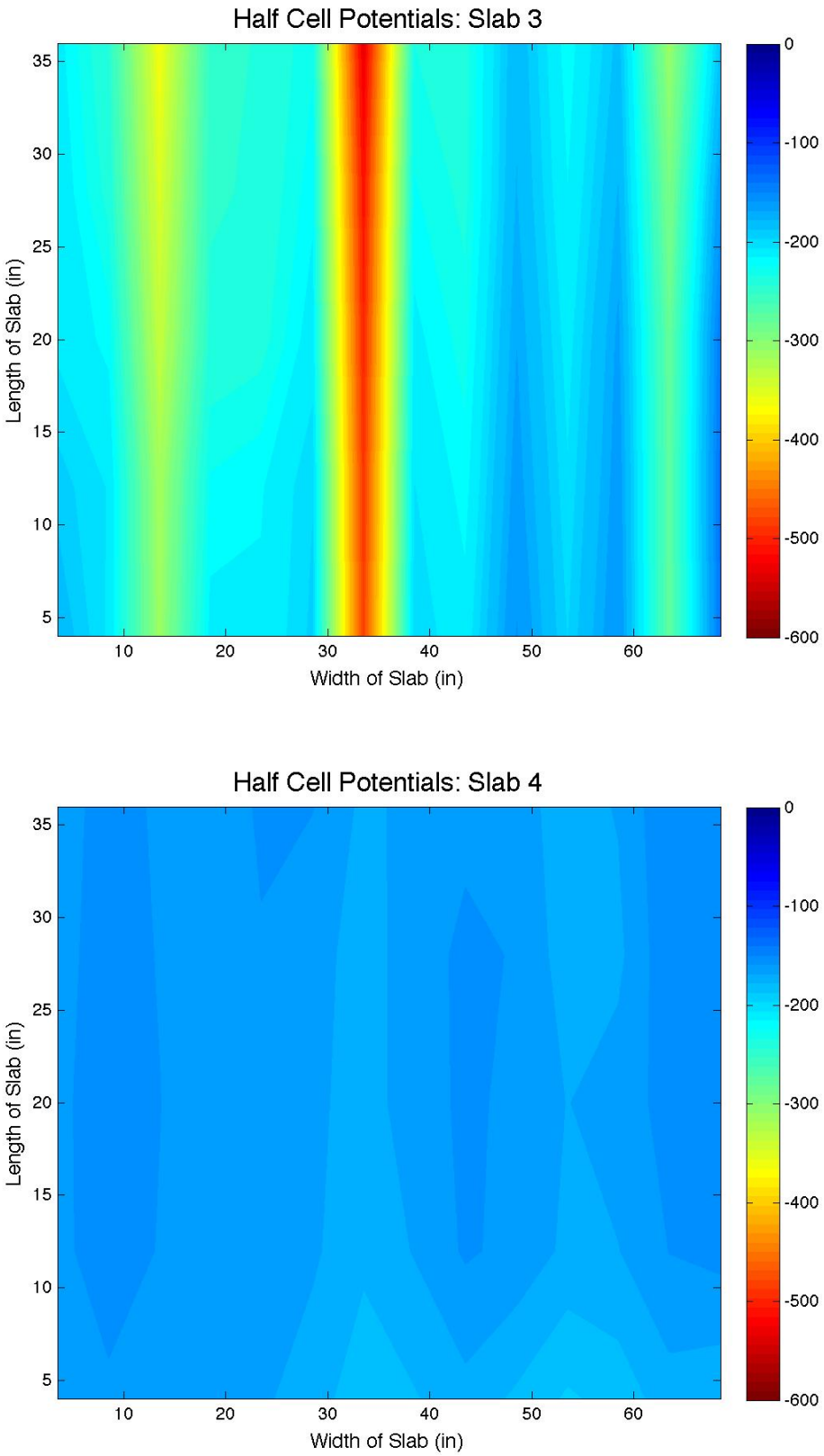

Figure A-19: Week of July 27, 2012

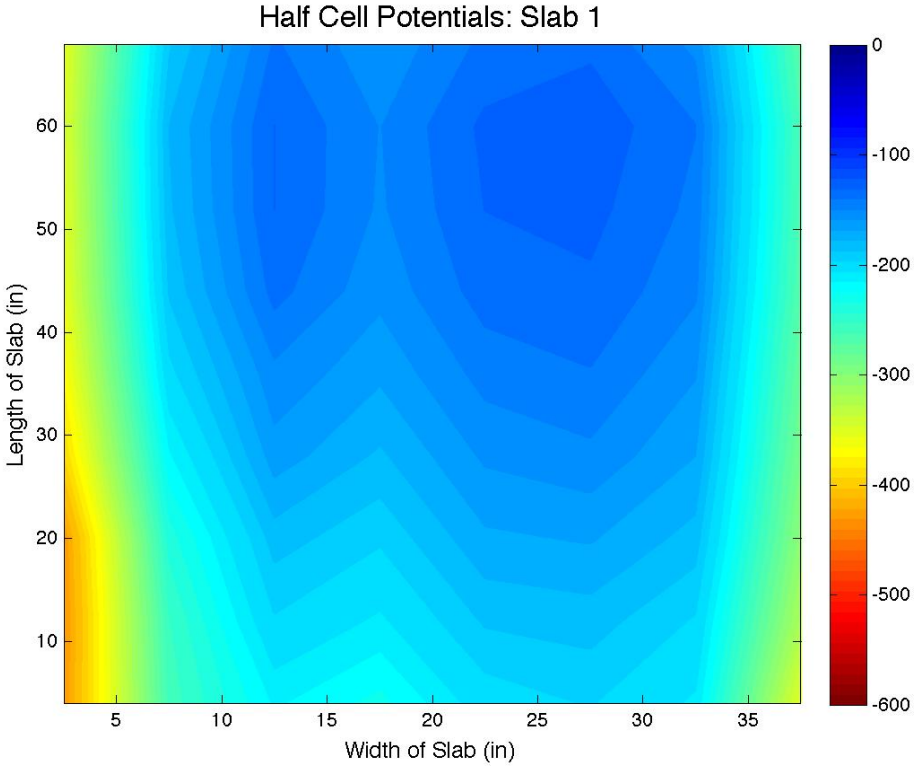
Half Cell Potentials: Slab 1
Length of Slab (in)
Width of Slab (in)
10
20
30
40
50
60
5
10
15
20
25
30
35
0
-100
-200
-300
-400
-500
-600

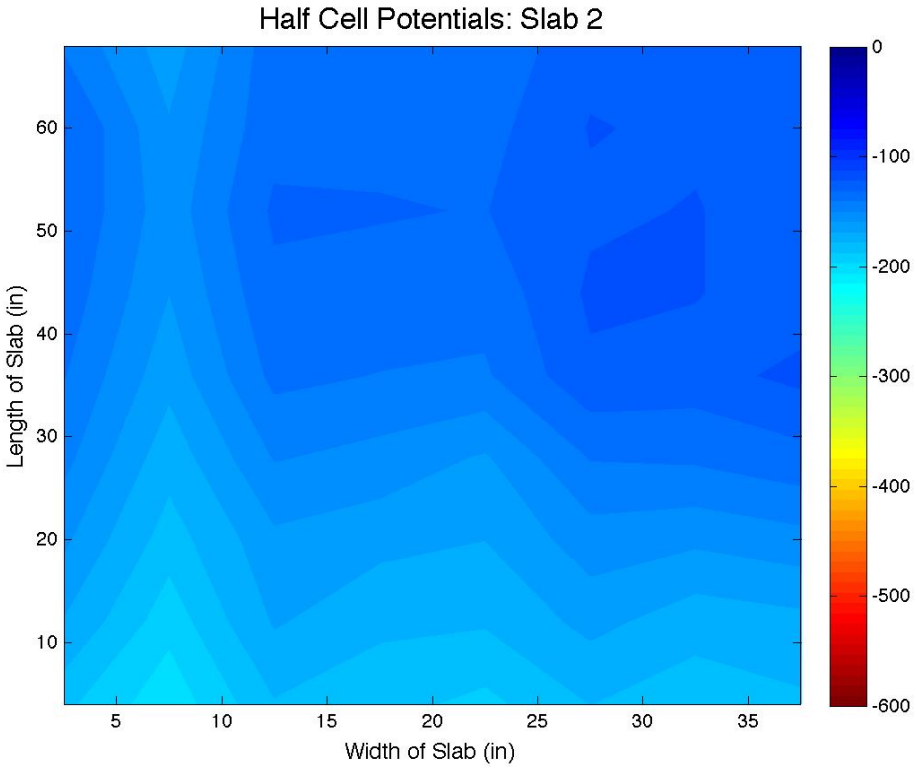
Half Cell Potentials: Slab 2
Length of Slab (in)
Width of Slab (in)
10
20
30
40
50
60
5
10
15
20
25
30
35
0
-100
-200
-300
-400
-500
-600

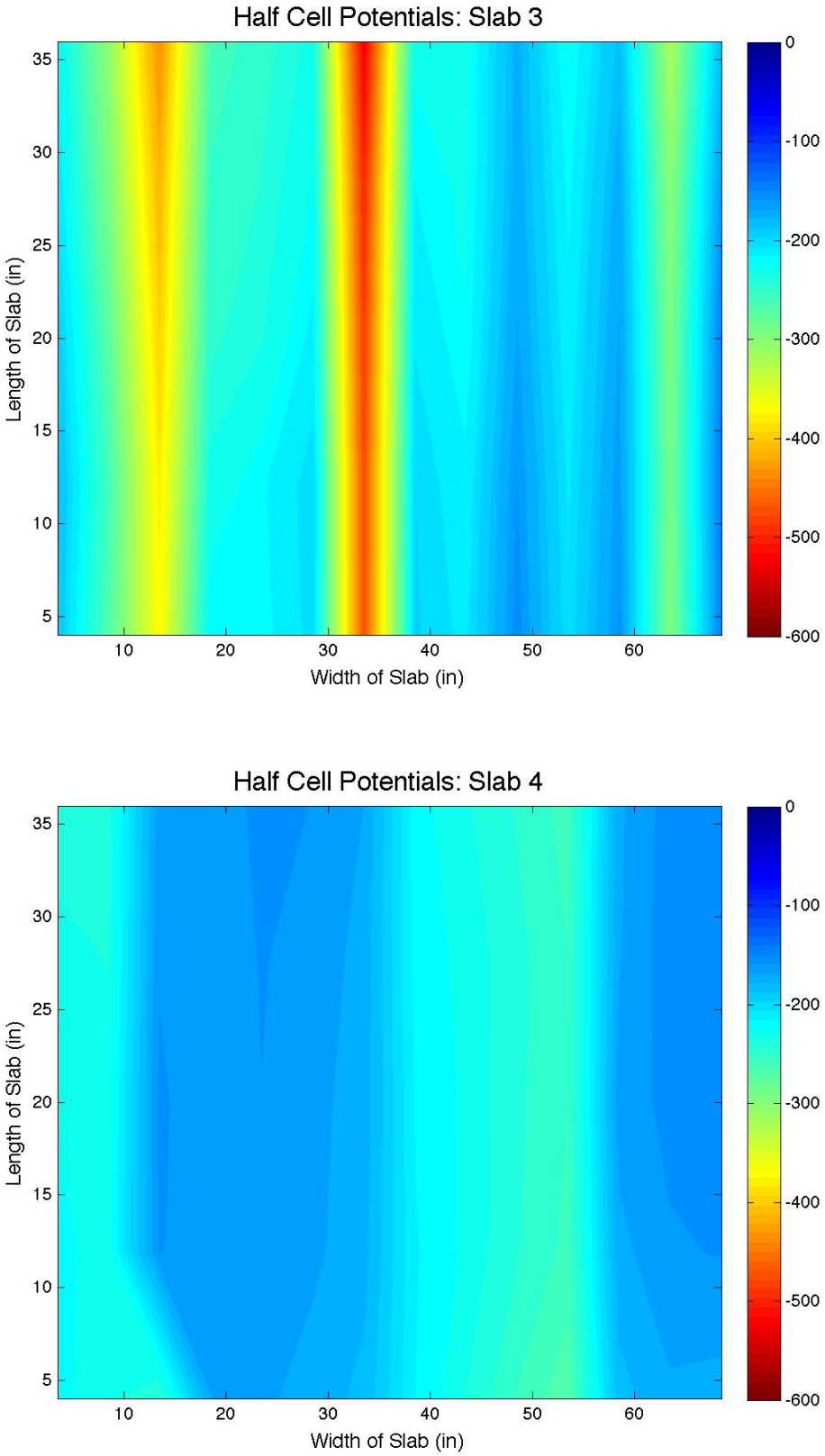

Figure A-20: Week of August 3, 2012

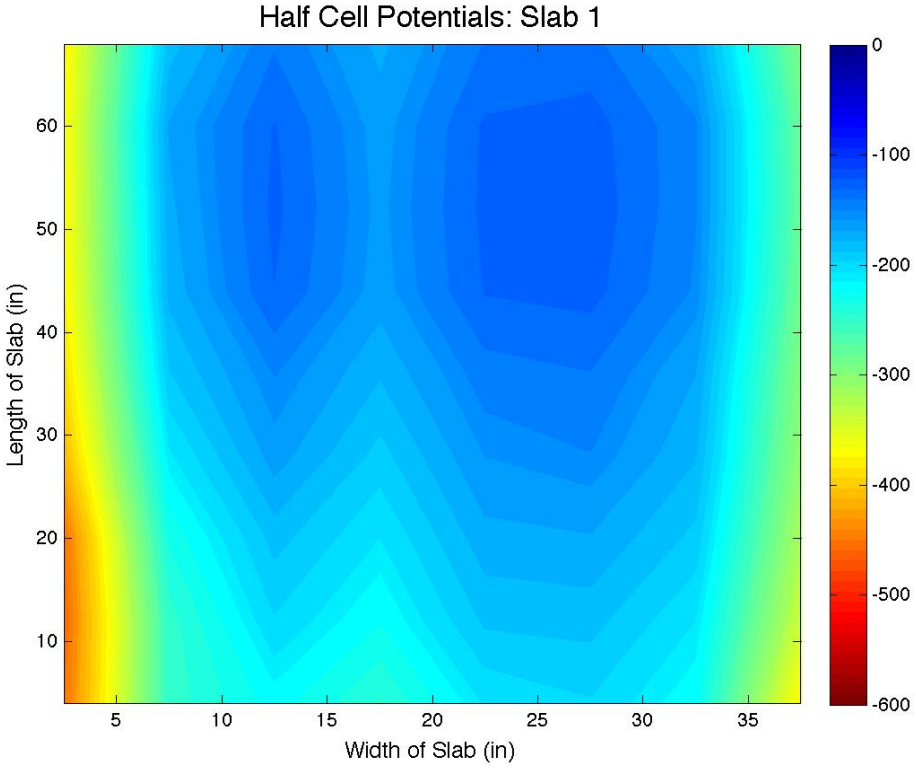
Half Cell Potentials: Slab 1
Length of Slab (in)
Width of Slab (in)
10
20
30
40
50
60
5
10
15
20
25
30
35
0
-100
-200
-300
-400
-500
-600

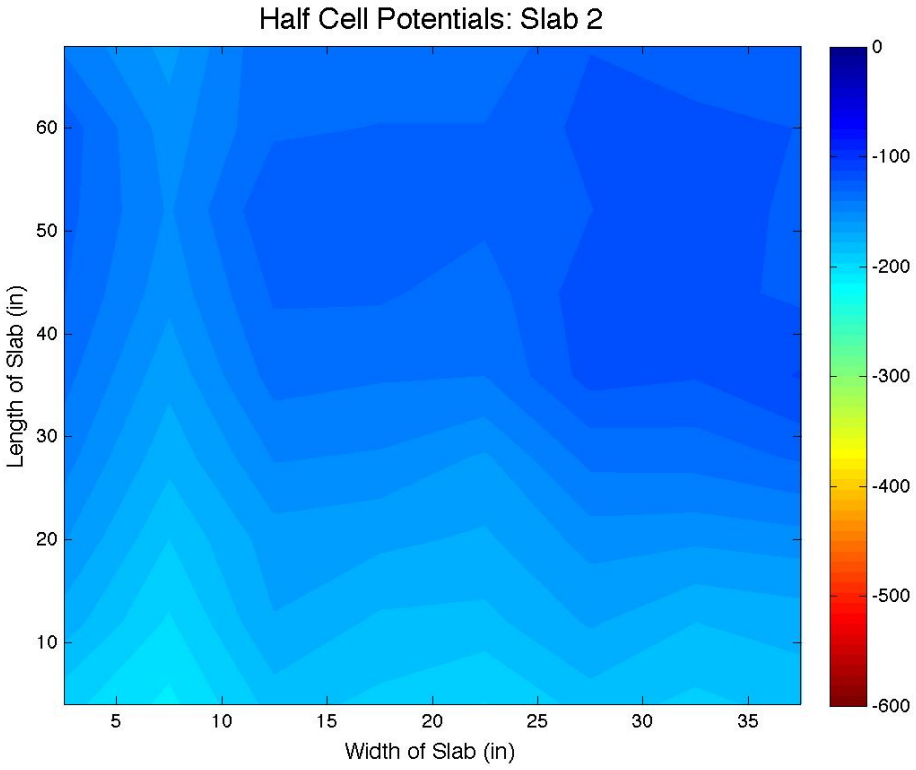
Half Cell Potentials: Slab 2
Length of Slab (in)
Width of Slab (in)
10
20
30
40
50
60
5
10
15
20
25
30
35
0
-100
-200
-300
-400
-500
-600

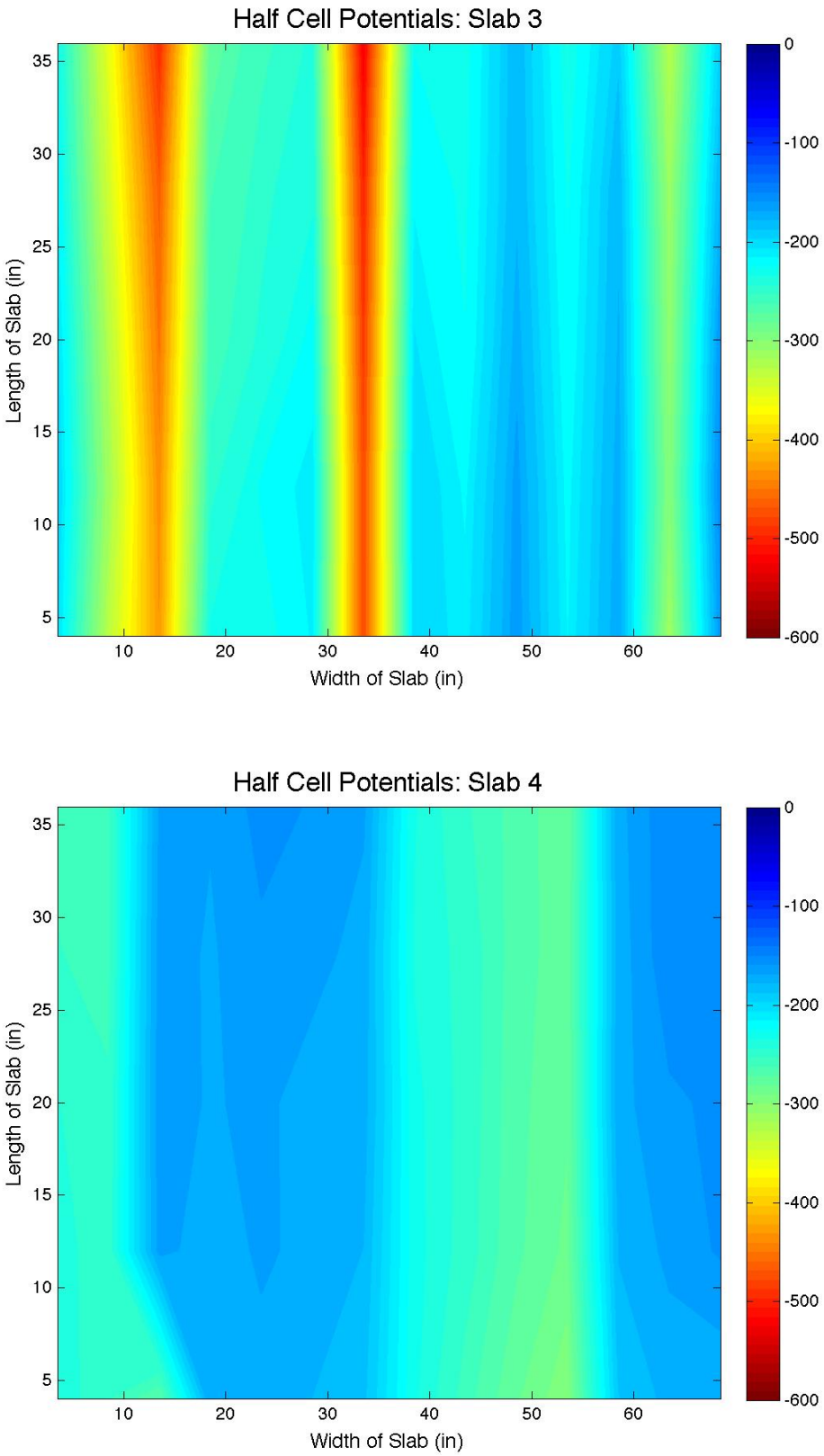

Figure A-21: Week of August 10, 2012

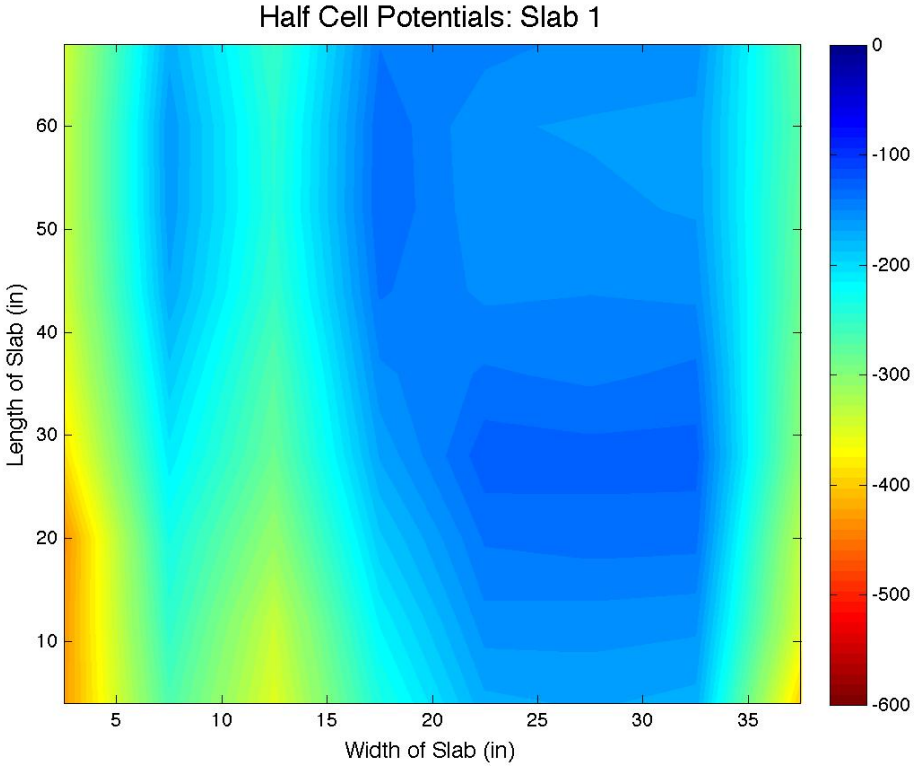
Half Cell Potentials: Slab 1
Length of Slab (in)
Width of Slab (in)
10
20
30
40
50
60
5
10
15
20
25
30
35
0
-100
-200
-300
-400
-500
-600

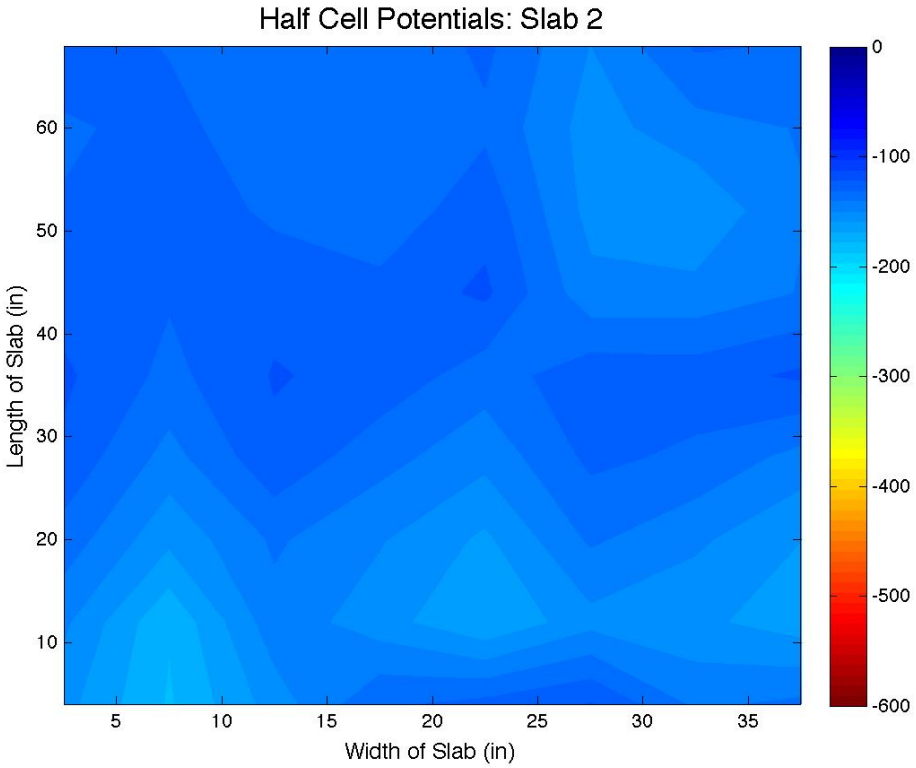
Half Cell Potentials: Slab 2
Length of Slab (in)
Width of Slab (in)
10
20
30
40
50
60
5
10
15
20
25
30
35
0
-100
-200
-300
-400
-500
-600

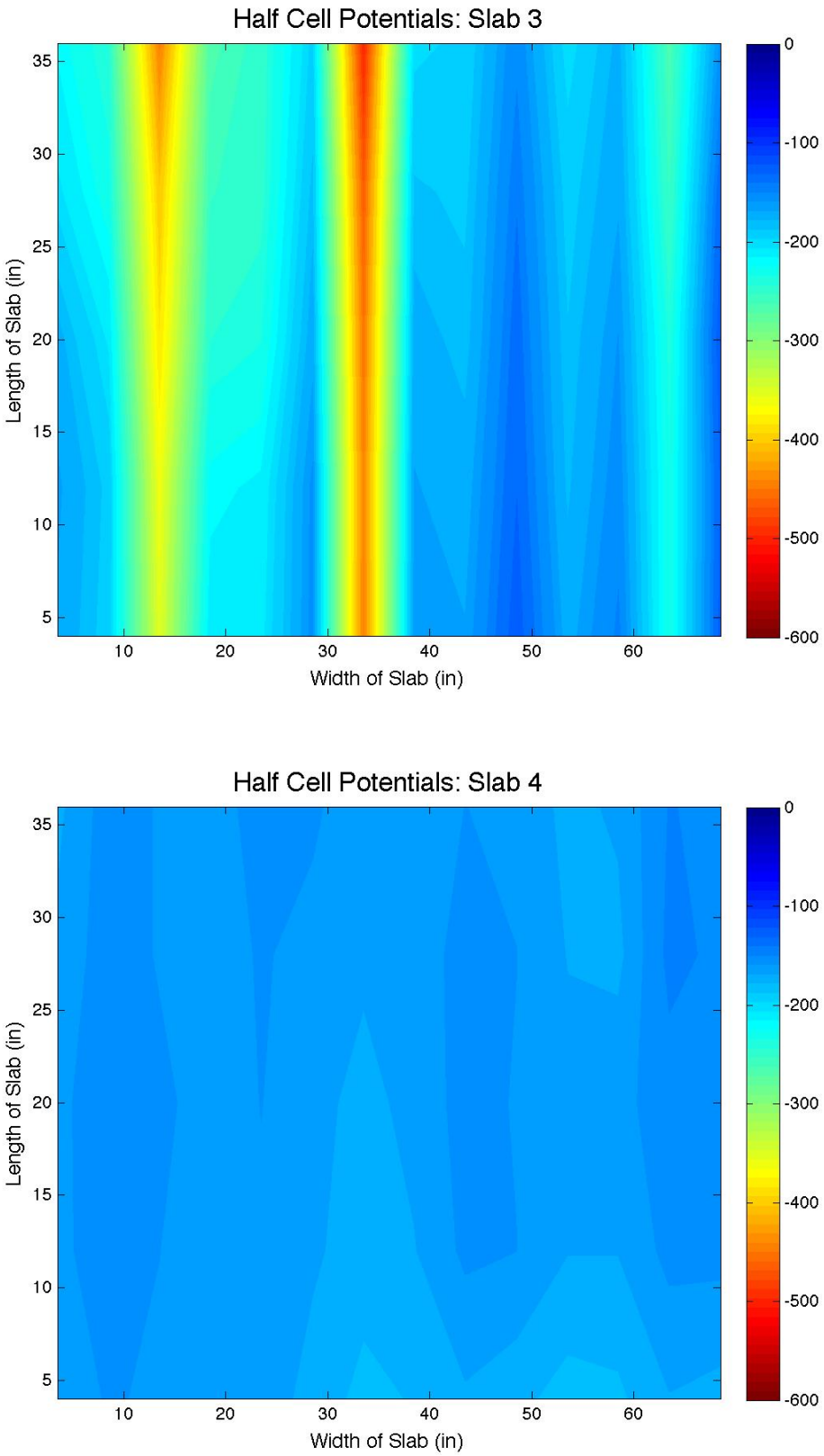

Figure A-22: Week of August 17, 2012

Appendix B

Statistical Analysis of Slabs

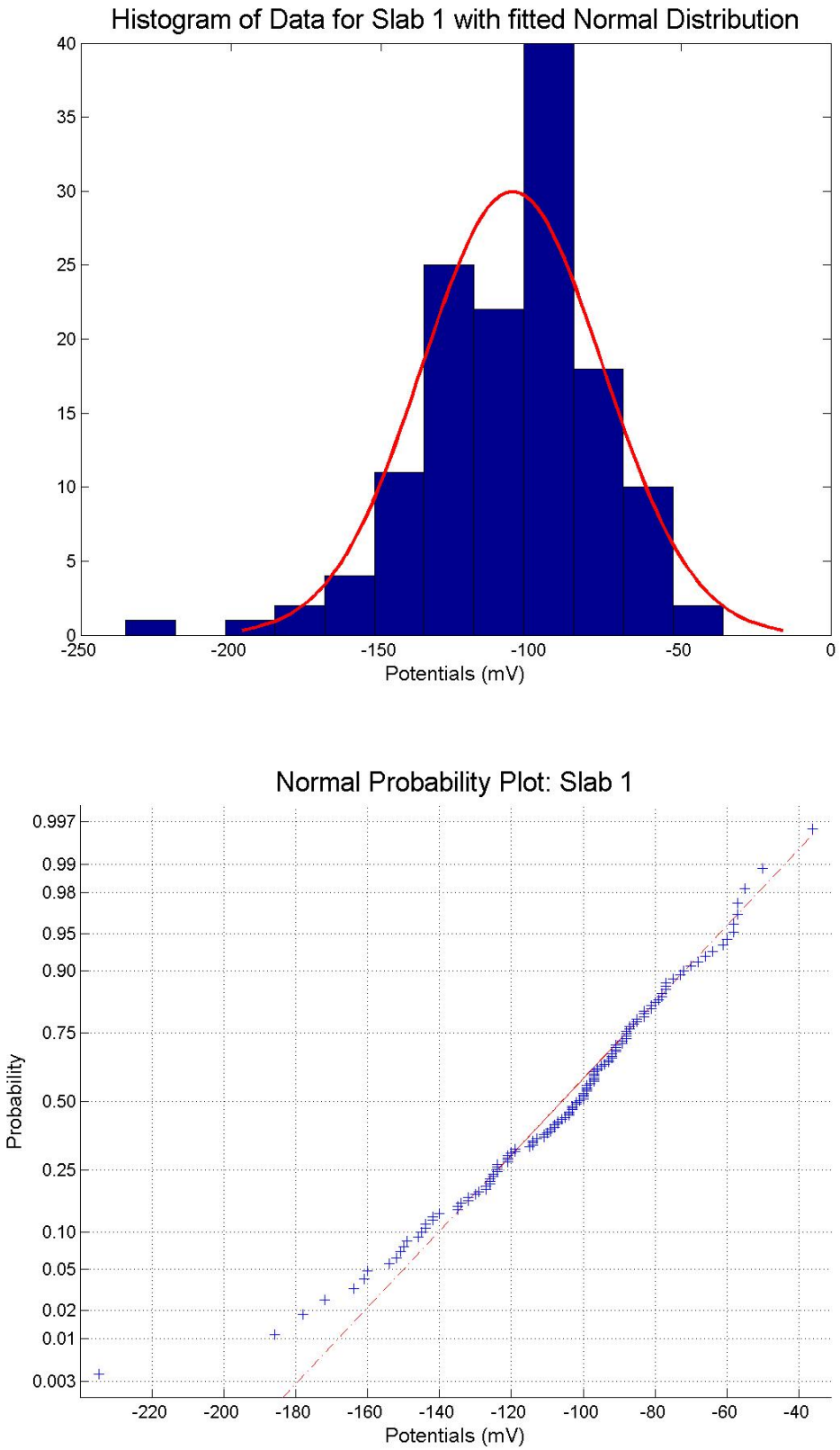

Figure B-1: Statistical Analys Slab 1: 12/22/2011

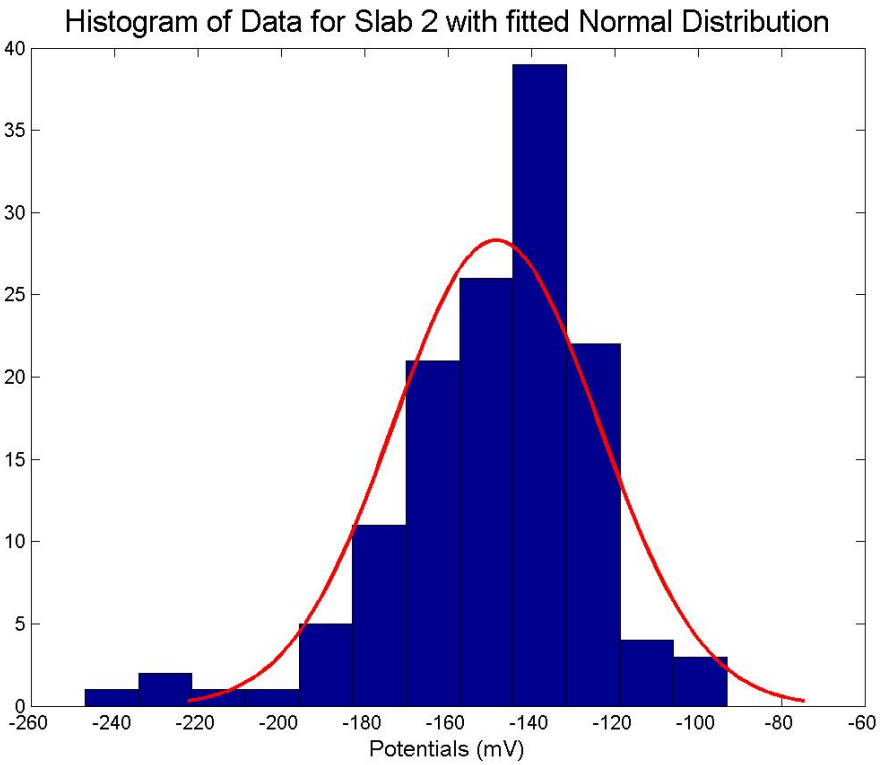

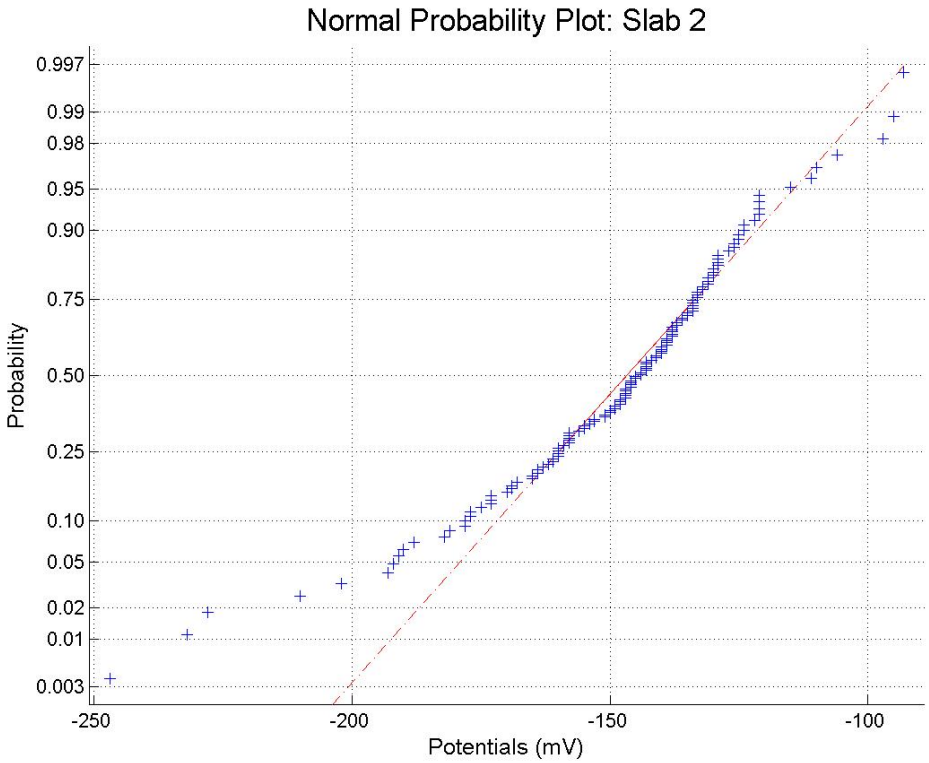

Figure B-2: Statistical Analys Slab 2: 12/22/2011

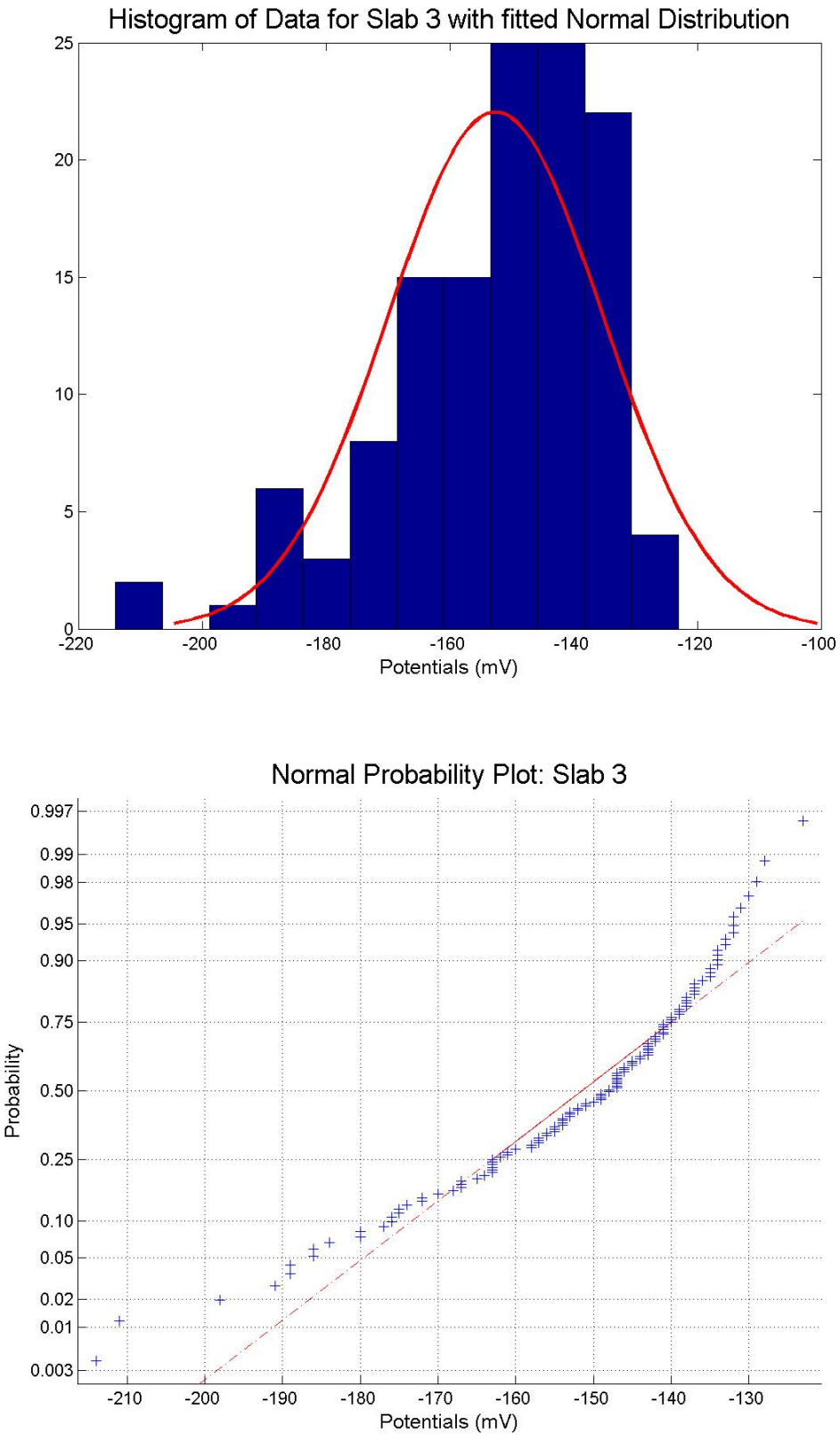

Figure B-3: Statistical Analys Slab 3: 12/22/2011

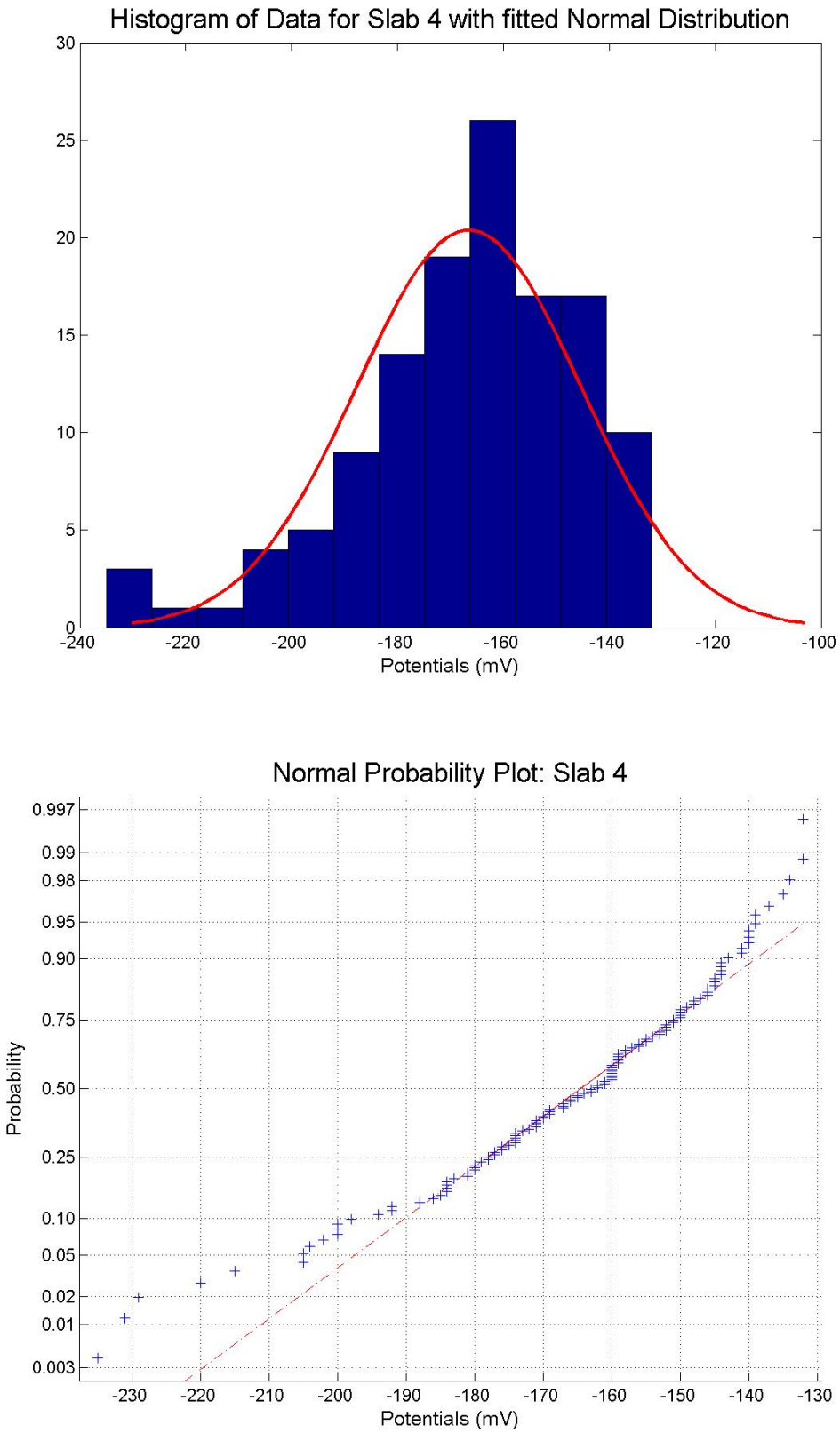

Figure B-4: Statistical Analys Slab 4: 12/22/2011

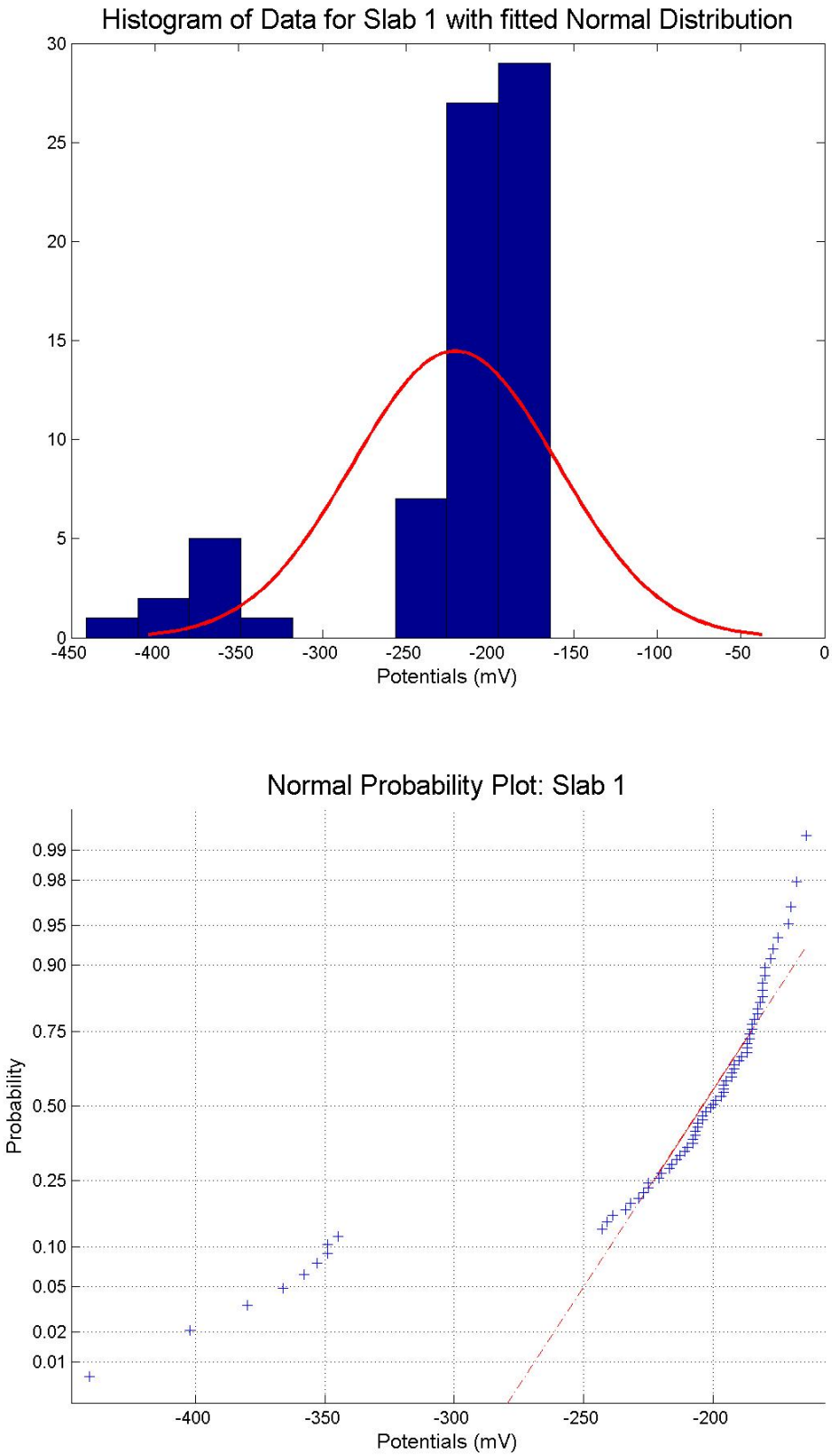

Figure B-5: Statistical Analys Slab 1: 03/23/2012

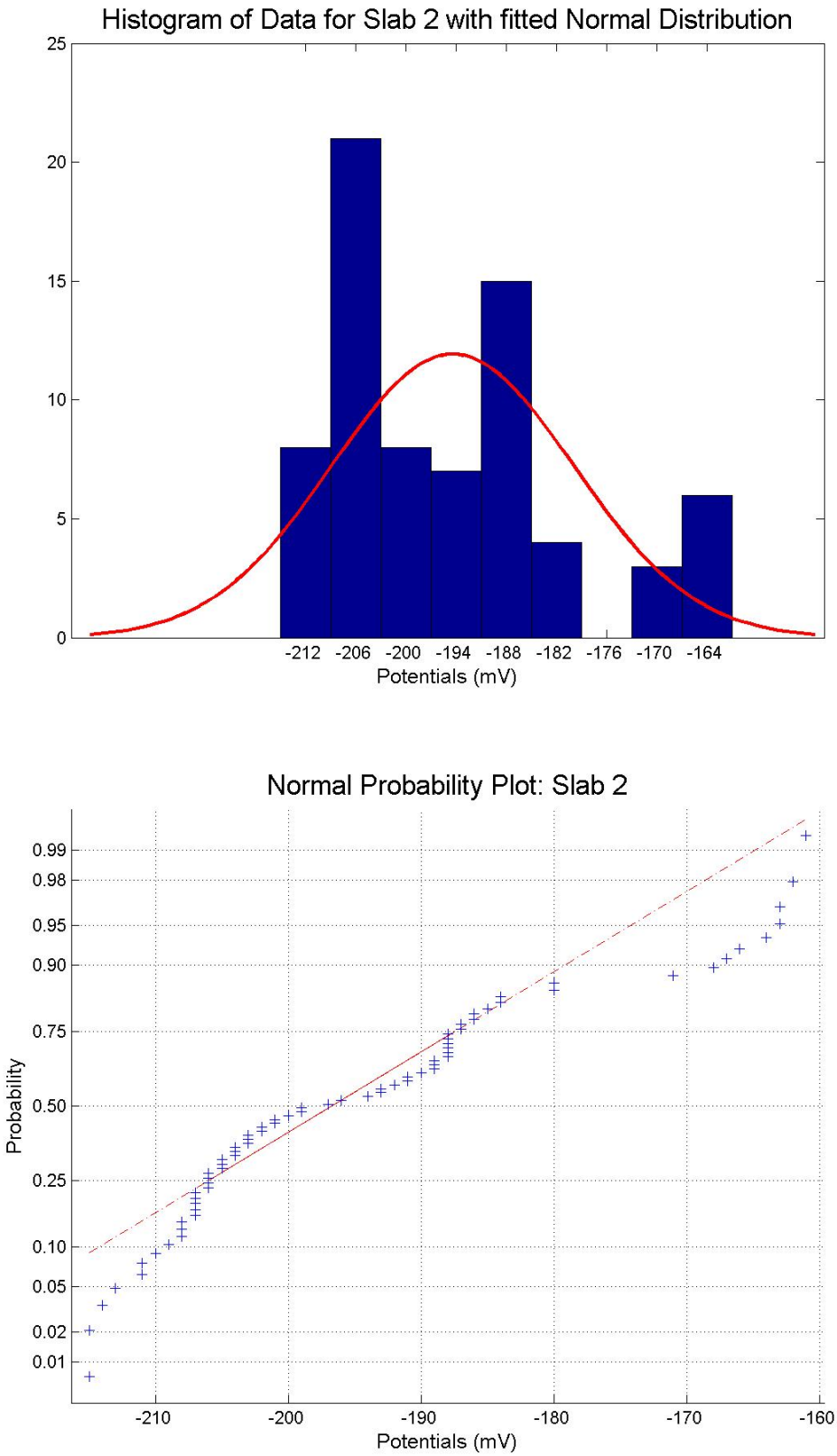

Figure B-6: Statistical Analys Slab 2: 03/23/2012

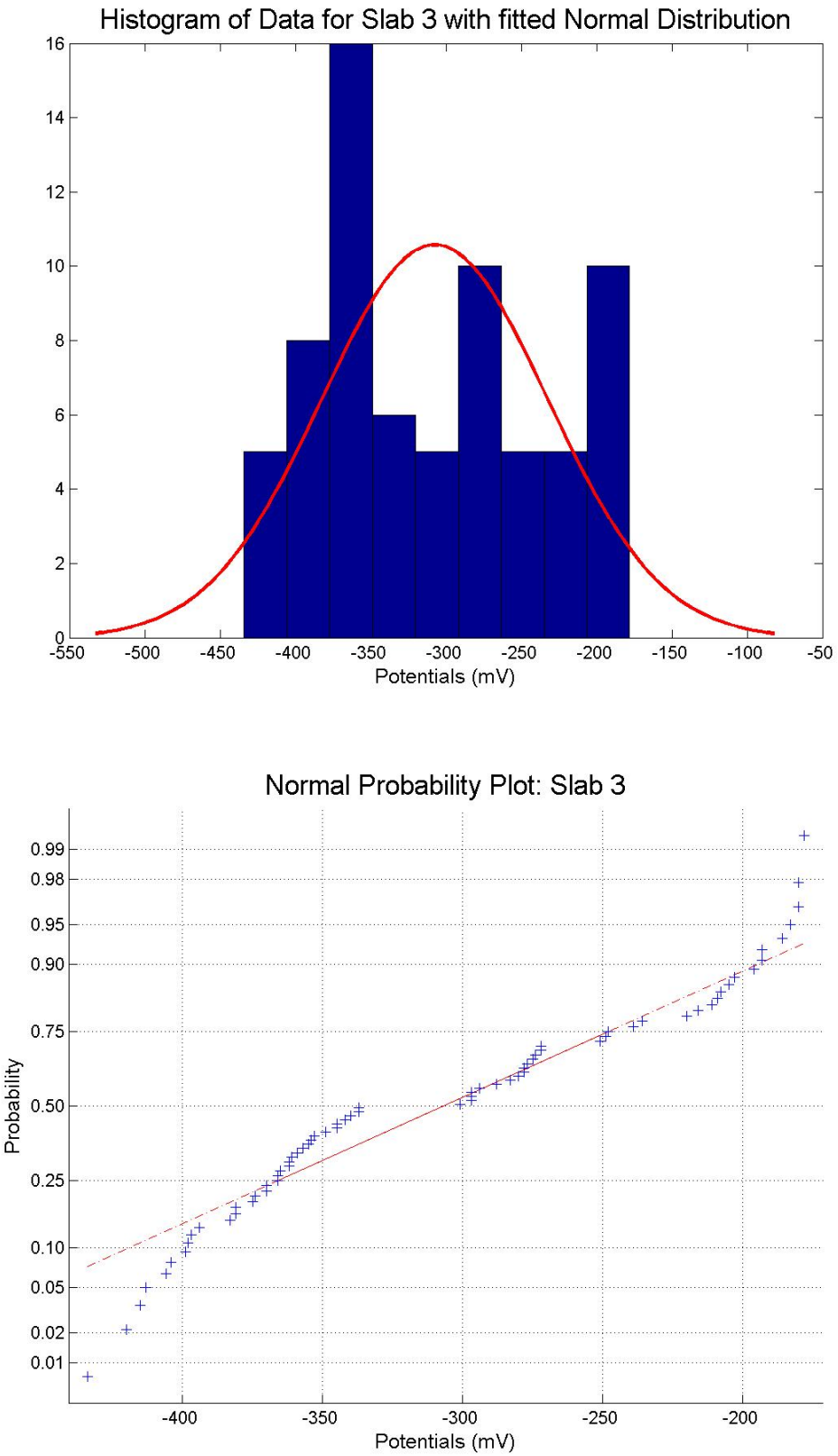

Figure B-7: Statistical Analys Slab 3: 03/23/2012

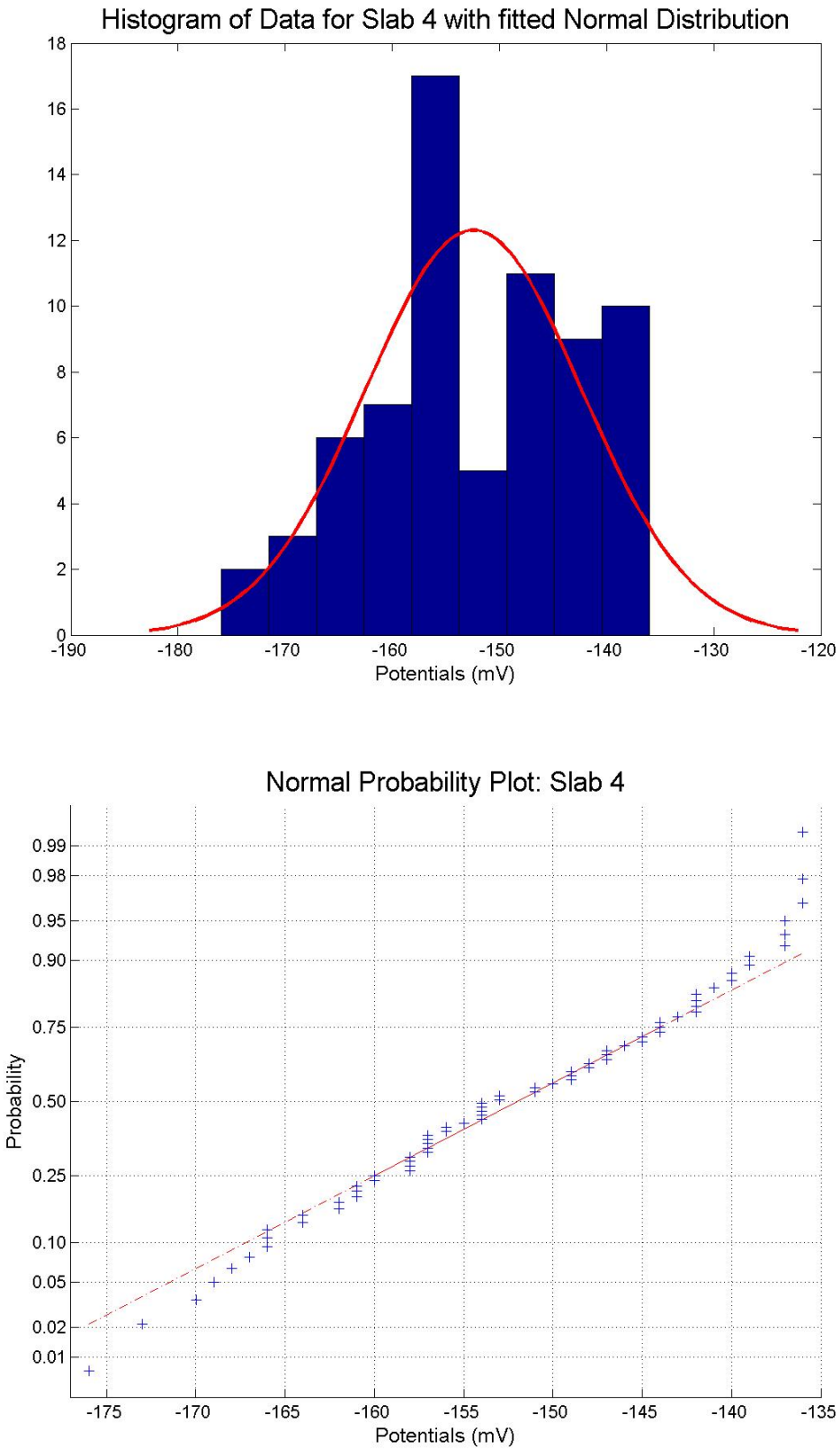

Figure B-8: Statistical Analys Slab 4: 03/23/2012

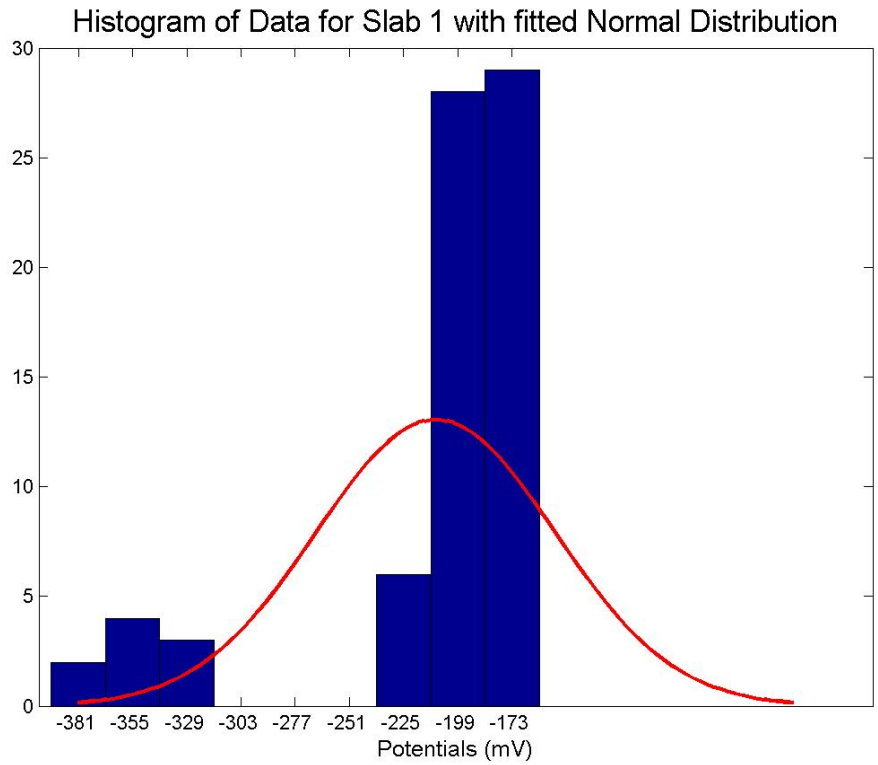

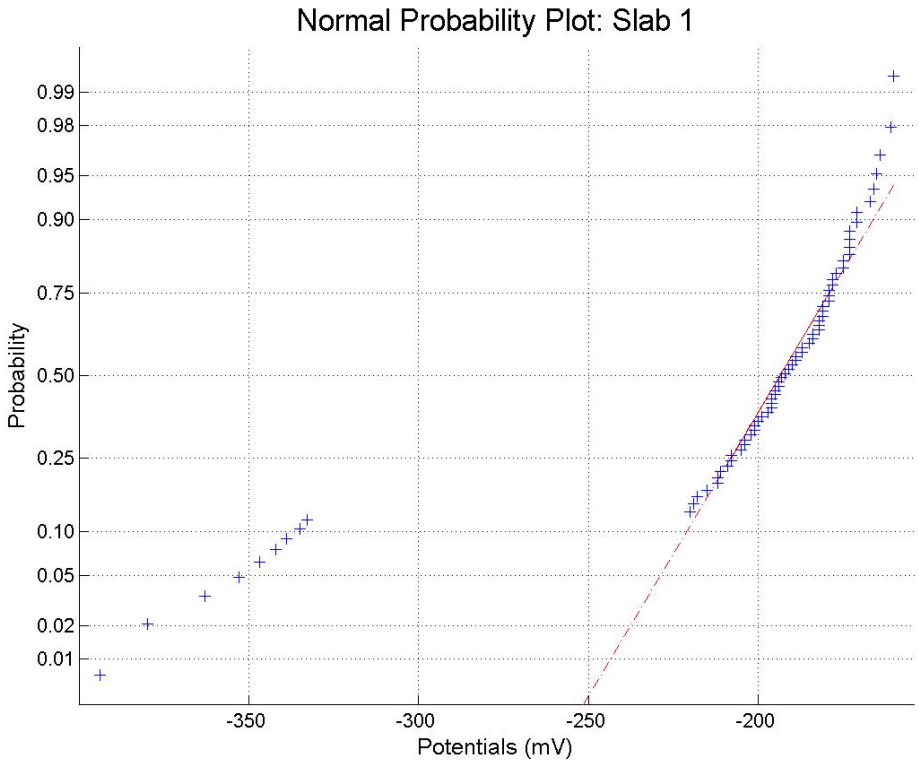

Figure B-9: Statistical Analys Slab 1: 03/30/2012

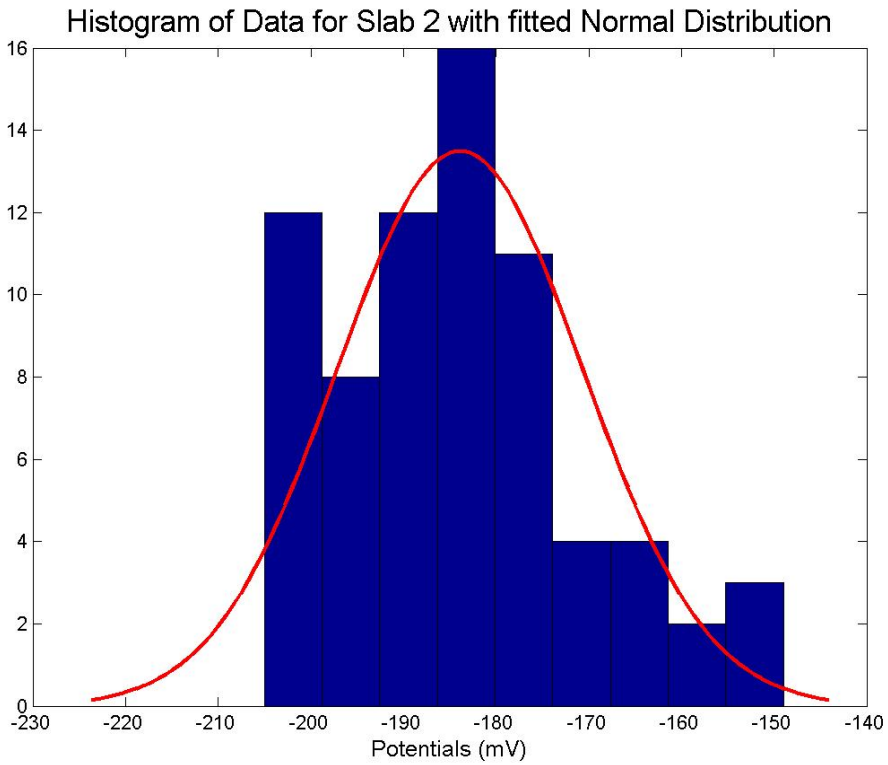

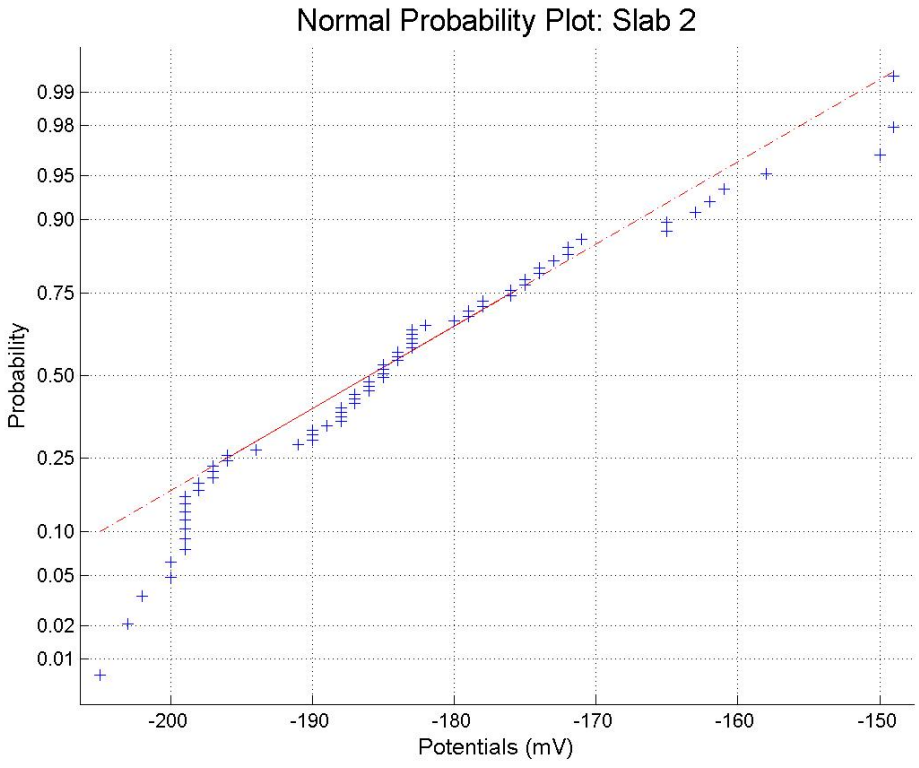

Figure B-10: Statistical Analys Slab 2: 03/30/2012

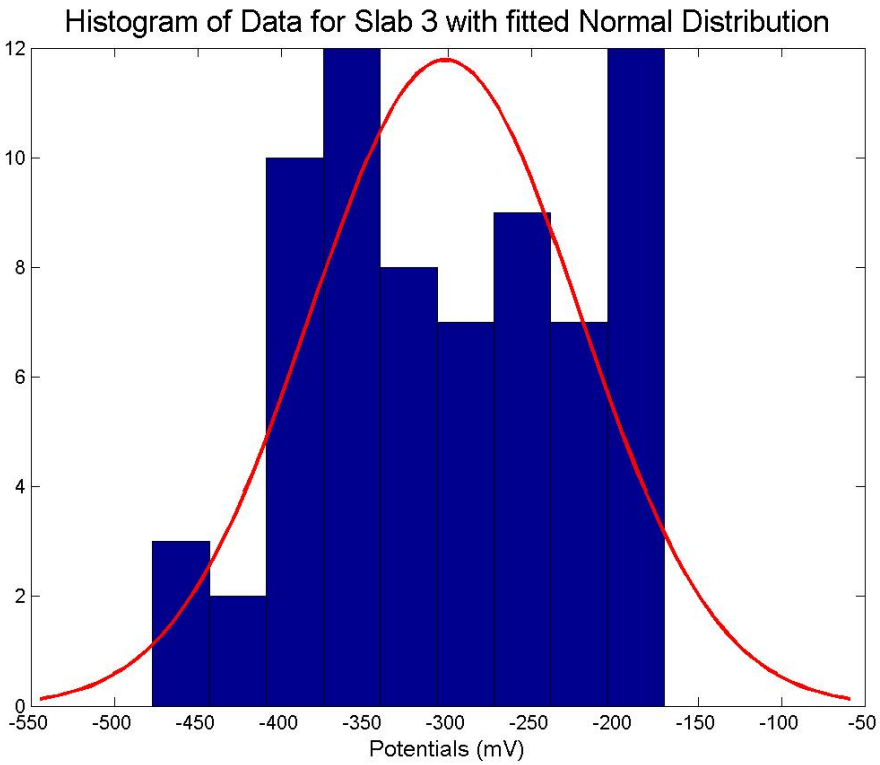

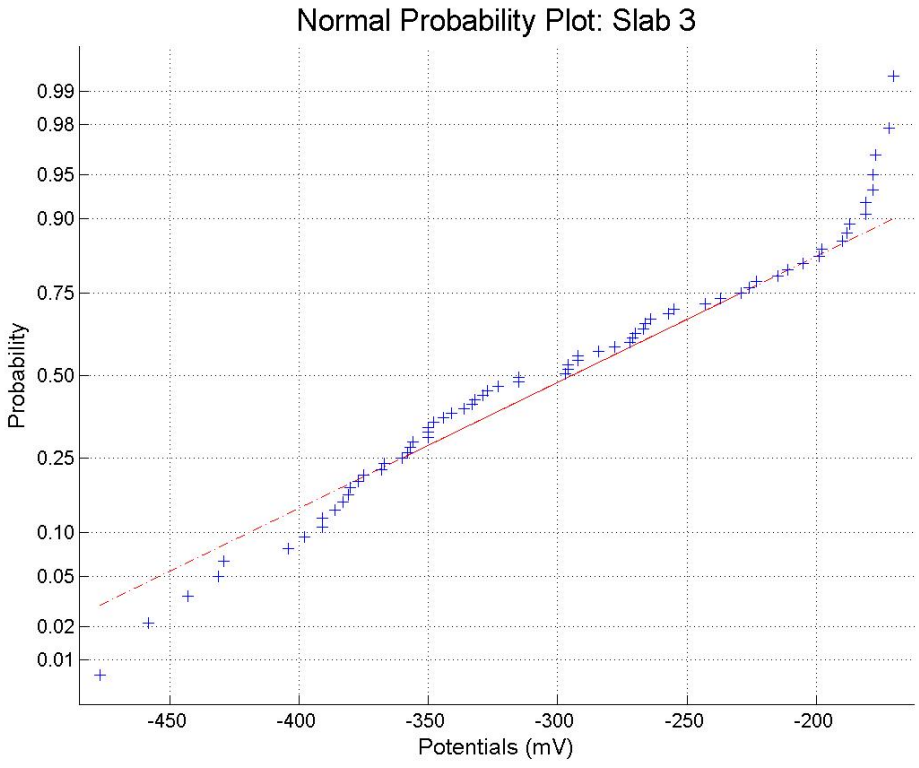

Figure B-11: Statistical Analys Slab 3: 03/30/2012

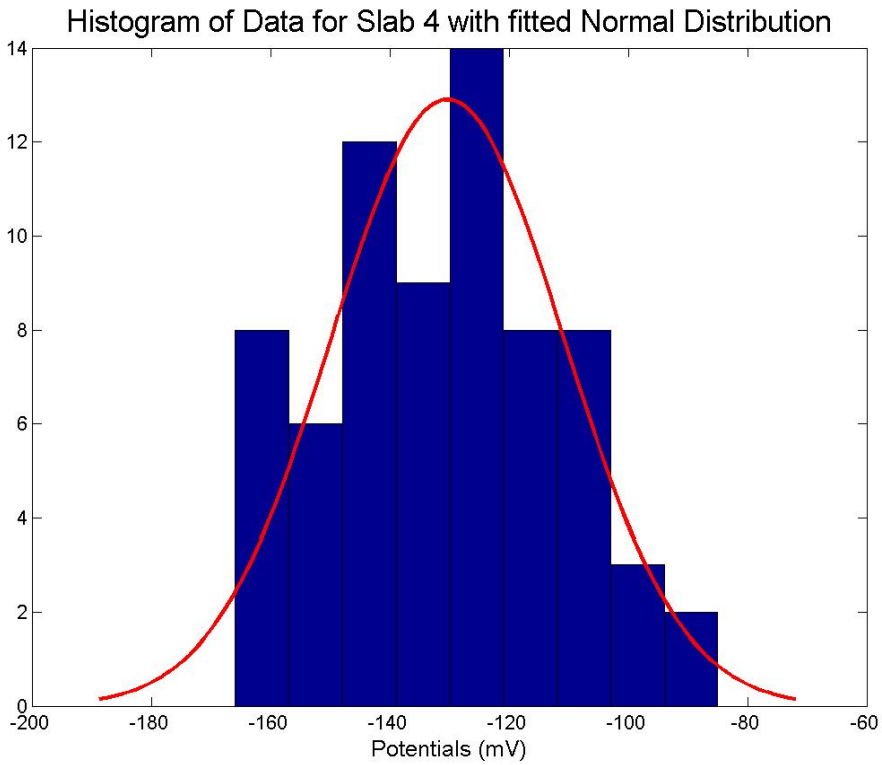

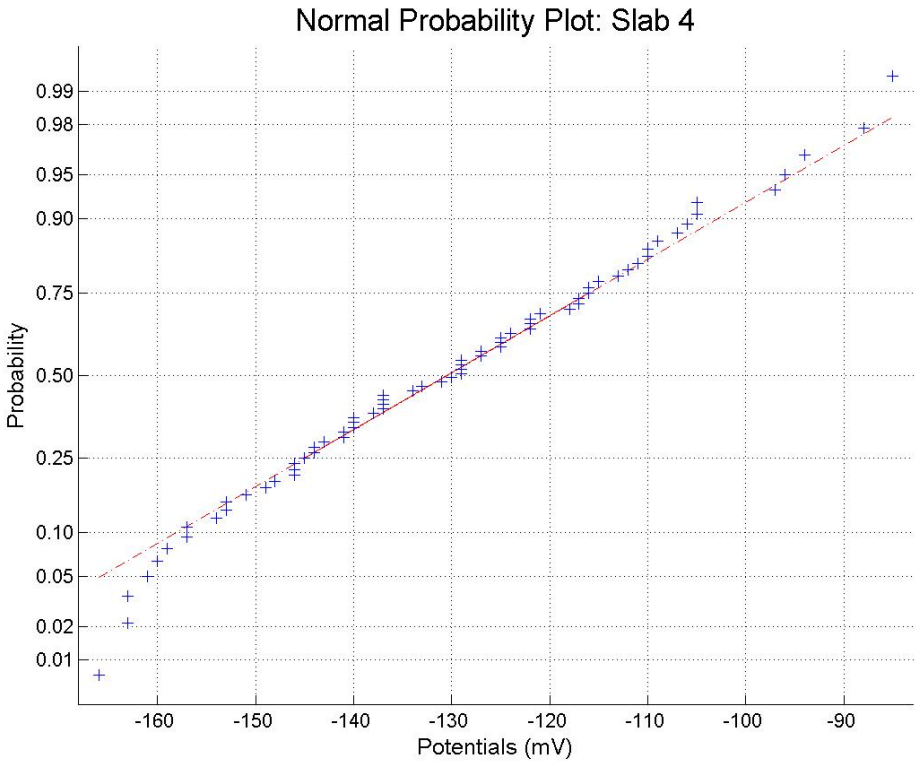

Figure B-12: Statistical Analys Slab 4: 03/30/2012

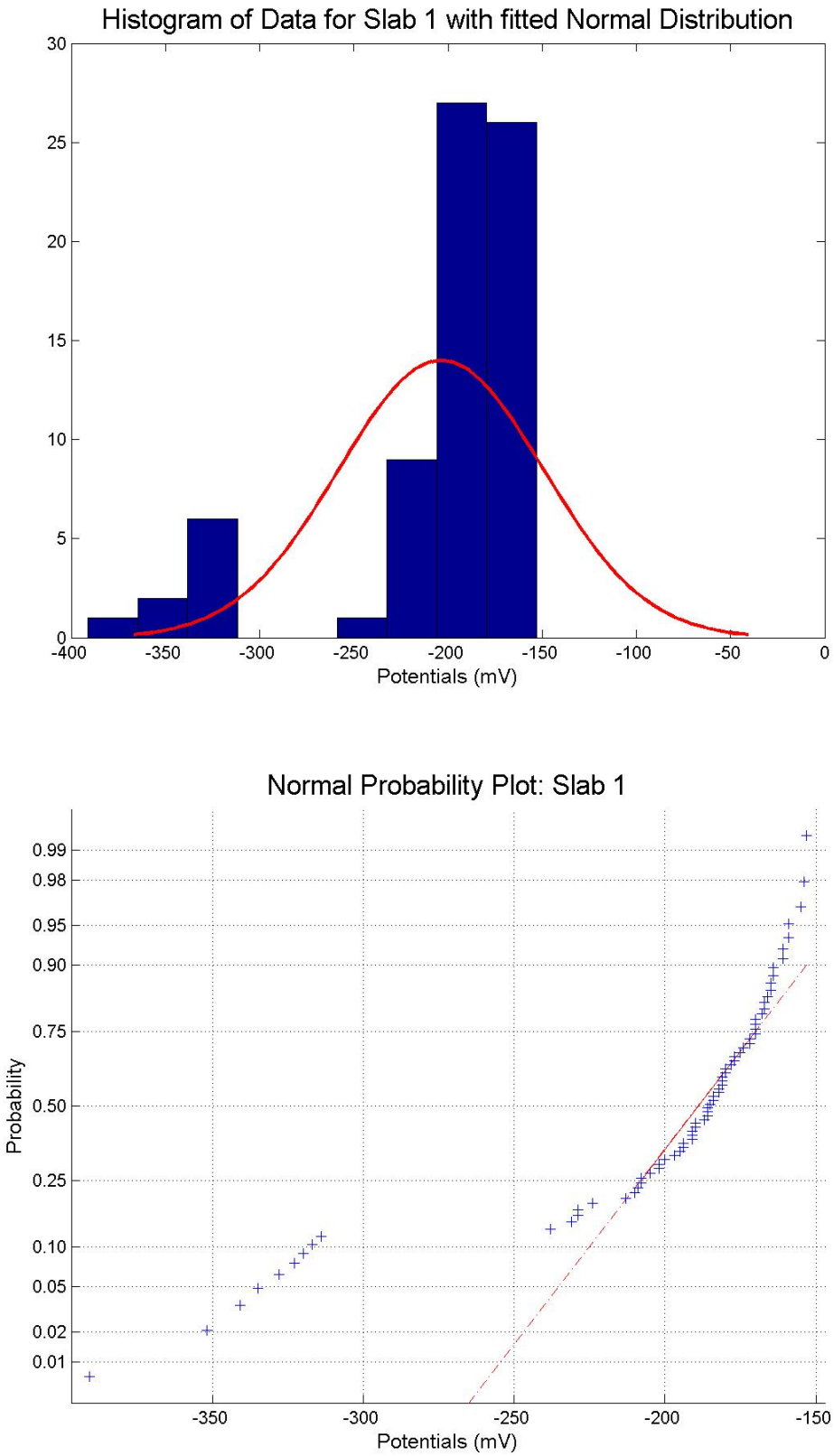

Figure B-13: Statistical Analys Slab 1: 04/06/2012

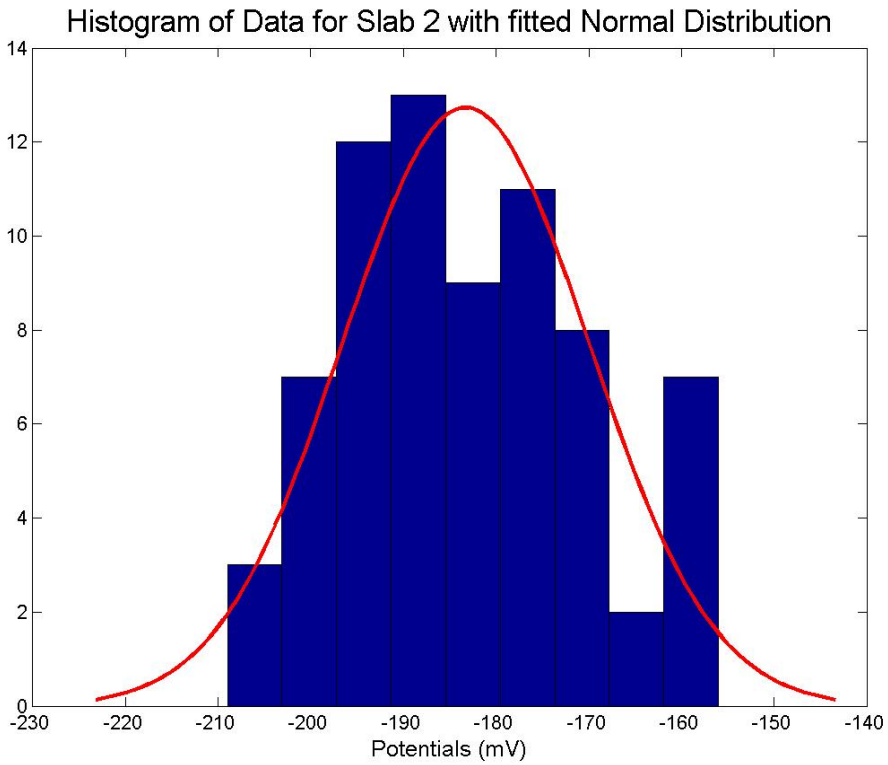

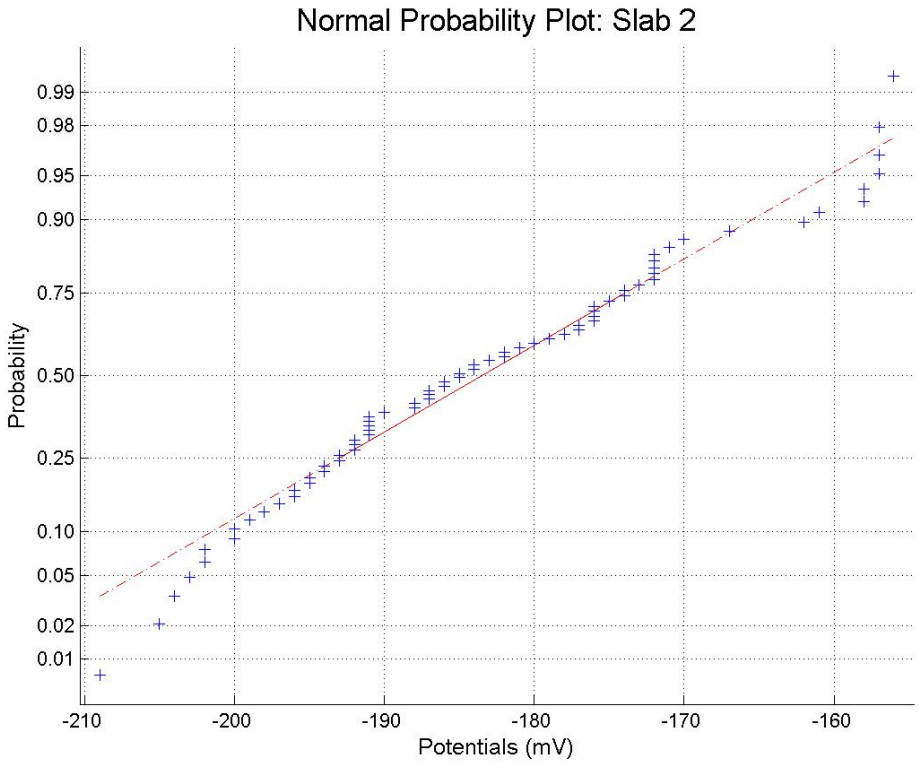

Figure B-14: Statistical Analys Slab 2: 04/06/2012

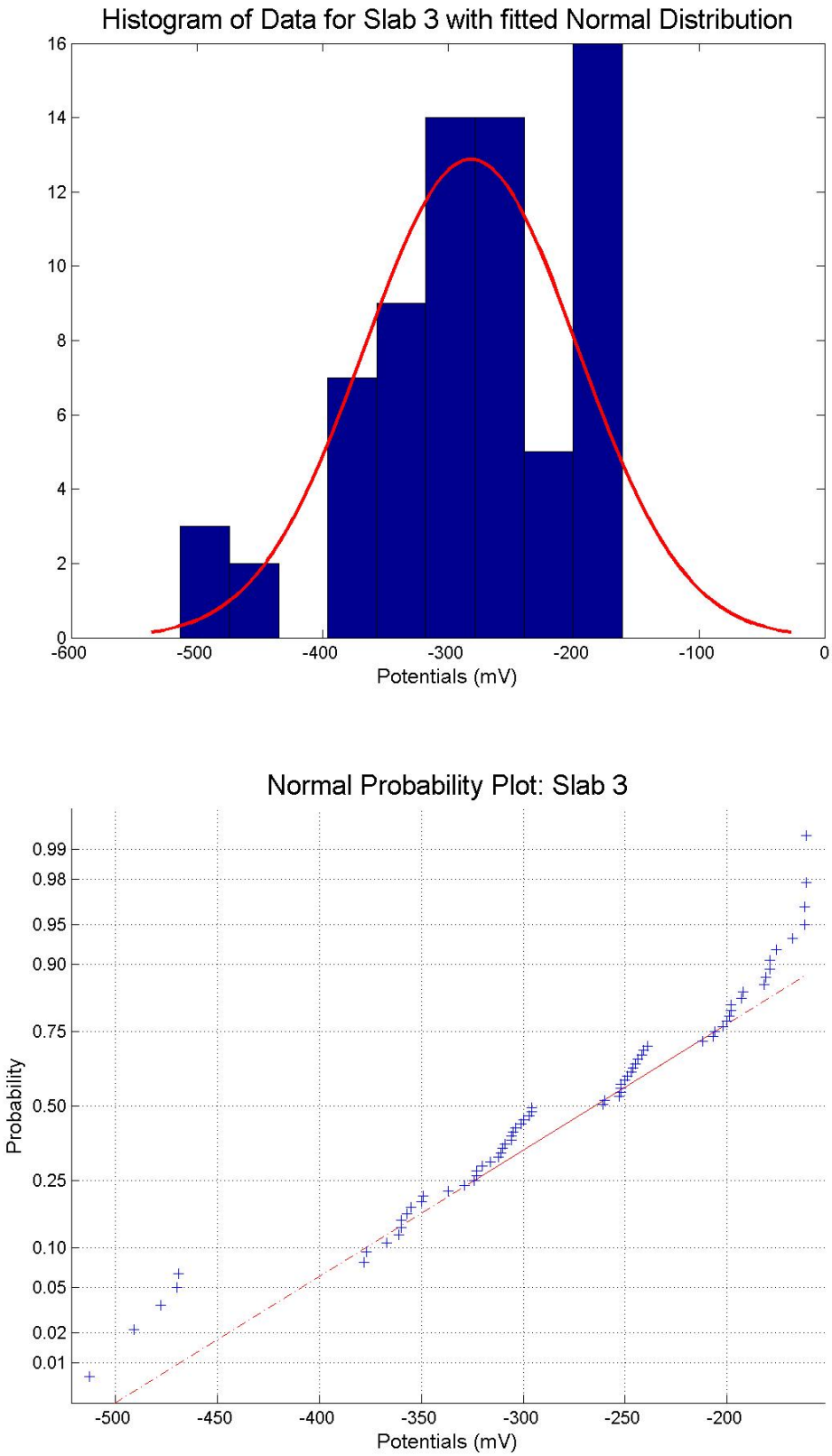

Figure B-15: Statistical Analys Slab 3: 04/06/2012

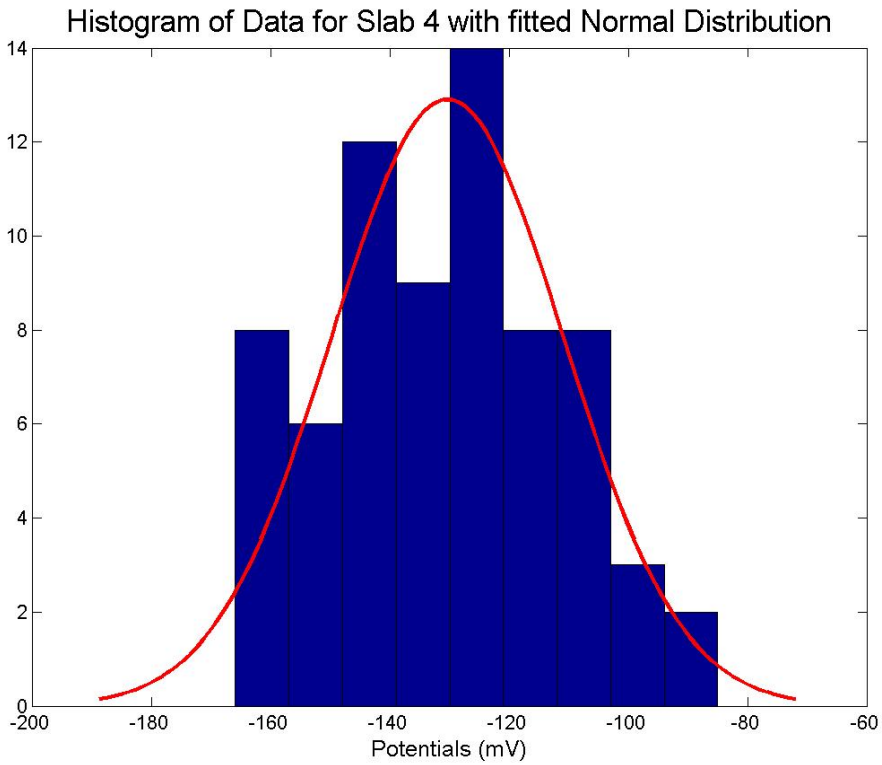

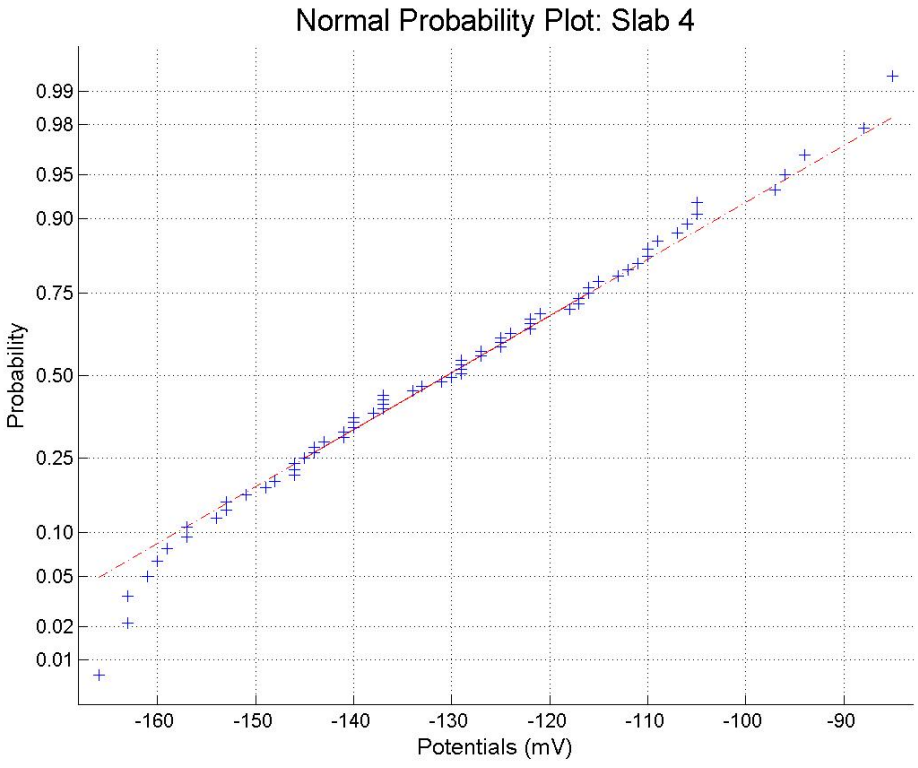

Figure B-16: Statistical Analys Slab 4: 04/06/2012

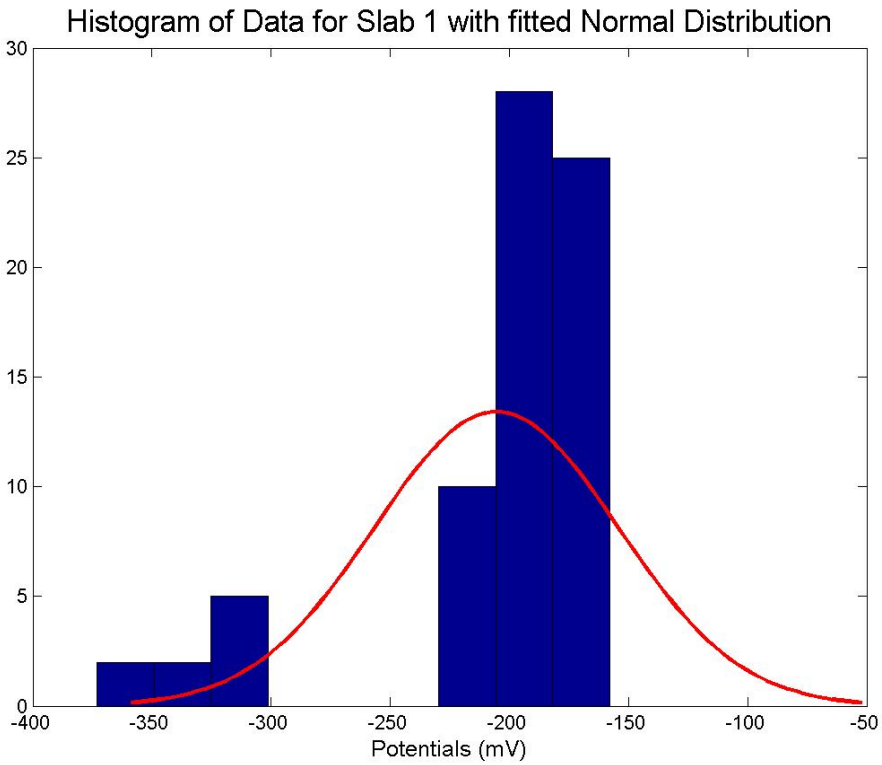

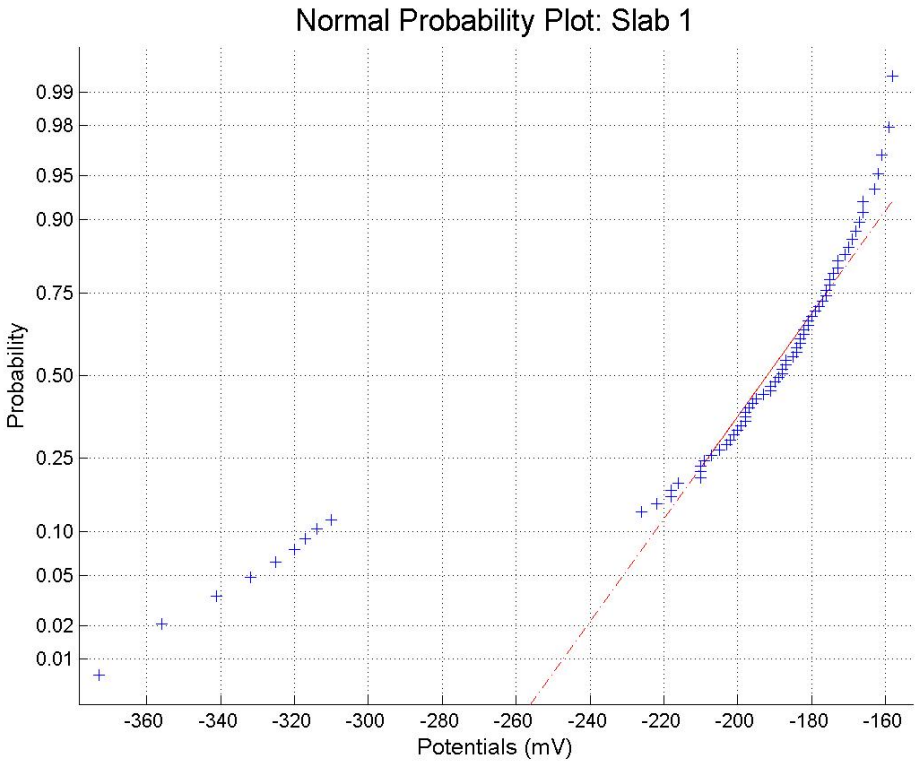

Figure B-17: Statistical Analys Slab 1: 04/13/2012

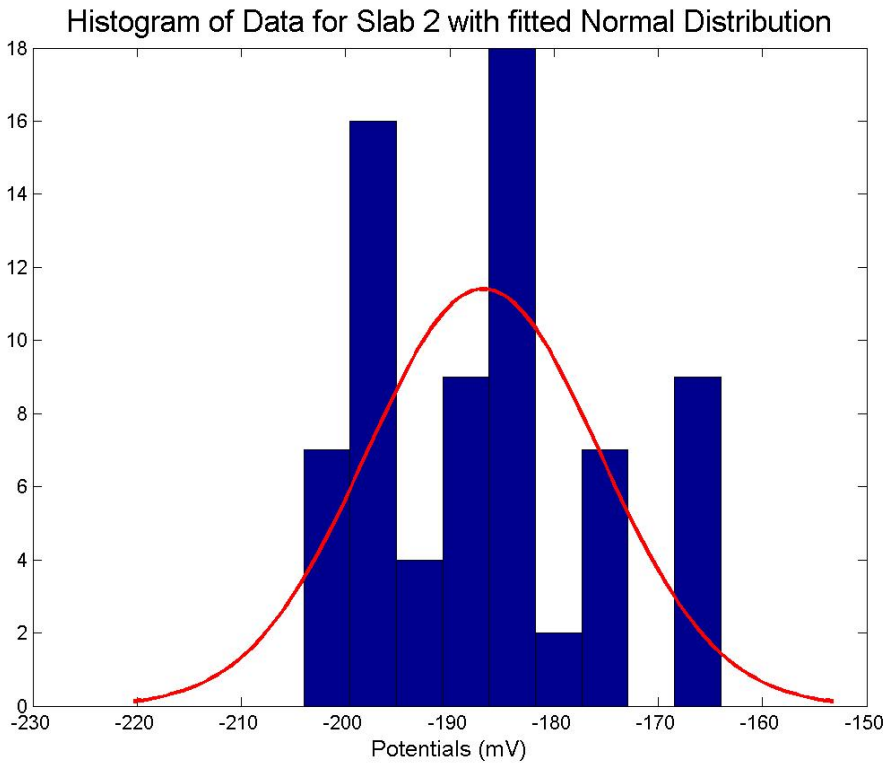

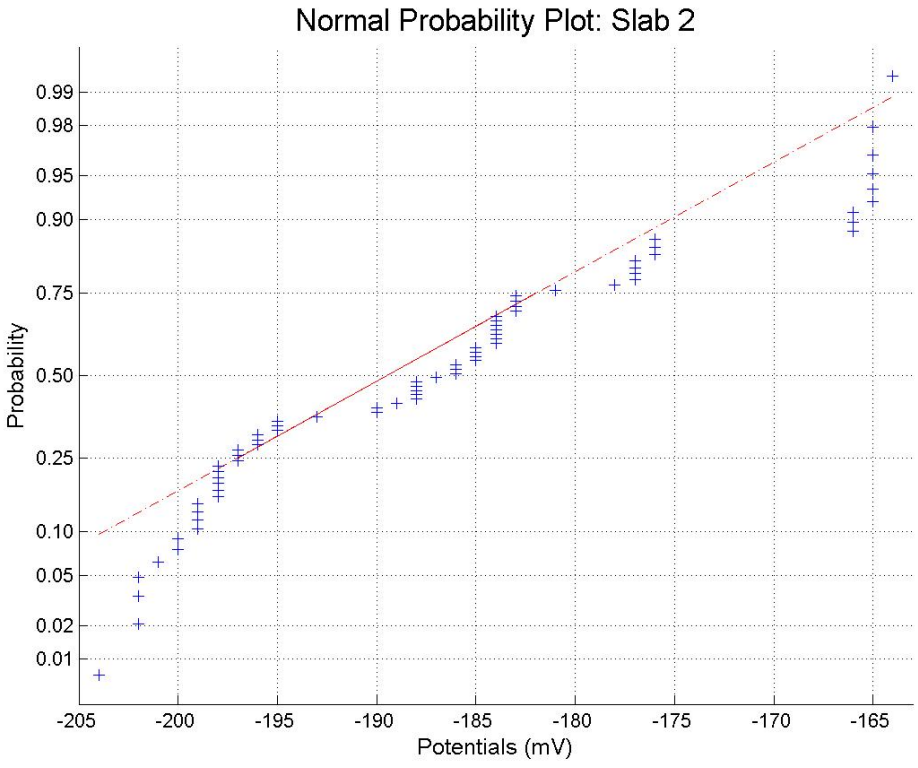

Figure B-18: Statistical Analys Slab 2: 04/13/2012

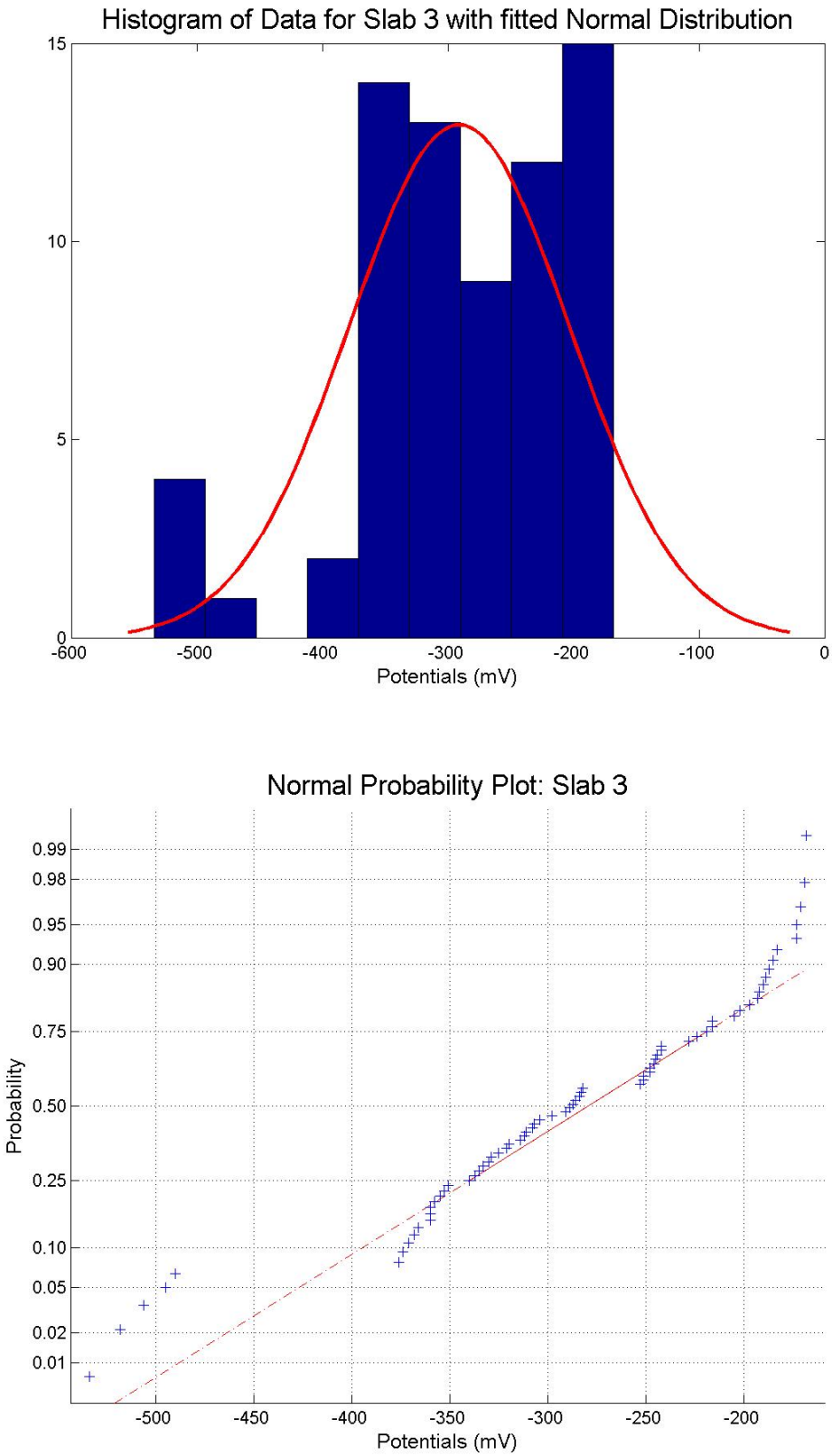

Figure B-19: Statistical Analys Slab 3: 04/13/2012

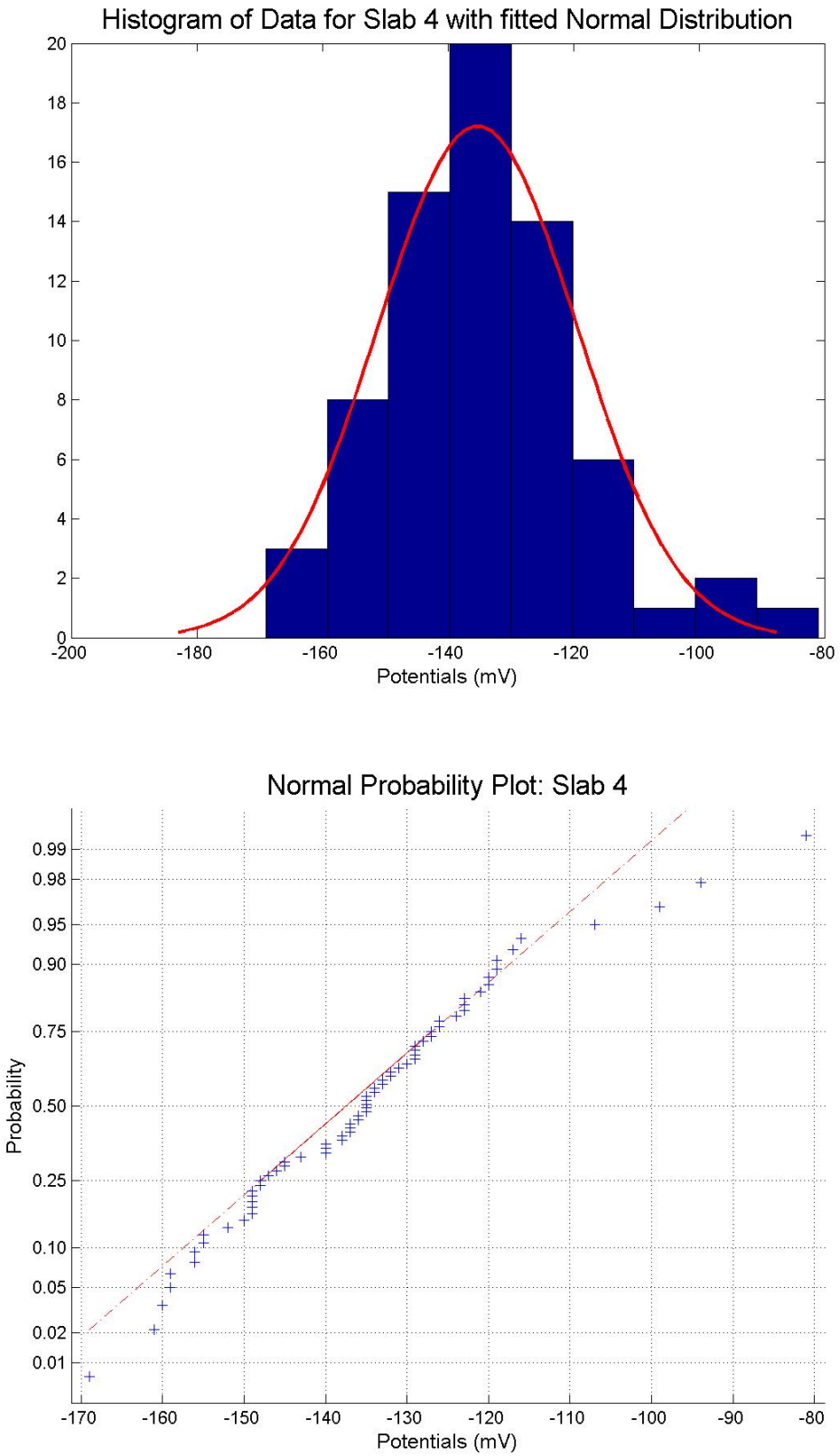

Figure B-20: Statistical Analys Slab 4: 04/13/2012

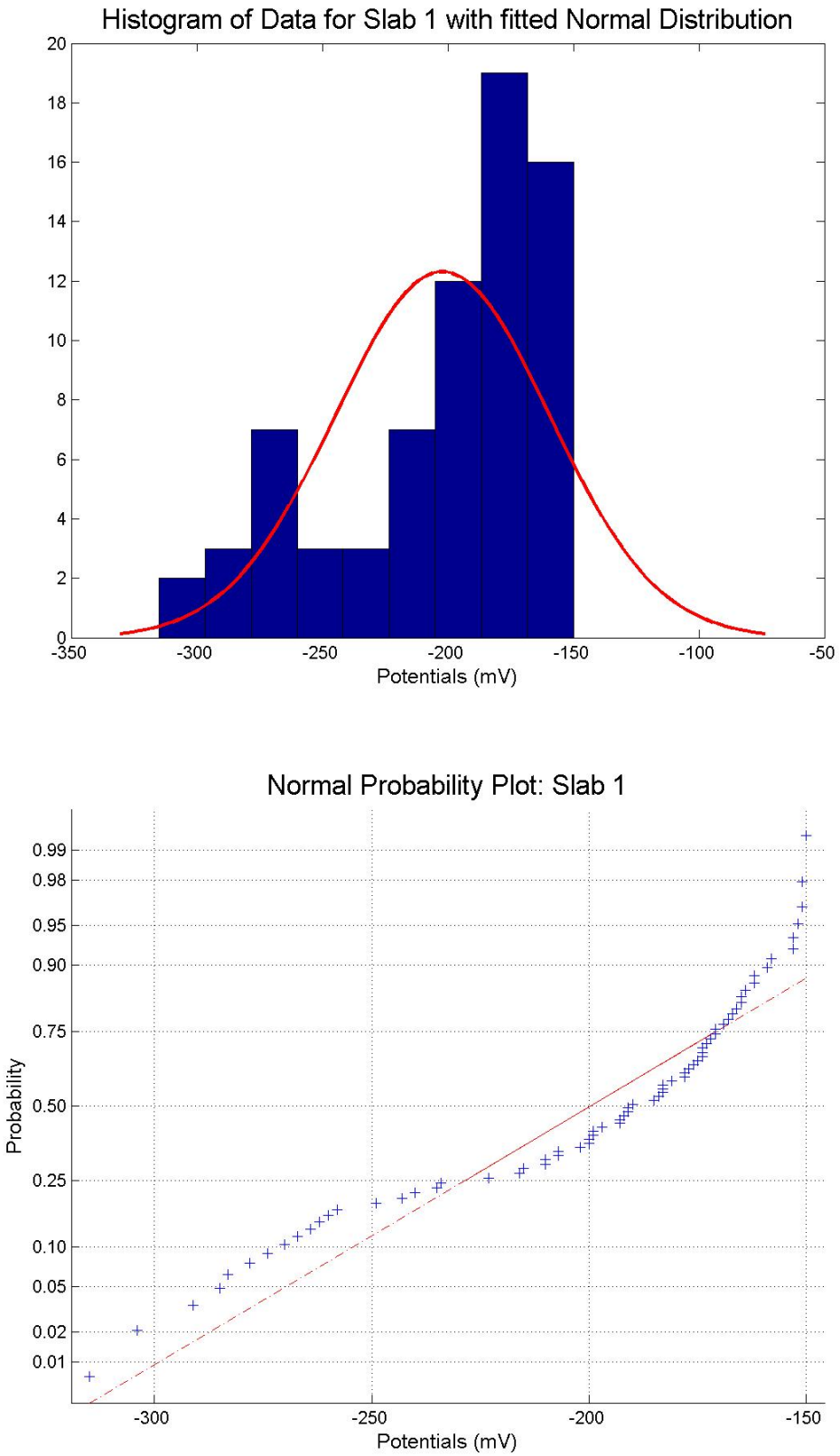

Figure B-21: Statistical Analys Slab 1: 04/20/2012

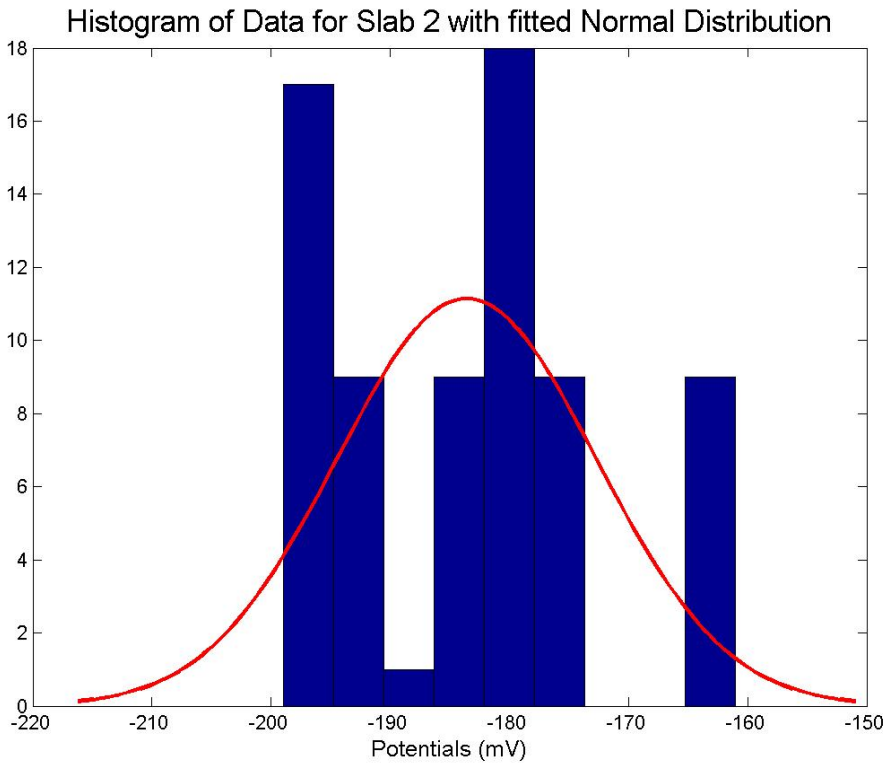

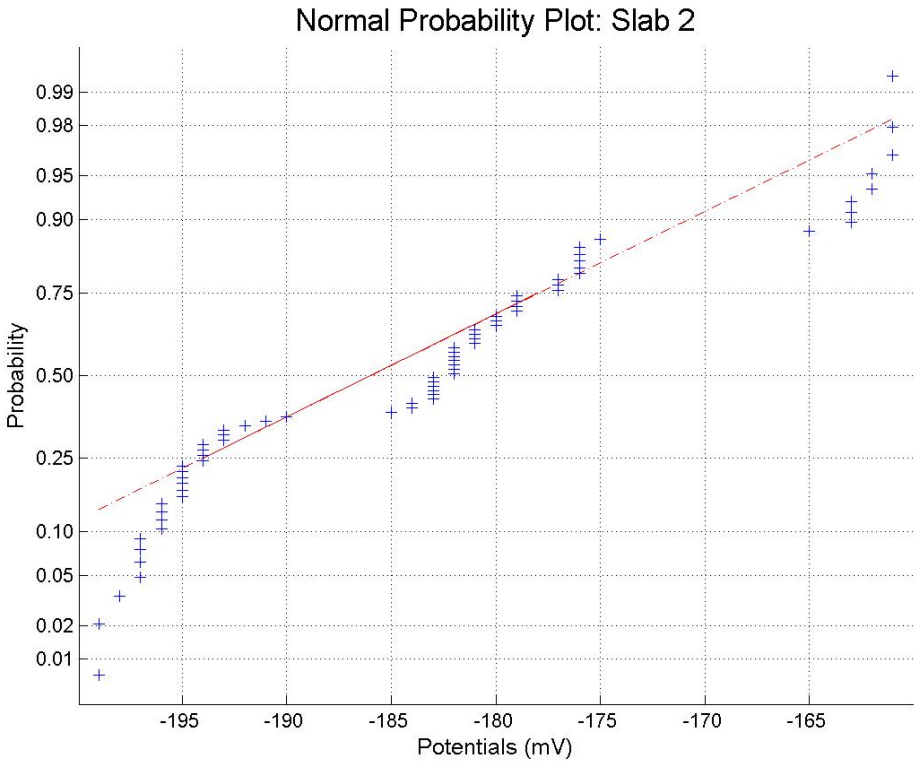

Figure B-22: Statistical Analys Slab 2: 04/20/2012

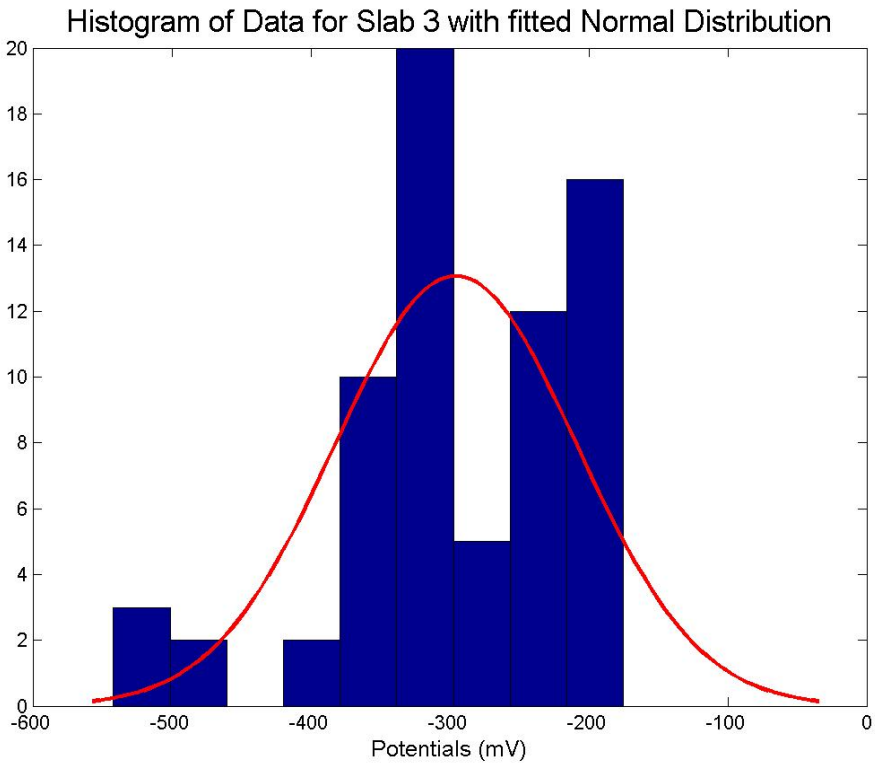

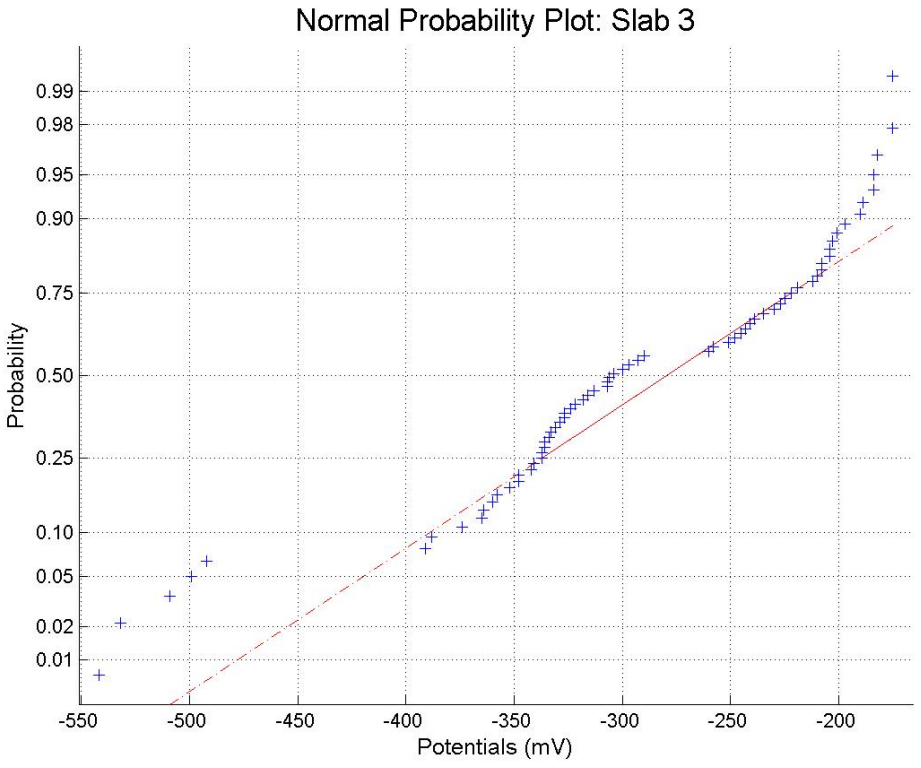

Figure B-23: Statistical Analys Slab 3: 04/20/2012

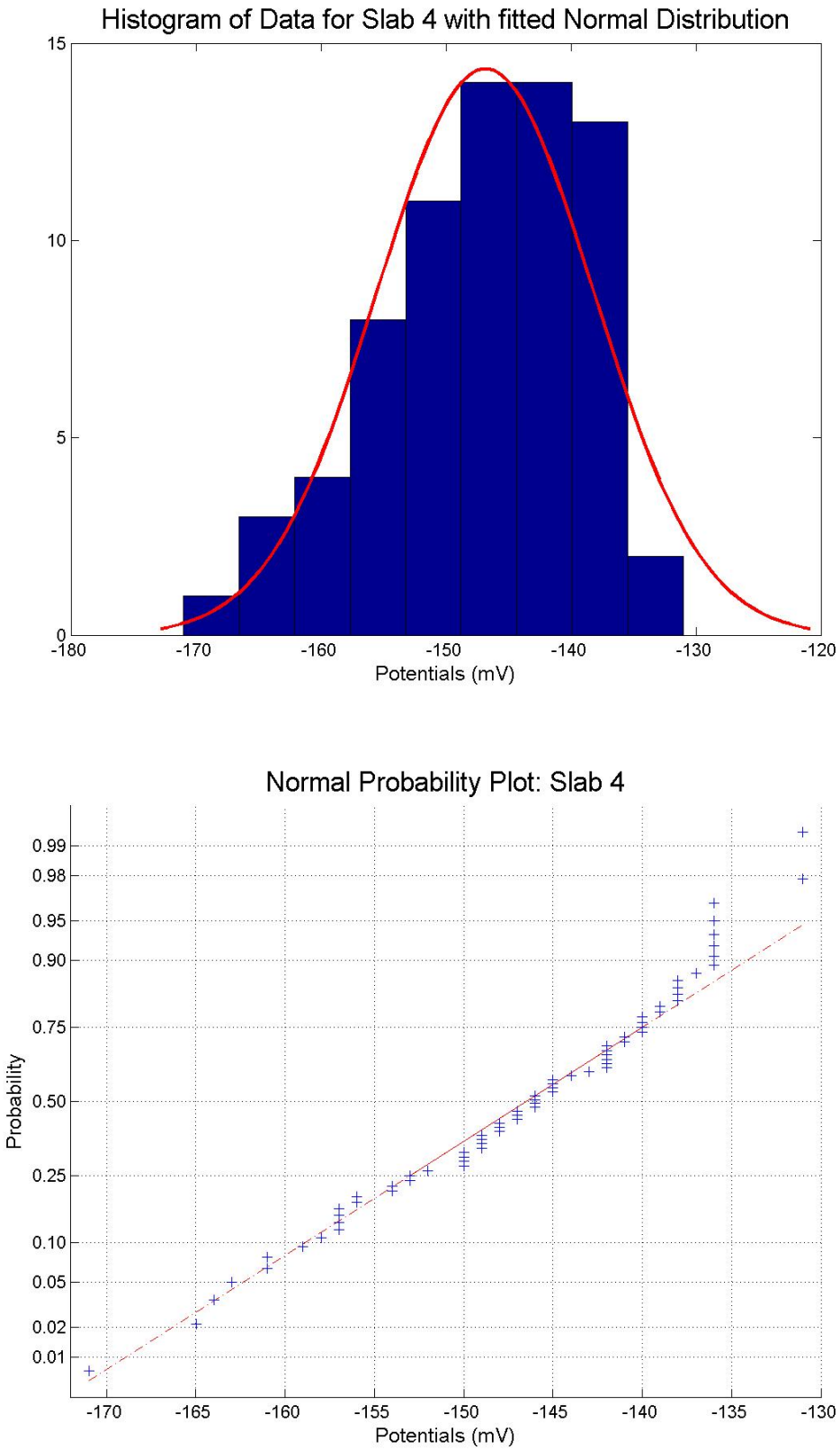

Figure B-24: Statistical Analys Slab 4: 04/20/2012

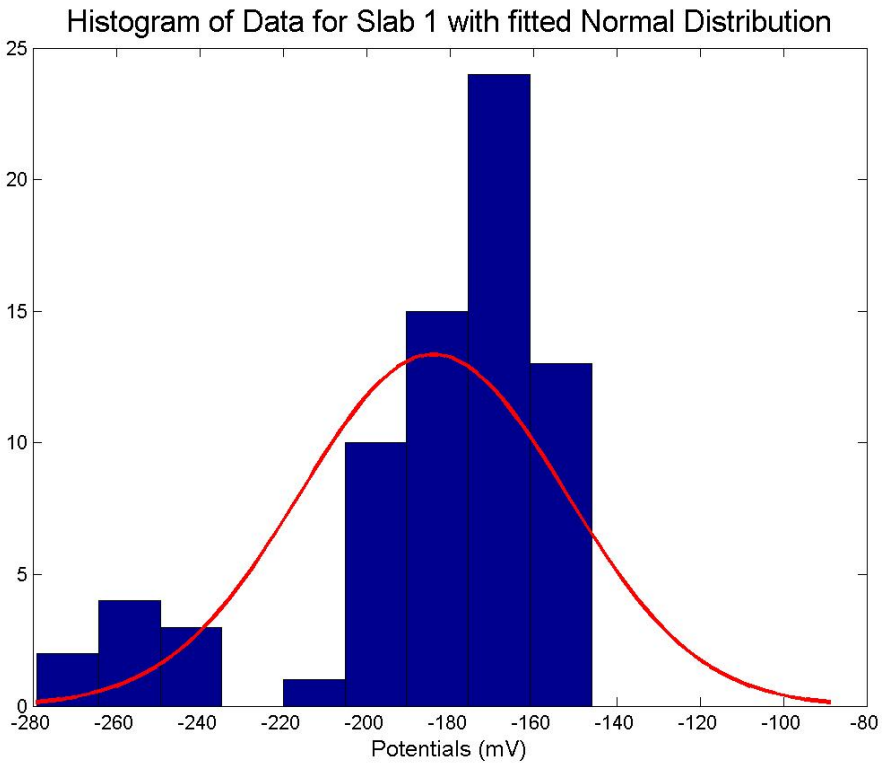

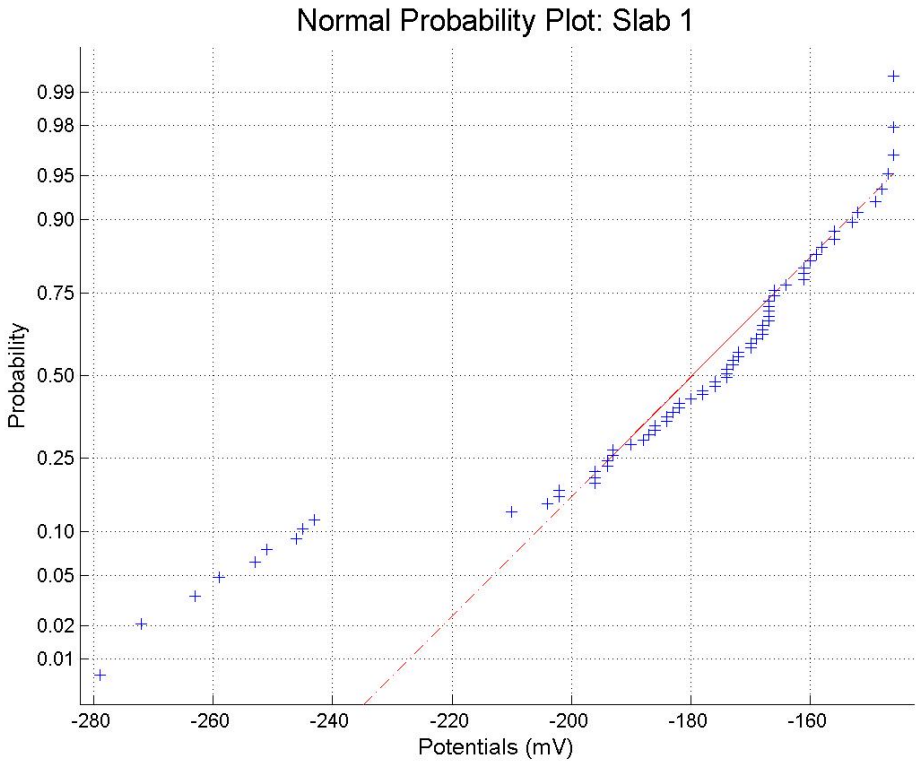

Figure B-25: Statistical Analys Slab 1: 04/27/2012

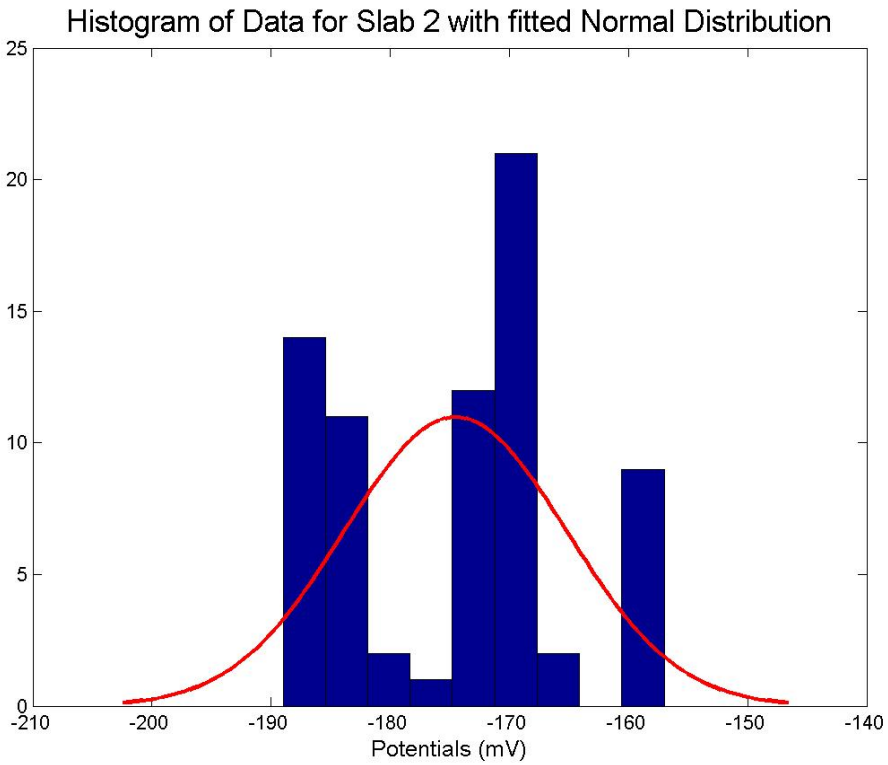

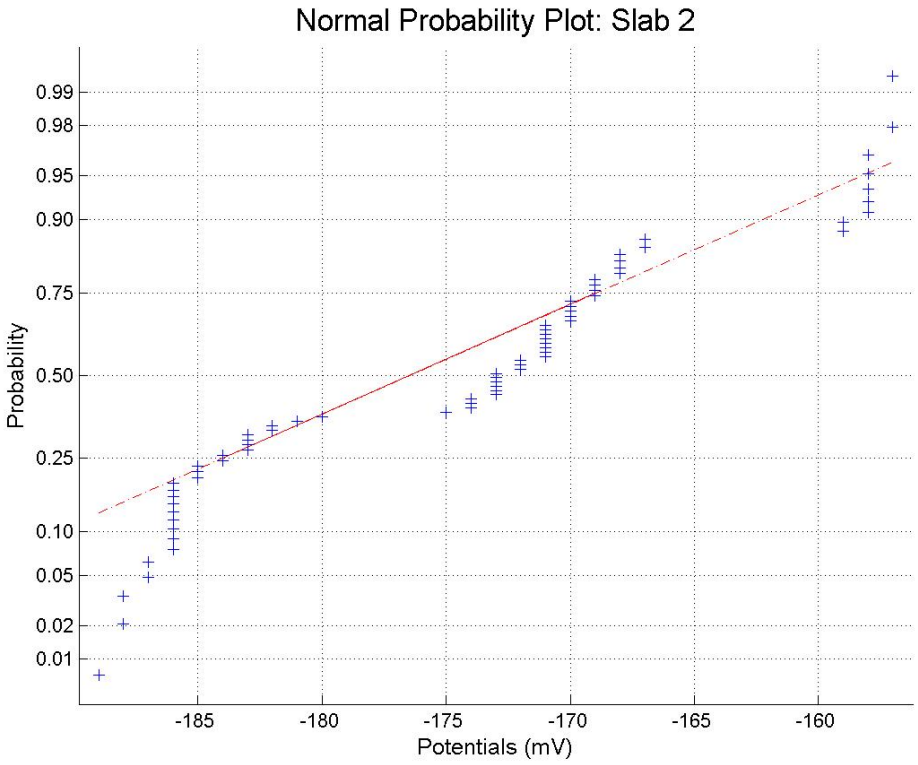

Figure B-26: Statistical Analys Slab 2: 04/27/2012

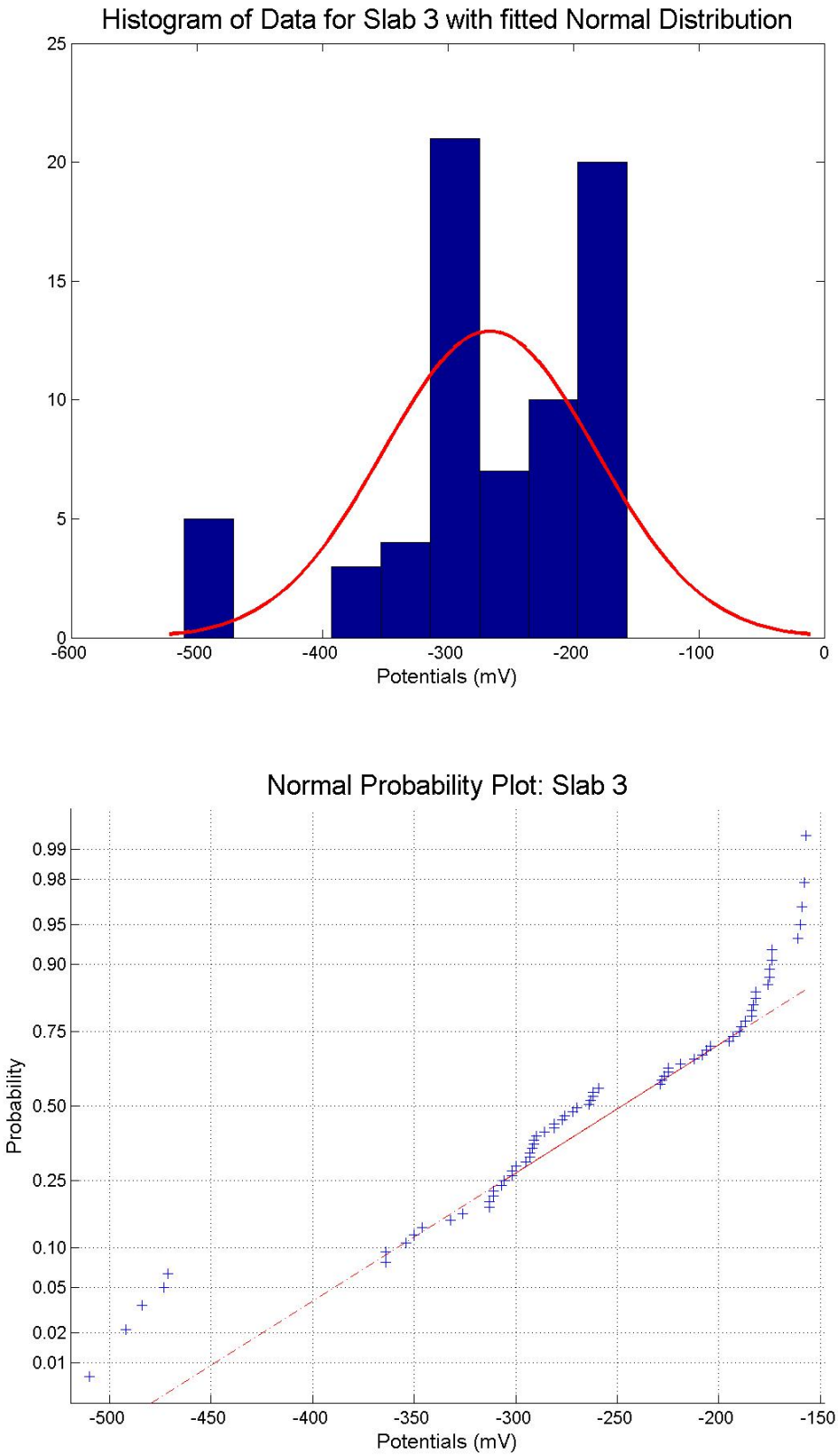

Figure B-27: Statistical Analys Slab 3: 04/27/2012

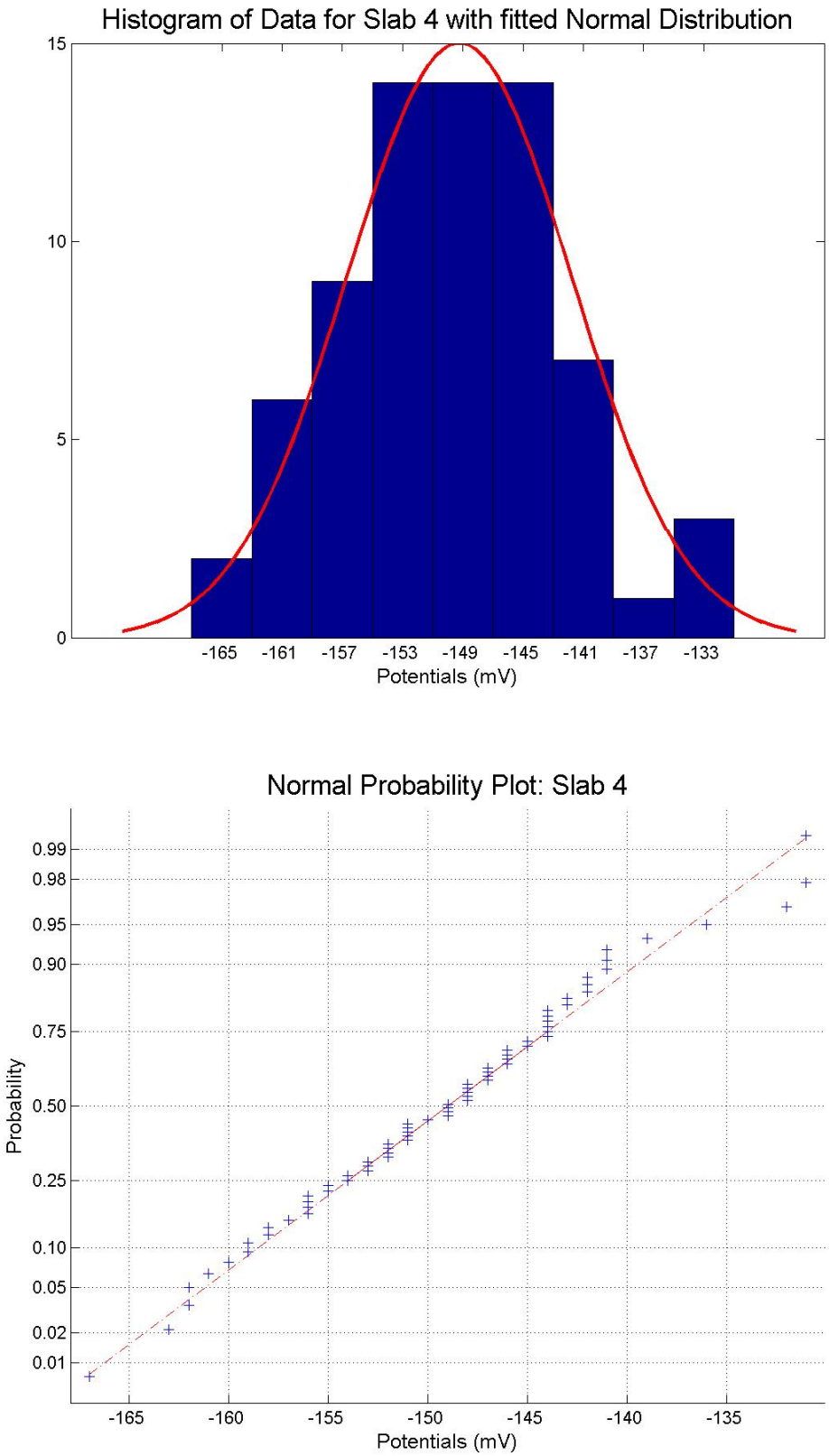

Figure B-28: Statistical Analys Slab 4: 04/27/2012

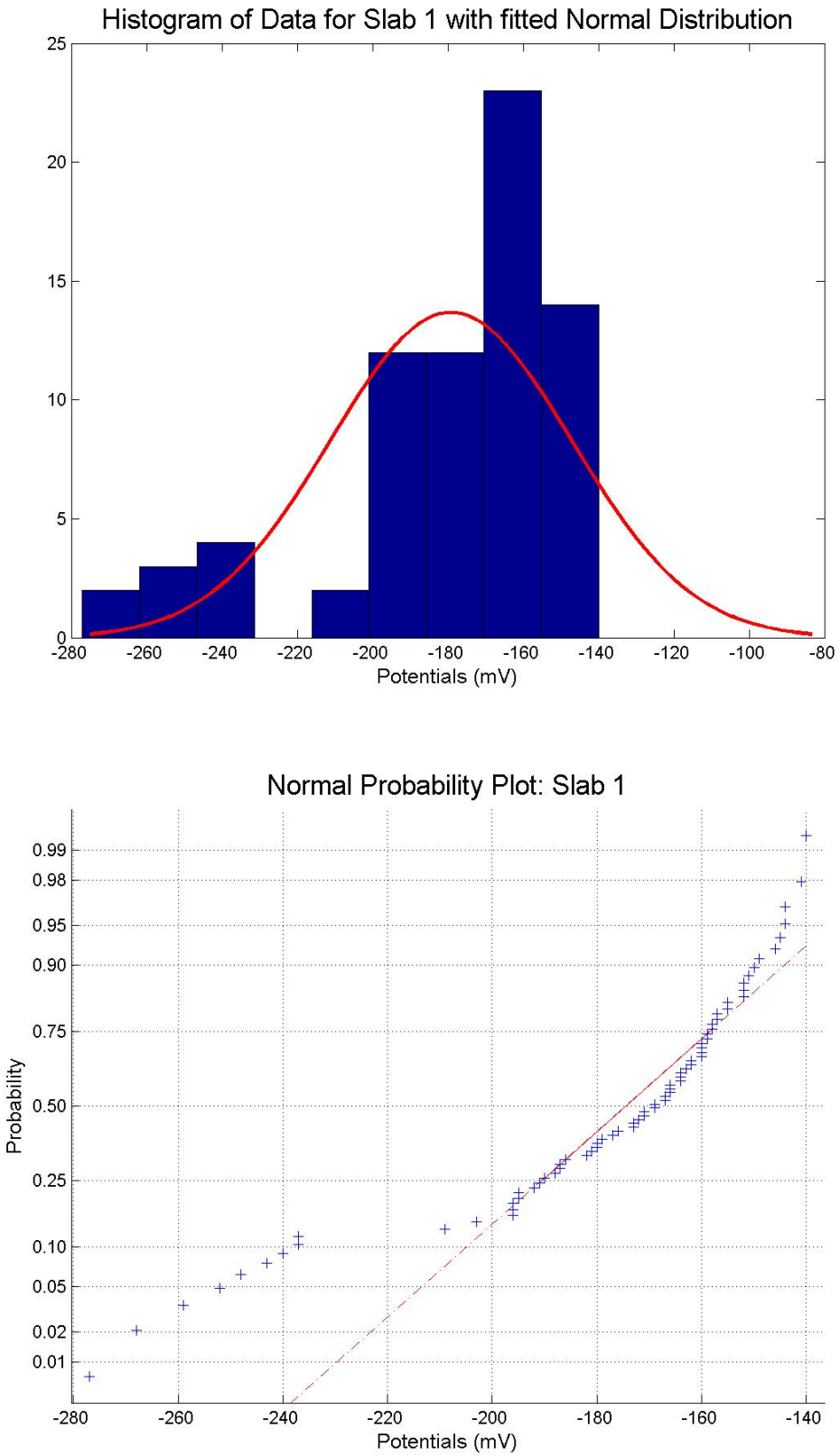

Figure B-29: Statistical Analys Slab 1: 05/04/2012

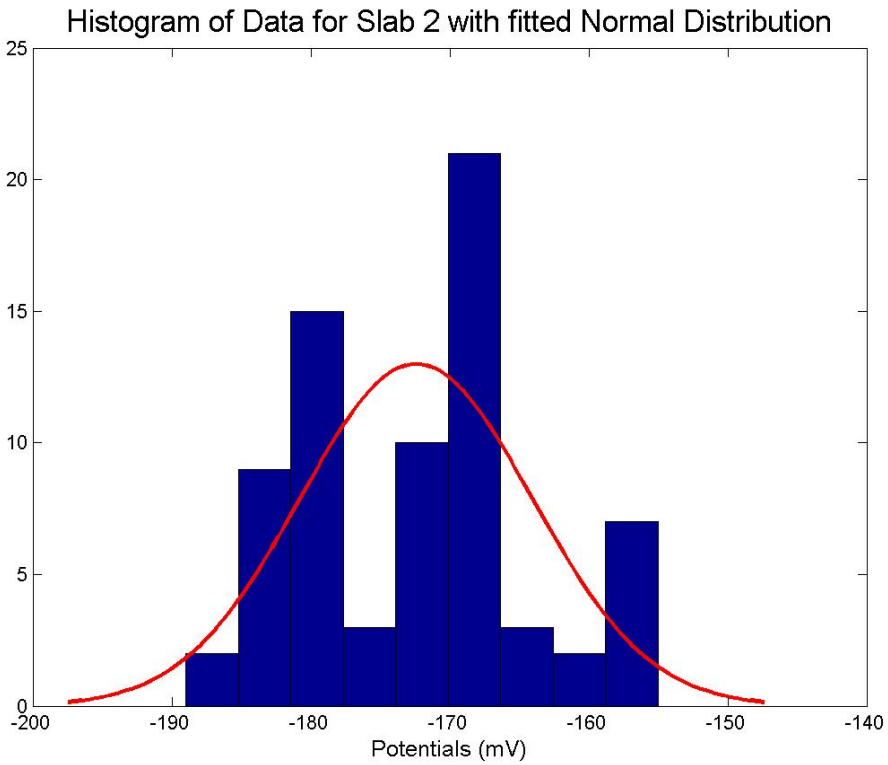

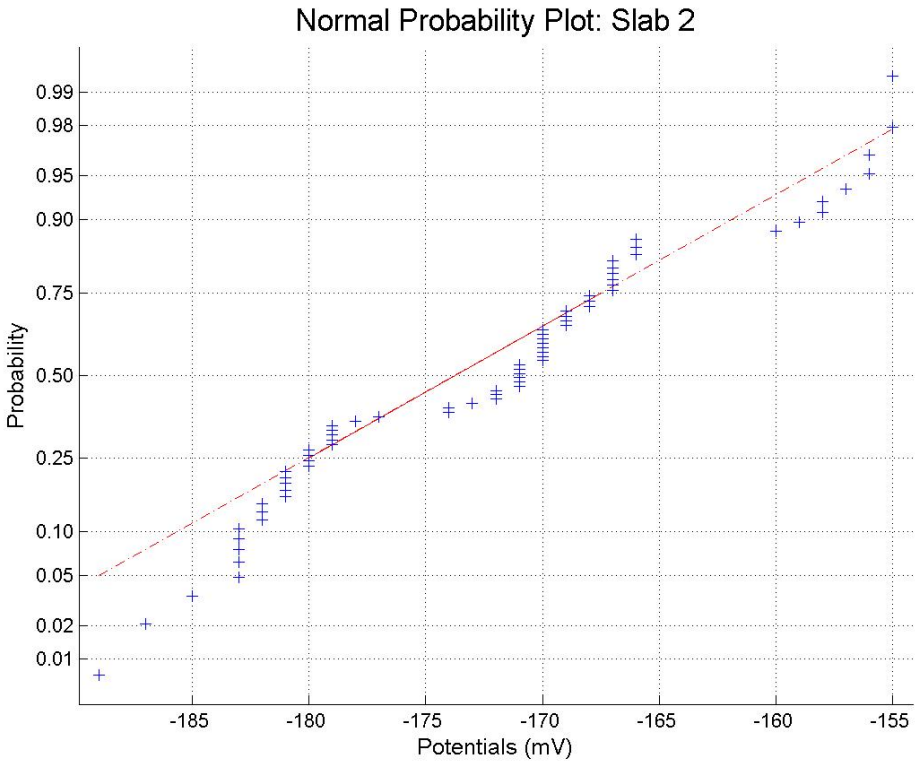

Figure B-30: Statistical Analys Slab 2: 05/04/2012

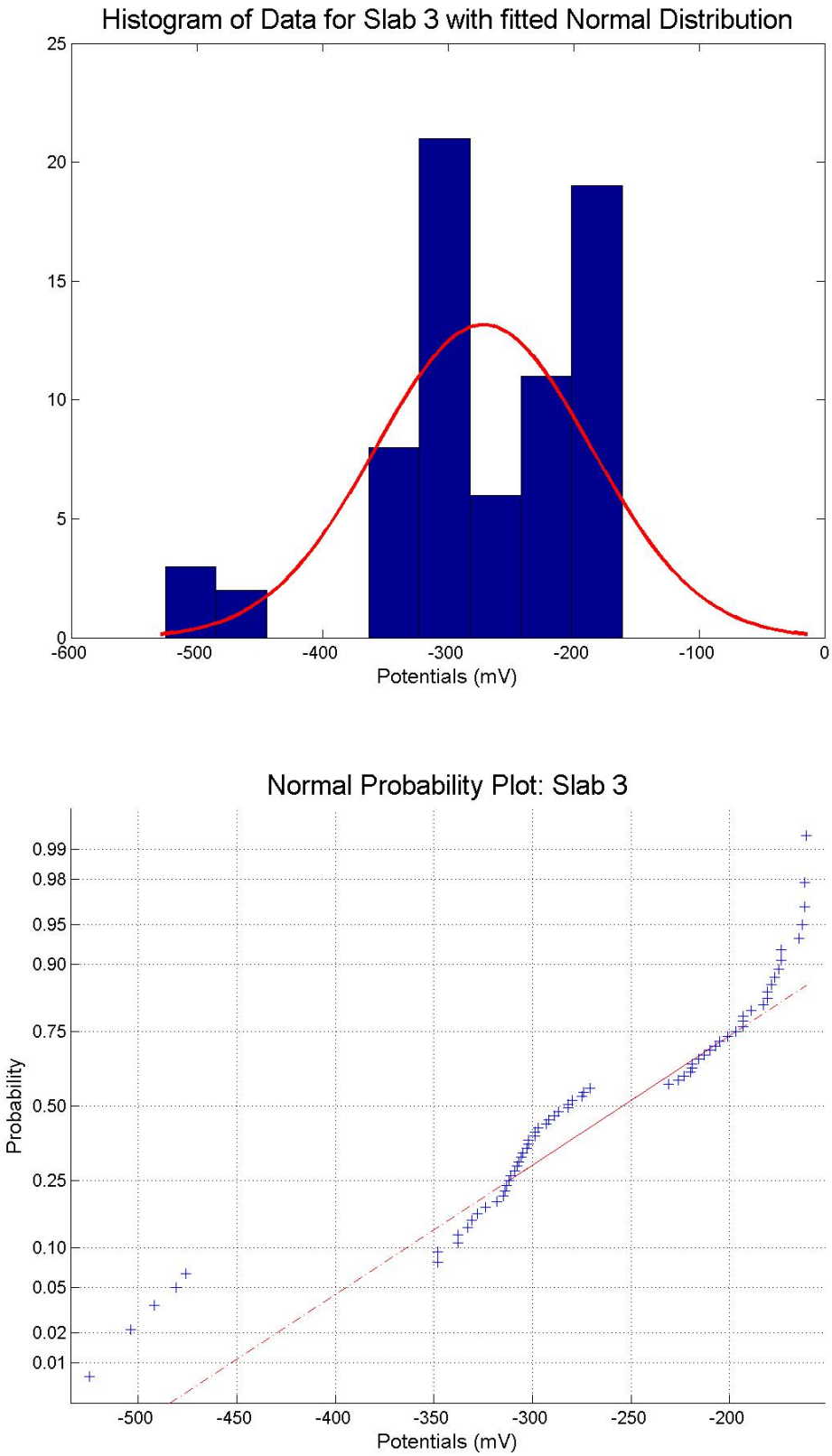

Figure B-31: Statistical Analys Slab 3: 05/04/2012

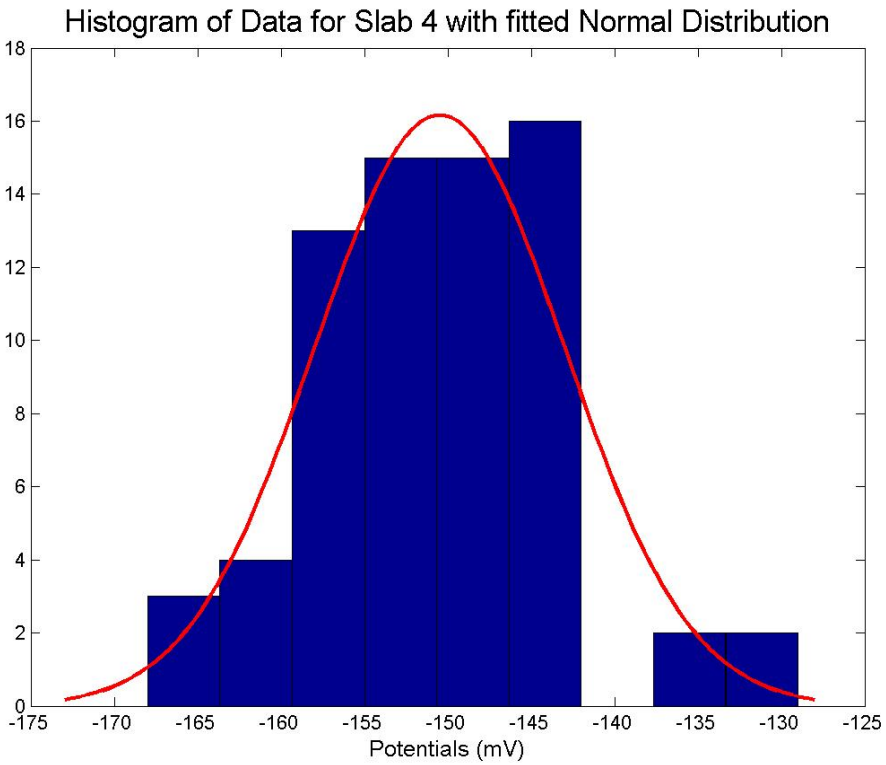

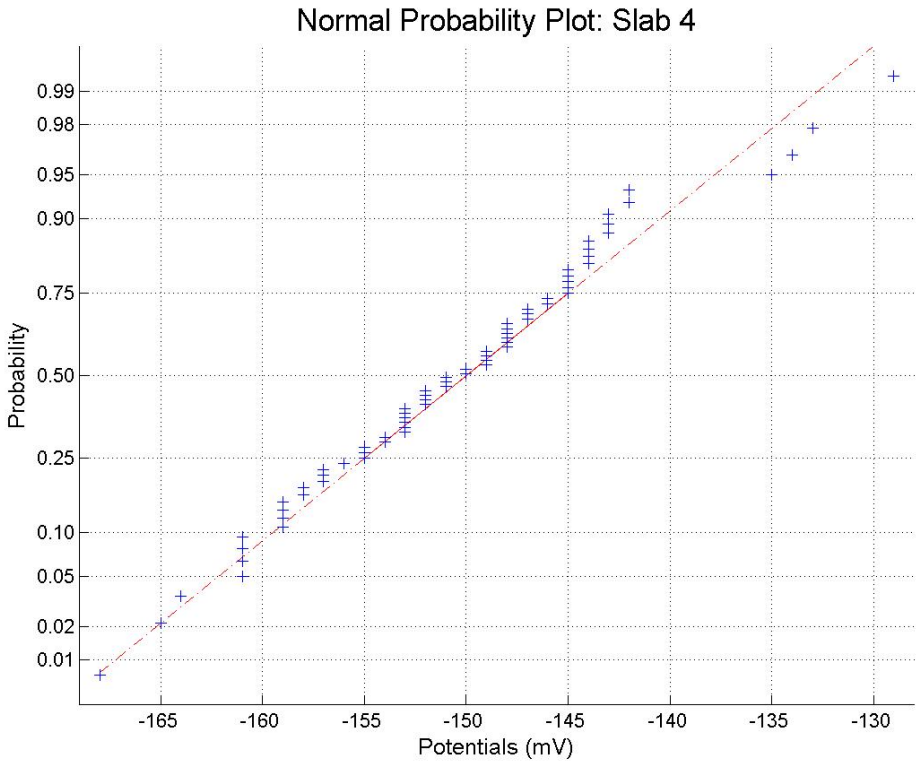

Figure B-32: Statistical Analys Slab 4: 05/04/2012

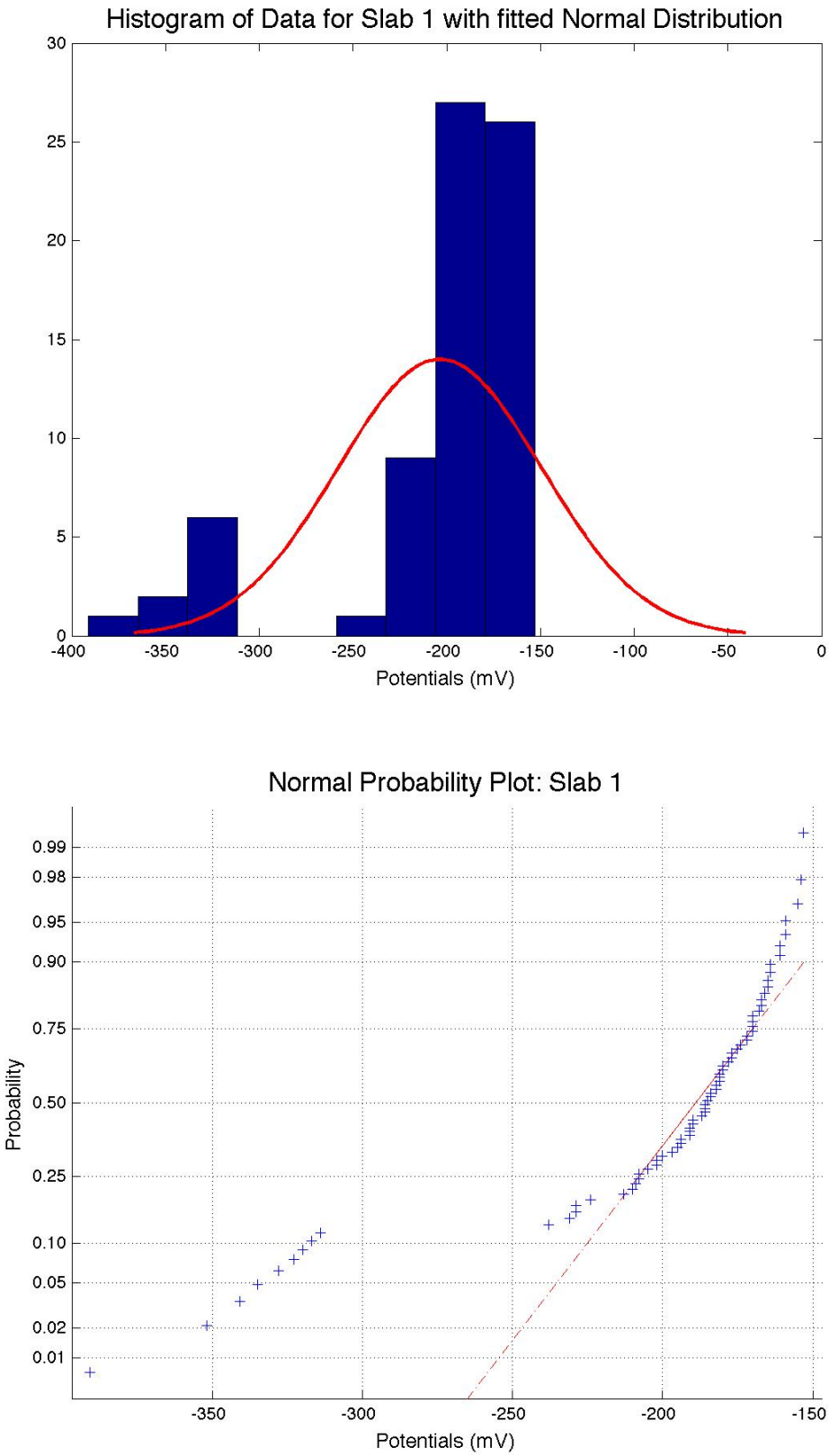

Figure B-33: Statistical Analys Slab 1: 05/11/2012

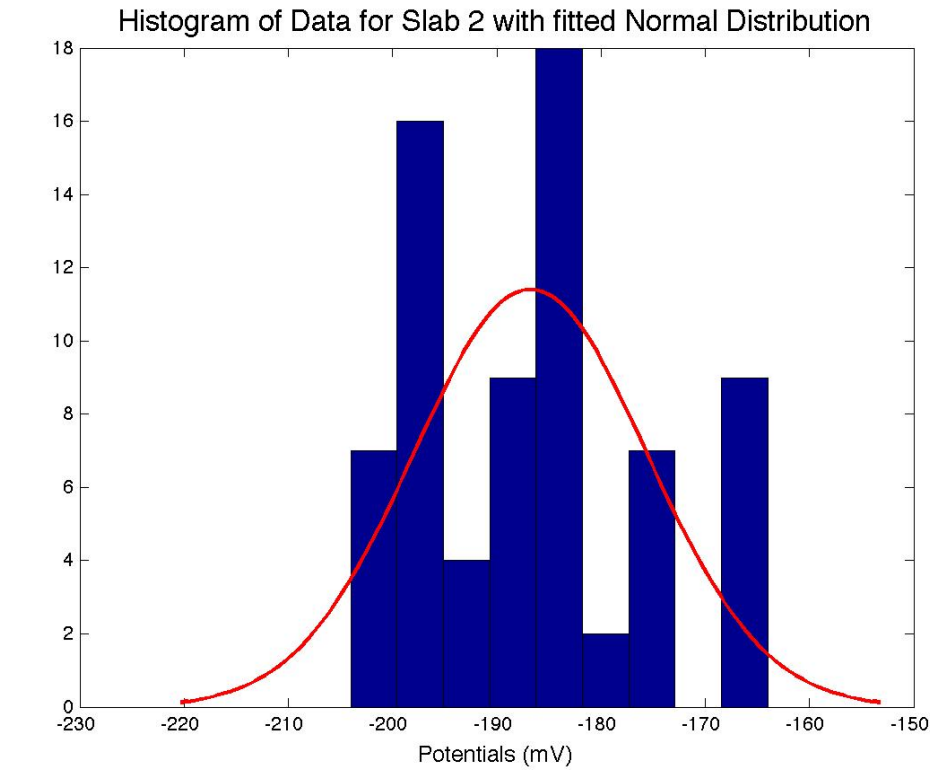

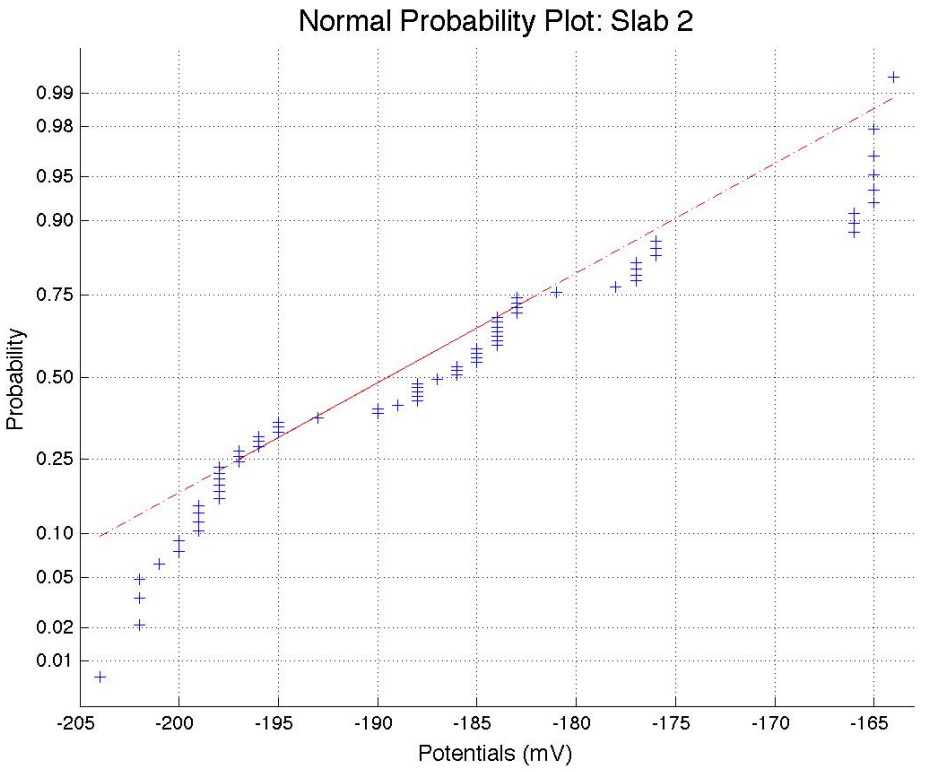

Figure B-34: Statistical Analys Slab 2: 05/11/2012

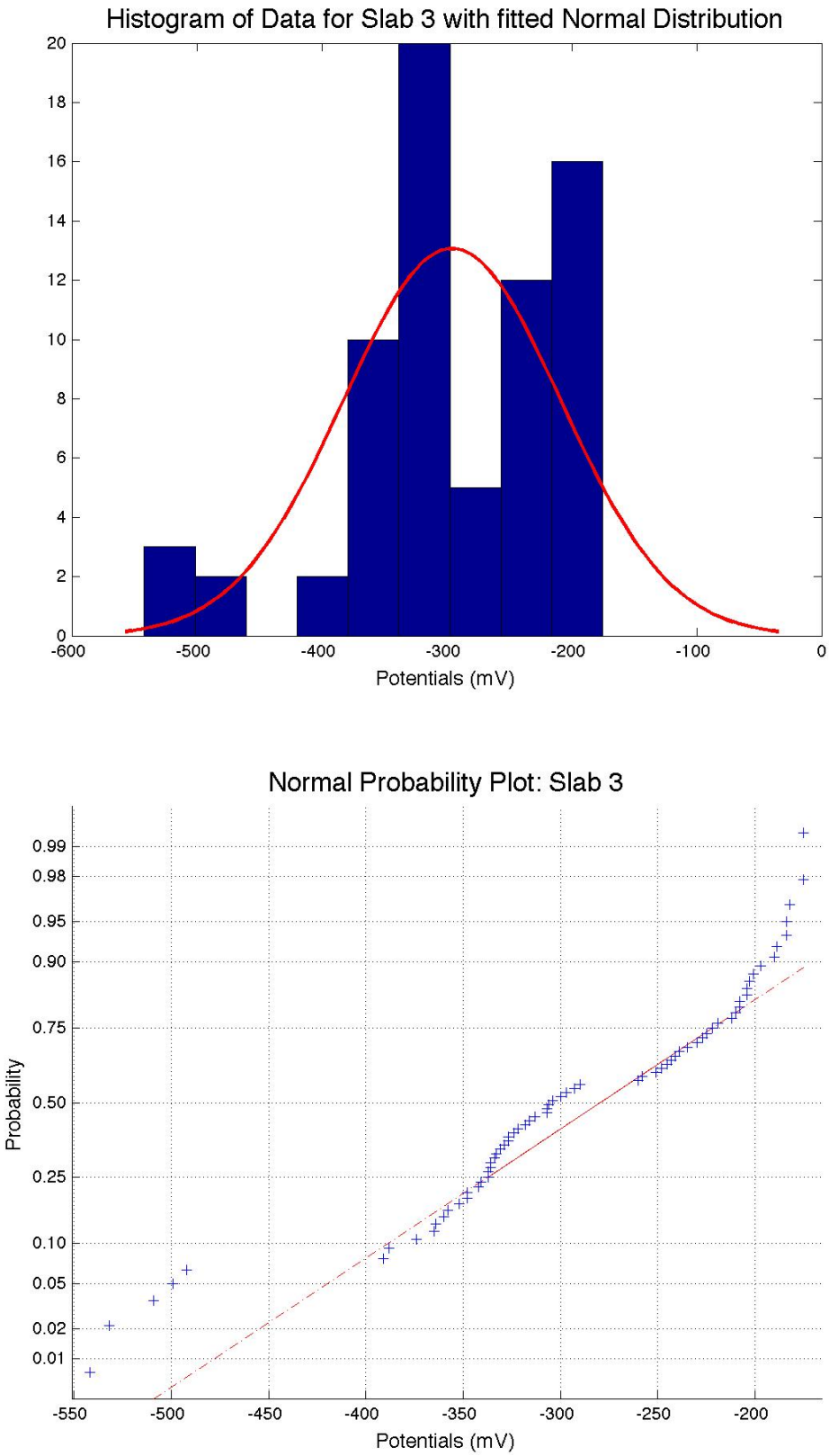

Figure B-35: Statistical Analys Slab 3: 05/11/2012

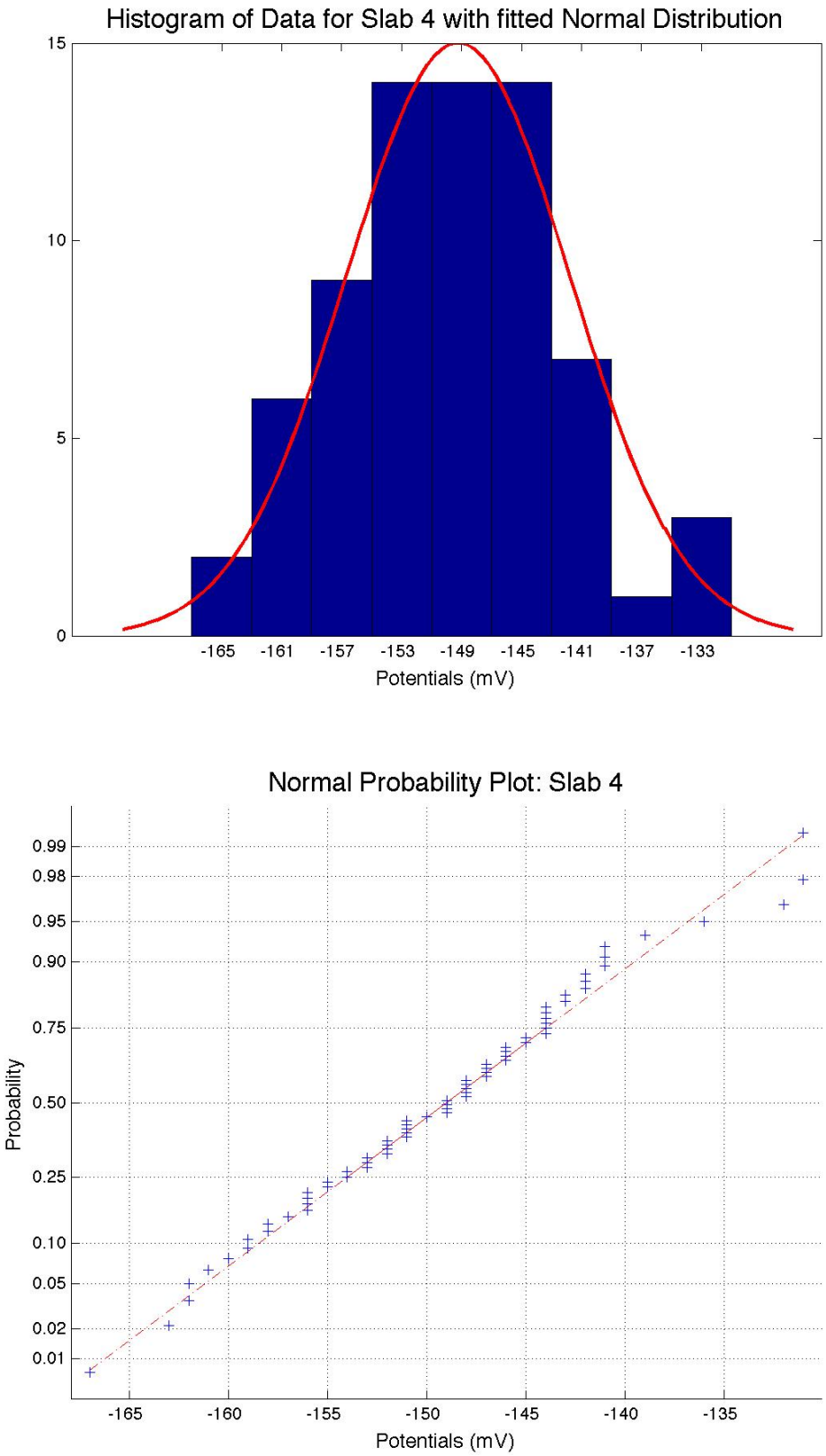

Figure B-36: Statistical Analys Slab 4: 05/11/2012

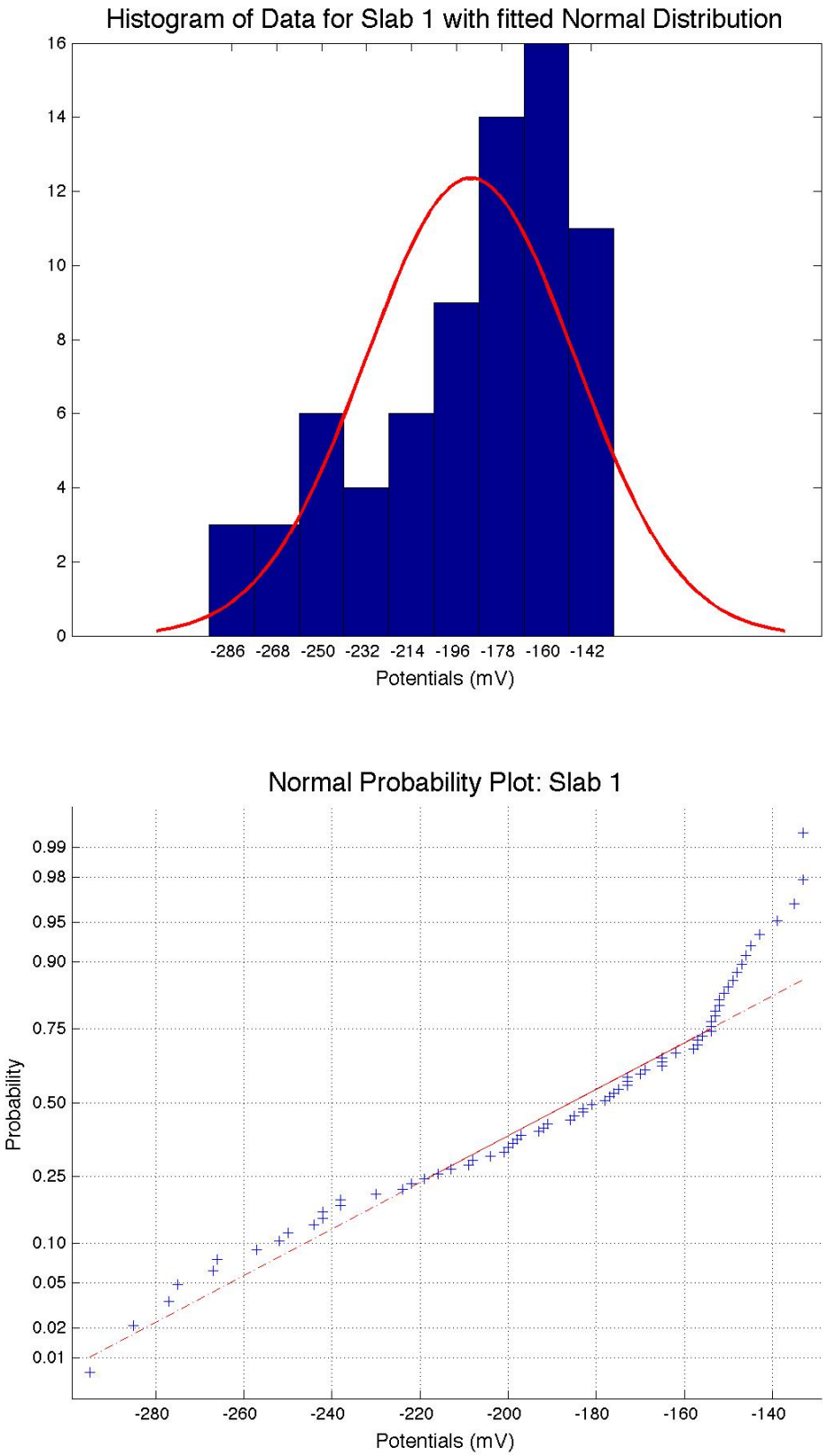

Figure B-37: Statistical Analys Slab 1: 05/25/2012

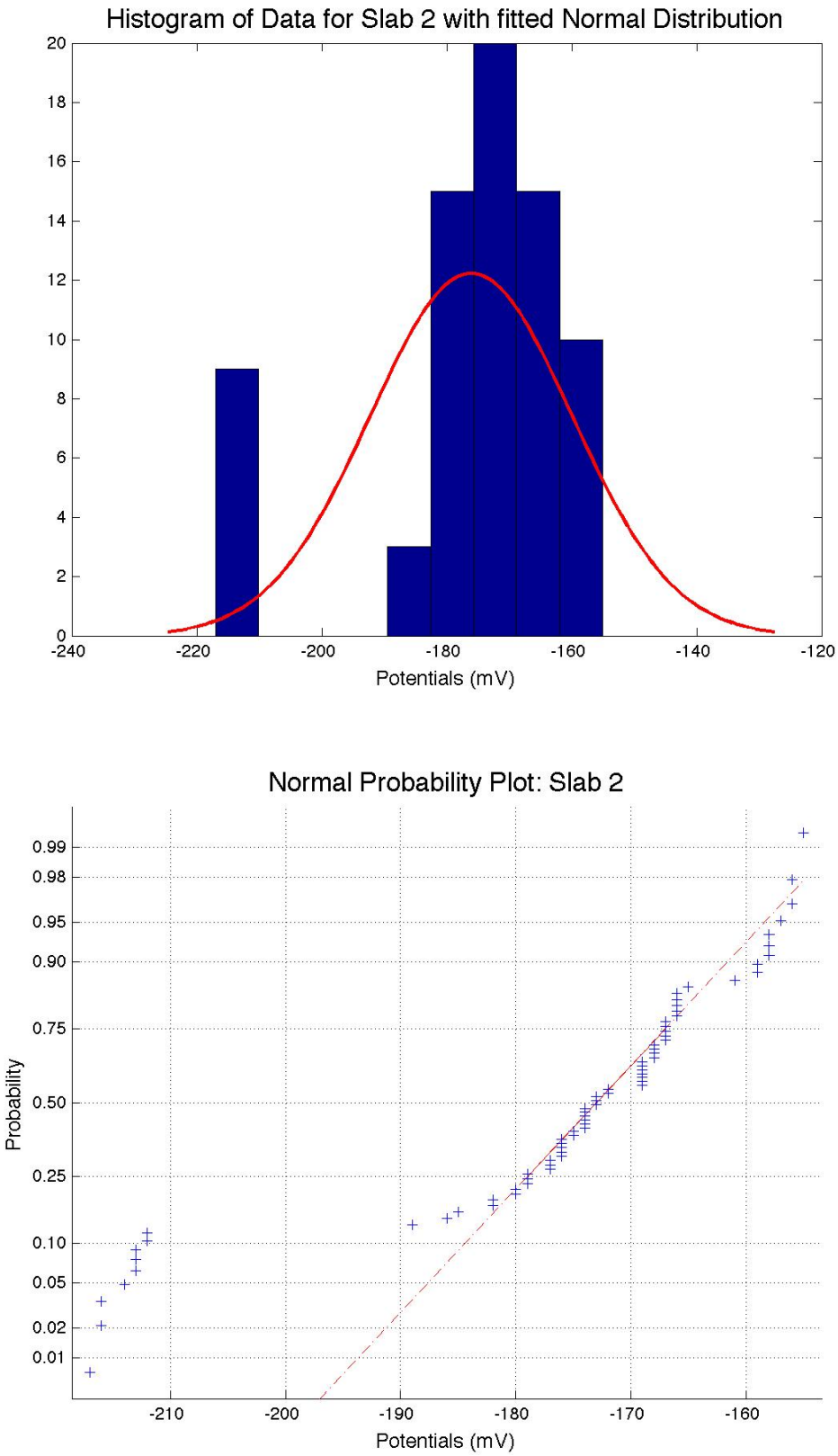

Figure B-38: Statistical Analys Slab 2: 05/25/2012

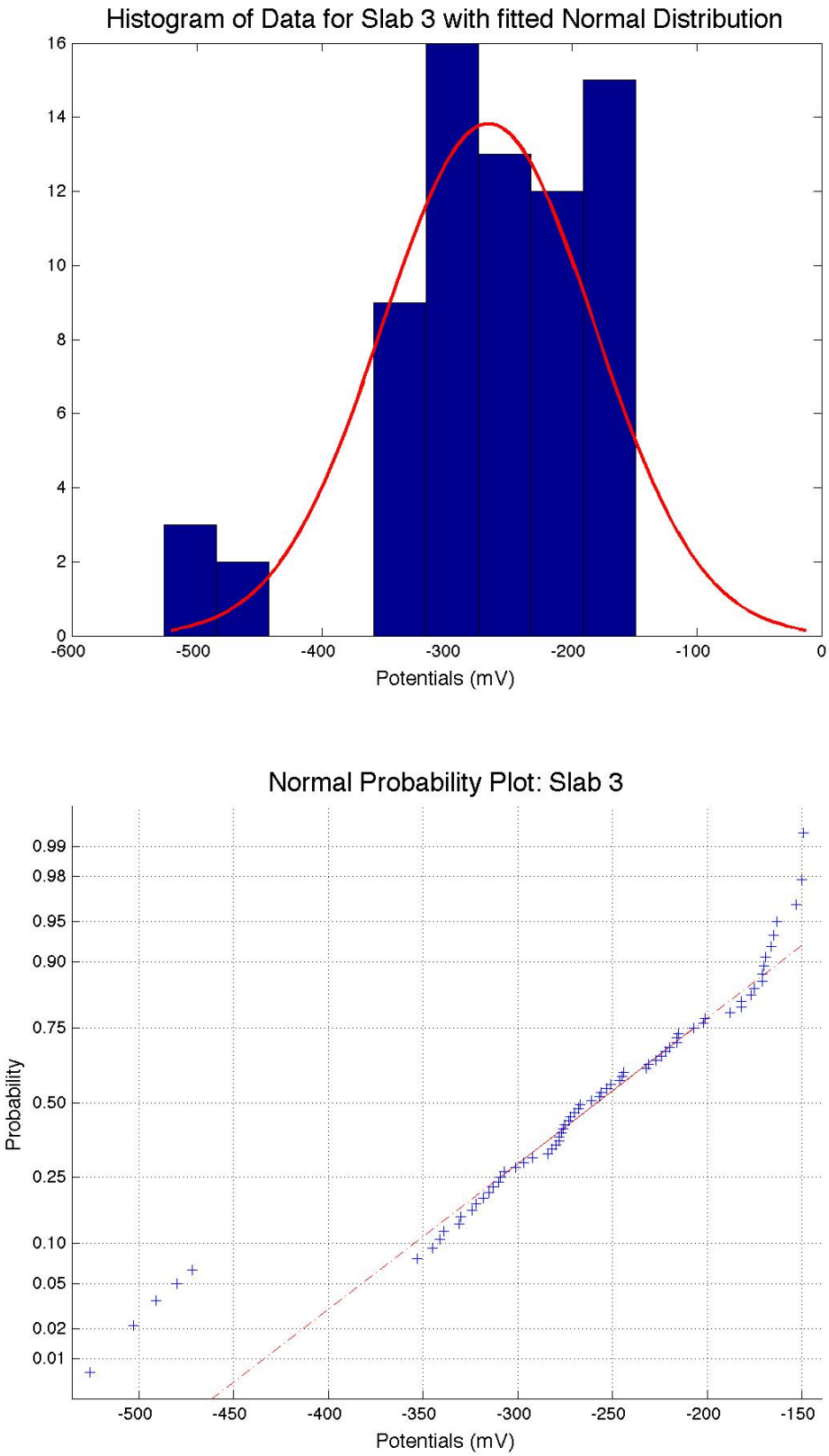

Figure B-39: Statistical Analys Slab 3: 05/25/2012

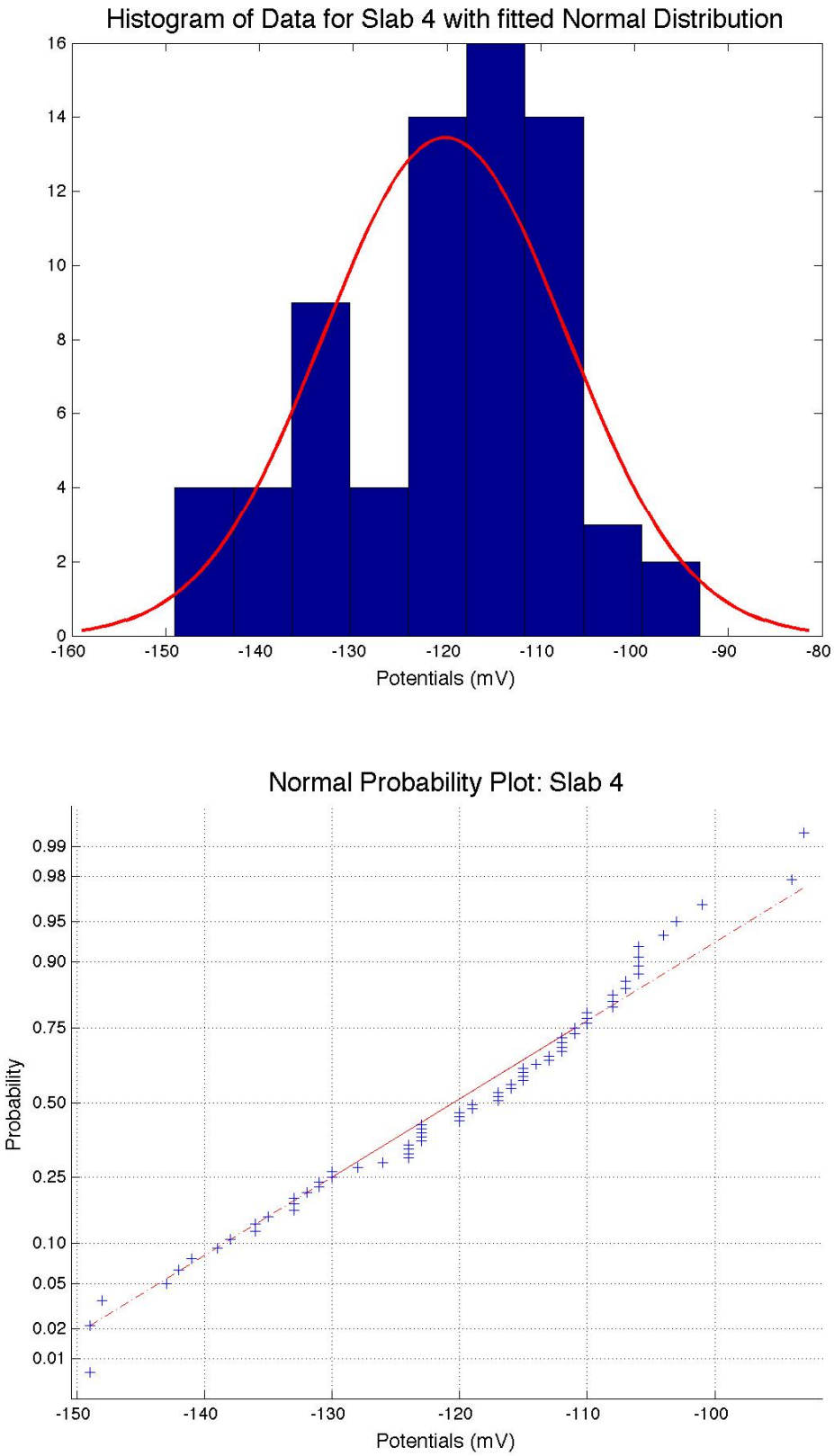

Figure B-40: Statistical Analys Slab 4: 05/25/2012

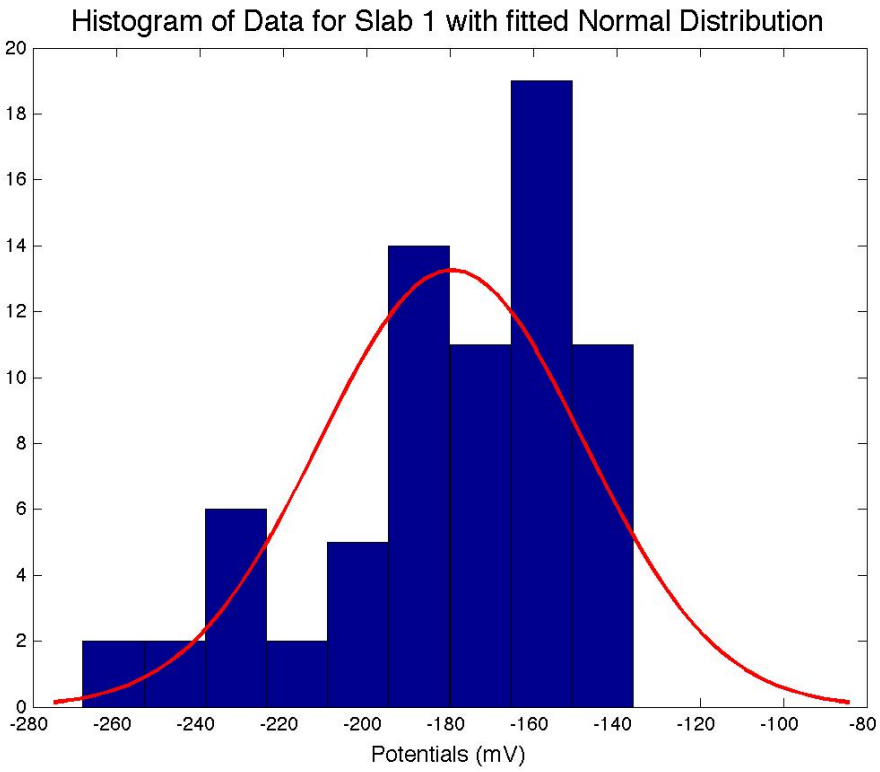

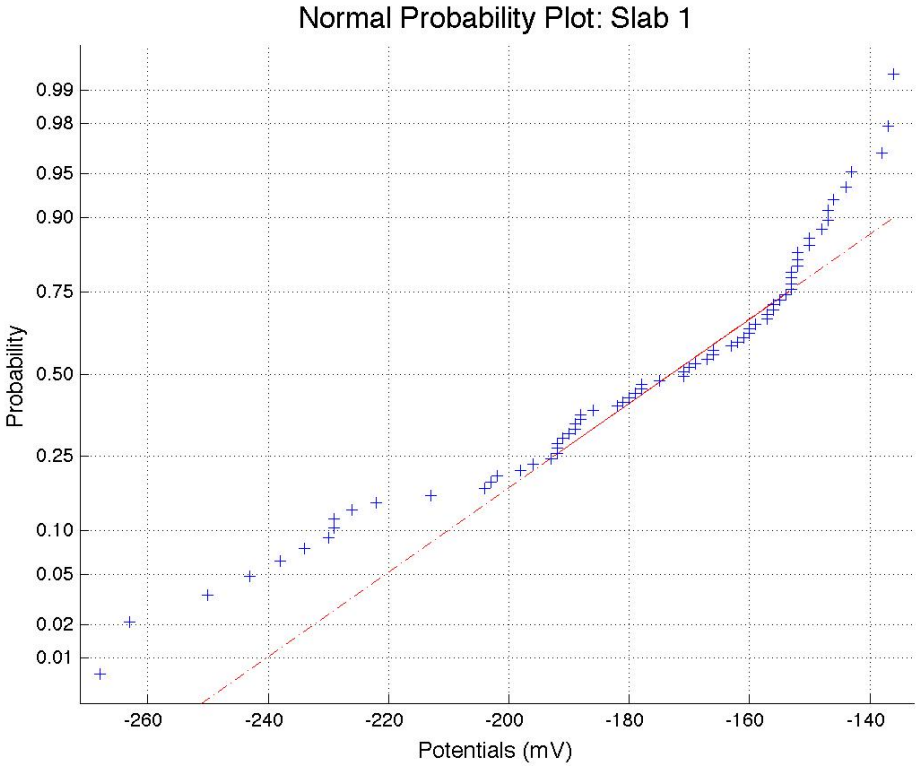

Figure B-41: Statistical Analys Slab 1: 06/01/2012

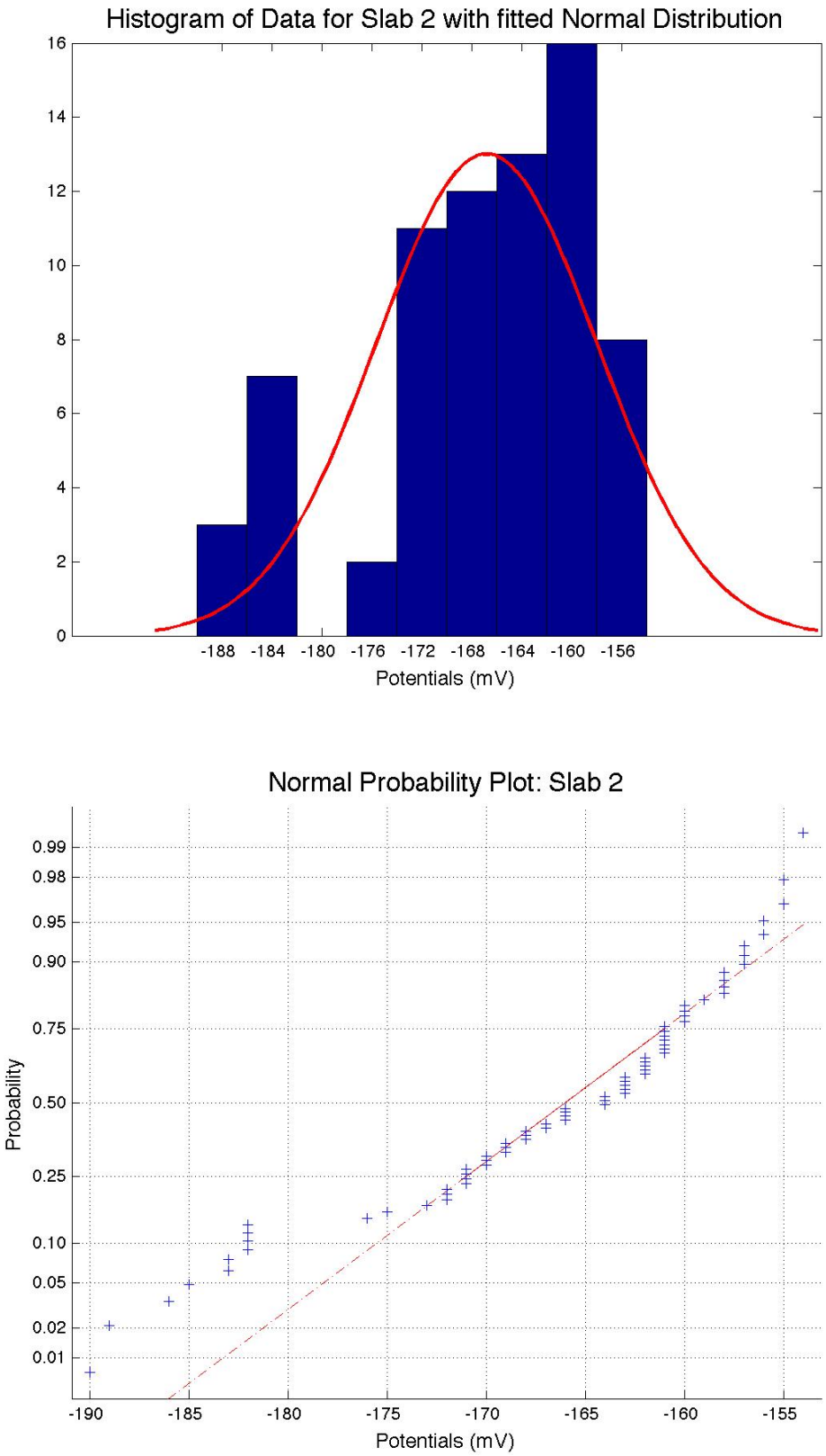

Figure B-42: Statistical Analys Slab 2: 06/01/2012

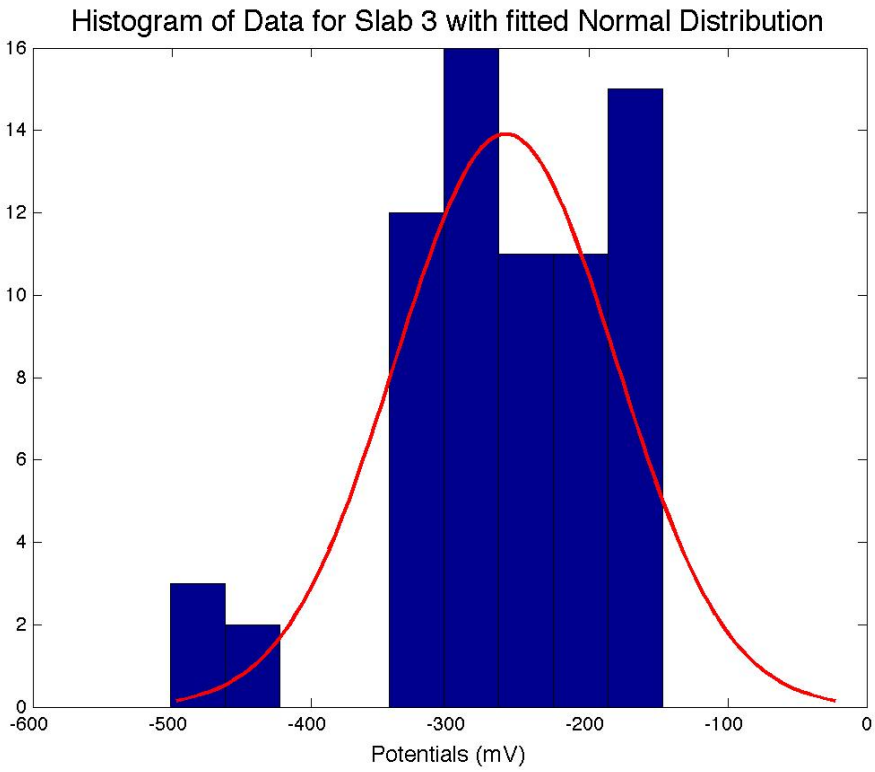

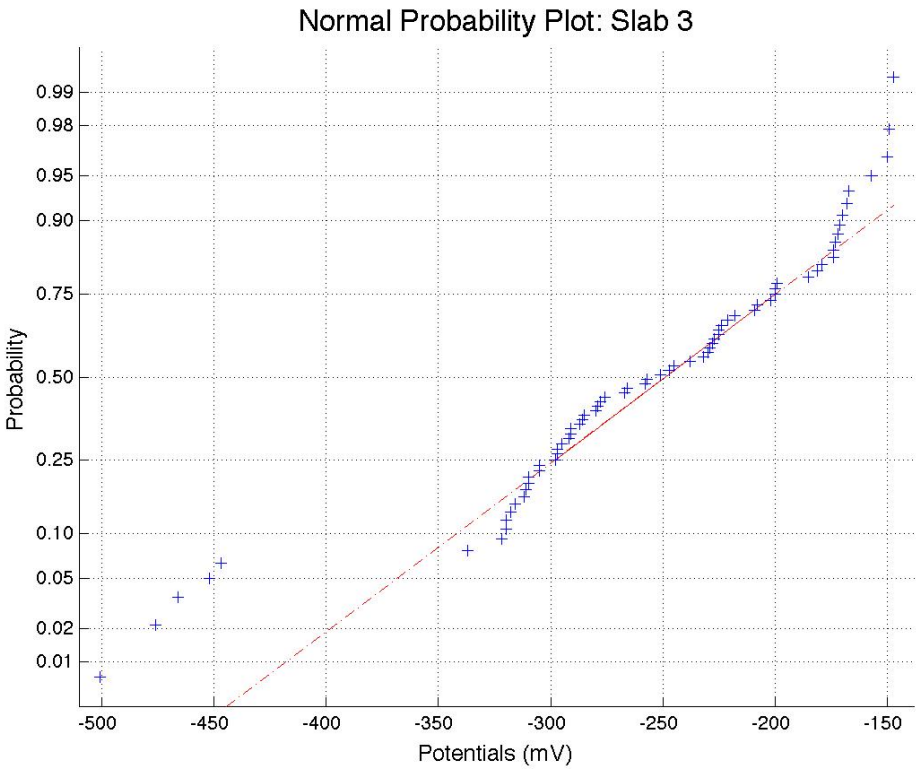

Figure B-43: Statistical Analys Slab 3: 06/01/2012

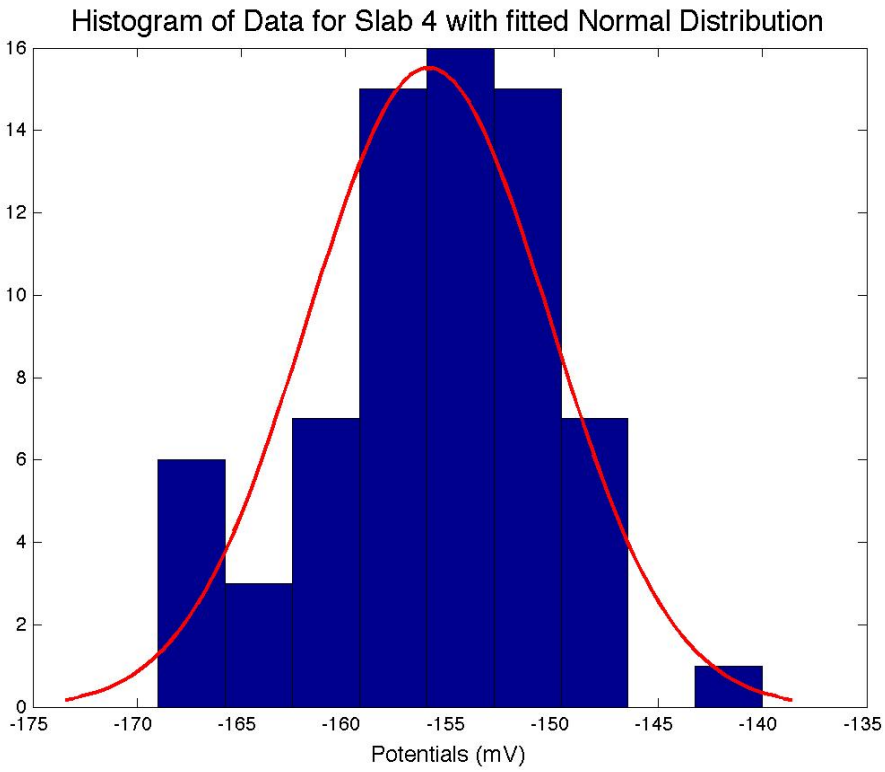

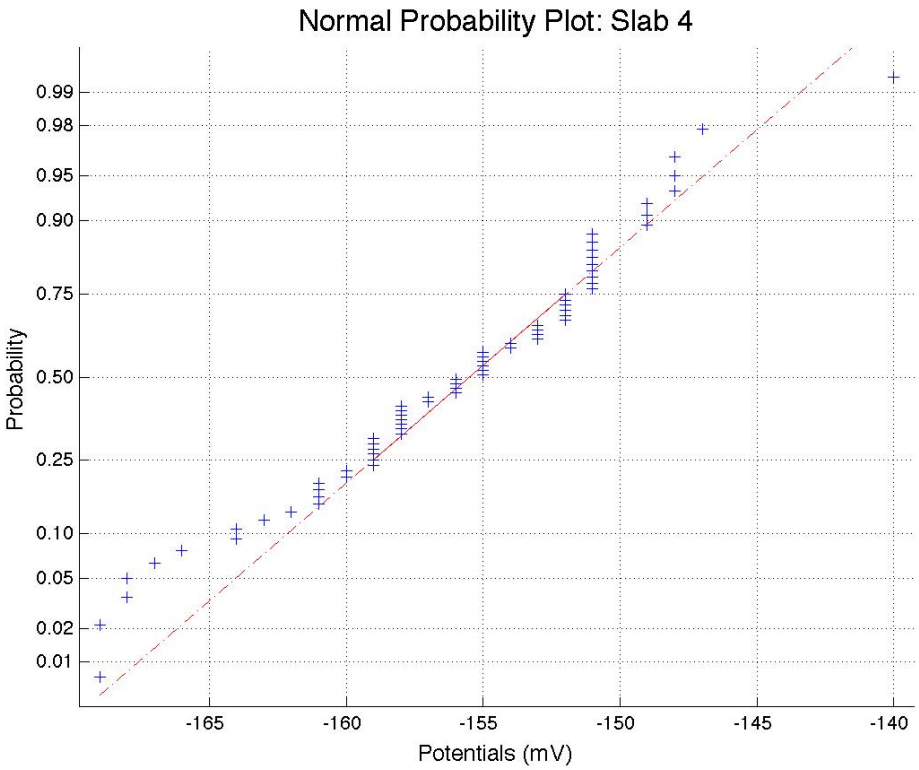

Figure B-44: Statistical Analys Slab 4: 06/01/2012

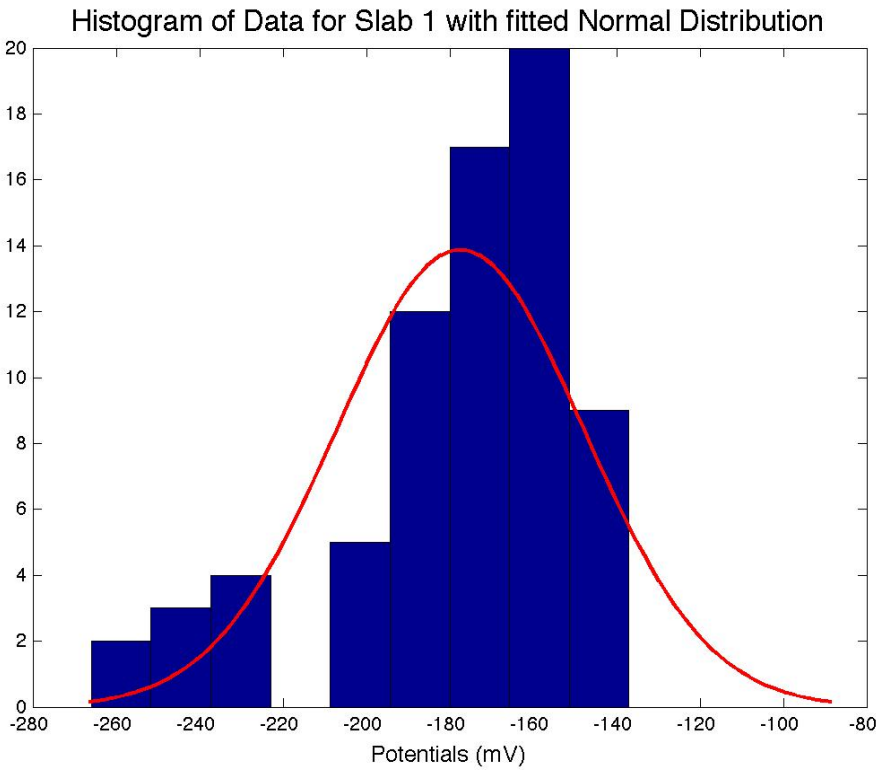

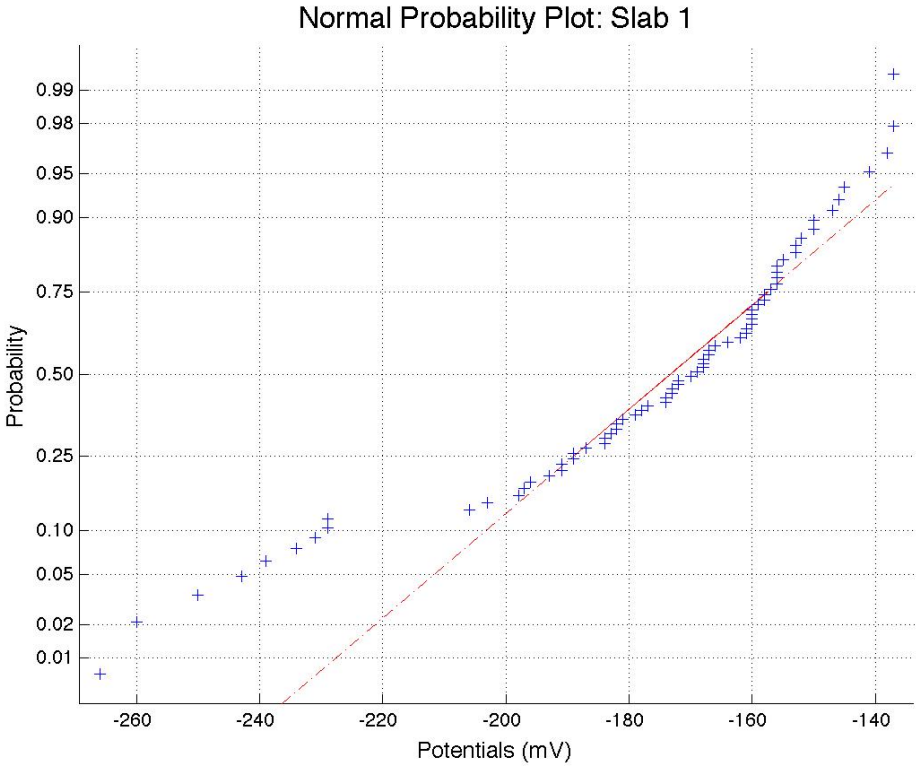

Figure B-45: Statistical Analys Slab 1: 06/08/2012

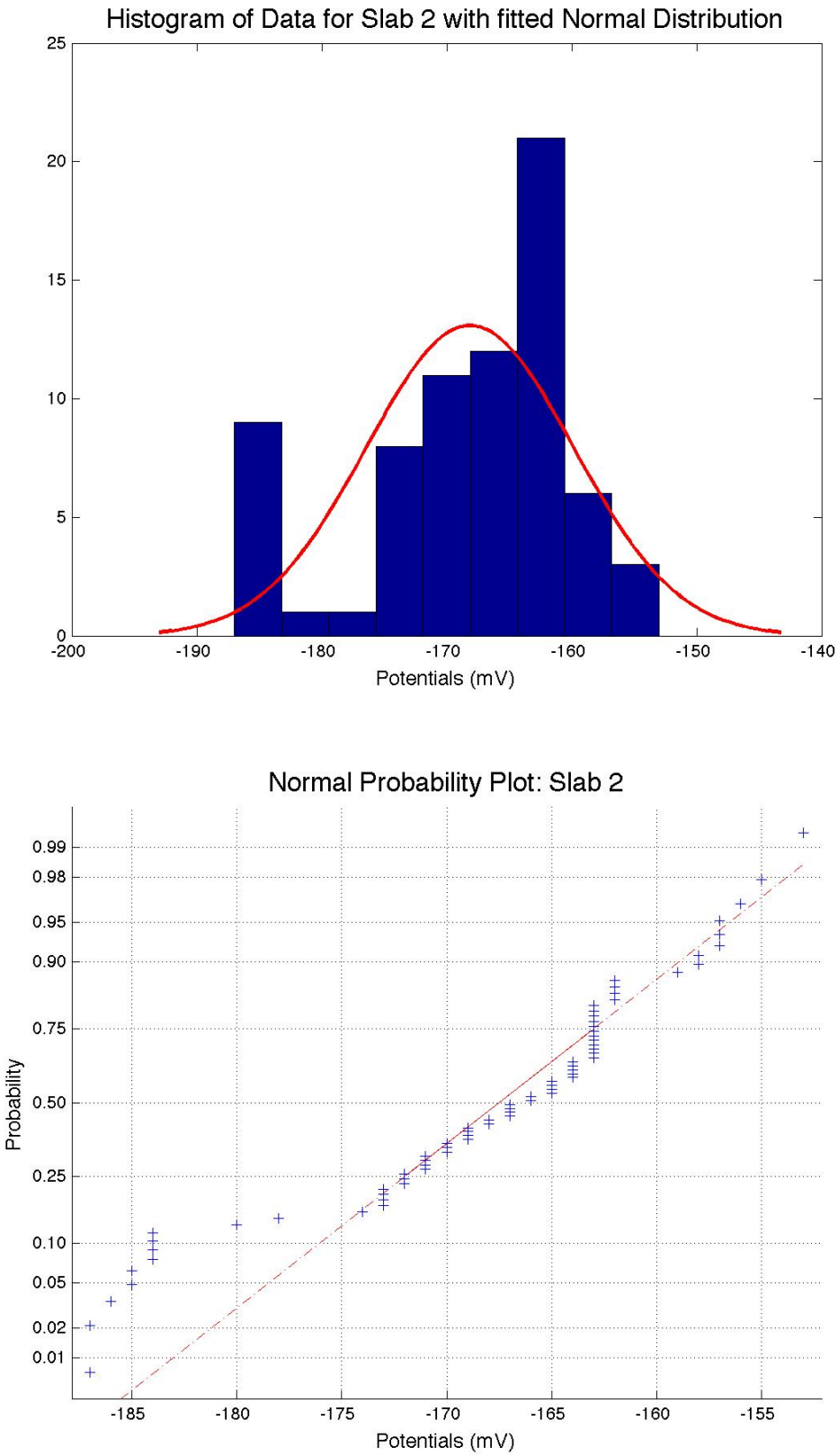

Figure B-46: Statistical Analys Slab 2: 06/08/2012

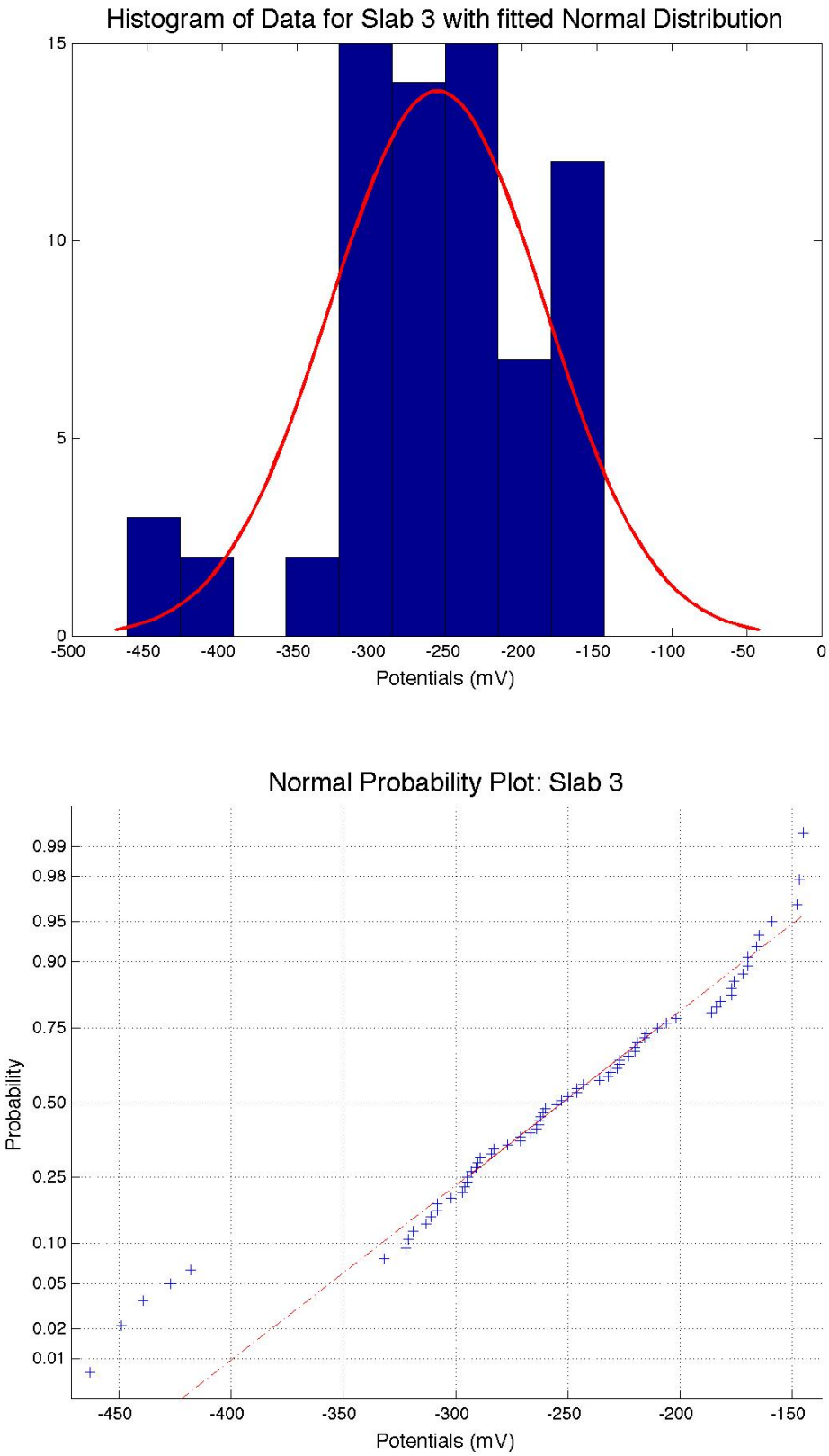

Figure B-47: Statistical Analys Slab 3: 06/08/2012

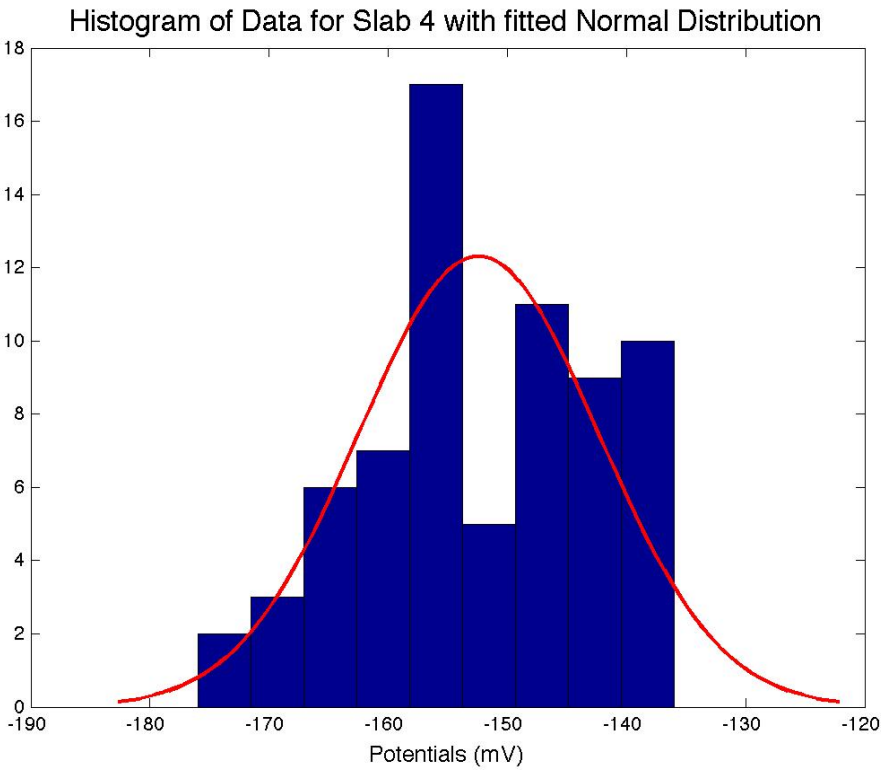

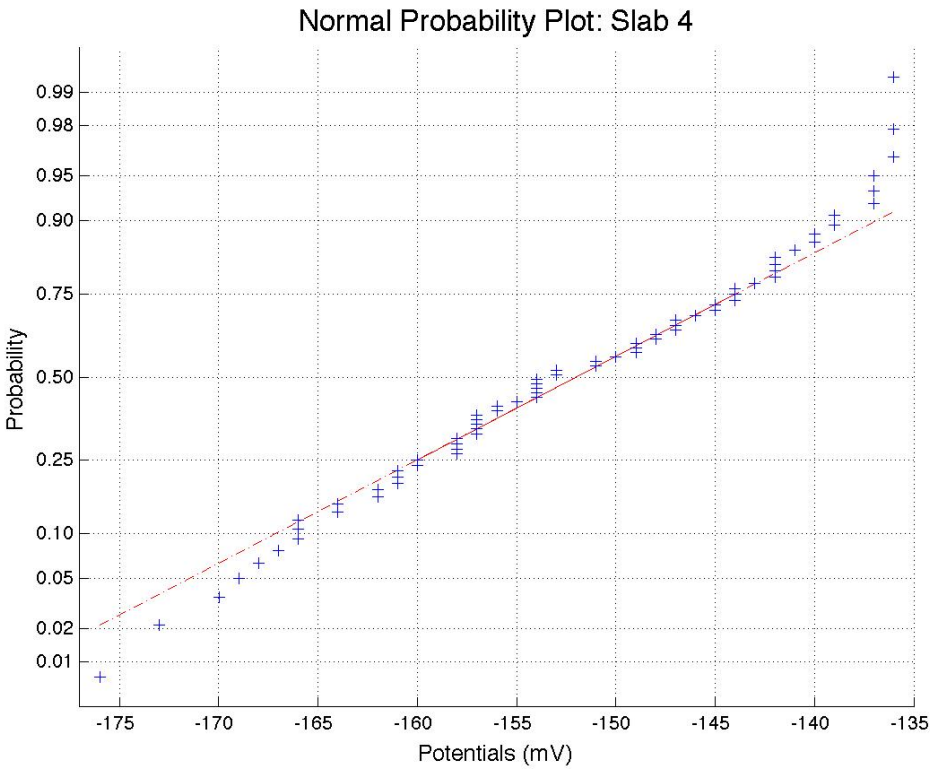

Figure B-48: Statistical Analys Slab 4: 06/08/2012

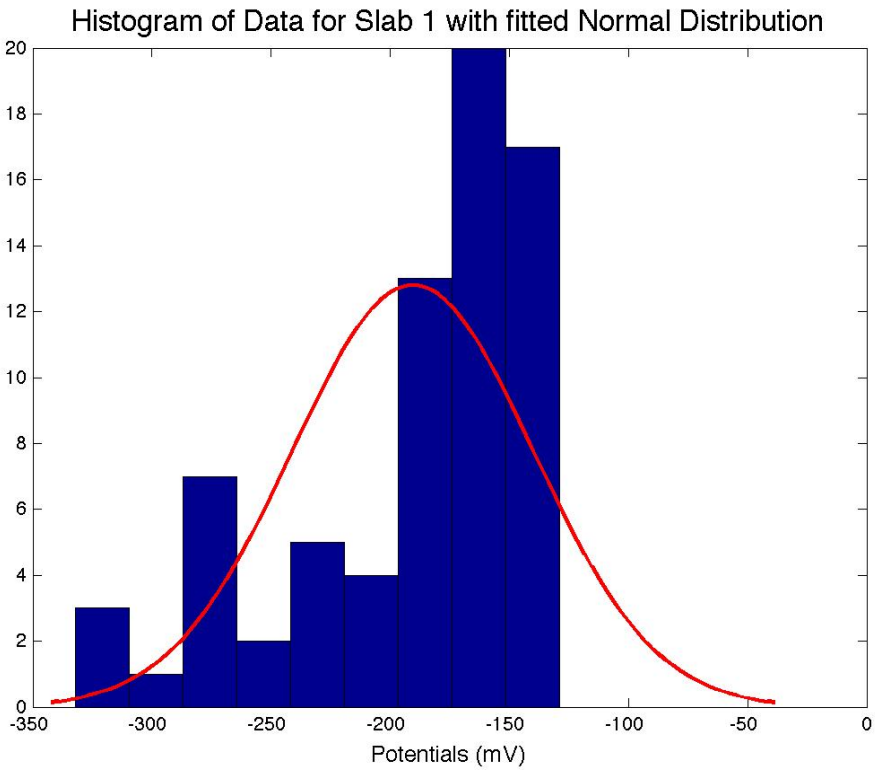

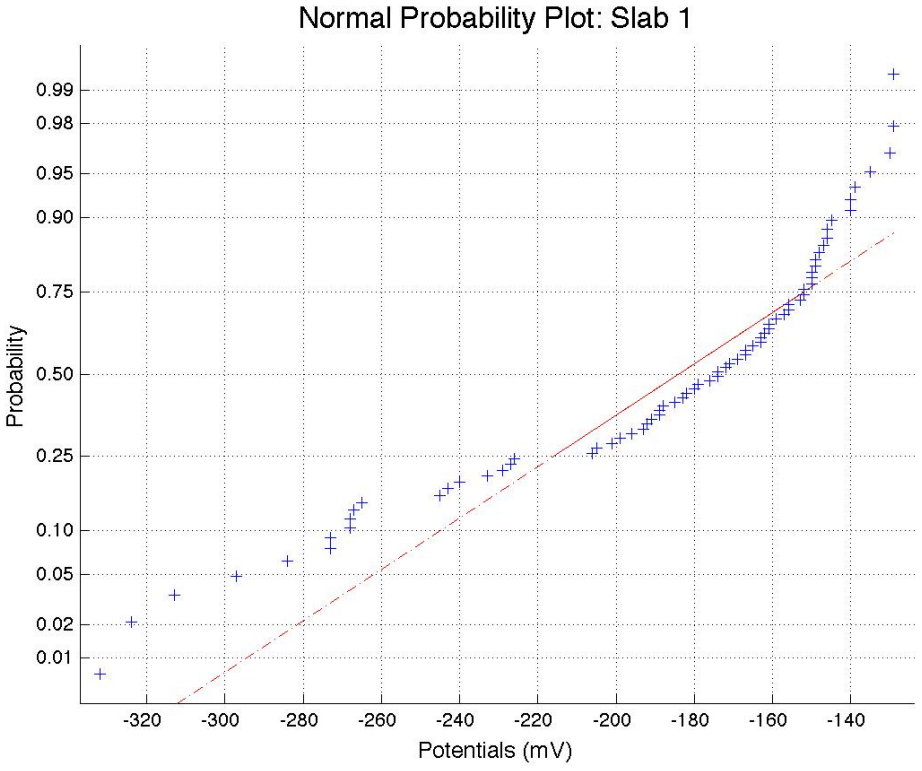

Figure B-49: Statistical Analys Slab 1: 06/15/2012

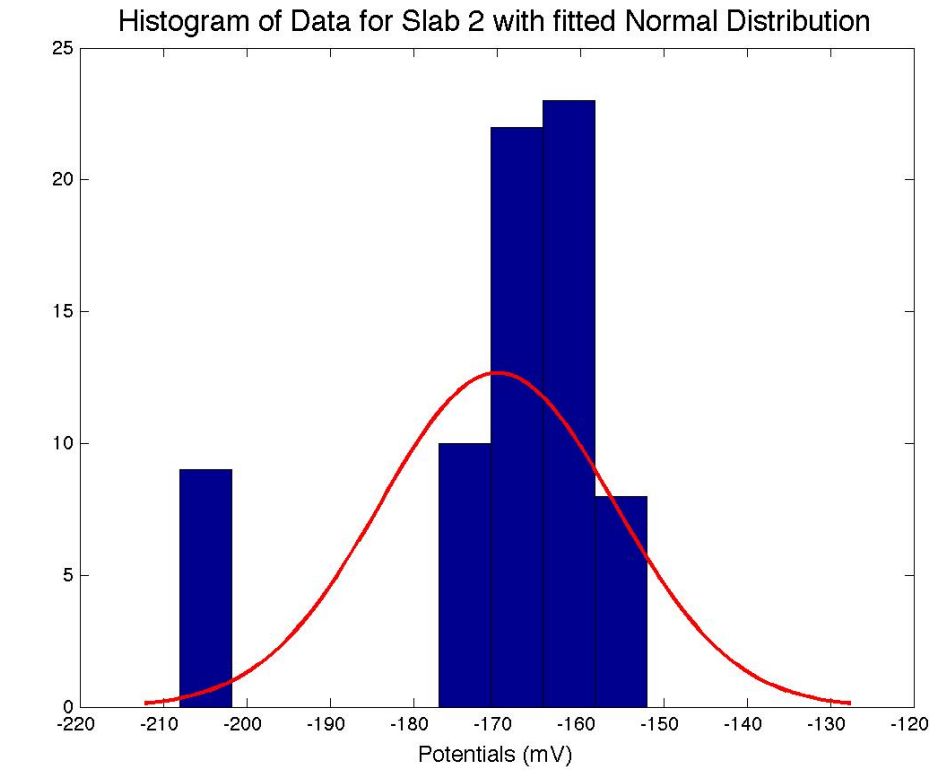

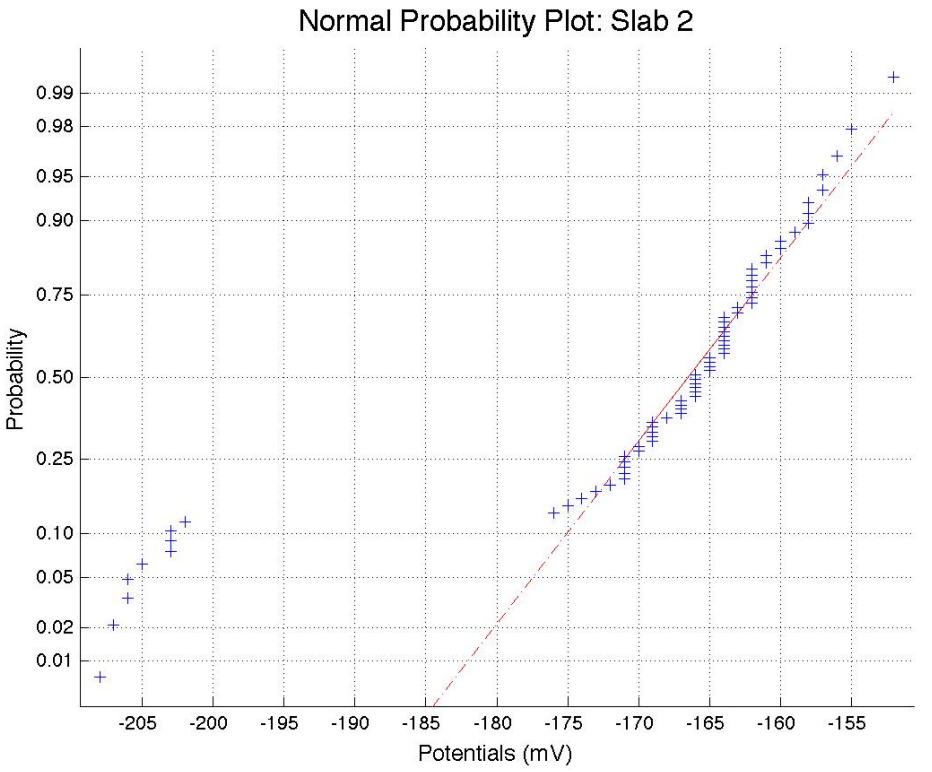

Figure B-50: Statistical Analys Slab 2: 06/15/2012

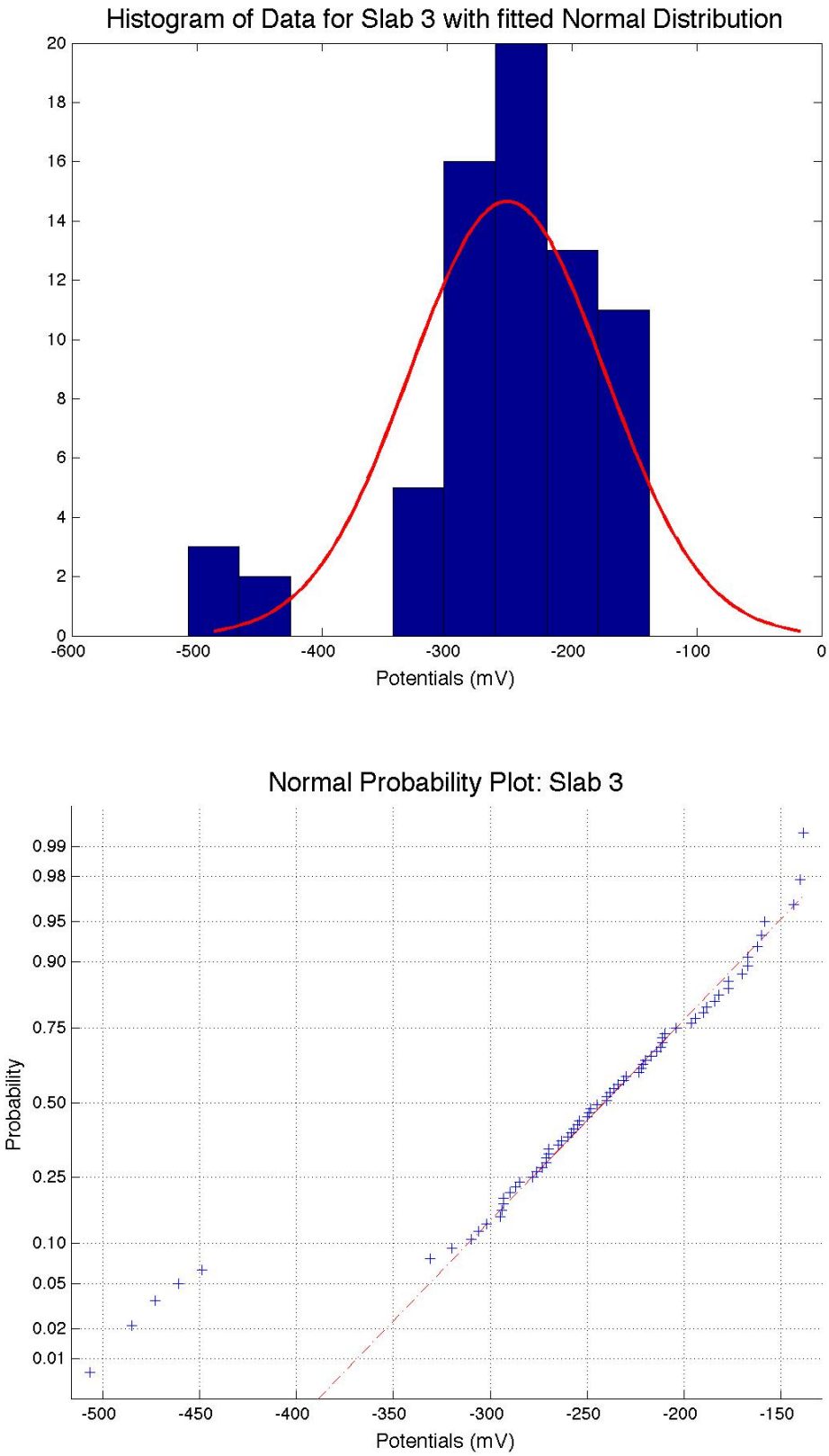

Figure B-51: Statistical Analys Slab 3: 06/15/2012

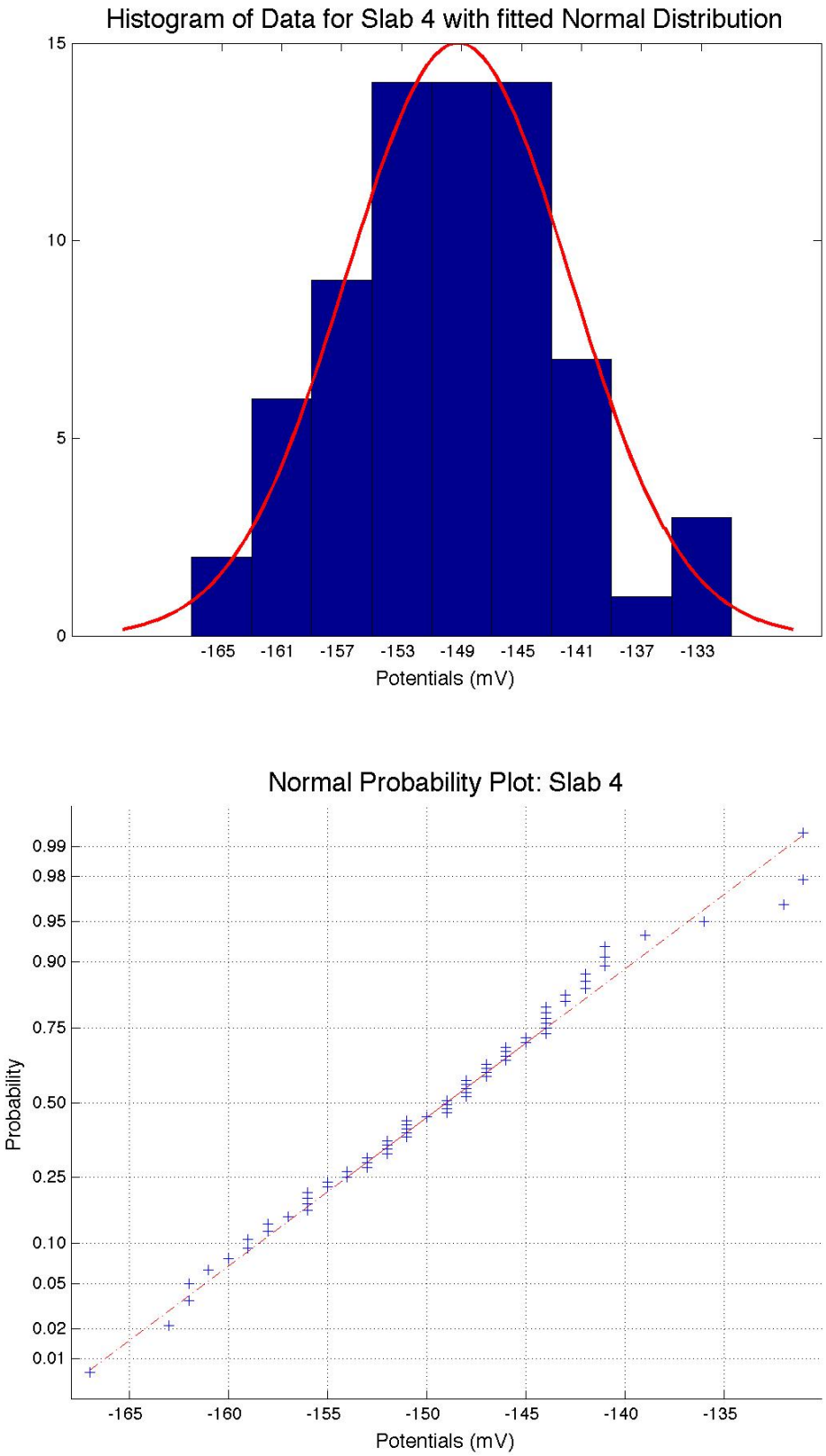

Figure B-52: Statistical Analys Slab 4: 06/15/2012

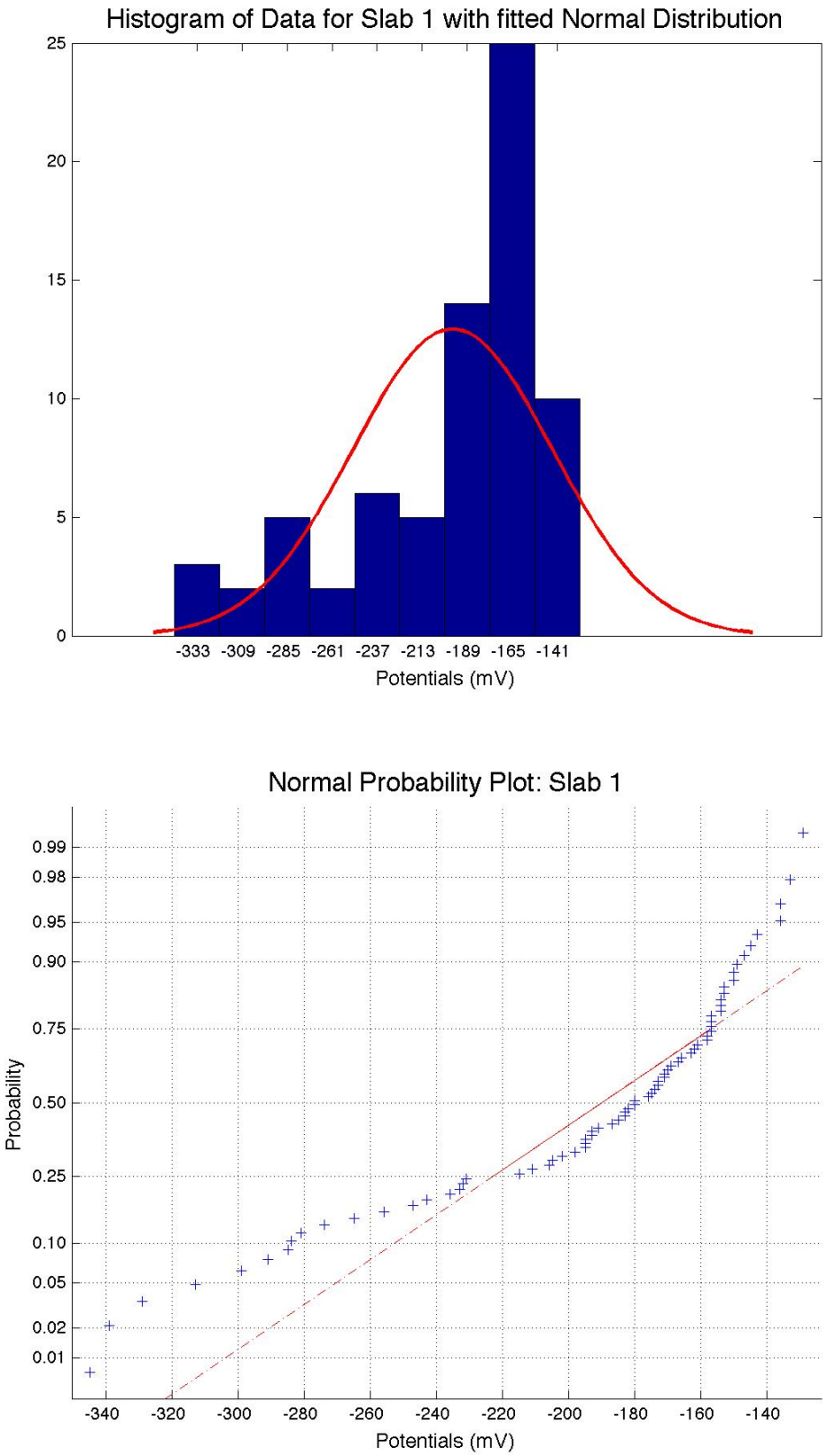

Figure B-53: Statistical Analys Slab 1: 06/22/2012

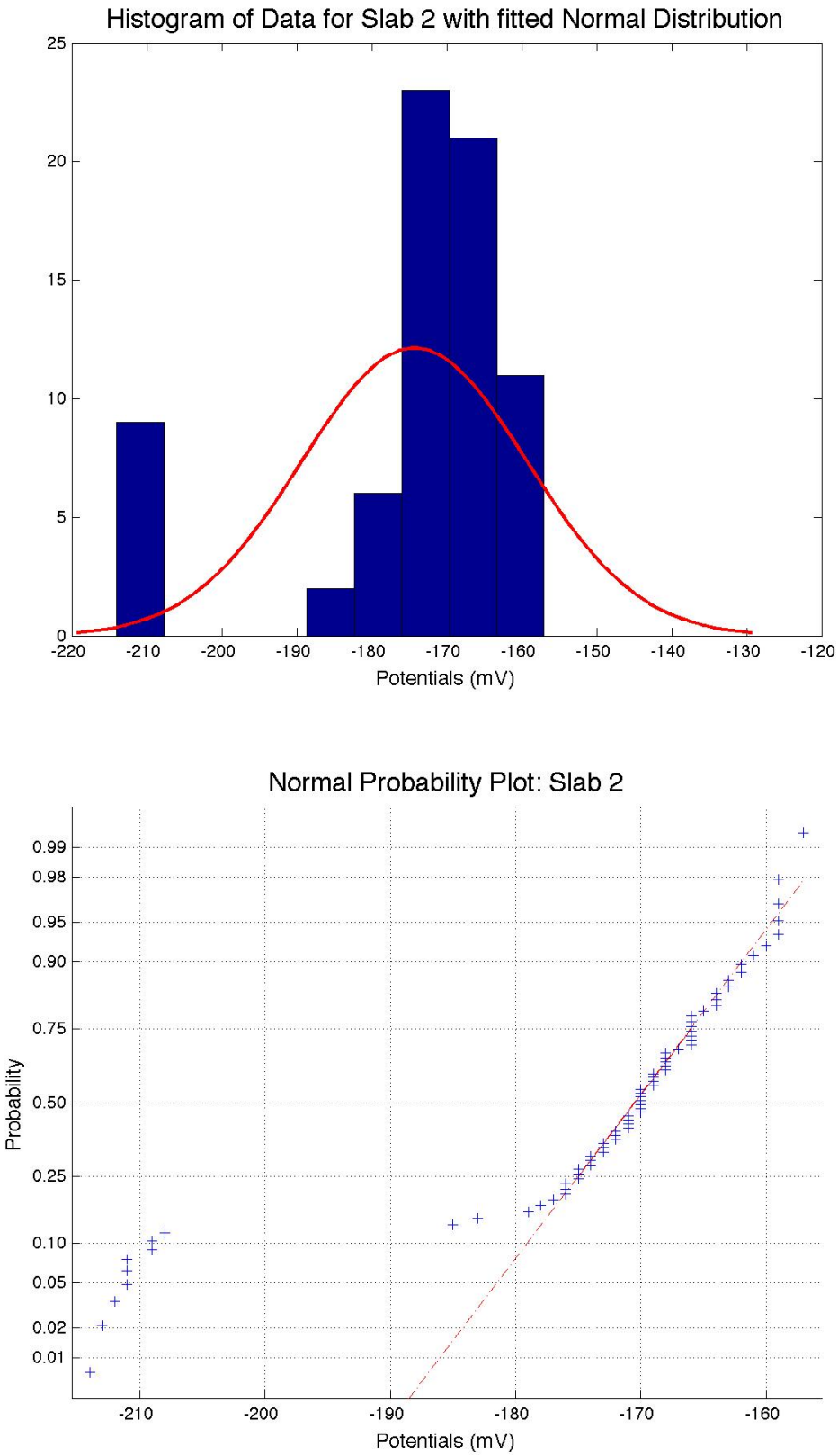

Figure B-54: Statistical Analys Slab 2: 06/22/2012

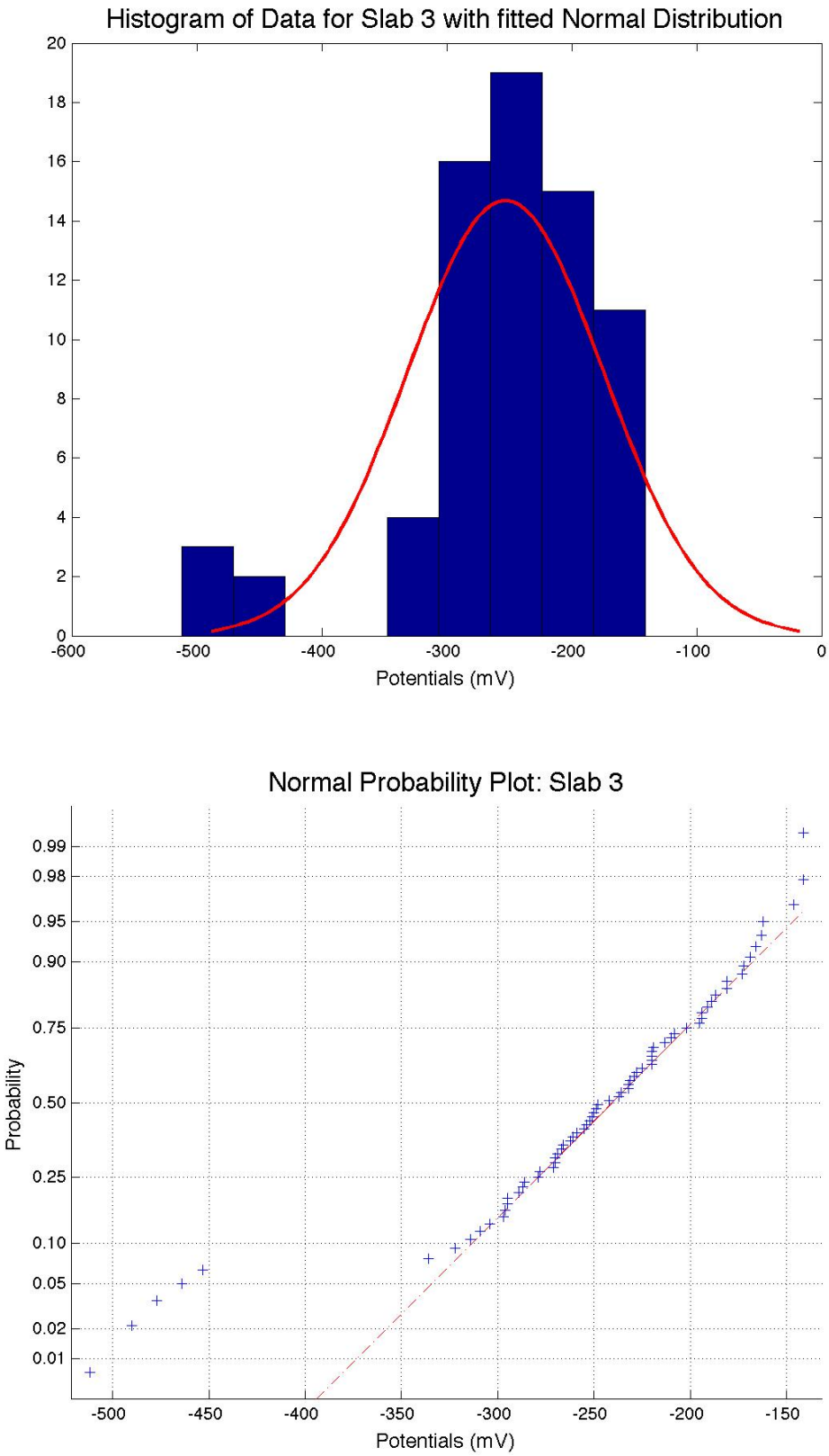

Figure B-55: Statistical Analys Slab 3: 06/22/2012

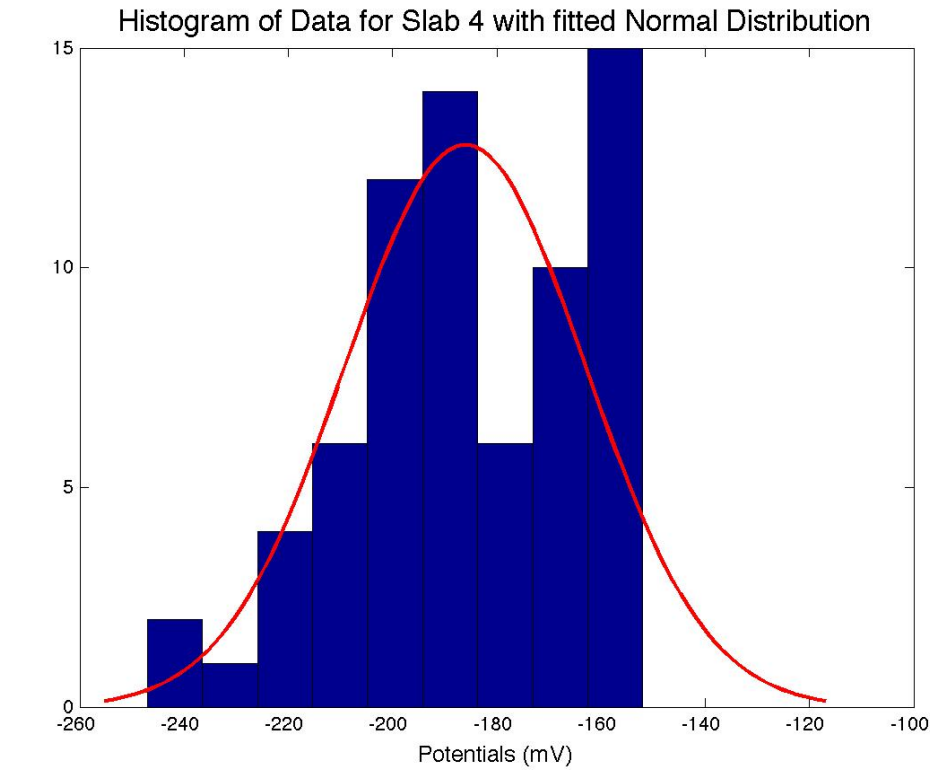

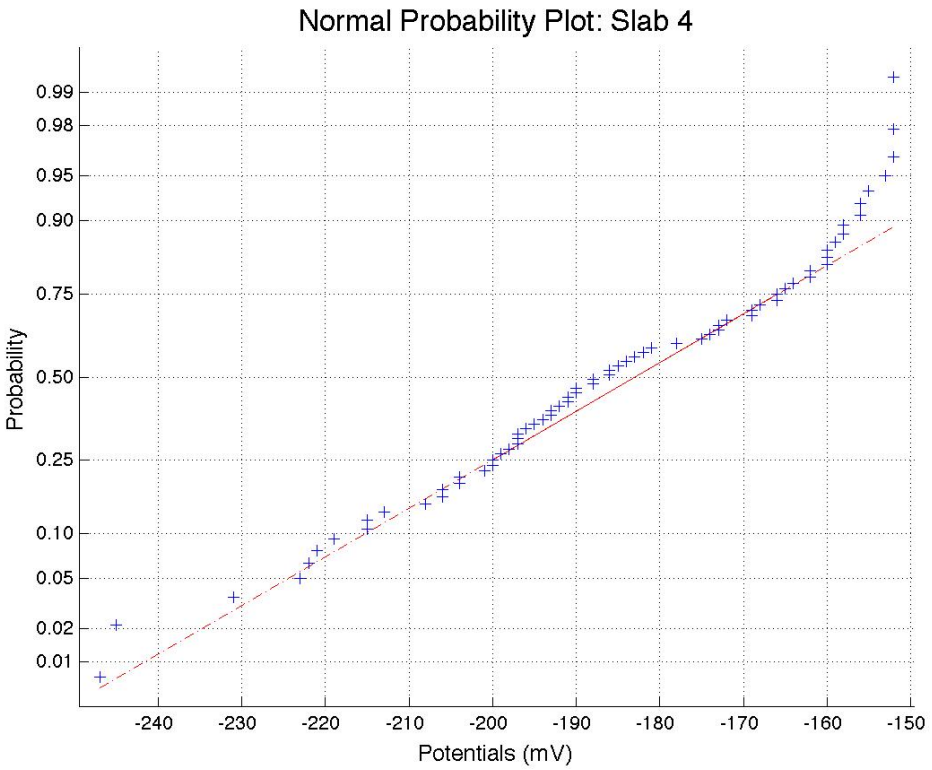

Figure B-56: Statistical Analys Slab 4: 06/22/2012

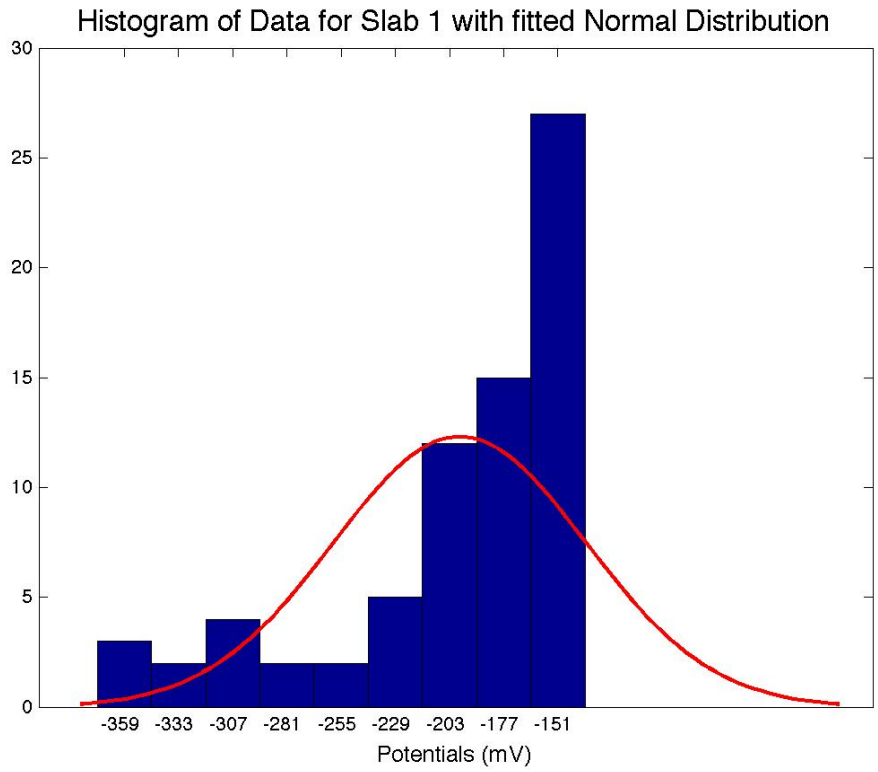

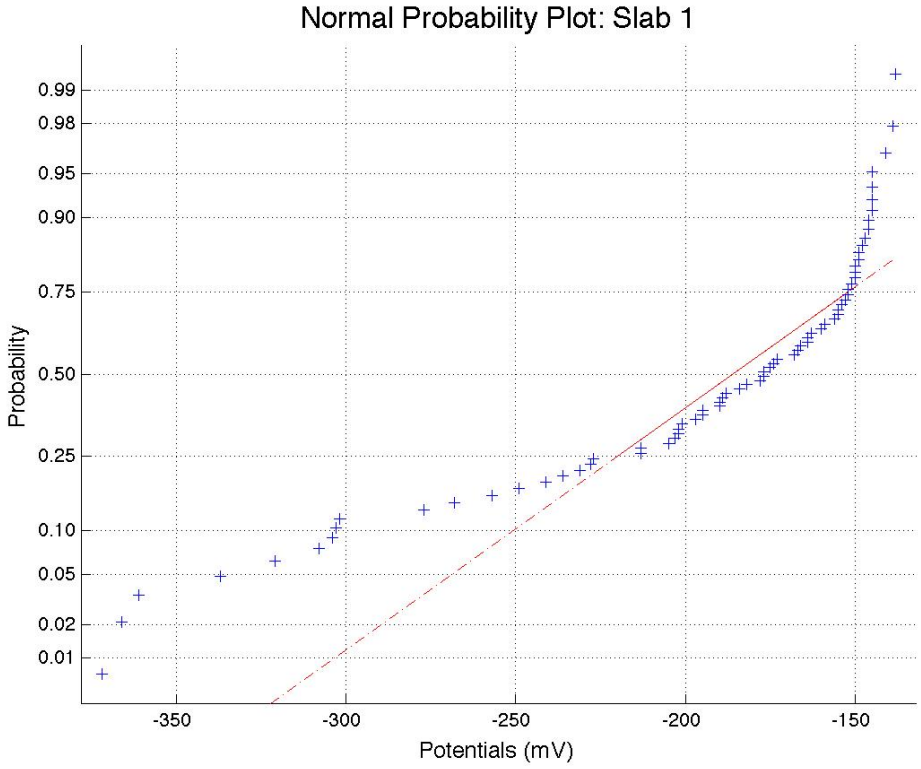

Figure B-57: Statistical Analys Slab 1: 06/29/2012

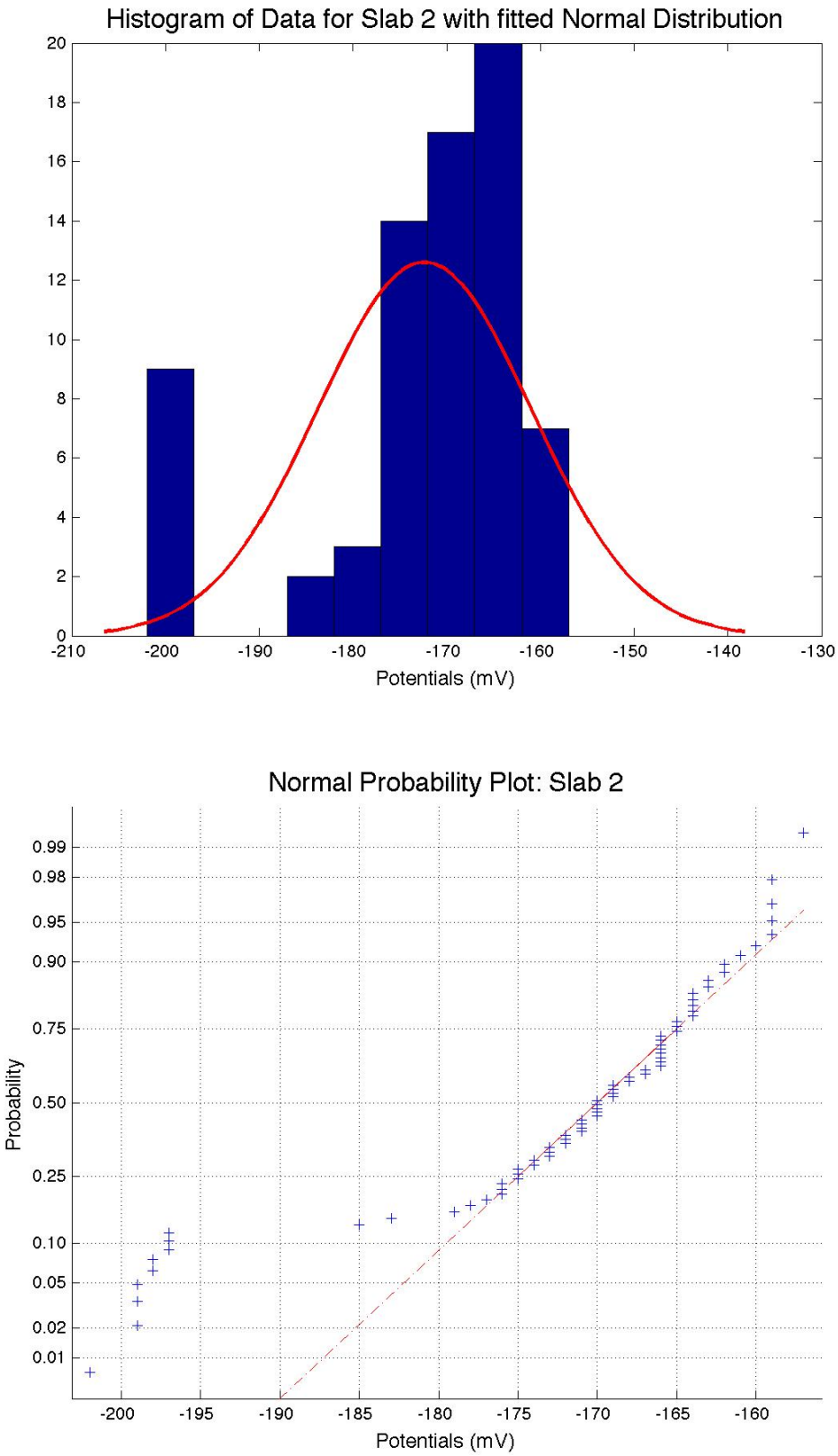

Figure B-58: Statistical Analys Slab 2: 06/29/2012

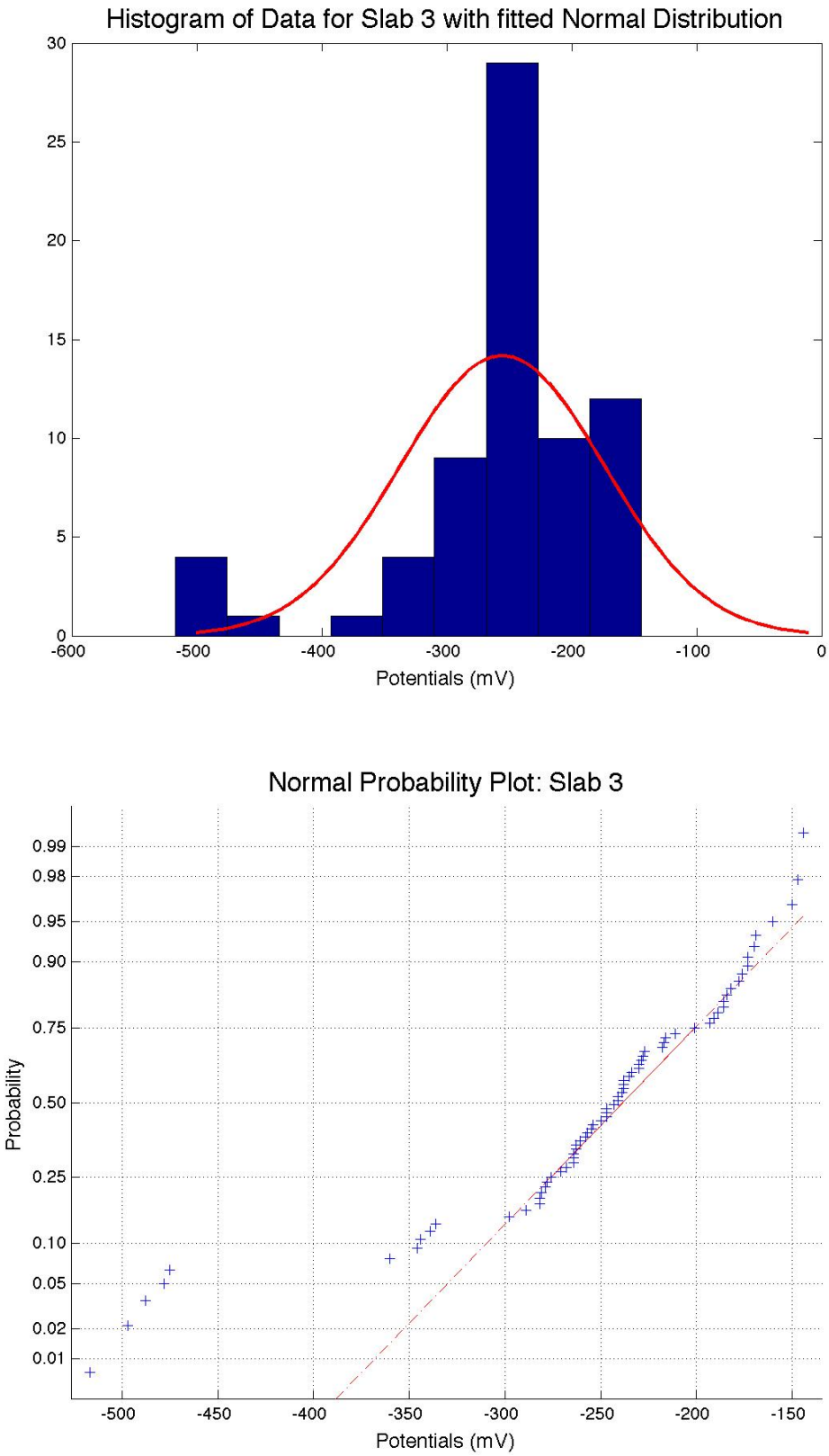

Figure B-59: Statistical Analys Slab 3: 06/29/2012

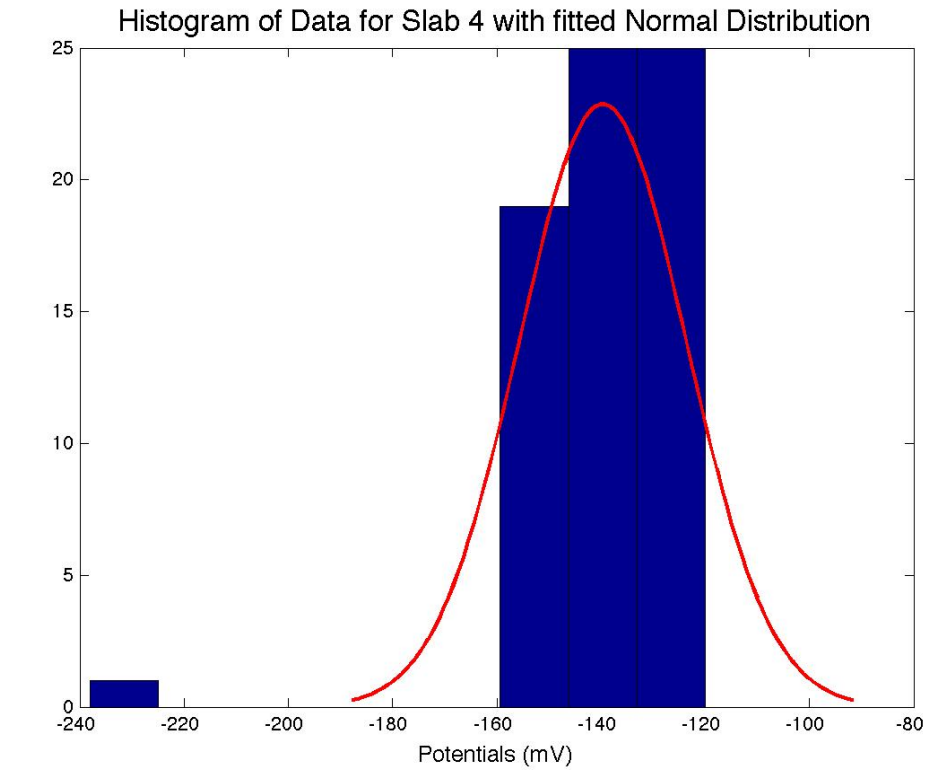

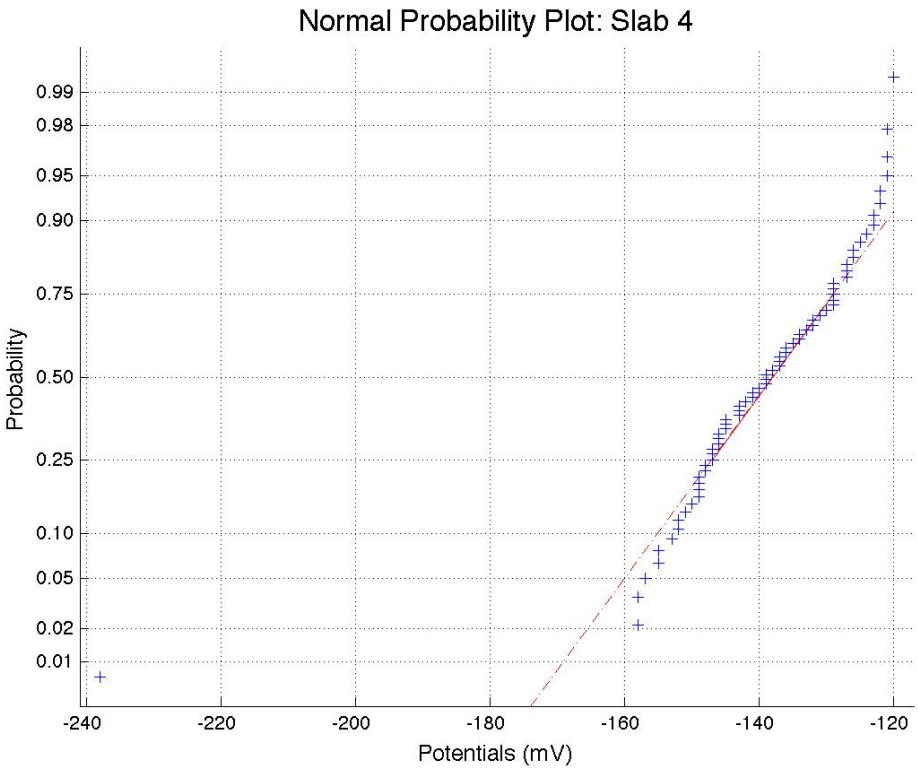

Figure B-60: Statistical Analys Slab 4: 06/29/2012

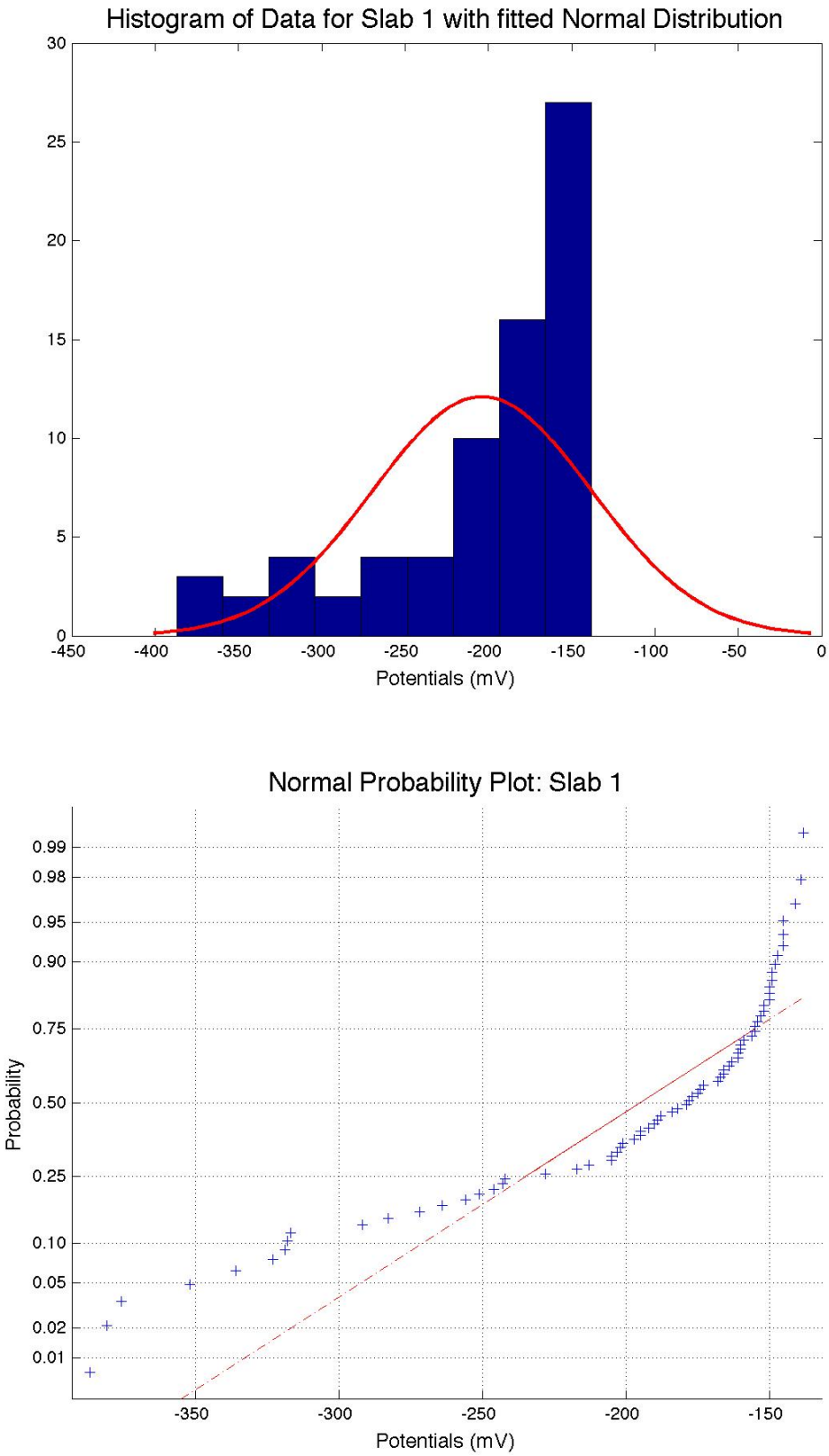

Figure B-61: Statistical Analys Slab 1: 07/06/2012

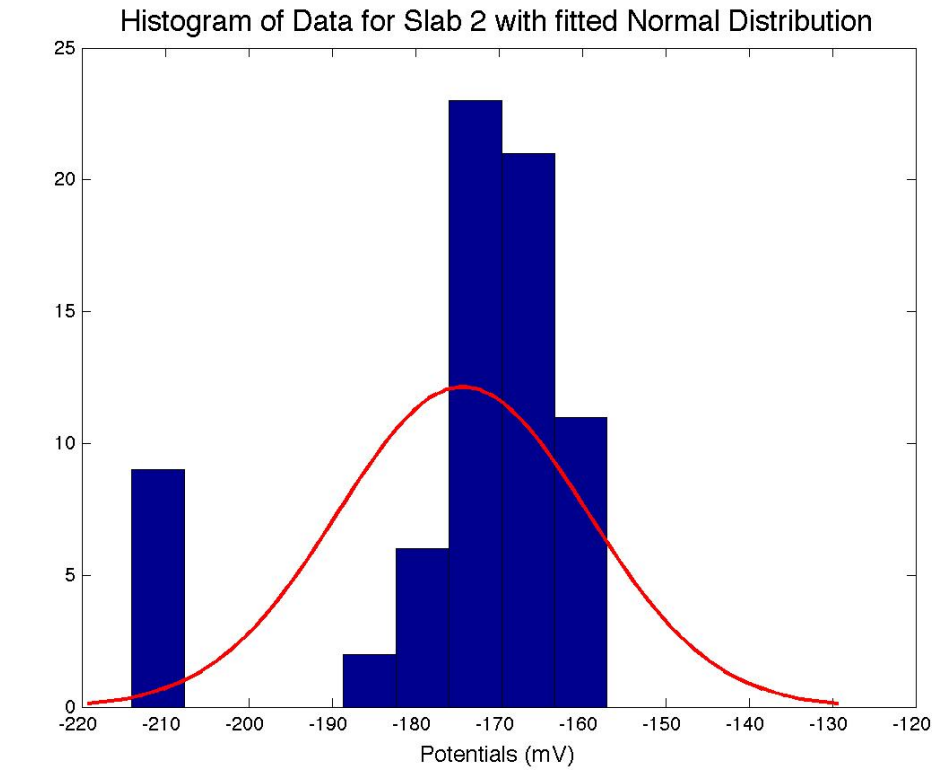

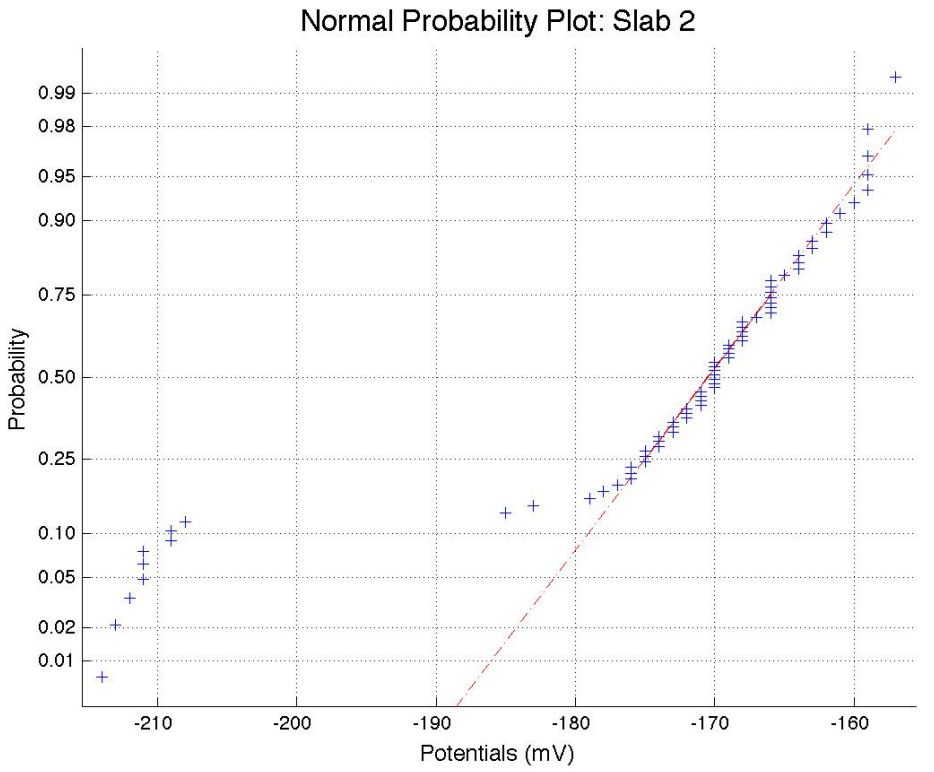

Figure B-62: Statistical Analys Slab 2: 07/06/2012

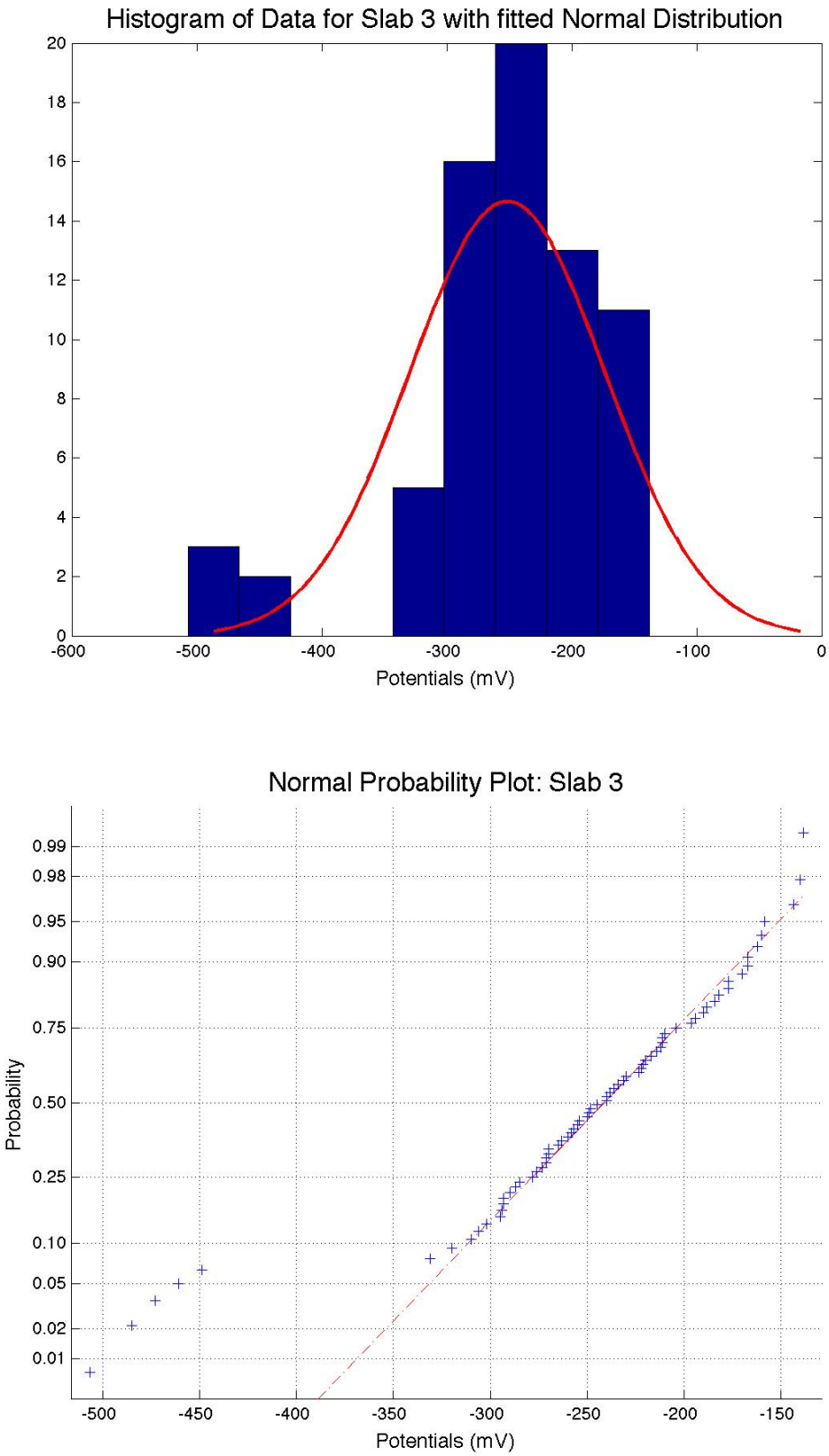

Figure B-63: Statistical Analys Slab 3: 07/06/2012

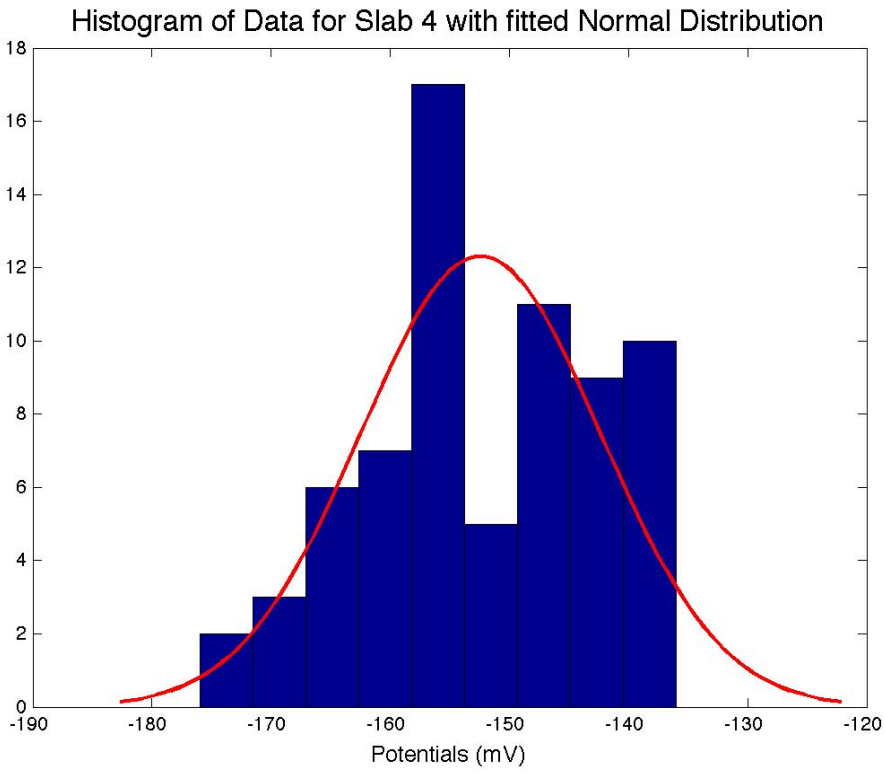

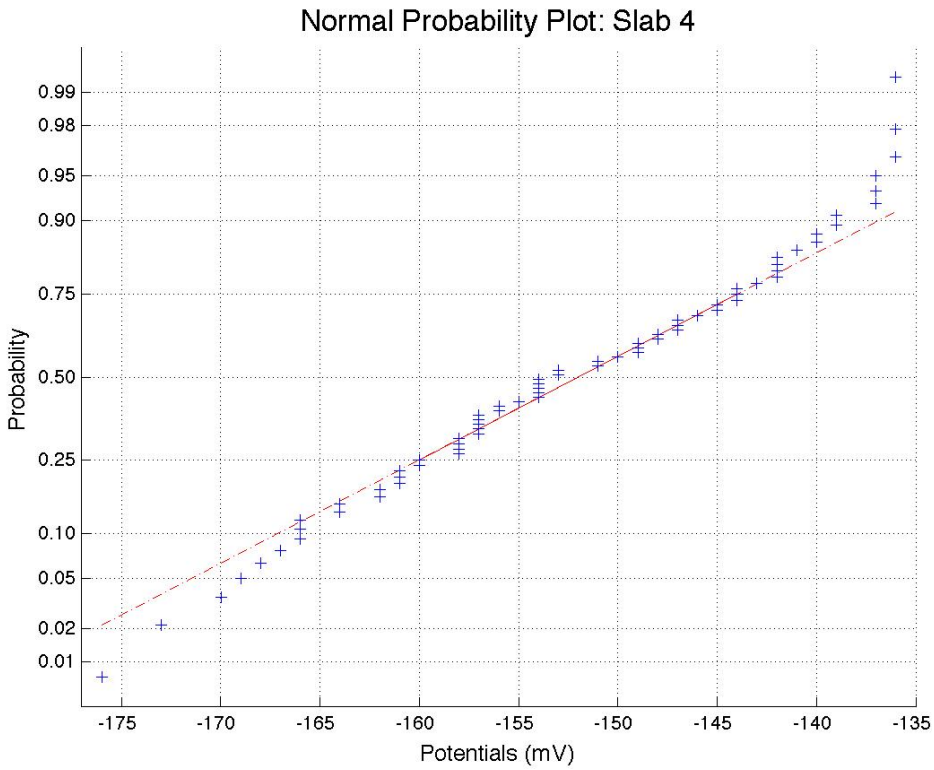

Figure B-64: Statistical Analys Slab 4: 07/06/2012

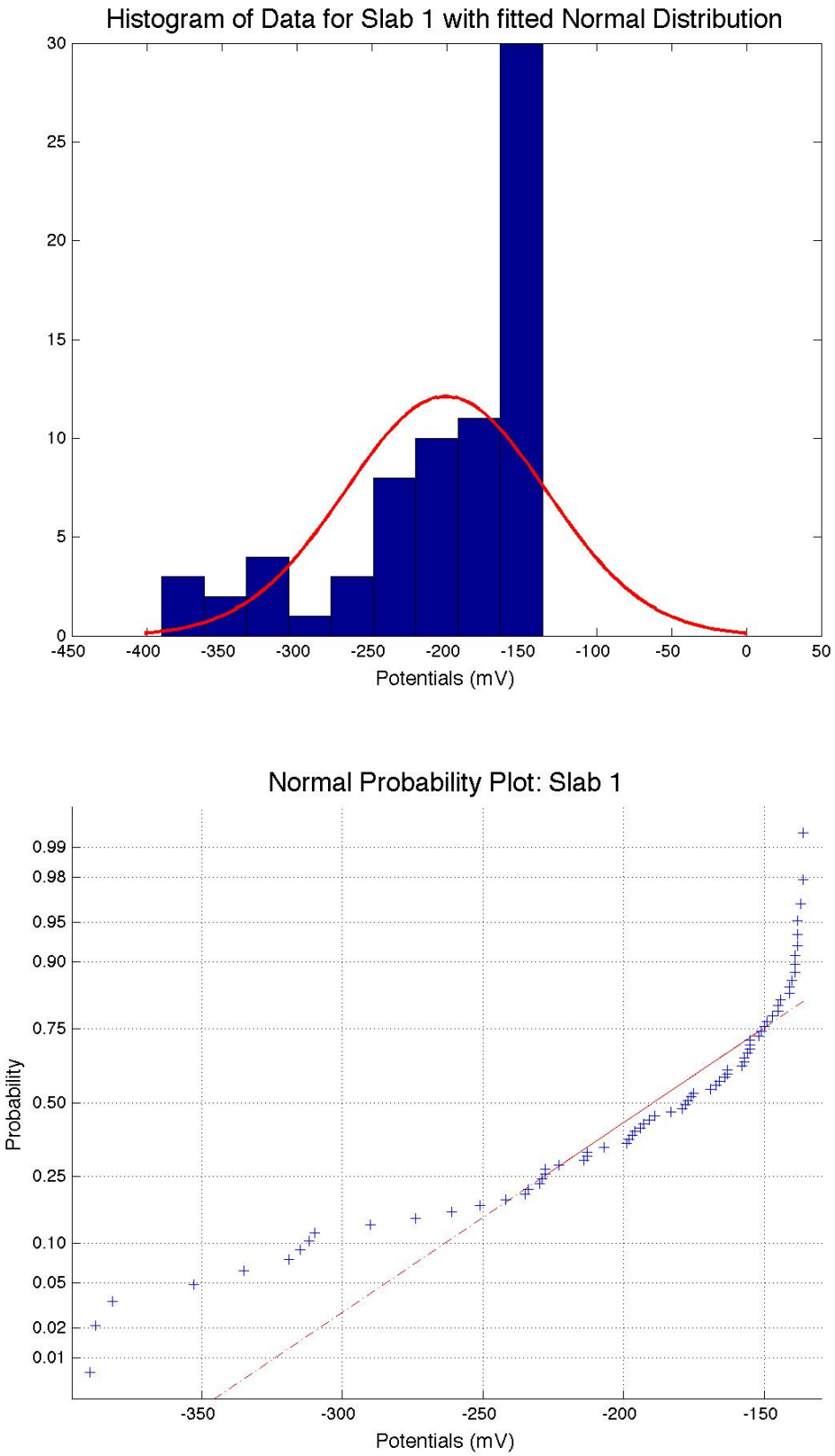

Figure B-65: Statistical Analys Slab 1: 07/13/2012

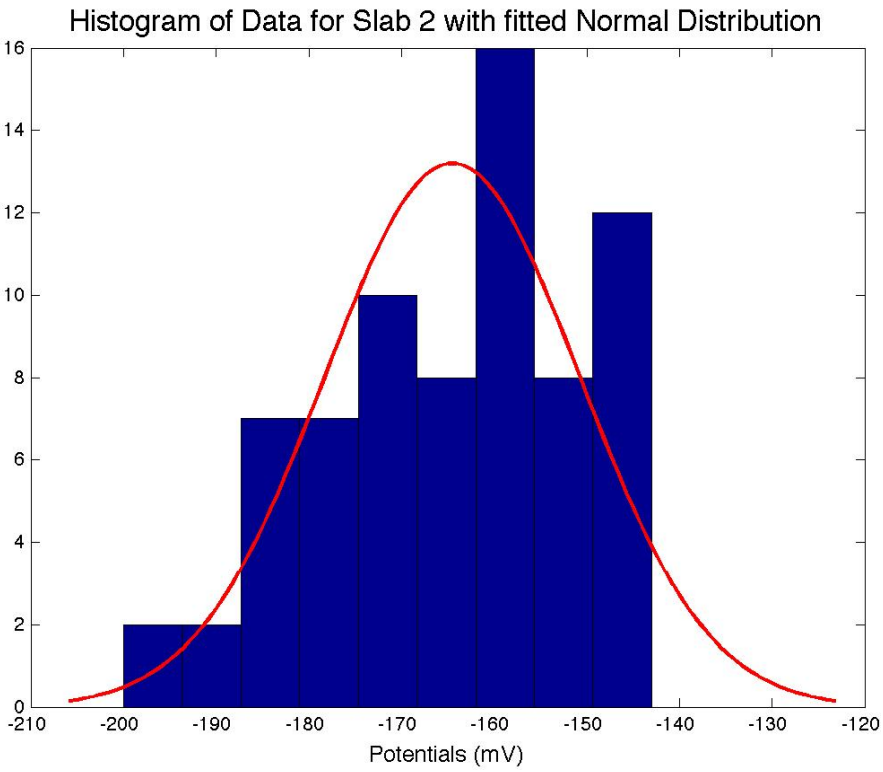

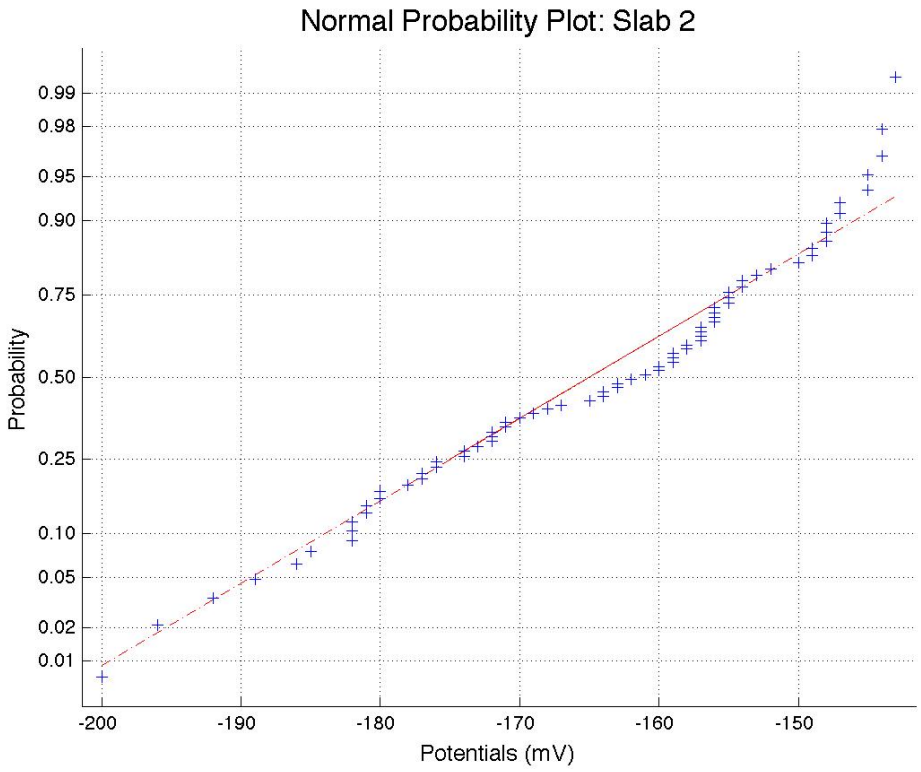

Figure B-66: Statistical Analys Slab 2: 07/13/2012

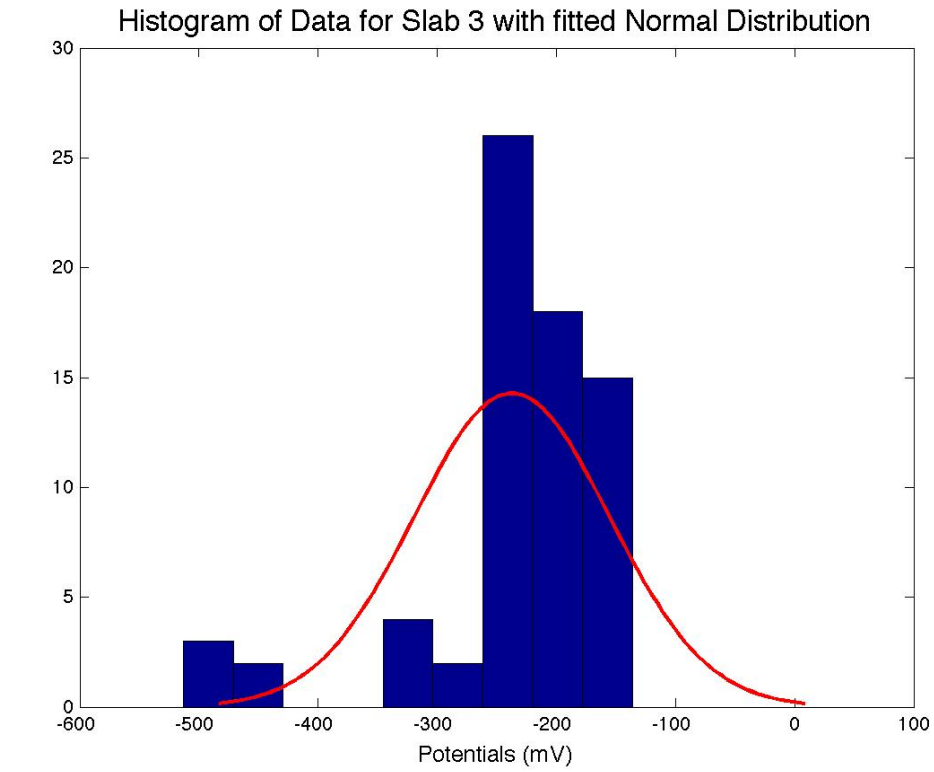

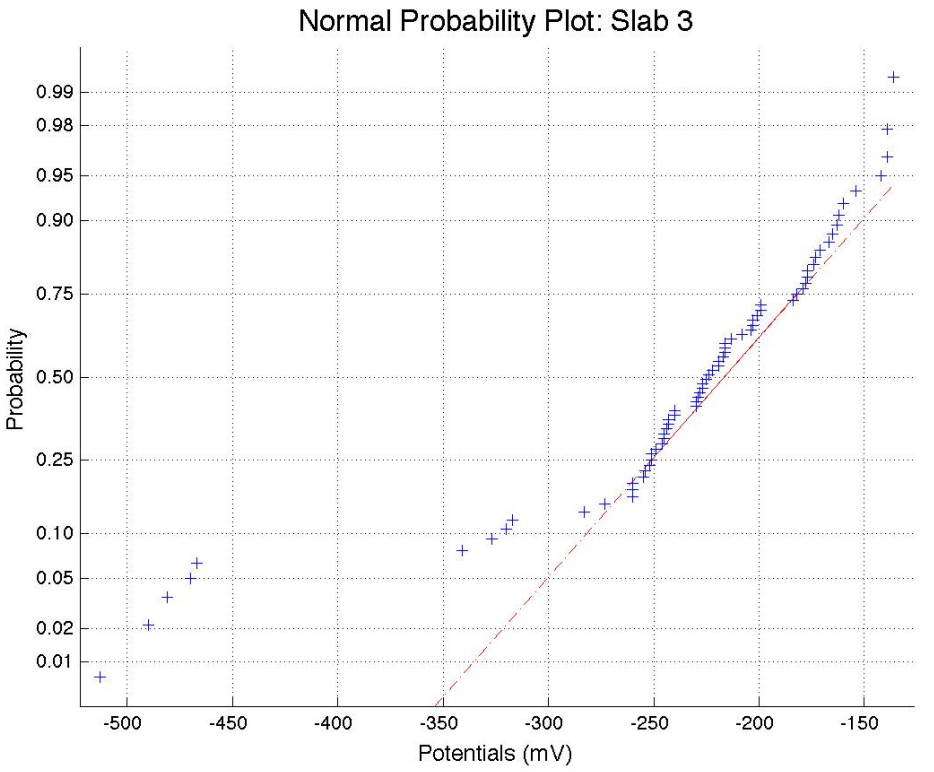

Figure B-67: Statistical Analys Slab 3: 07/13/2012

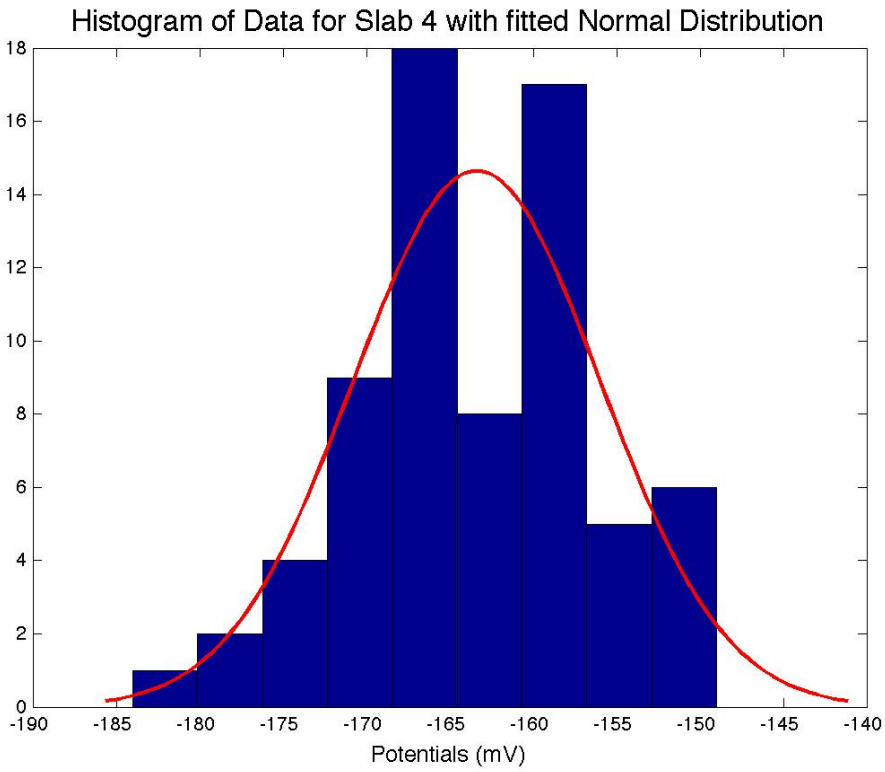

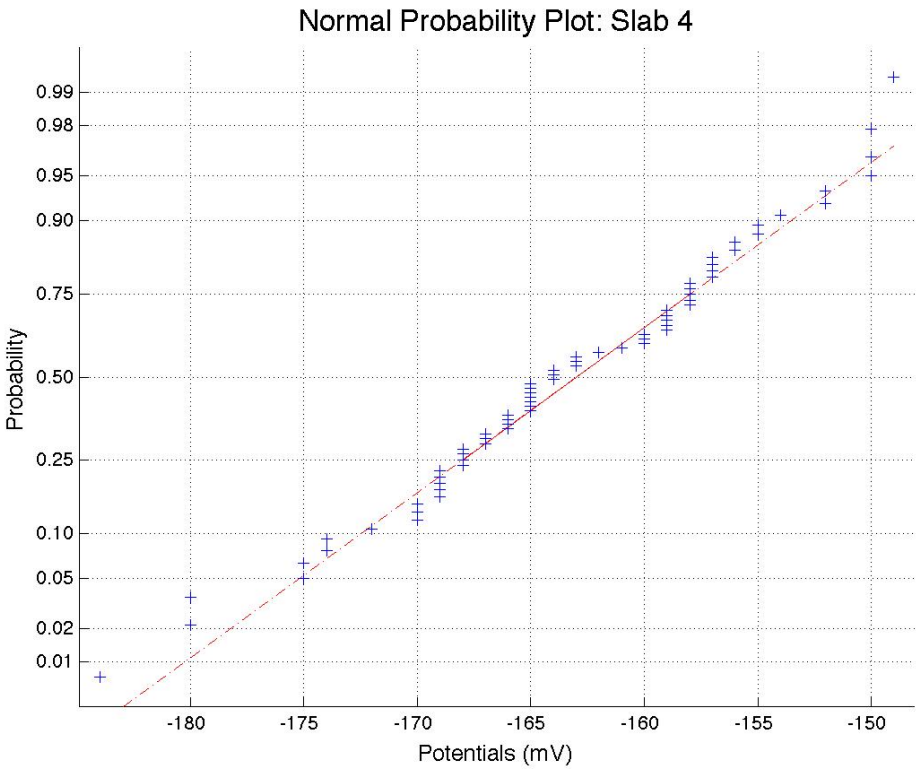

Figure B-68: Statistical Analys Slab 4: 07/13/2012

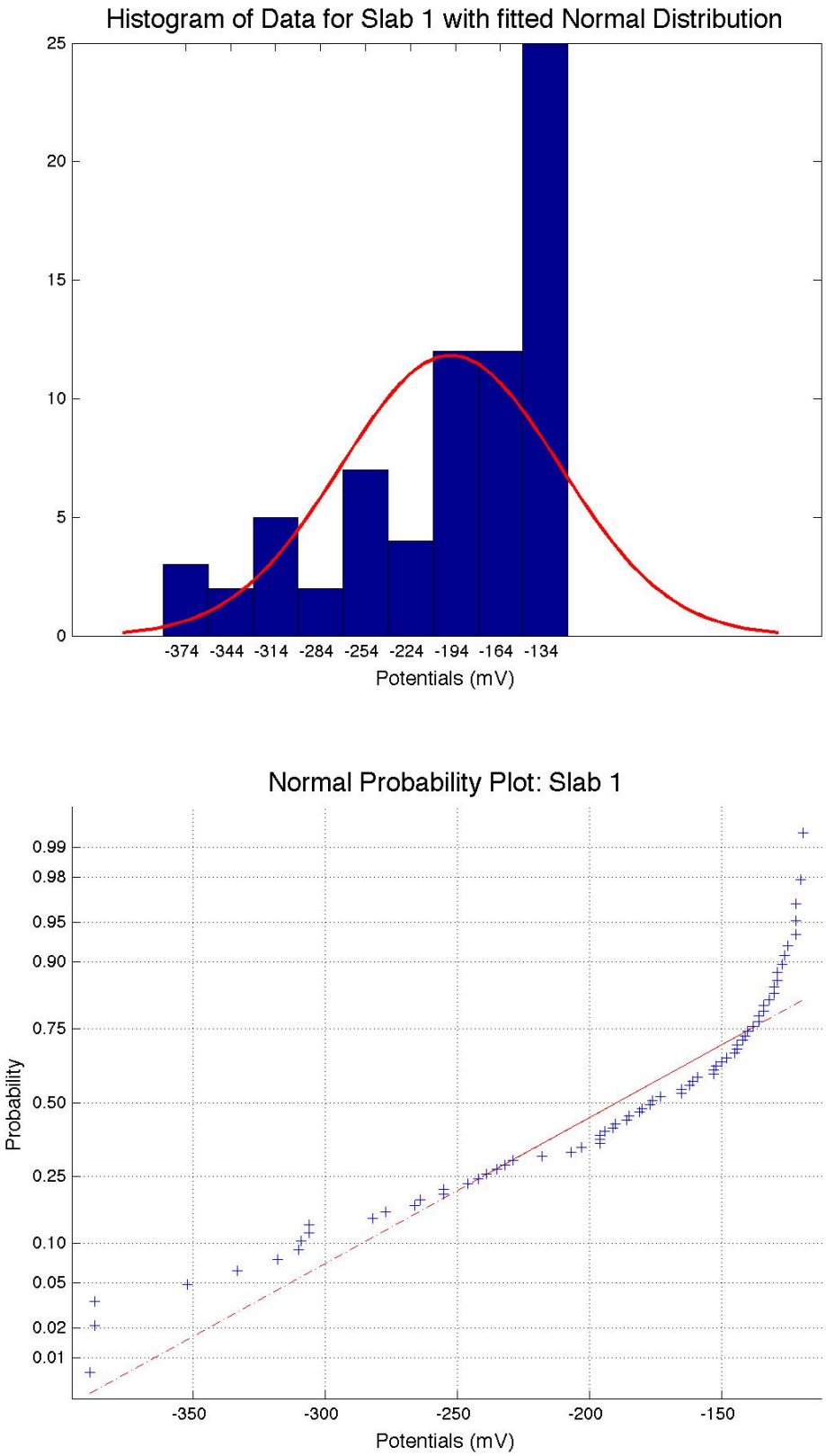

Figure B-69: Statistical Analys Slab 1: 07/20/2012

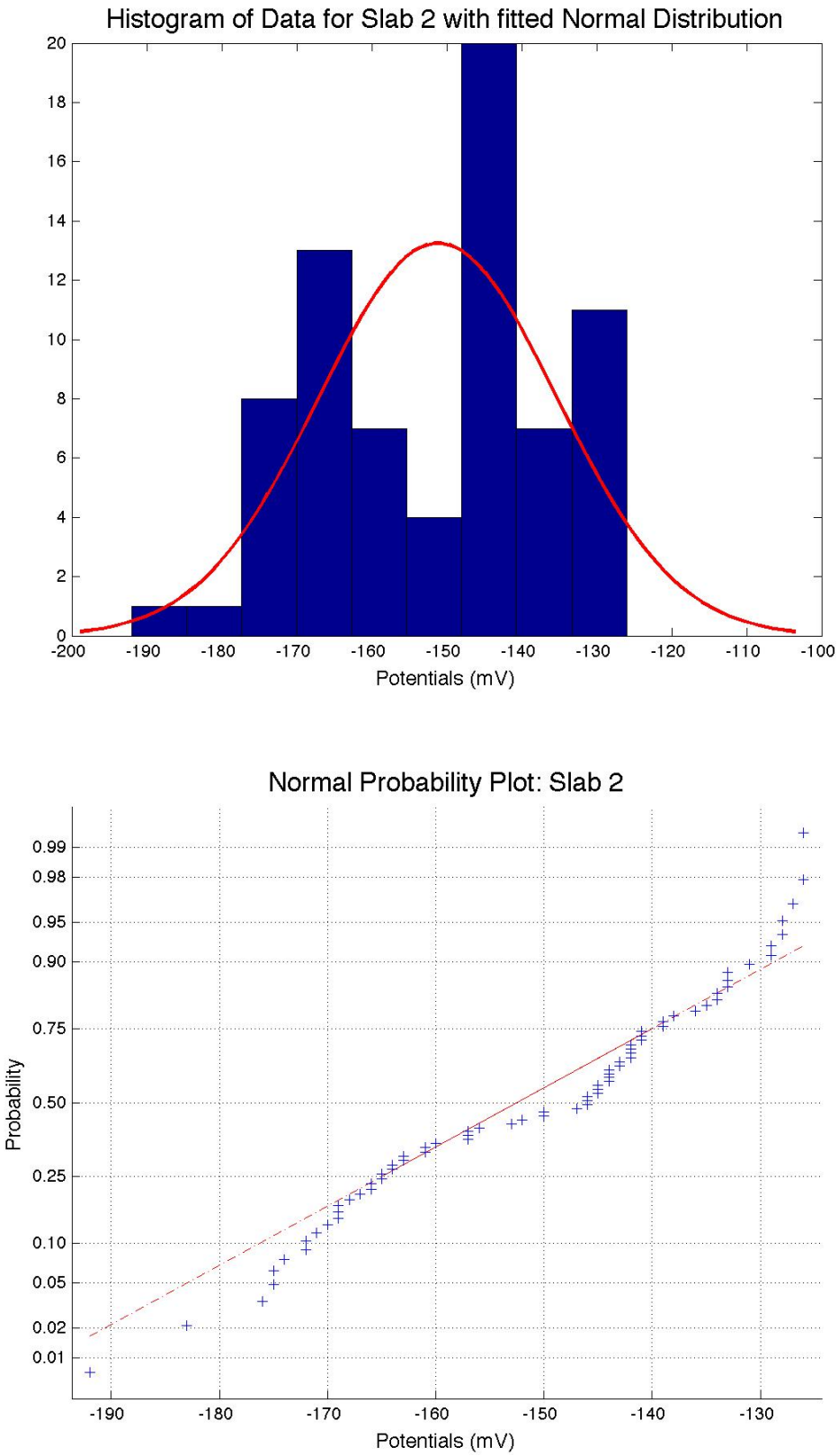

Figure B-70: Statistical Analys Slab 2: 07/20/2012

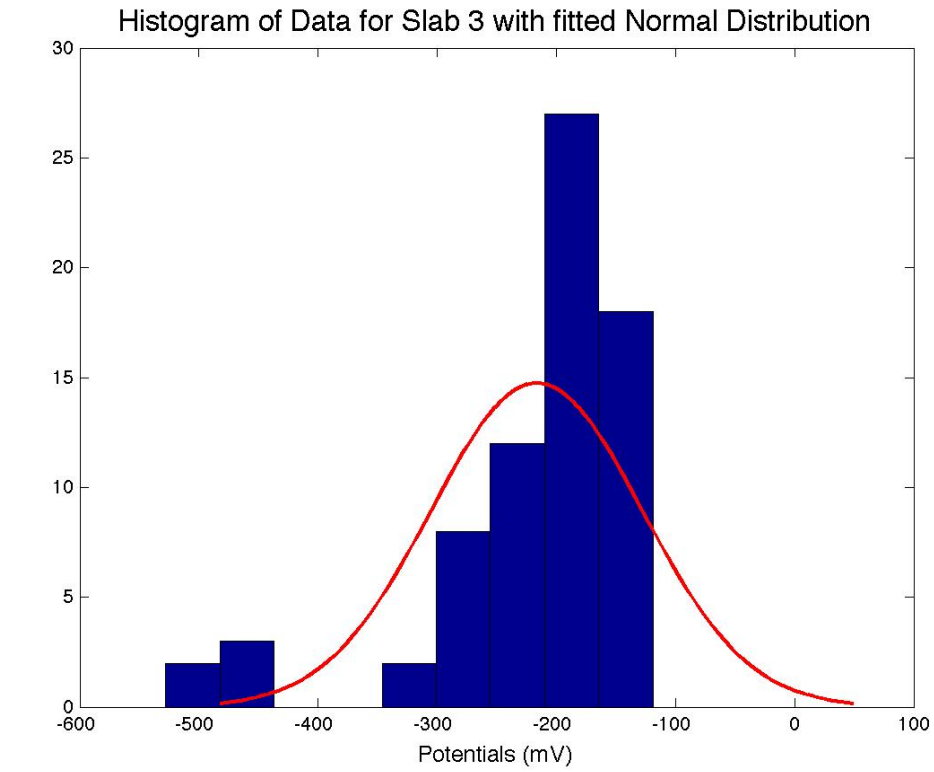

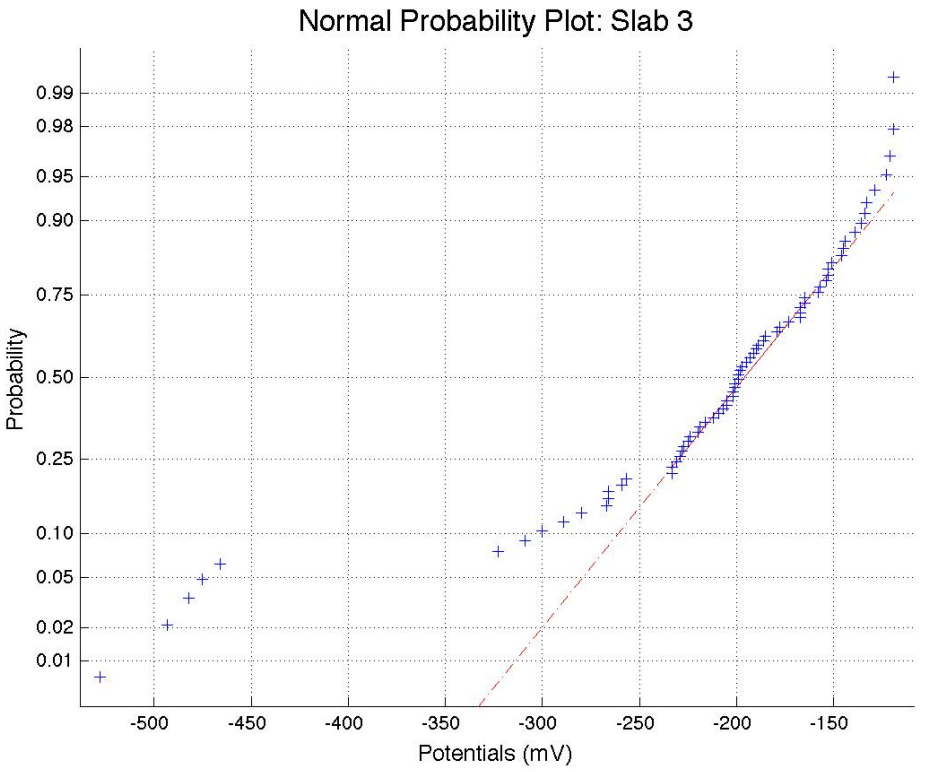

Figure B-71: Statistical Analys Slab 3: 07/20/2012

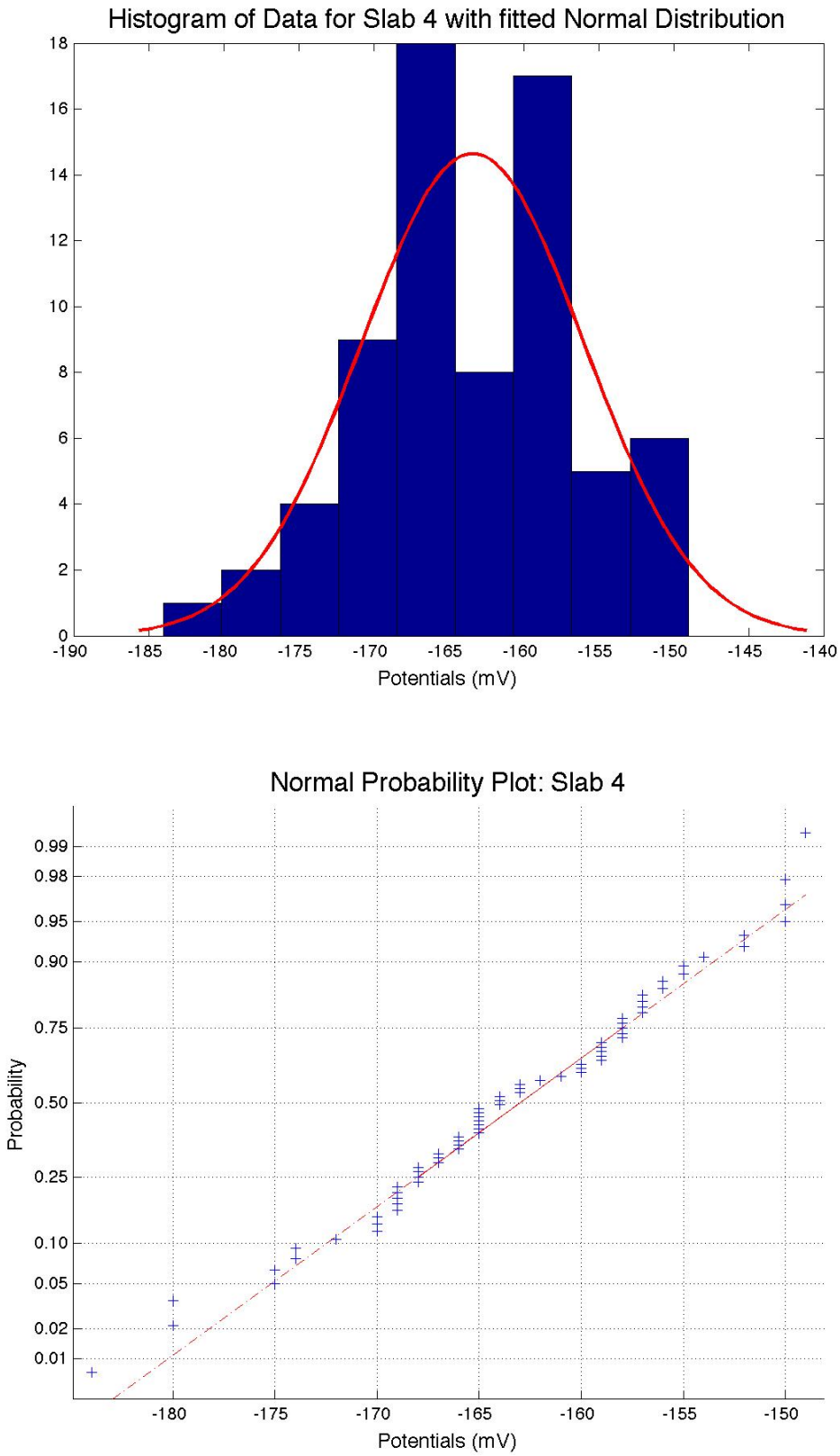

Figure B-72: Statistical Analys Slab 4: 07/20/2012

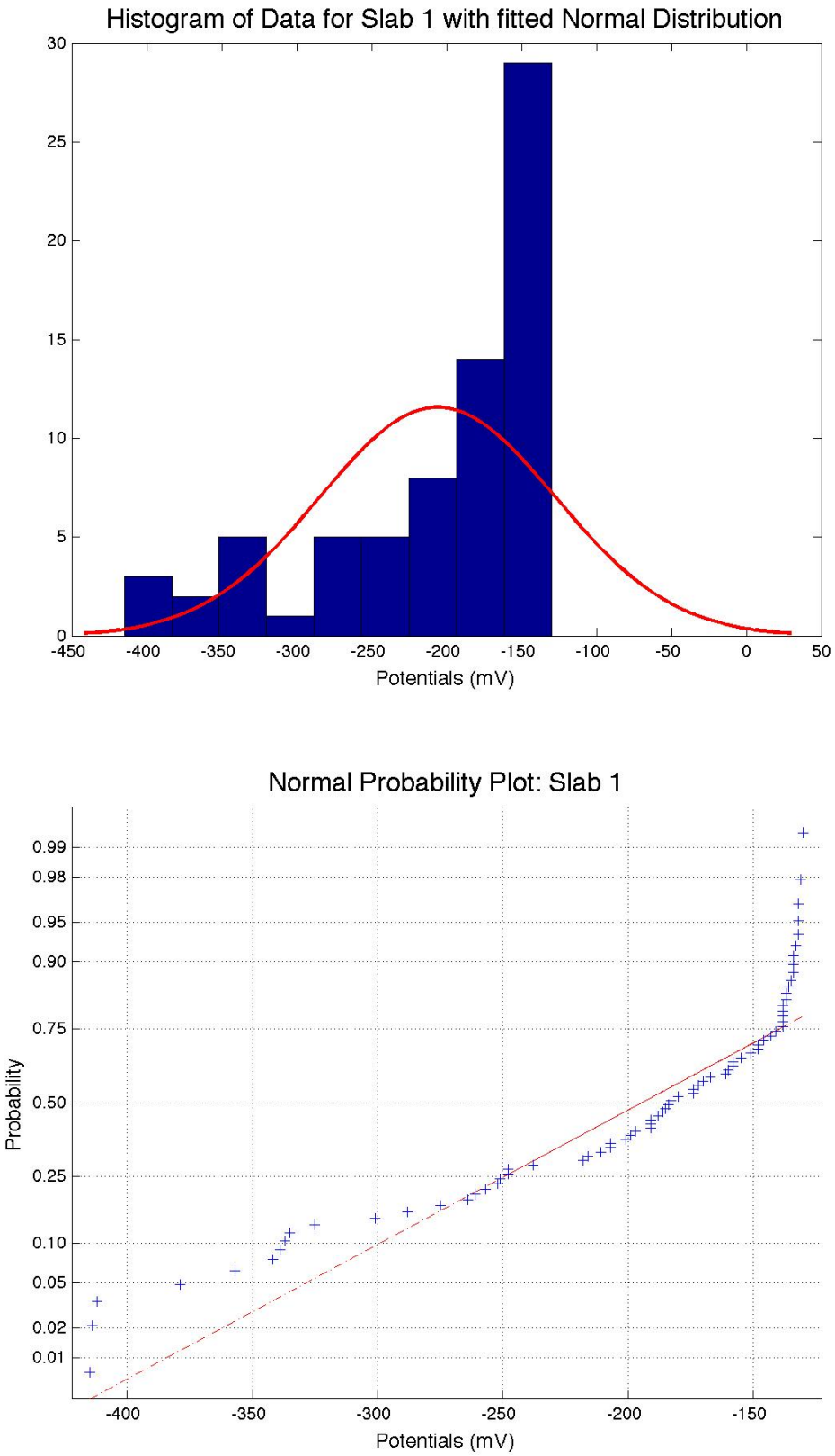

Figure B-73: Statistical Analys Slab 1: 07/27/2012

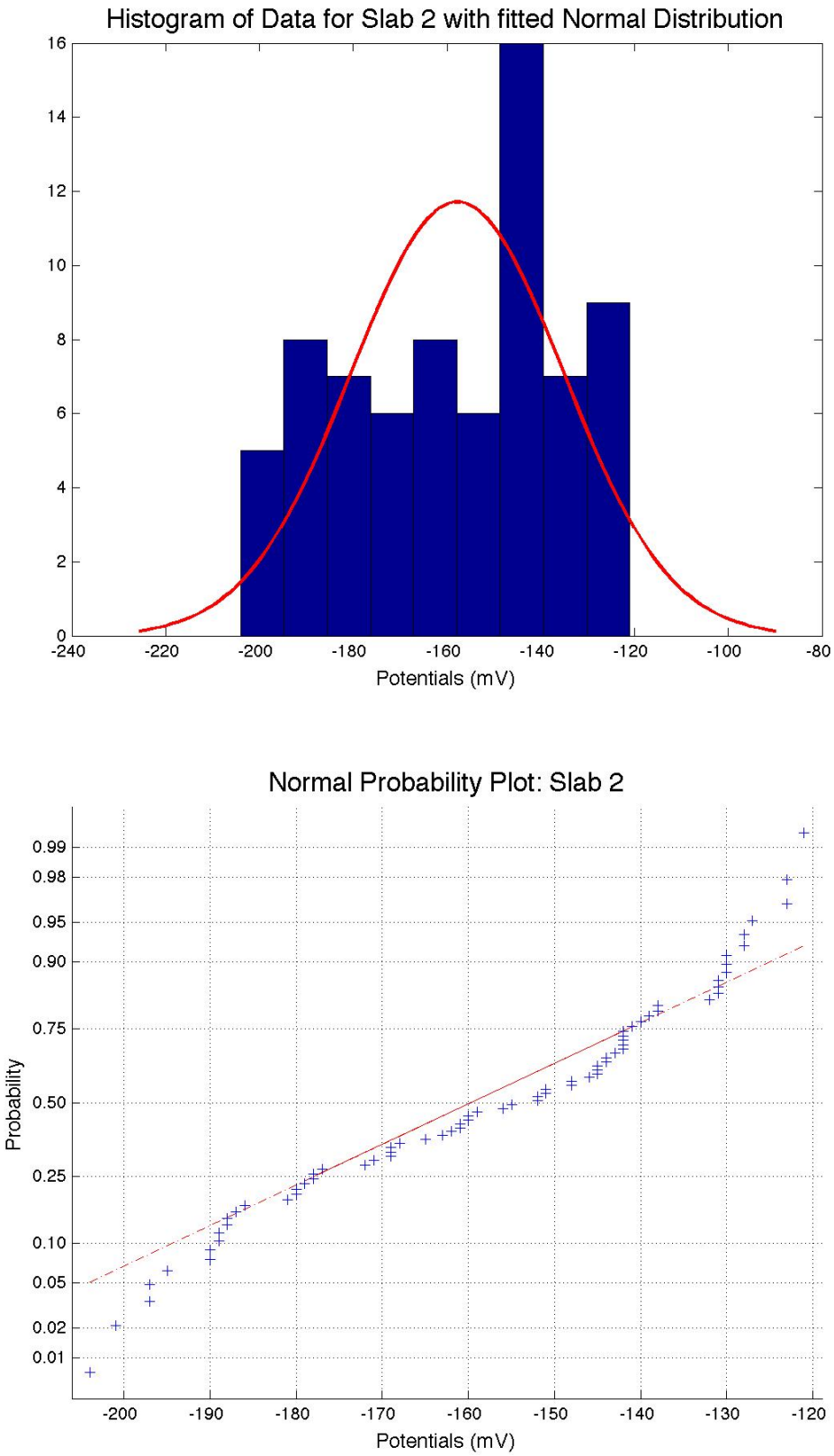

Figure B-74: Statistical Analys Slab 2: 07/27/2012

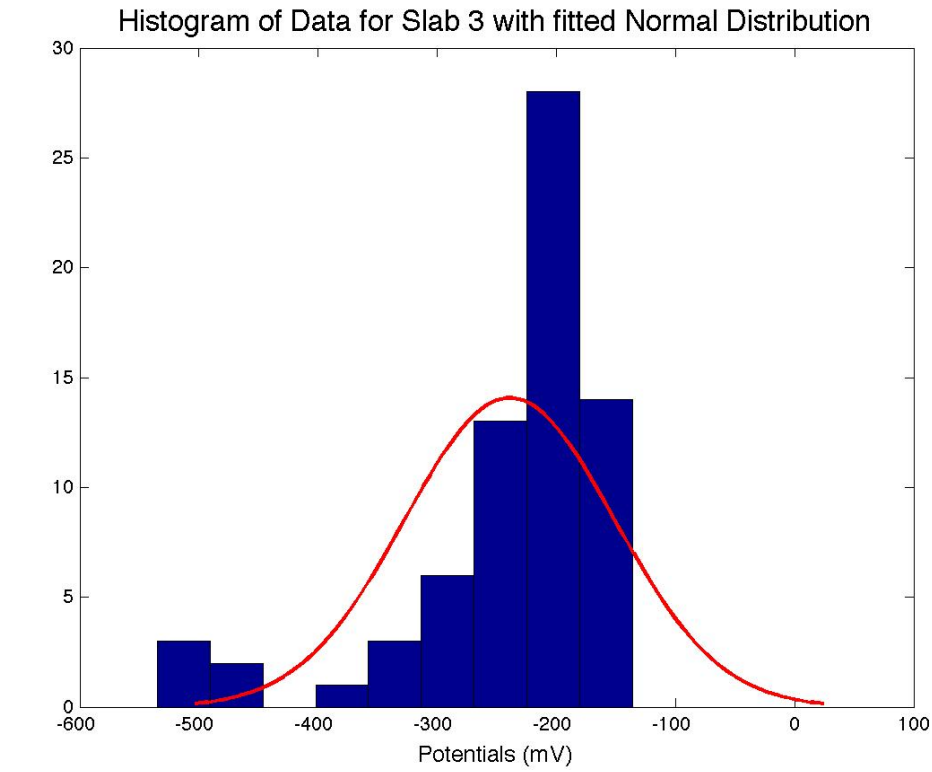

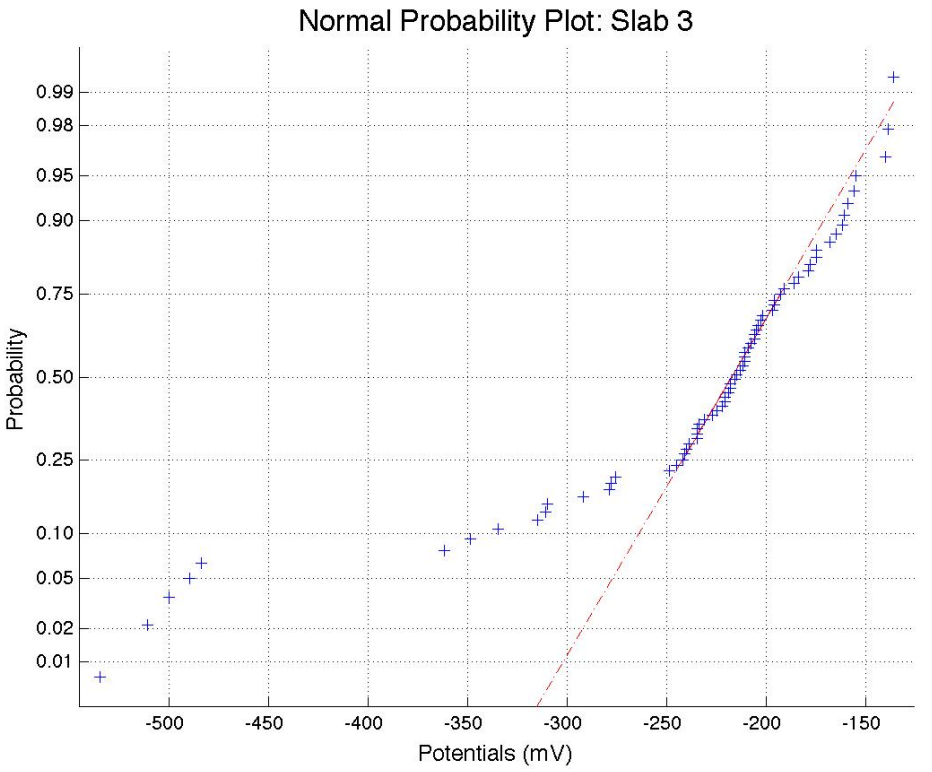

Figure B-75: Statistical Analys Slab 3: 07/27/2012

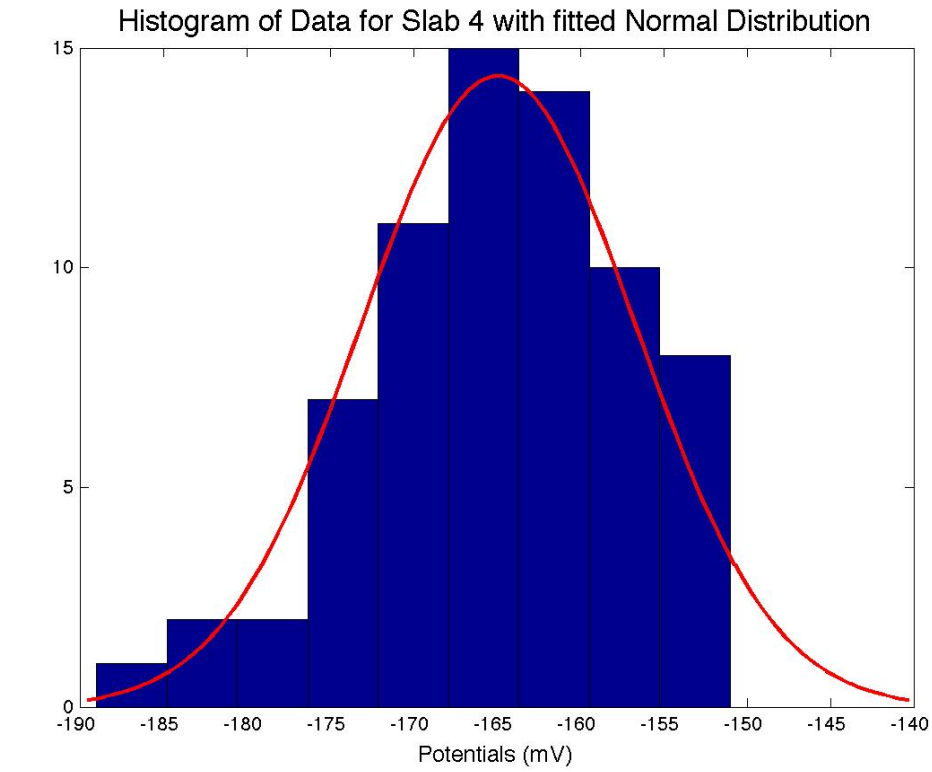

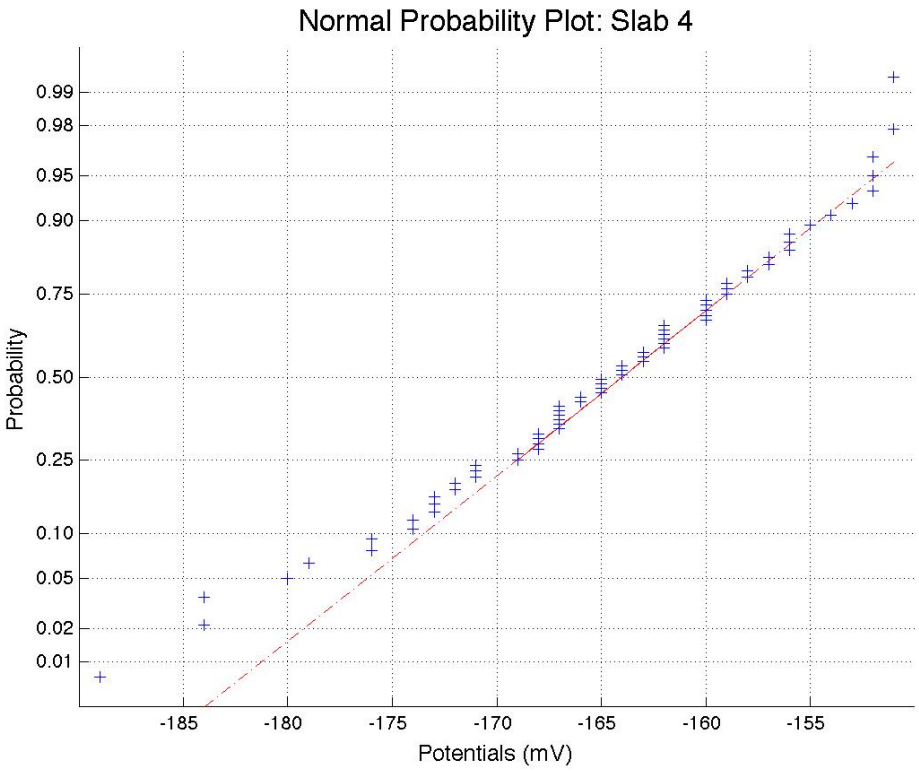

Figure B-76: Statistical Analys Slab 4: 07/27/2012

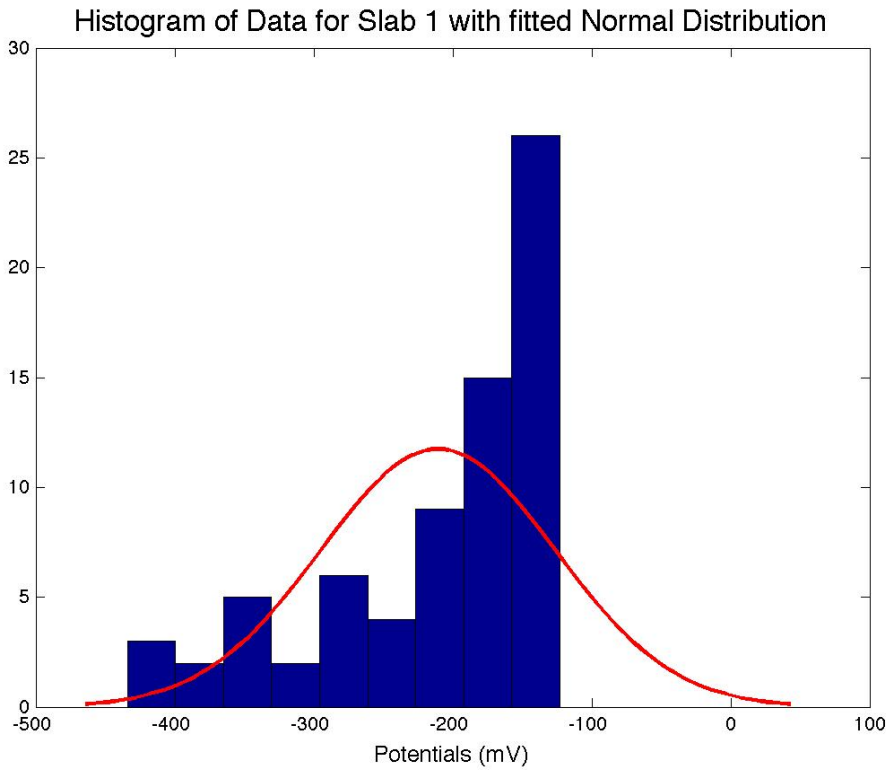

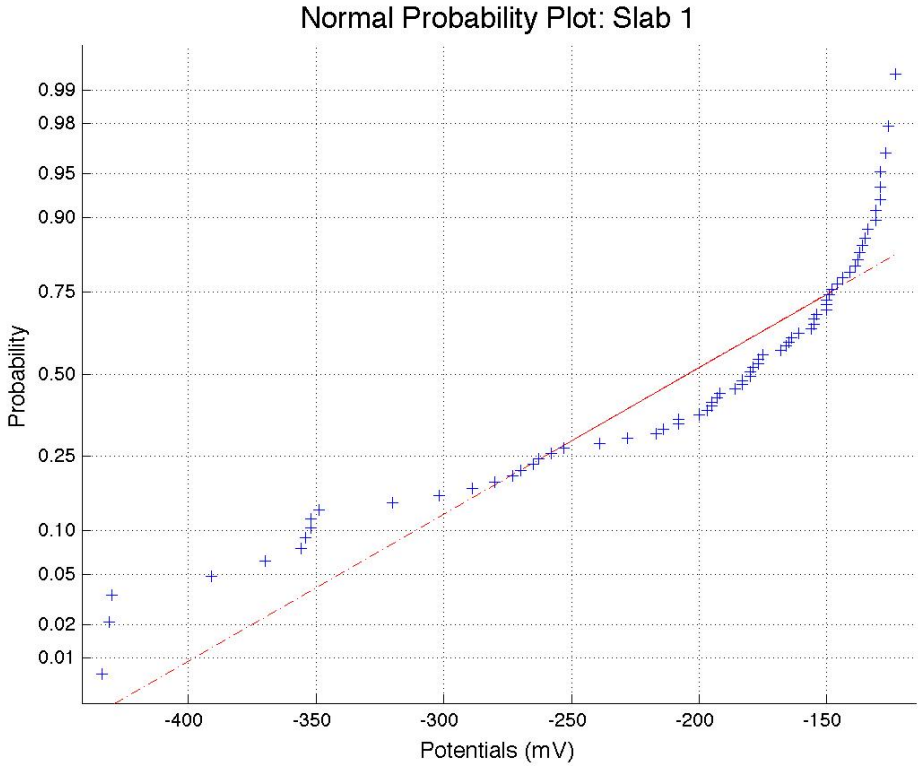

Figure B-77: Statistical Analys Slab 1: 08/03/2012

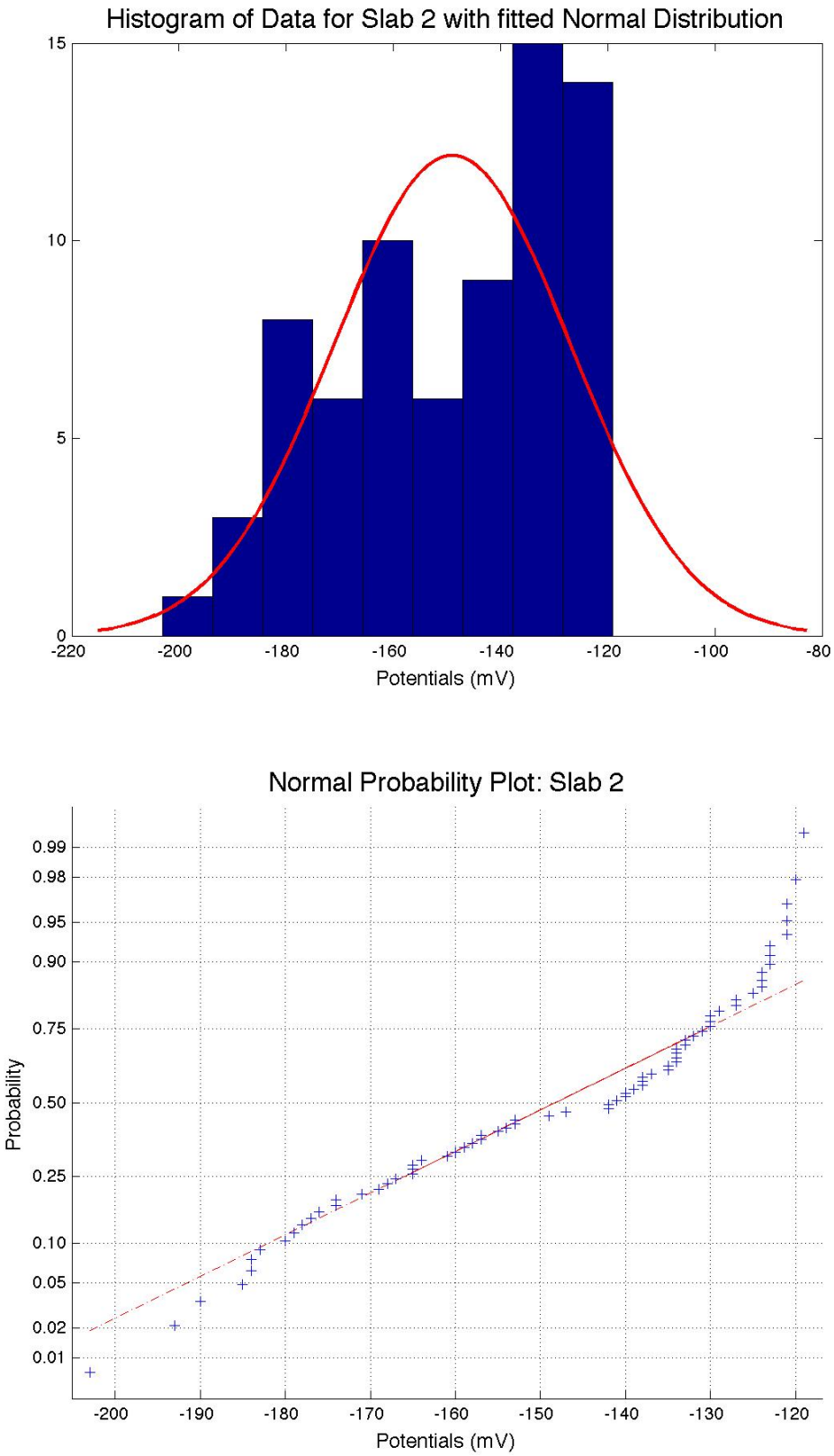

Figure B-78: Statistical Analys Slab 2: 08/03/2012

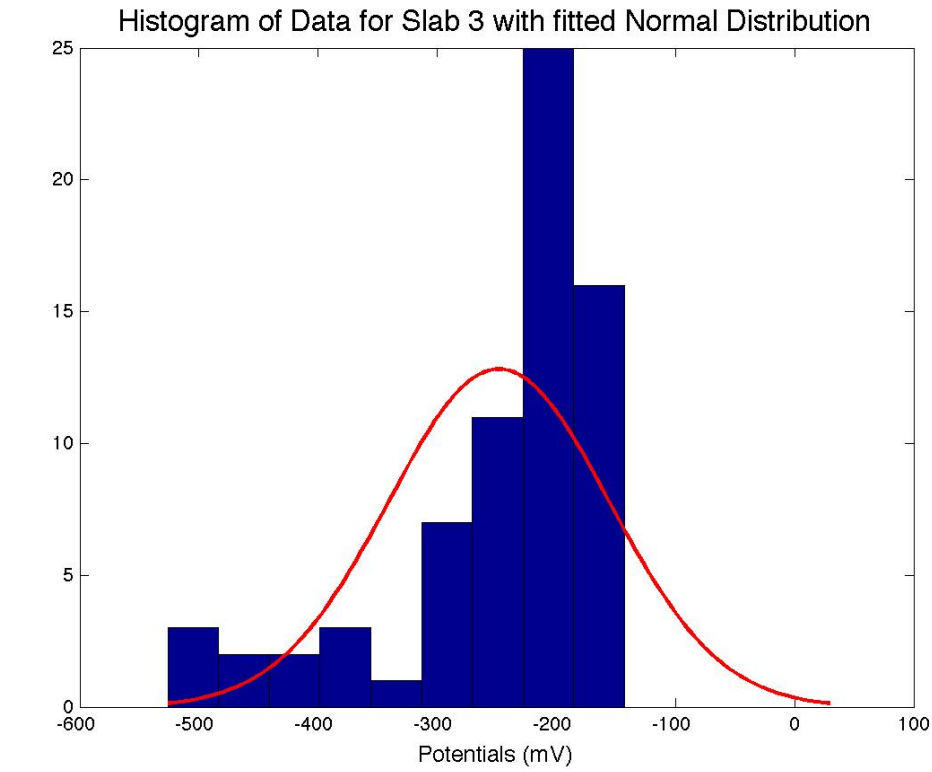

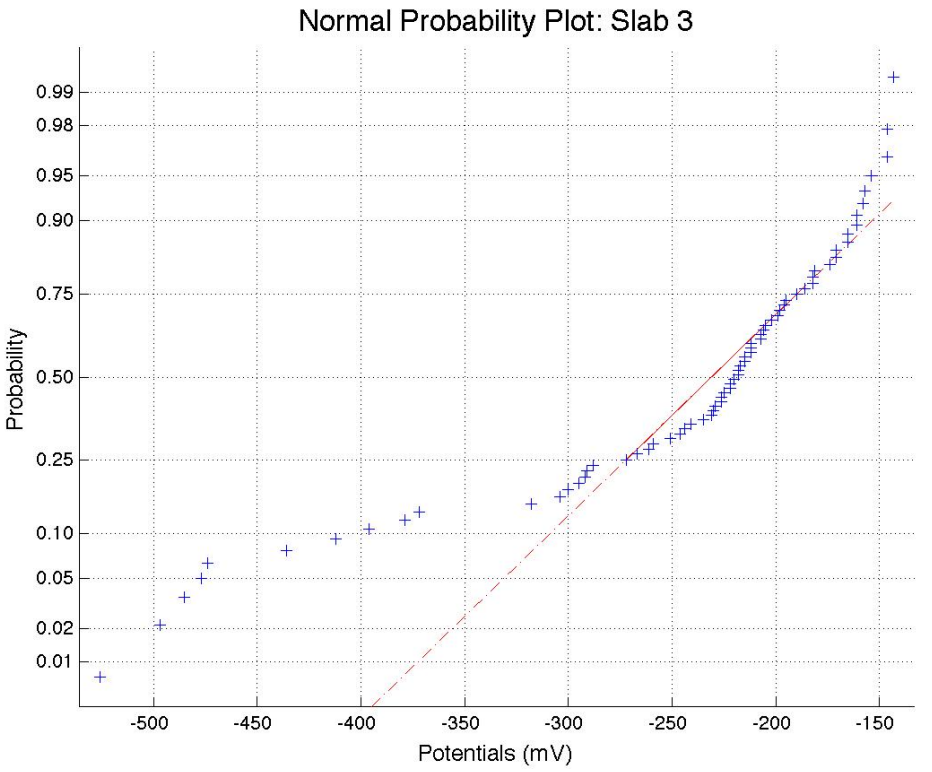

Figure B-79: Statistical Analys Slab 3: 08/03/2012

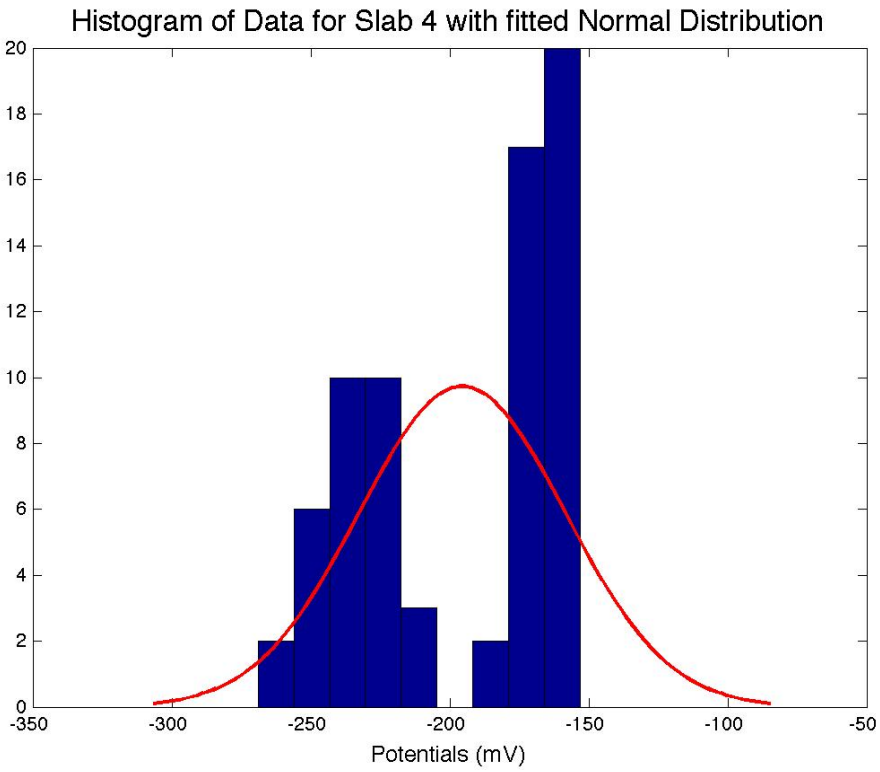

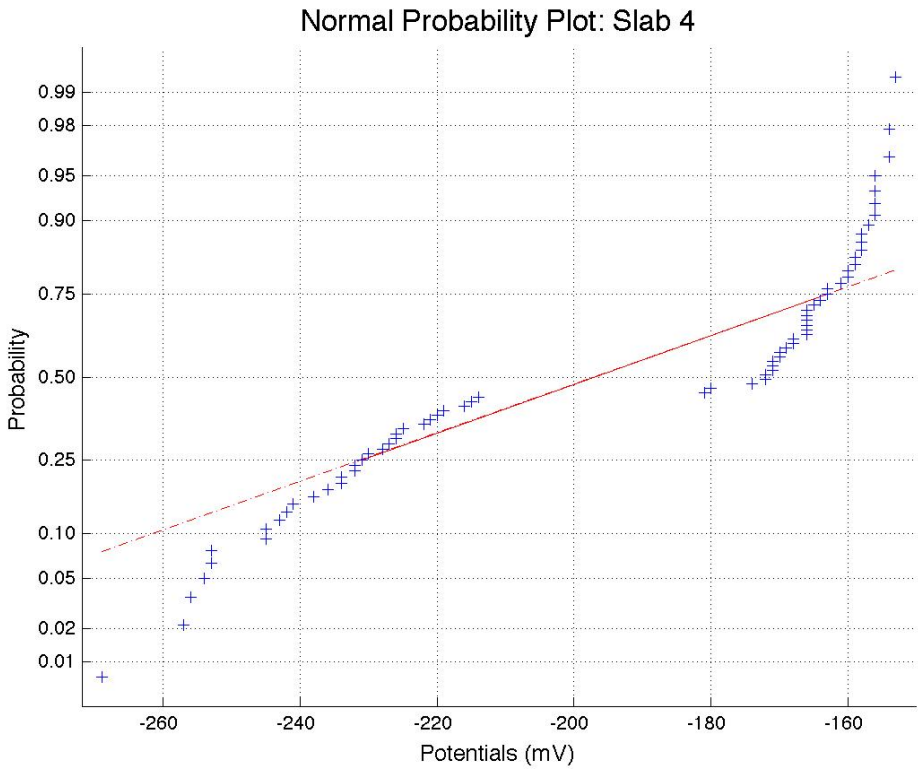

Figure B-80: Statistical Analys Slab 4: 08/03/2012

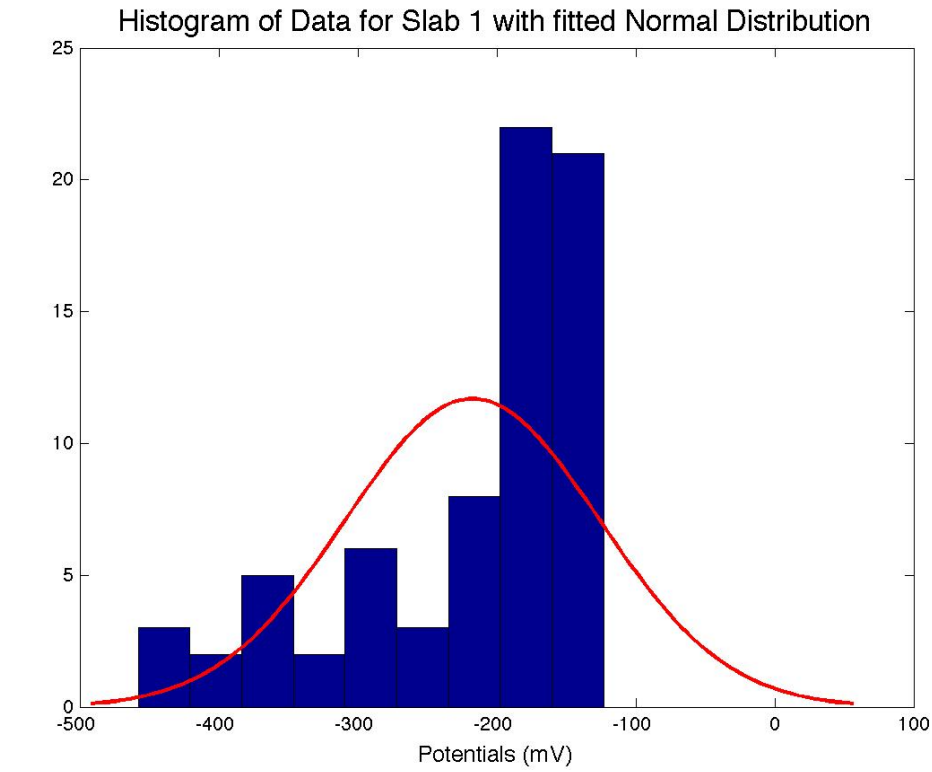

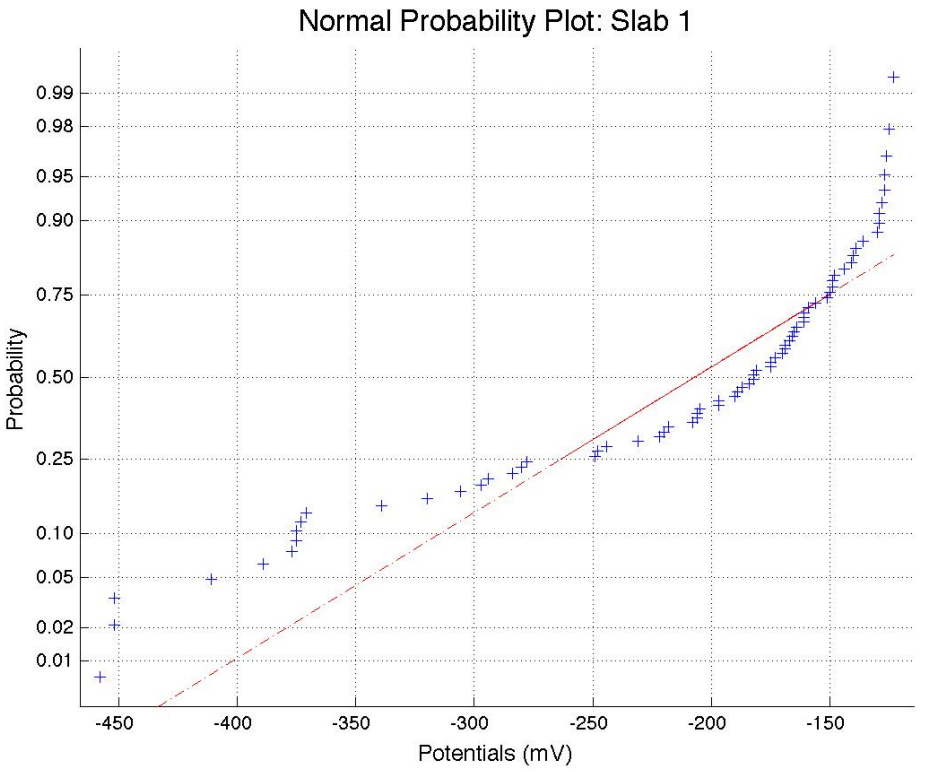

Figure B-81: Statistical Analys Slab 1: 08/10/2012

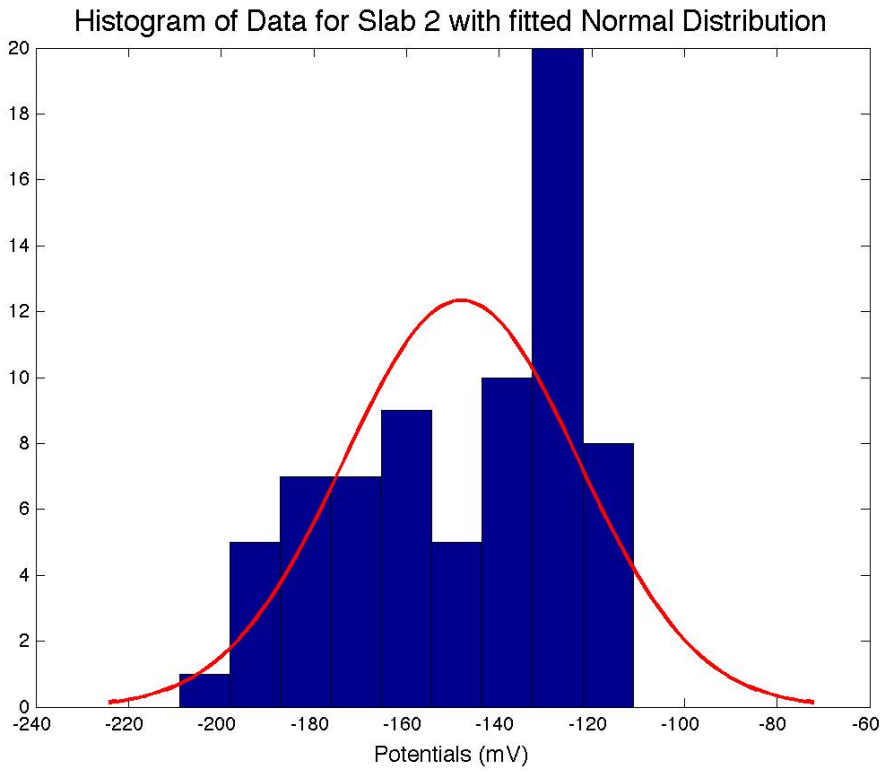

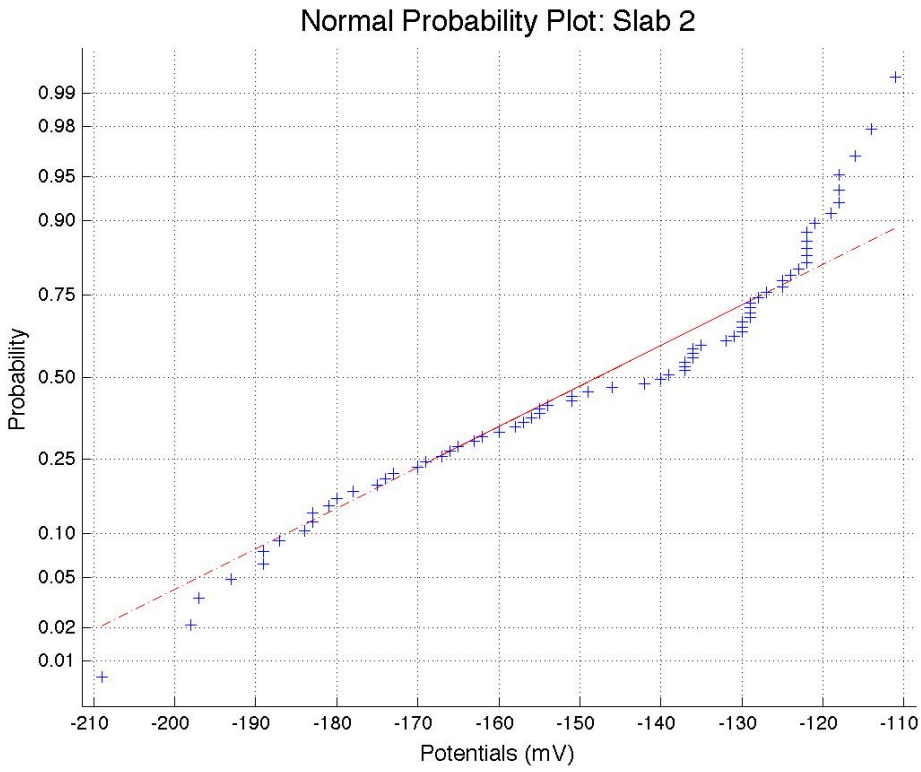

Figure B-82: Statistical Analys Slab 2: 08/10/2012

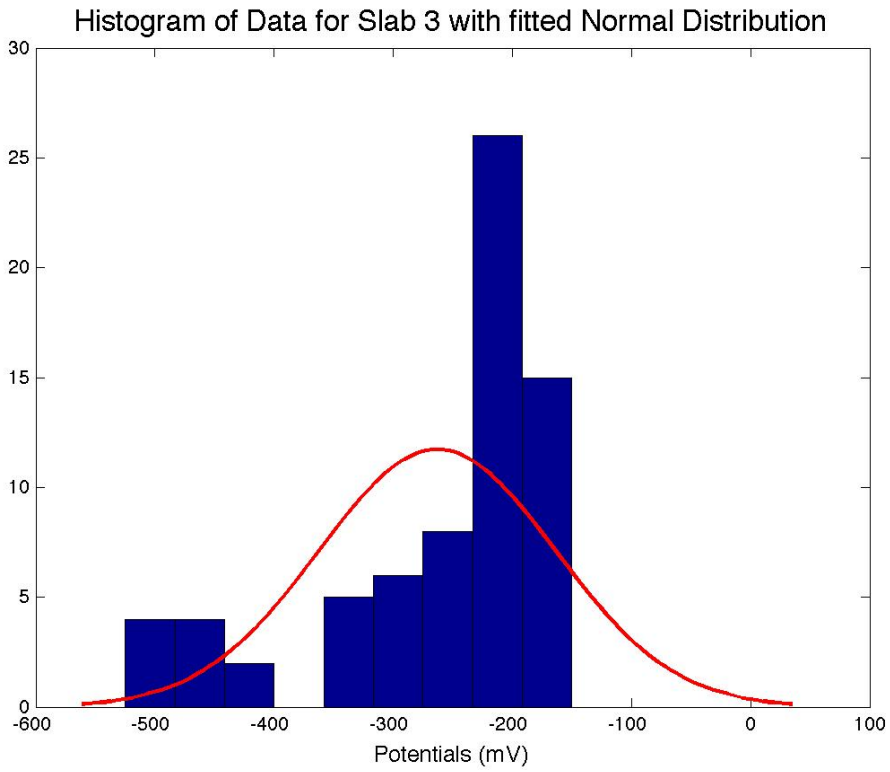

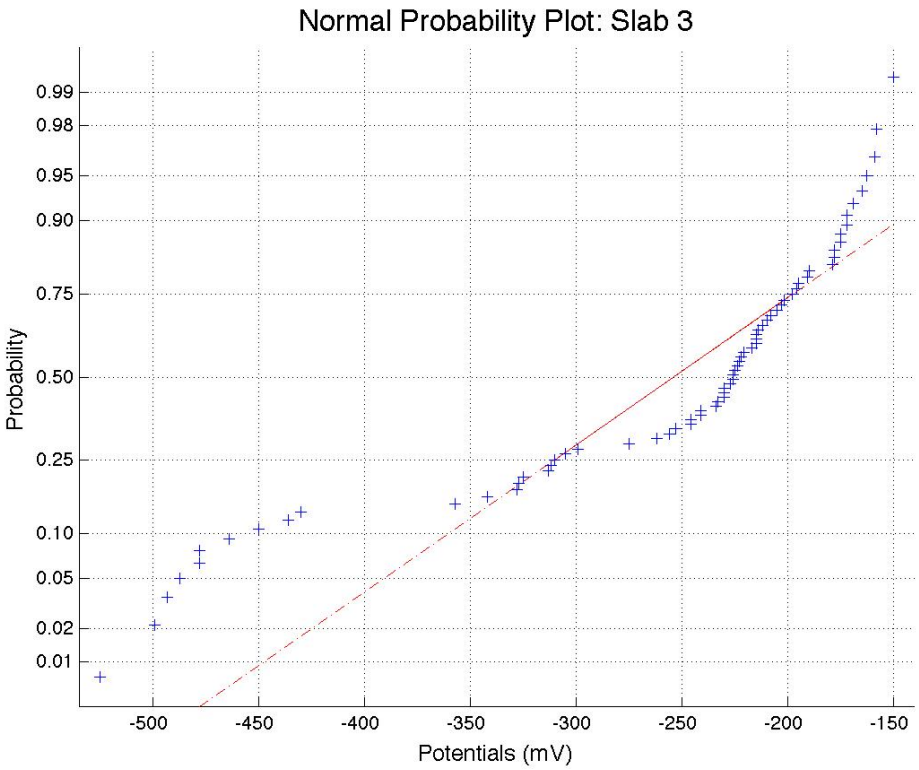

Figure B-83: Statistical Analys Slab 3: 08/10/2012

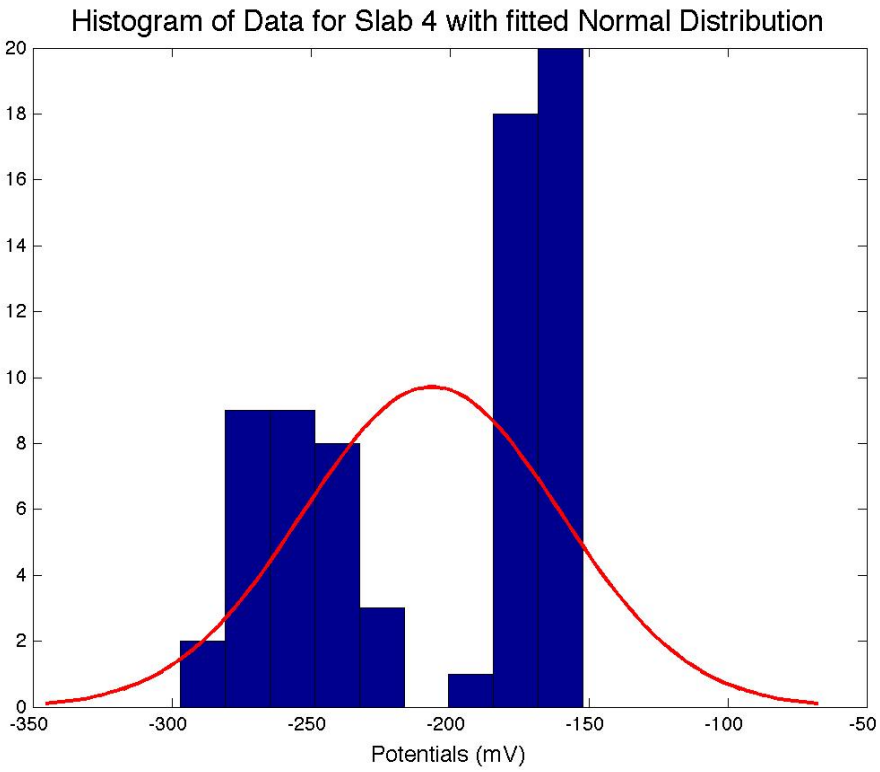

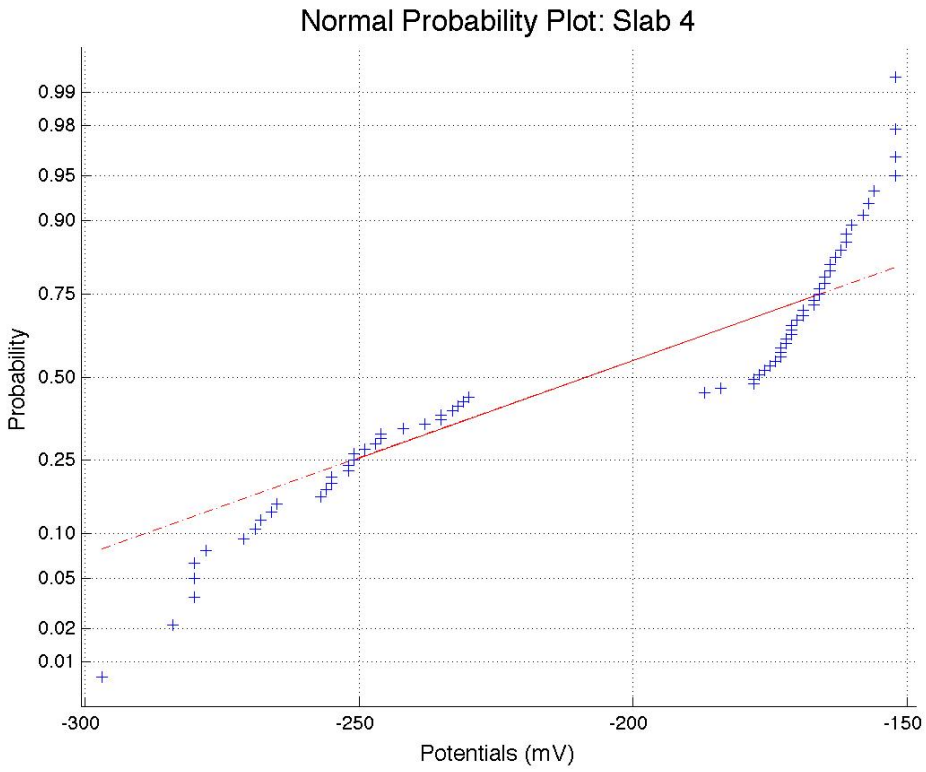

Figure B-84: Statistical Analys Slab 4: 08/10/2012

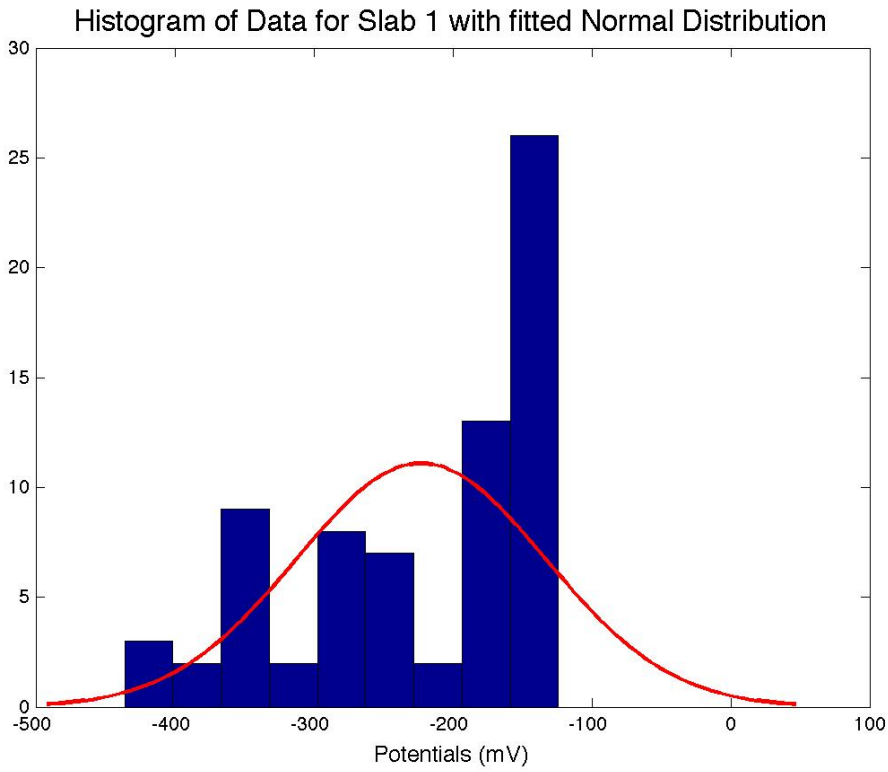

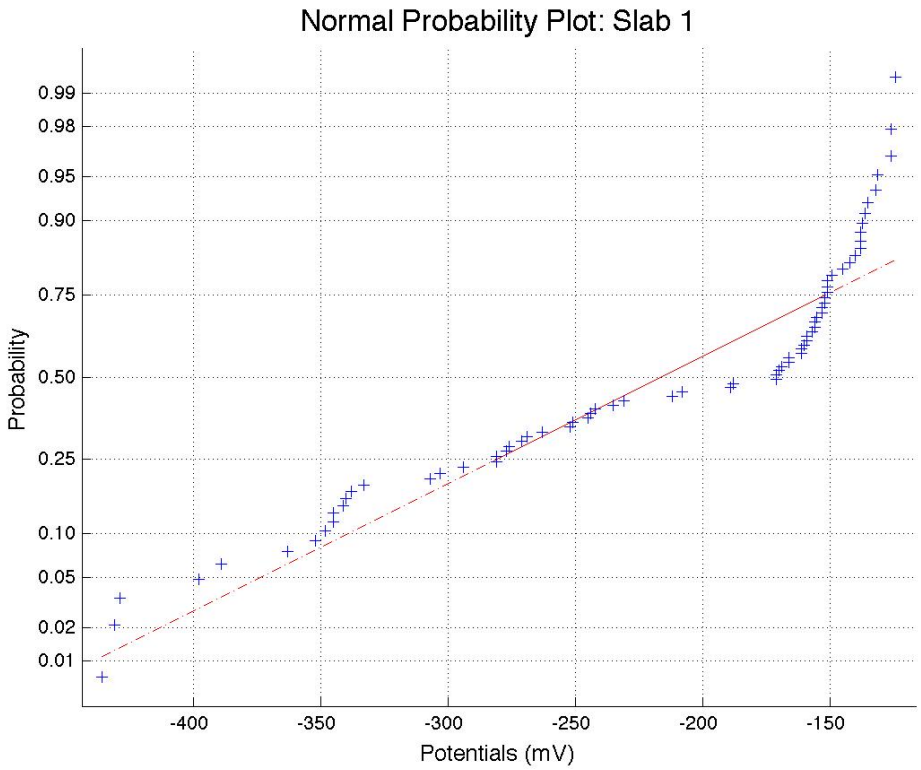

Figure B-85: Statistical Analys Slab 1: 08/17/2012

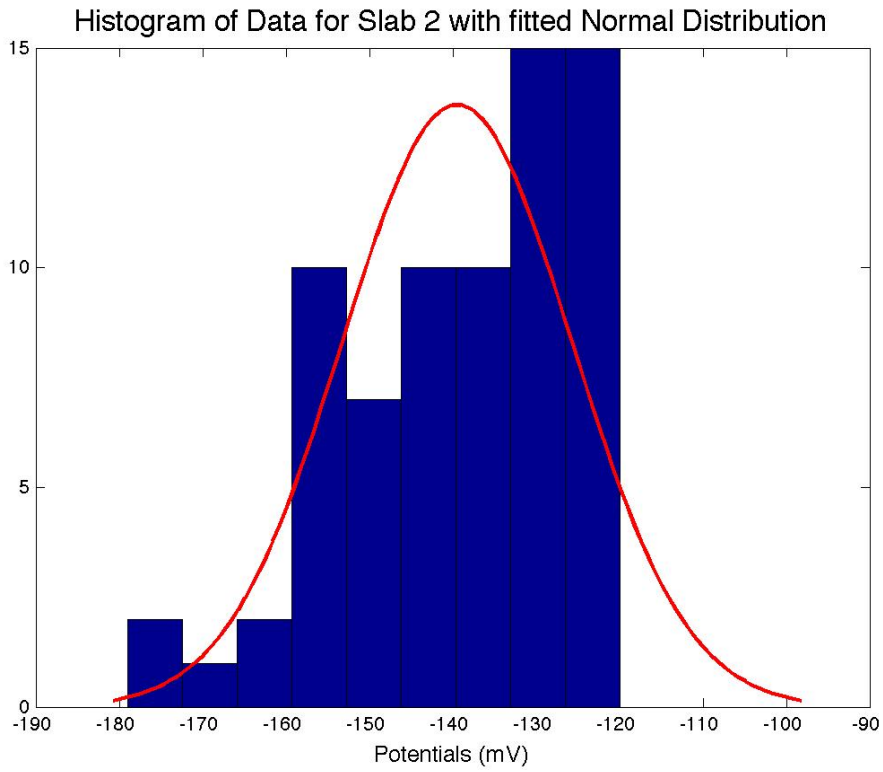

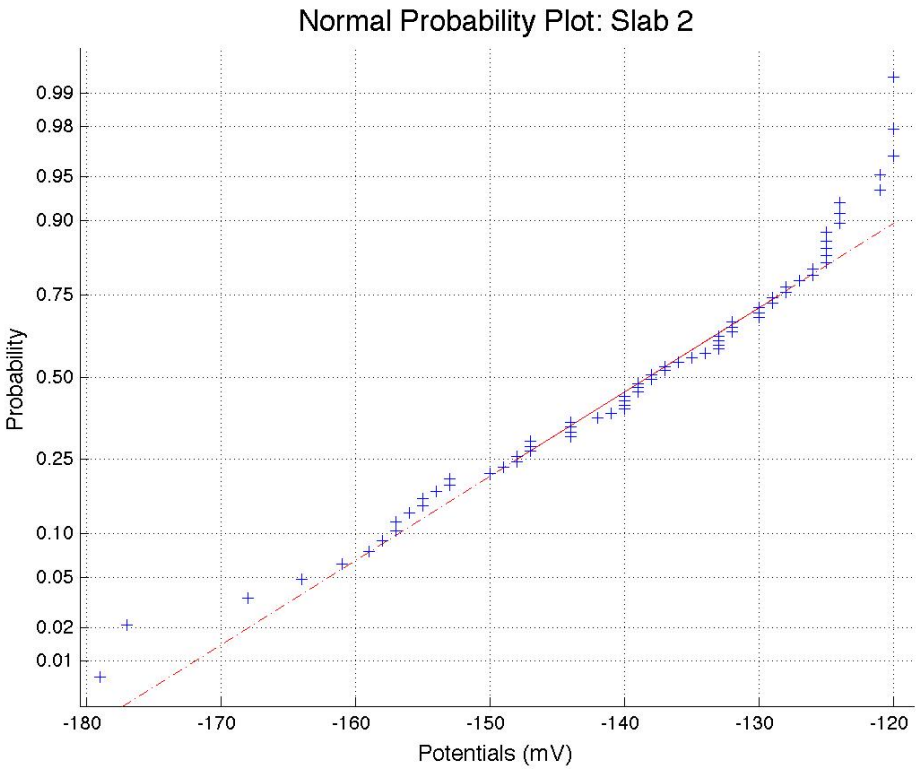

Figure B-86: Statistical Analys Slab 2: 08/17/2012

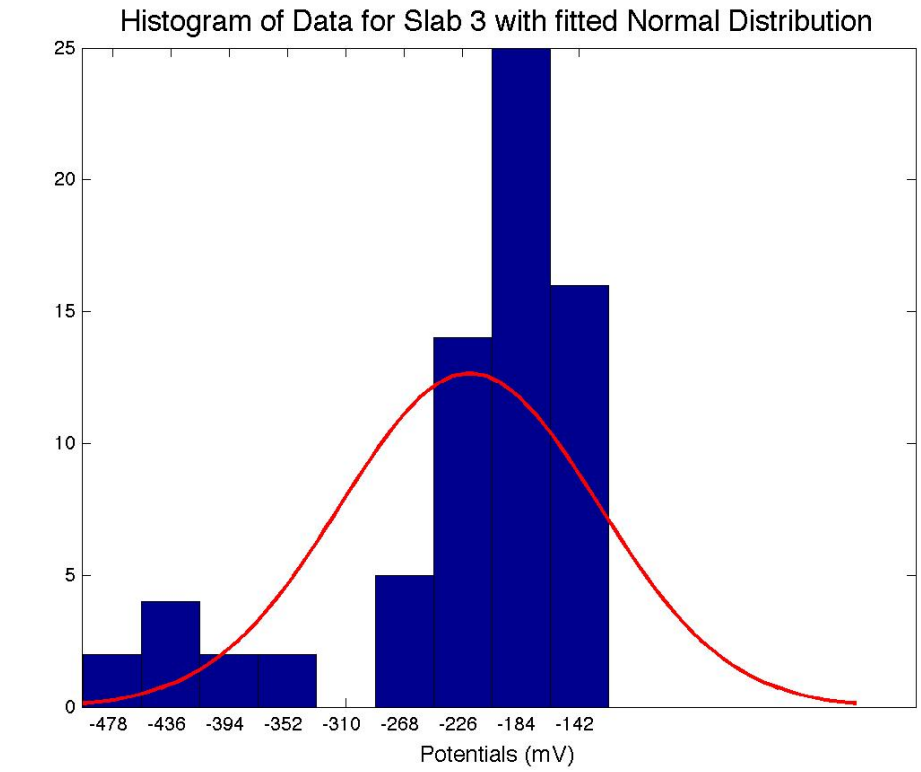

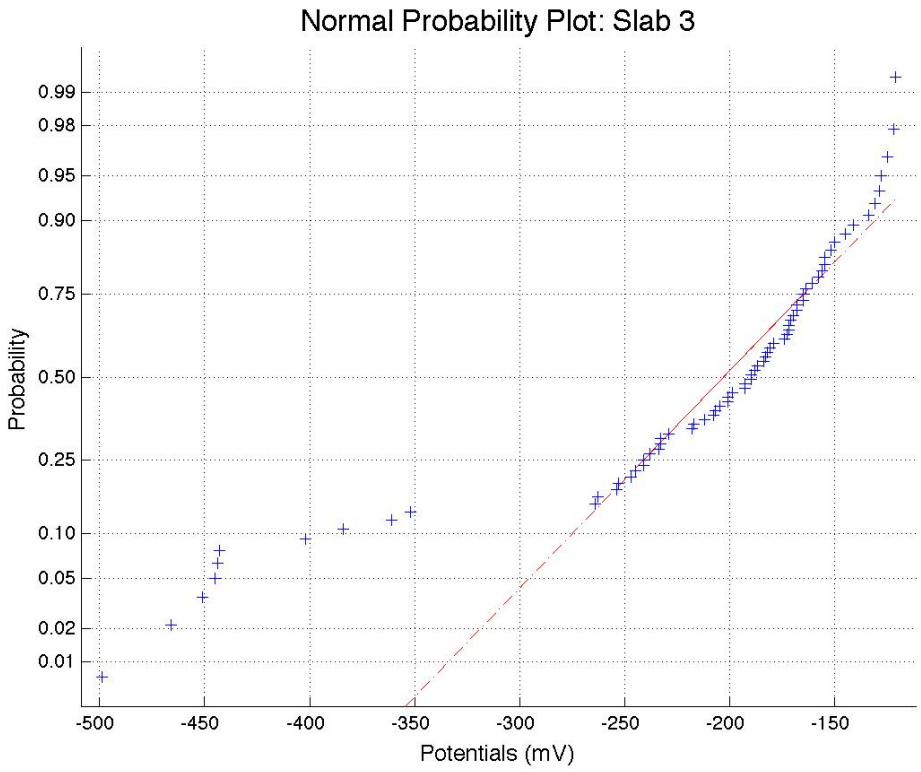

Figure B-87: Statistical Analys Slab 3: 08/17/2012

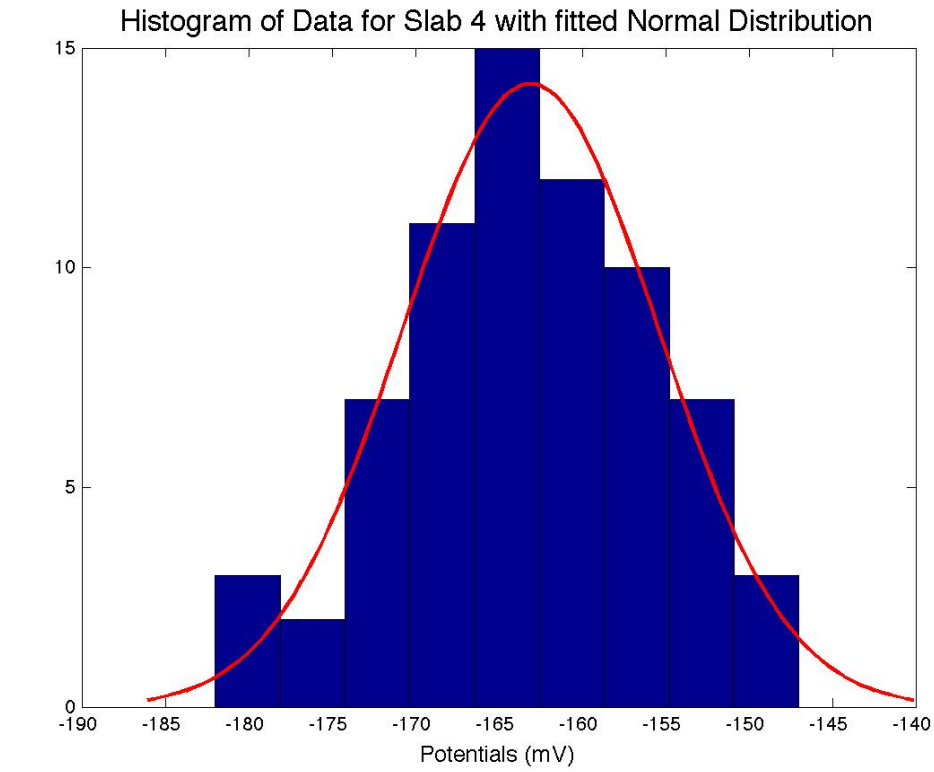

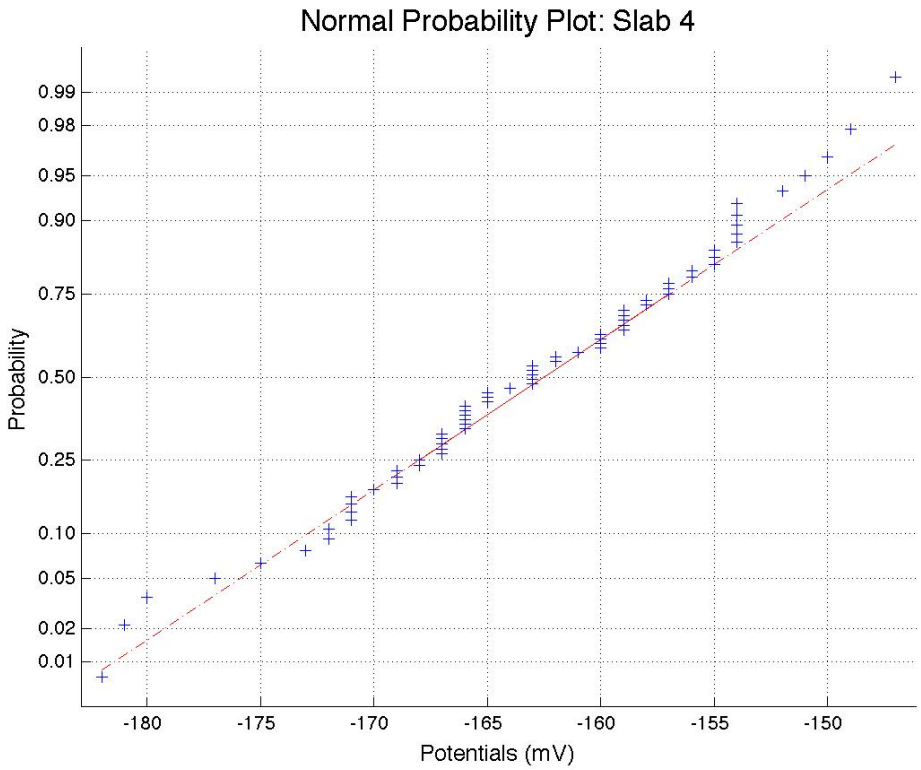

Figure B-88: Statistical Analys Slab 4: 08/17/2012

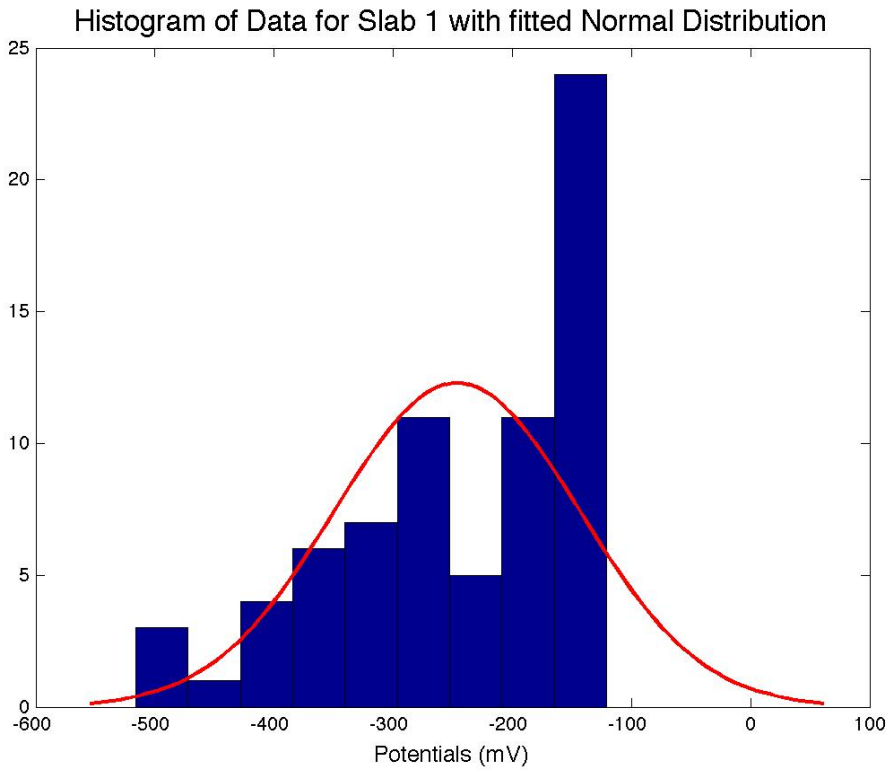

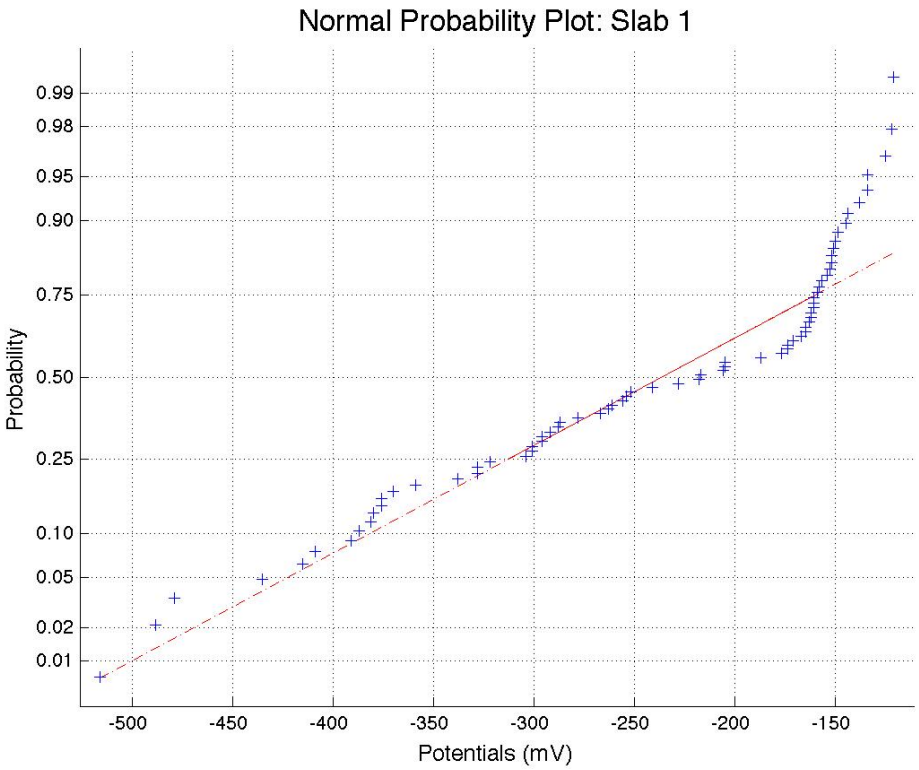

Figure B-89: Statistical Analys Slab 1: 08/24/2012

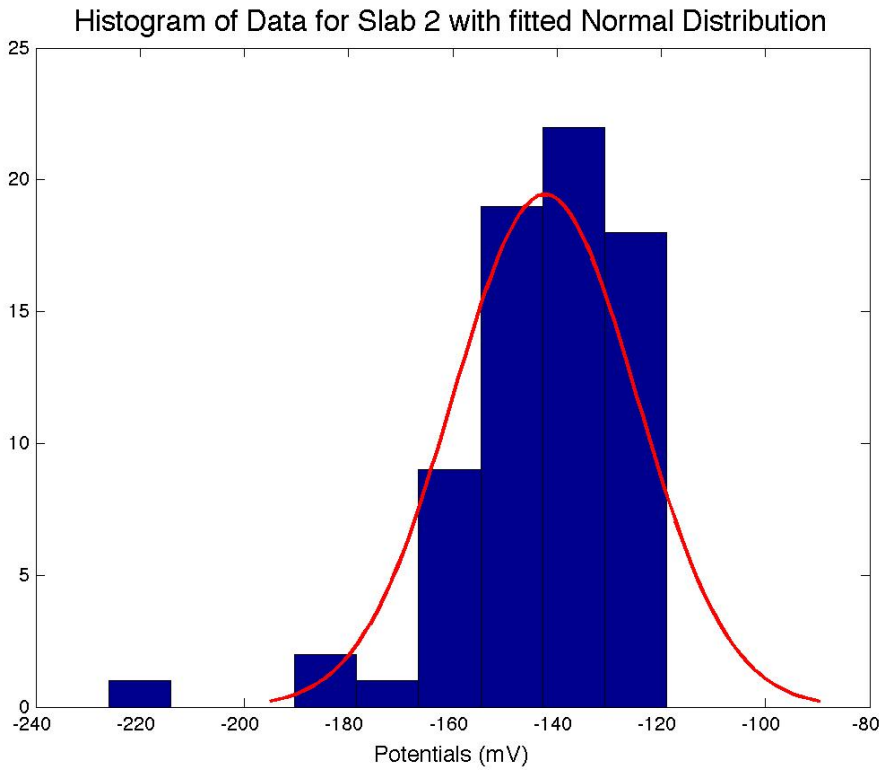

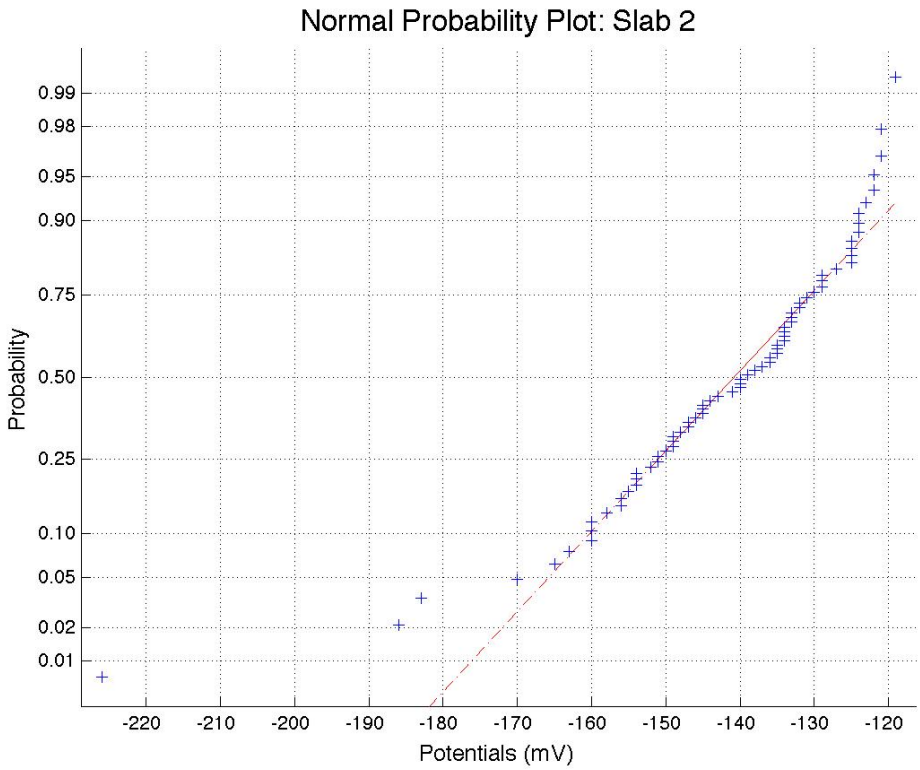

Figure B-90: Statistical Analys Slab 2: 08/24/2012

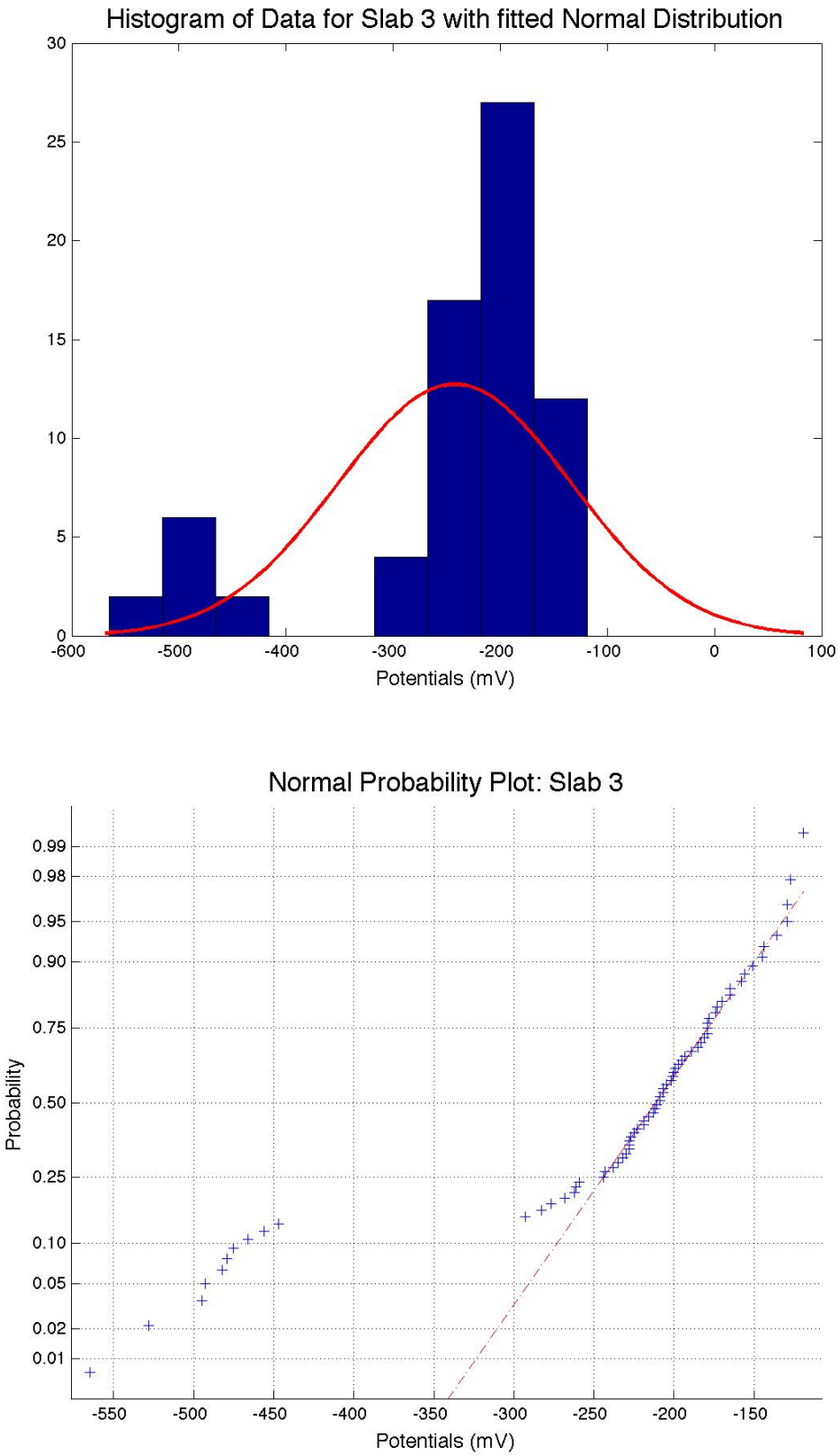

Figure B-91: Statistical Analys Slab 3: 08/24/2012

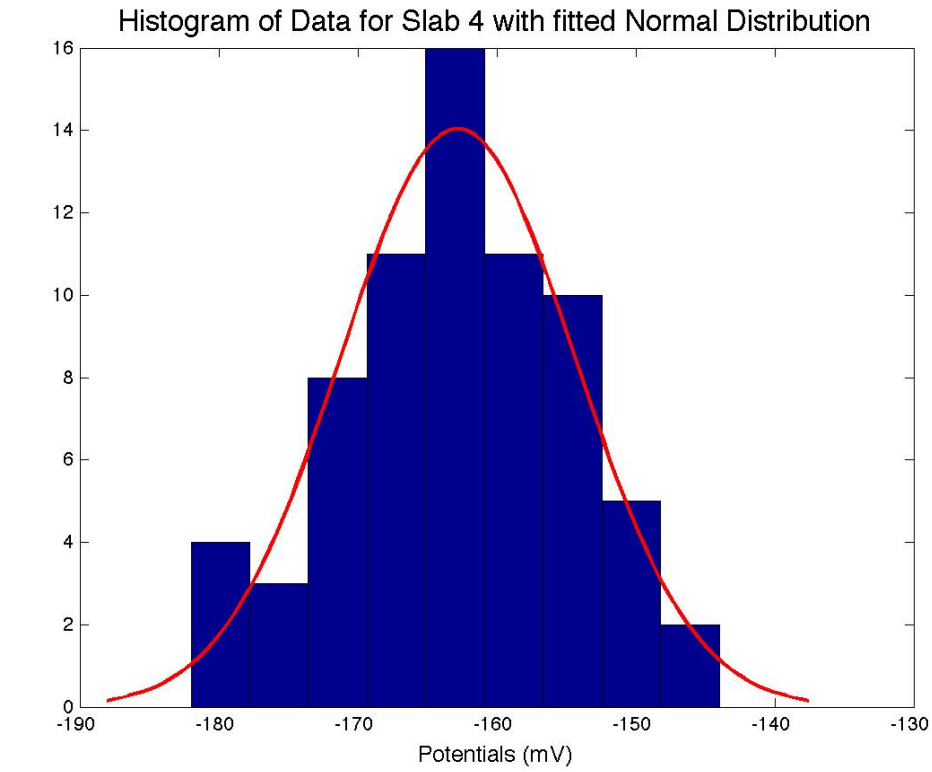

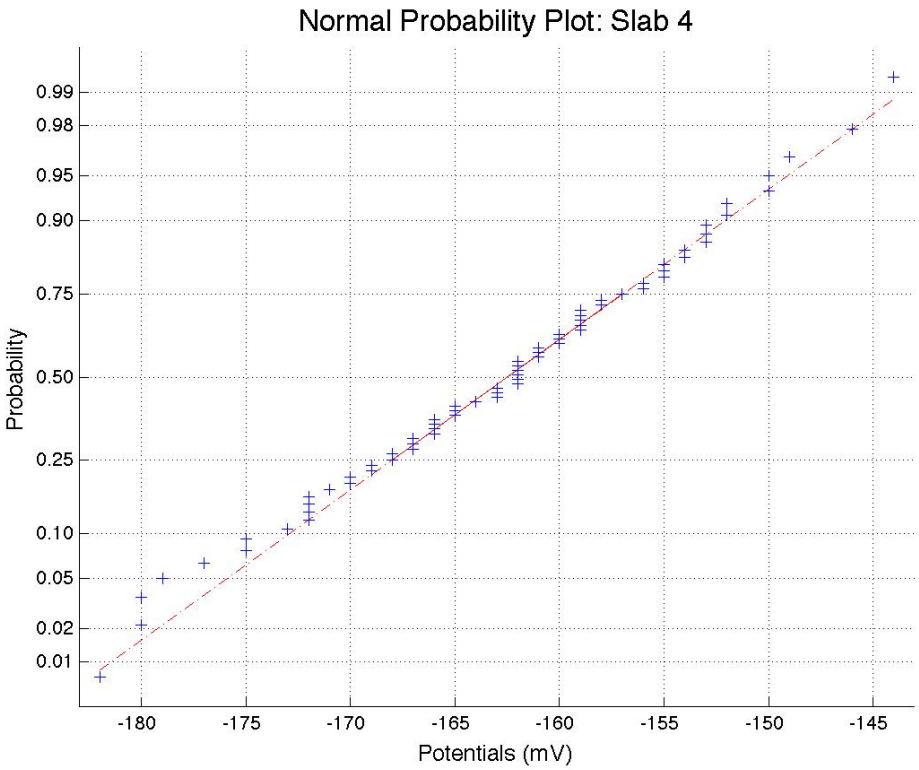

Figure B-92: Statistical Analys Slab 4: 08/24/2012

Bibliography

[1] A. A. Almusallam. Effect of degree of corrosion on the properties of reinforcing steel rebars. *Construction and Building Materials*, 15:361–368, 2001.

[2] C. Arya and P. Vassie. Influence of cathode-to-anode area ratio and separation distance on galvanic corrosion currents of steel in concrete containing chlorides. *Cement and Concrete Research*, 25(5):989–998, 1995.

[3] B. Assouli, G. Ballivy, and P. Rivard. Influence of environmental parameters on application of standard ASTM C876-91: half cell potential measurements. *Corrosion Engineering, Science and Technology*, 43(1):93–96, 2008.

[4] ASTM Standard C876. *Standard Test Method for Corrosion Potentials of Uncoated Reinforcing Steel in Concrete*. ASTM International, West Conshohocken, PA, 2009.

[5] ASTM Standard G1- 03. *Standard Practice for Preparing, Cleaning, and Evaluating Corrosion Test Specimens*. ASTM International, West Conshohocken, PA, 2003.

[6] ASTM Standard G109. *Standard Test Method for Determining Effects of Chemical Admixtures on Corrosion of Embedded Steel Reinforcement in Concrete Exposed to Chloride Environments*. ASTM International, West Conshohocken, PA, 2007.

[7] ASTM Standard G16-95. *Standard Guide for Applying Statistics to Analysis of Corrosion Data*. ASTM International, West Conshohocken, PA, 2010.

[8] J. G. Cabrera. Deterioration of concrete due to reinforcement steel corrosion. *Cement and Concrete Composites*, 18:47–59, 1996.

[9] L. Chung, S.-H. Cho, J.-H. J. Kim, and S.-T. Yi. Correction factor suggestion for ACI development length provisions based on flexural testing of RC slabs with various levels of corroded reinforcing bars. *Engineering Structures*, 26:1013–1026, 2004.

[10] L. Chung, J.-H. J. Kim, and S.-T. Yi. Bond strength prediction for reinforced concrete members with highly corroded reinforcing bars. *Cement and Concrete Composites*, 30:603–611, 2008.

[11] D. Darwin, J. Balma, J. C. E. Locke, and T. V. Nguyen. Accelerated corrosion testing for concrete reinforcing bar corrosion protection systems. In P. J. M. Monteiro, K. Chong, J. Larsen-Basse, and K. Komvopoulos, editors, *Duability 2000*, Proceedings of Durability Workshop, pages 91–108, Berkeley, CA, 2001. Oxford, Elsevier Science Ltd.

[12] B. Elsener. Half-cell potential mapping to assess repair work on RC structures. *Construction and Building Materials*, 15:133–139, 2001.

[13] B. Elsener. Macrocell corrosion of steel in concrete - implications for corrosion monitoring. *Cement and Concrete Composites*, 24:65–72, 2002.

[14] C. Fang, K. Lundgren, L. Chen, and C. Zhu. Corrosion influence on bond in reinforced concrete. *Cement and Concrete Research*, 34:2159–2167, 2004.

[15] S. H. Gamidi. Non destructive testing of structures, November 2009.

[16] P. Gaydecki, I. Silva, B. Fernandes, and Z. Yu. A portable inductive scanning system for imaging steel-reinforcing bars embedded within concrete. *Sensors and Actuators*, 84:25–32, 2000.

[17] G. K. Glass and N. R. Buenfeld. The presentation of the chloride threshold level for corrosionof steel in concrete. *Corrosion Science*, 39(5):1001–1013, 1997.

[18] P. Gu, P. Xie, and J. Beaudoin. A discussion of the paper "ELECTRODE POTENTIAL MEASUREMENTS OF CONCRETE REINFORCEMENT FOR CORROSION EVALUATION" by R. Francois, G. Arliguie and D. Bardy. *Cement and Concrete Research*, 25(5):1111–1114, 1995.

[19] J. Gulikers. Experimental investigations on macrocell corrosion in chloride-contaminated concrete. *HERON*, 41(2):107–123, 1996.

[20] P. Huang, Y. Bao, and Y. Yao. Influence of HCl corrrosion on the mechanical properties of concrete. *Cement and Concrete Research*, 35:584–589, 2005.

[21] R. Huang, J.-J. Chang, and J.-K. Wu. Correlation between corrosion potential and polarization resistance of rebar in concrete. *Materials Letters*, 28:445–450, October 1996.

[22] R. Huang and C. Yang. Condition assessment of reinforced concrete beams relative to reinforcement corrosion. *Cement and Concrete Composites*, 19:131–137, 1997.

[23] S. S. Hubbard et al. Experimental detection of reinforcing bar corrosion using nondestructive geophysical techniques. *ACI Materials Journal*, 100(6):501–510, November-December 2003.

[24] R. R. Hussain. Underwater half-cell corrosion potential bench mark measurements of corroding steel in concrete influenced by a variety of material science and environmental engineering variables. *Measurement*, 44:274–280, 2011.

[25] Industrial Applications and Chemistry Section. *Guidebook on Non-Destructive Testing of Concrete Structures*. IAEA, Wagramer Strasse 5, P.O. Box 100, A-1400 Vienna, Austria, September 2002.

[26] G. H. Kock, M. P. Brongers, N. G. Thompson, Y. P. Virmani, and J. Prayer. CORROSION COSTS AND PREVENTIVE STRATEGIES IN THE UNITED STATES. Technical Report FHWA-RD-01-156, FHWA, U.S

Federal Highway Administration, Turner-Fairbank Highway Research Center, McLean, Virginia, March 2002.

[27] H.-S. Lee, T. Noguchi, and F. Tomosawa. Evaluation of the bond properties between concrete and reinforcement as a function of the degree of reinforcement corrosion. *Cement and Concrete Research*, 32:1313–1318, 2002.

[28] V. Leelalerkiet, J.-W. Kyung, M. Ohtsu, and M. Yokota. Analysis of half-cell potential measurement for corrosion of reinforced concrete. *Construction and Building Materials*, 18:155–162, 2004.

[29] J. Makar and R. Desnoyers. Magnetic field techniques for the inspection of steel under concrete cover. *NDT&E International*, 34:445–456, 2001.

[30] G. Markeset and R. Myrdal. Modelling of reinforcement corrosion in concrete - State of the art. Technical Report COIN Project report 7, SINTEF Building and Intrastructure, Forskningsveien 3 B, POBox 124 Blindern, N-0314 Oslo, Norway, 2008.

[31] G. Miller et al. Detection and imaging of surface corrosion on steel reinforcing bars using a phase-sensitive inductive sensor intended for use with concrete. *NDT&E International*, 36:19–26, 2003.

[32] W. Norris, D. Naus, and H. G. III. Inspection of nuclear power plants containment structures. *Nuclear Engineering and Design*, 192:303–329, 1999.

[33] M. Ohtsu and T. Yamamoto. Compensation procedure for half-cell potential measurement. *Construction and Building Materials*, 11(7-8):395–402, 1997.

[34] N. Polydorides, G. Georghiou, D. Kim, and C. Won. Subspace constrained regularization for corrosion detection with magnetic induction tomography. *NDT&E International*, 41:510–516, 2008.

[35] M. Pour-Ghaz, O. B. Isgor, and P. Ghods. Quantitative interpretation of half-cell potential measurements in concrete structures. *Journal of Materials in Civil Engineering*, 21(9):467–475, 2009.

[36] A. Poursaee and C. Hansson. Potential pitfalls in assessing chloride-induced corrosion of steel in concrete. *Cement and Concrete Research*, 39:391–400, 2009.

[37] J. Prabakar, B. Bharathkumar, and A. Chellappan. Prediction of rebar profile in a earth retaining RCC structure using cover meter survey. *Construction and Building Materials*, 21:873–878, 2007.

[38] B. Pradhan and B. Bhattacharjee. Half-cell potential as an indicator of chloride-induced rebar corrosion initiation in RC. *Journal of Materials in Civil Engineering*, 21(10):543–552, 2009.

[39] B. Pradhan and B. Bhattacharjee. Rebar corrosion in chloride environment. *Construction and Building Materials*, 25:2565–2575, 2011.

[40] R. W. Revie and H. H. Uhlig. *Corrosion and Corrosion Control : An Introduction to Corrosion Science and Engineering.* John Wiley and Sons, Inc., Hoboken, New Jersey, 4th edition, 2008.

[41] J. Rodriguez, L. M. Ortega, and J. Casal. Load carrying capacity of concrete structures with corroded reinforcement. *Construction and Building Materials*, 11(4):239–248, 1997.

[42] V. Singh, G. M. Lloyd, and M. L. Wang. Effects of temperature and corrosion thickness and composition on magnetic measurements of structural streel wires. *NDT&E International*, 37:525–538, 2004.

[43] R. Vedalakashmi, K. Rajagopal, and N. Palaniswamy. Longterm corrosion performance of rebar embedded in blended cement concrete under macro cell corrosion condition. *Construction and Building Materials*, 22:186–199, 2008.

[44] H. Yashiro et al. Development of a magnetic corrosion probe for nondestructive evaluation of concrete against corrosion of reinforcing bar. *Corrosion Science*, 50:1005–1010, 2008.